The Institute of Paper Chemistry

Appleton, Wisconsin

Doctor's Dissertation

Raman Spectra of Celluloses

James Hugh Wiley

June, 1986

RAMAN SPECTRA OF CELLULOSES

A thesis submitted by

James Hugh Wiley

B.S. (Chem.) 1980, The University of Puget Sound, Tacoma, WA

M.S. 1982, Lawrence University

in partial fulfillment of the requirements
of The Institute of Paper Chemistry
for the degree of Doctor of Philosophy
from Lawrence University
Appleton, Wisconsin

June, 1986

TABLE OF CONTENTS

SUMMARY

A Raman microprobe was used to investigate the vibrational spectra of celluloses. The objectives were to further assign the bands in the vibrational spectrum of cellulose; study the structural differences between cellulose polymorphs; and study molecular orientation in cellulose fibers. The long-term goal of this work is to establish a basis for the use of vibrational spectroscopy in the study of plant cell wall architecture.

Several series of spectra in which the polarization of the incident light was varied relative to the fiber axis were recorded from oriented fibers. Analysis of band intensities as a function of polarization revealed information about the directional character of the vibrational motions. A study of deuterated celluloses identified the modes which involve OH and CH motions. This study, together with normal coordinate analyses of model compounds performed by previous researchers, enabled us to identify the types of vibrational motions responsible for most of the bands. The motions identified in this manner agree qualitatively in most cases with traditional group frequency assignments, but the vibrational motions are much more complex. Therefore, this novel approach provides a more thorough characterization of the Raman spectrum of cellulose and establishes a basis for future studies of native tissues.

Spectral differences between cellulose polymorphs were studied by comparing the spectra of Valonia (predominantly I_α), ramie (predominantly I_β), and mercerized ramie (II) celluloses. The spectra indicate that celluloses I_α and I_β have similar molecular conformations, but have distinct hydrogen bonding patterns. In cellulose II, the molecular conformation as well as the hydrogen bonding pattern differs from those in native cellulose.

Cellulose orientation in the plane perpendicular to the chain axis was studied by varying the polarization of the incident light relative to the cell wall surface of ramie cross sections. The results indicate that the cellulose is oriented randomly in the lateral direction perpendicular to the chain axis. In addition, a comparison of spectra from freely-dried and tension-dried cotton fibers indicated that the cellulose was oriented randomly in the lateral direction in freely-dried fibers, but nonrandomly in tension-dried fibers.

PREFACE

THESIS SCOPE

In this thesis, the Raman microprobe was used to generate new information to aid in the interpretation of the vibrational spectrum of native celluloses. The objectives were to advance the assignment of the Raman spectrum of cellulose, to study cellulose orientation in fibers, and to study the structural differences between native celluloses from various sources. The thesis was part of a larger program to study the molecular architecture of wood fibers. It served to build a foundation for the study of native woody tissues.

BACKGROUND

The wood fiber cell wall is a complex composite structure containing cellulose, hemicellulose, and lignin.[1-2] Cellulose, the β-1,4 linked polymer of anhydroglucopyranose, is the major load bearing component in the composite. Although the chemical structure of cellulose is well known, many aspects of its organization in the cell wall are poorly understood.

At The Institute of Paper Chemistry, a variety of spectroscopic and diffractometric techniques have been used to study the structure of cellulose. Raman spectroscopy has played a major part in this multifaceted approach. The Raman experiment is represented schematically in Fig. 1.[3] The monochromatic light from a laser is focused on the sample and the scattered light is analyzed. In the case of a nonvibrating system, the scattered light will have the same frequency as the incident light. If the molecules vibrate with a frequency, ω_k, then a small component of the scattered light will be shifted $\pm \omega_k$ relative to the incident light. A Raman spectrum is a plot of the intensity of the scattered

light vs. the frequency shift of the scattered light relative to the incident monochromatic light. Since the frequency shift corresponds to the vibrational frequencies of the molecules, Raman spectroscopy provides information analogous to infrared spectroscopy.

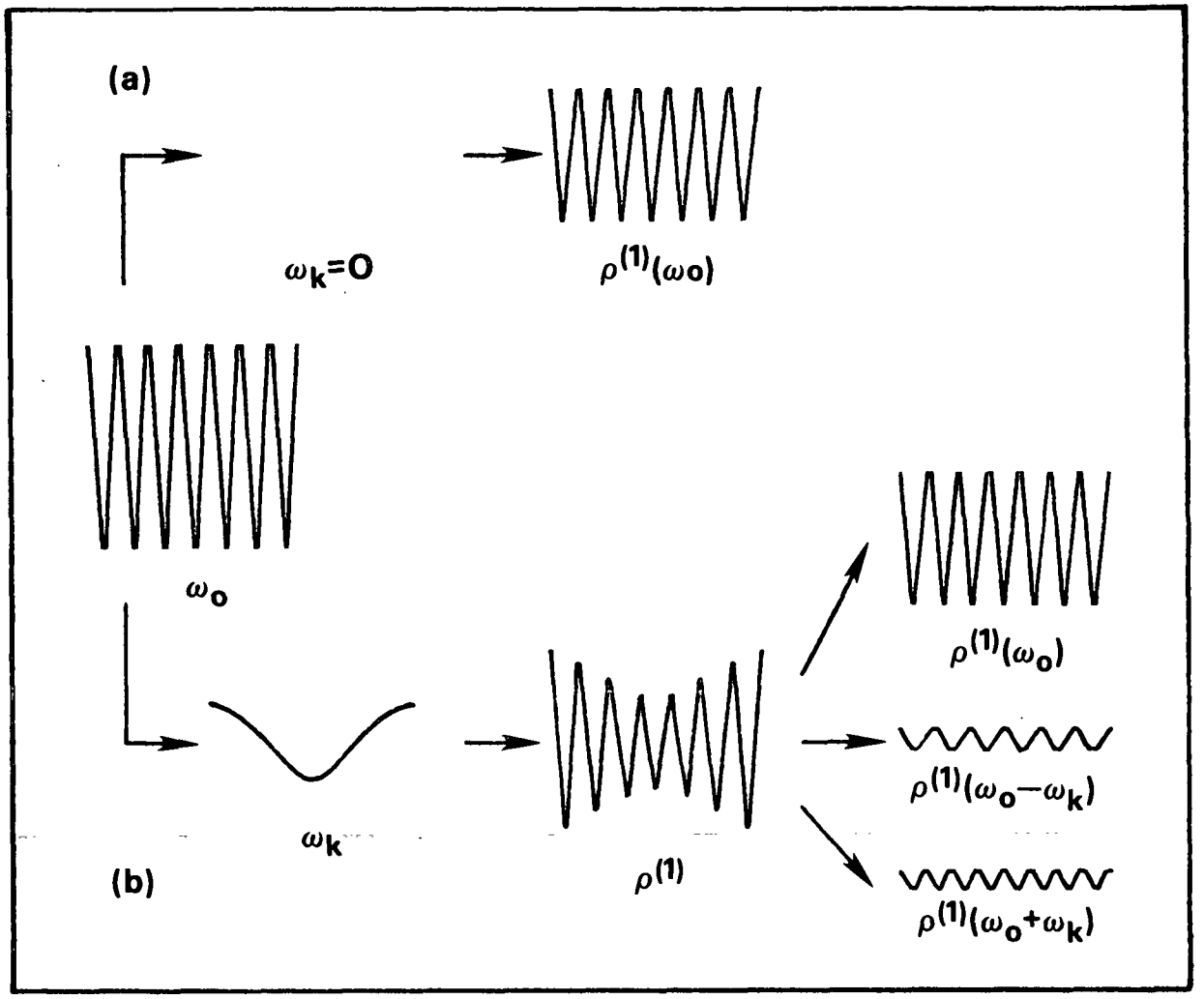

Figure 1. The Raman scattering experiment. ω_o = frequency of incident light; ω_k = vibrational frequency of the molecules; ρ = frequency of scattered light. (a) Nonvibrating system; (b) vibrating system.[3]

Both Raman and infrared spectroscopy yield information about chemical functionality, molecular conformation, and hydrogen bonding. Raman spectroscopy, however, has some important advantages for the study of cell wall structure. Highly polar bond systems, which result in intense infrared bands, have relatively low polarizabilities and, hence, weak Raman intensities. Water, therefore, has very weak Raman bands and does not interfere with the spectrum of cellulose. The low frequency region, which is observed with difficulty using infrared spectrometers, is easily observed with Raman spectrometers. Finally, cellulosic materials are often optically heterogeneous substrates. Any processes other than absorption which cause attenuation of the incident beam are problematic in infrared spectroscopy. Since the refractive index of the sample will often go through large changes in the neighborhood of absorption bands, the scattering losses will vary greatly with frequency over the infrared region. In Raman spectroscopy, refractive index variations are not a problem since the excitation frequency is far removed from any absorption bands. Therefore, Raman spectra of samples such as cellulose, which scatter light strongly, are more accurate representations of the vibrational motions and the characteristic vibrational transitions.

A recent innovation in Raman spectroscopy was the development of the Raman microprobe.[4-6] The microprobe is a specially designed optical microscope coupled to a conventional Raman spectrometer. The microprobe performs two key functions. It focuses the exciting light down to a spot as small as 1 micron in diameter,[5] then it gathers the scattered light and transmits it to the spectrometer. The microprobe makes it possible to identify the morphological features from which spectra are recorded. Orientation, composition, and structure can be related to morphology.

The present investigation utilized the ability of the microprobe to record spectra from morphologically homogeneous domains using polarized light to derive new information from the Raman spectrum of cellulose. This report has been divided into three chapters. Chapter One concerns the band assignment work; Chapter Two covers the structural differences between cellulose polymorphs; and Chapter Three discusses cellulose orientation.

CHAPTER I. ASSIGNMENT OF THE VIBRATIONAL SPECTRUM OF CELLULOSE

INTRODUCTION

Band assignments are descriptions of the vibrational motions occurring at the observed frequencies. The amount of structural information obtainable from vibrational spectra is related to the accuracy and completeness of the band assignments. Assignment of the vibrational spectrum of cellulose is difficult because cellulose is structurally complex, has many vibrational degrees of freedom, and possesses low symmetry. A variety of empirical and theoretical techniques have been used in order to assign the cellulose spectrum. Each approach has provided useful information but none have rigorously assigned the vibrational spectrum of cellulose.

In this thesis, new information for the assignment of the cellulose vibrational spectrum has been generated from Raman microprobe spectra of oriented celluloses. The dependence of band intensities on the polarization of the exciting light relative to the orientation of the molecules was studied. Vibrational modes behave like directional antennae toward polarized light. They interact with the exciting radiation most strongly when the electric vector is parallel to the direction in which the maximum change in the polarizability associated with the vibrational motions occurs. Since this direction is related to the direction of the vibrational displacements, studying the dependence of band intensities on the orientation of the incident electric vector can yield information about the direction of the vibrational motions. The intensity study also serves to build a foundation for investigations of woody tissues by providing a much more complete characterization of the bands in the Raman spectrum of cellulose than has been available previously.

In addition to the intensity study, a limited investigation of deuterated celluloses was done to identify the modes which involve hydrogen. Deuterium substitution causes those modes which involve hydrogen to shift in frequency due to the greater mass of the deuterium atom while the modes that do not involve hydrogen remain unshifted. Although the hydroxyl groups on cellulose can be partially deuterated by exposing cellulose to D_2O, fully deuterated cellulose is difficult to prepare without destroying the crystalline structure. We chose a novel approach for the preparation of deuterated cellulose. Cellulose producing algae were grown in D_2O. This method yields cellulose that is deuterated at both the oxygen and carbon atoms, allowing the effects of deuteration to be studied more completely than is possible with celluloses prepared by the deuterium exchange method.

The new experimental information discussed above was used to build upon the results from previous studies of cellulose and cellulose model compounds. These previous studies will be reviewed in the background section.

BACKGROUND

THEORETICAL ASSIGNMENT METHODS

Normal coordinate analysis provides the most rigorous means of assigning vibrational spectra. The method is described in detail in several textbooks on vibrational spectroscopy.[7-10] Since the results from normal coordinate analyses will be used extensively in this thesis, the method will be described briefly here. A normal coordinate analysis uses a simplified molecular model to calculate the form and frequency of the normal modes of vibration. A molecule is modeled as a system of point masses connected by massless springs. When an atom is displaced from its equilibrium position, the springs connected to the other atoms exert a restoring force and the atoms oscillate in space. The potential energy of an atom is proportional to the displacement of the atom from its equilibrium position. Under the harmonic oscillator approximation, it is assumed that the vibrations are sufficiently small so that the potential energy is a simple quadratic function of the displacements.

Application of Newton's laws of motion to the simple molecular model results in a set of linear equations called secular equations. The system of equations may be written in matrix form as follows:

$$\det \left| \underline{GF} - \lambda \underline{E} \right| = 0 \qquad (1)$$

where $\underline{G}$ = the kinetic energy matrix
$\underline{F}$ = the potential energy matrix
$\underline{E}$ = a diagonal unit matrix
λ = a row matrix of constants proportional to the normal frequencies.

The normal frequencies calculated by Eq. (1) are the eigenvalues of the $\underline{GF}$ product matrix. The form of each normal mode is calculated by finding the eigenvectors of the $\underline{GF}$ matrix.

The eigenvectors are used to calculate potential energy distributions (PED's) which give the relative contributions of the internal coordinates to each normal mode. Internal coordinates use the changes in bond lengths and angles to describe the positions of the atoms in the molecule. They are the most chemically meaningful coordinates for describing vibrational motion.

Several pieces of information are necessary to perform a normal coordinate analysis. The kinetic energy matrix, G, requires the masses of the atoms, the definitions of the internal coordinates, and the structure of the molecule (bond angles and lengths, etc.). The potential energy matrix, F, requires the values of the force constants for the molecule. While information about molecular structure is often available, the force constants are unknown and must be obtained from the observed frequencies. Since the number of force constants generally exceeds the number of observed frequencies, simplified force fields must be used. The force constants in the simplified field are calculated by assuming initial values based on those for chemically similar systems, then refining these values against the observed frequencies until an acceptable agreement is achieved. The choice of initial force constants is critical because the force fields derived by the refinement procedure are not necessarily unique. Two different force fields can predict the observed frequencies equally well but yield significantly different potential energy distributions.

Several normal coordinate analyses for carbohydrates have appeared in the literature.[11-22] Two different approaches have been taken. In the approach taken at The Institute of Paper Chemistry, a force field specifically tailored to complex carbohydrates was developed by using model systems such as the 1,5-anhydropentitols,[11-12] the straight chain pentitols,[13] the pentose sugars,[13] the inositols,[15-16] and the hexose sugars.[17] The goal of these investigations was

to develop a framework within which the spectra of complex carbohydrates such as cellulose could be interpreted. For each group of compounds, the force constants were refined against the observed frequencies until a satisfactory fit was obtained. The derived force fields enabled successful prediction of the spectra of compounds not included in the refinements, and the calculated potential energy distributions were reasonable in comparison with the group frequency literature on the carbohydrates. The analyses were, thus, successful in developing a physically meaningful force field.

The hexose force field was used to extend the normal coordinate method to the cellodextrins[18] whose vibrational spectra more closely resemble the spectrum of cellulose. Because the number of vibrational degrees of freedom greatly exceeds the number of bands observed in the spectra of these compounds, it was neither possible nor meaningful to refine the constants. Although the calculations predicted many more bands than are actually observed, the distribution of the calculated frequencies was in qualitative agreement with the observed spectra. The force field developed for the model compounds, therefore, appears to provide a good model for understanding the vibrational spectra of the cellodextrins and cellulose.

In the second approach, workers have concentrated on normal coordinate calculations for glucose and its polymers using force fields transferred from noncarbohydrate systems.[19-22] The calculations are more approximate than the calculations done at the Institute because the force constants were not refined or rigorously tested to determine their meaningfulness. Furthermore, the calculations for cellulose[21-22] are based on a questionable structural model. The potential energy distributions from these studies are qualitatively similar to the distributions calculated using the first approach to a large extent. There

are some significant differences, however, which will be covered in the discussion.

The potential energy distributions calculated by the two approaches were quite complex. Except for the internal vibrations of the methylene groups, the modes below 1500 cm^{-1} are delocalized motions involving several internal coordinates. Above 1500 cm^{-1}, the CH and OH stretching modes did not appear to mix with the other internal coordinates.

EMPIRICAL ASSIGNMENT METHODS

The size and number of equations to be solved in a normal coordinate analysis becomes very large as the number of atoms in a molecule increases. Even in simplified force fields, the number of force constants exceeds the number of observed frequencies. It is not surprising then that most interpretations of the cellulose vibrational spectrum were based on more approximate empirical methods. The most common method used to interpret the spectra of large molecules is the group frequency method.[23] In this approximation, the vibrational motions are assumed to be localized in particular groups of atoms within the molecule. The frequency and form of these group vibrations are approximately constant from molecule to molecule if the chemical environment of the group remains the same. Therefore, the group frequencies determined for simple molecules can be used to interpret the spectrum of larger molecules.

In the literature,[24-28] the group frequency approximation has been used extensively together with information from the spectra of deuterated celluloses and polarized infrared spectra to assign the vibrational spectrum of cellulose. Although these have been useful in studies of cellulose structure, the normal coordinate calculations have shown that the group frequency approximation is

valid for only a few of the observed bands. Above 1500 cm^{-1}, the C-H and O-H stretching modes do behave as relatively pure group modes. Below 1500 cm^{-1}, however, only the internal vibrations of the CH_2OH groups approximate group modes.

In this thesis, new experimental information has been generated through the use of the Raman microprobe and the preparation of deuterated celluloses. This new information has been used together with previous theoretical and empirical information as an aid in the interpretation of the vibrational spectrum of cellulose.

THEORY

The dependence of band intensities on the polarization of the incident light was studied to facilitate assignment of the Raman spectrum of cellulose. The relationship between band intensities and the nature of the vibrational motions can be understood by considering the classical theory of Raman intensities. Only the essential points will be discussed here. The reader is referred to the textbooks for a more detailed treatment.[3] Raman scattered light arises from the dipoles induced in the molecules by the incident light. Raman intensities are, therefore, proportional to the square of the induced dipole moment. The direction and magnitude of the induced dipole moment is related to the intensity and direction of the electric vector of the incident light through the following equation:

$$\vec{P} = \underline{\alpha}' \vec{E} \tag{2}$$

where $\vec{P}$ = the induced dipole

$\underline{\alpha}'$ = the derived polarizability tensor

$\vec{E}$ = the electric vector of the incident light

Equation (2) implies a set of linear equations:

$$P_x = \alpha_{xx}E_x + \alpha_{xy}E_y + \alpha_{xz}E_z \tag{3}$$

$$P_y = \alpha_{yx}E_x + \alpha_{yy}E_y + \alpha_{yz}E_z \tag{4}$$

$$P_z = \alpha_{zx}E_x + \alpha_{zy}E_y + \alpha_{zz}E_z \tag{5}$$

where xyz = an arbitrary Cartesian coordinate system

P_i = the components of P in the xyz system

E_i = the components of E in the xyz system

α_{ij} = the components of $\underline{\alpha}$ in the xyz system[a]

Polarized light with the electric vector in the x direction can induce dipoles with components in the y and z directions as well as in the x direction. Thus, the polarization of the light can be changed by the scattering process.

The elements of the derived polarizability tensor are equal to the derivatives of the equilibrium polarizability tensor with respect to the vibrational coordinates. The dependence of the band intensities on the polarization of the incident and scattered beams depends on the relative magnitudes of the tensor elements, α_{ij}, which are determined by the directions of the vibrational motions. Measurement of the angle of the incident electric vector relative to the fiber axis that corresponds to the maximum intensity can reveal which tensor element is predominant and thereby provides information about the direction of the vibrational motion.

Intensity maxima were measured by performing the experiment shown in Fig. 2a using ramie fibers and fiberlike aggregates extracted from the cell wall of the alga Valonia macrophysa. Electron microscopy indicated that the cellulose chains are approximately parallel to the axis of the fiberlike aggregates and ramie fibers. The angle between the electric vector of the incident and scattered beams and the fiber axis, Θ, was varied from 0 to 90° in 15° increments. A regression technique was used to derive equations describing the dependence of the observed intensities on Θ. The locations of the intensity maxima were derived from these regression equations.

---

[a]In Eq. (3)-(5) and throughout the rest of the thesis the primes have been omitted when writing the elements of the derived polarizability tensor.

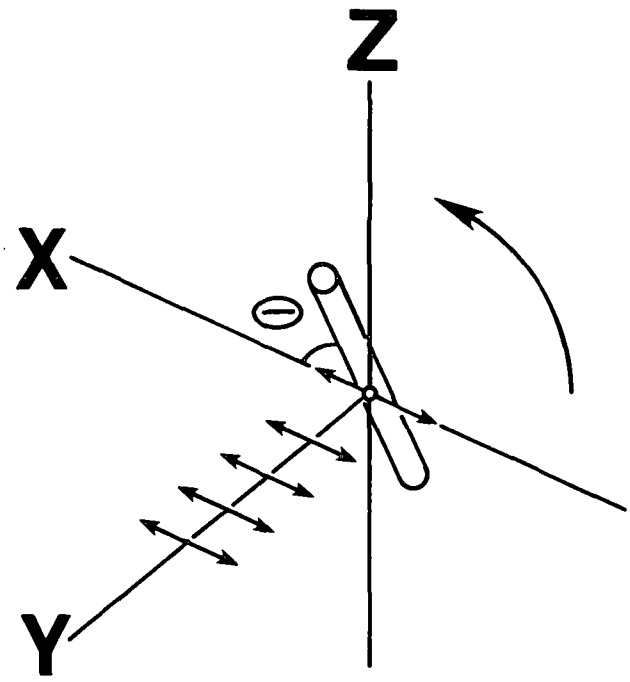

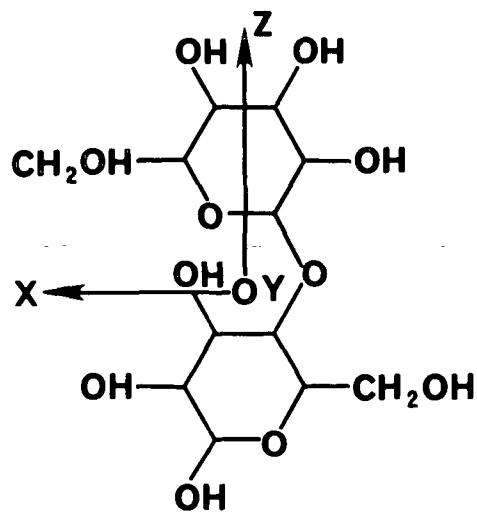

Figure 2. Experiment where the polarization of the incident beam was varied. Θ = the angle between the electric vector and the fiber axis; XYZ = laboratory coordinate system; xyz = molecule based coordinate system.

The form of the regression equation was derived following Snyder's treatment for Raman scattering from partially oriented polymers.[29] We defined xyz as a molecule based coordinate system with the z axis parallel to the chain axis. The laboratory based coordinates are XYZ, where the X axis is parallel to the electric vector of the incident and scattered beams and the direction of propagation is along the Y axis. The coordinate definitions are shown in Fig. 2a and 2b. We assumed that the chains are oriented parallel to the axis of the ramie fibers and the fiberlike aggregates of Valonia cellulose and that the chains are oriented randomly in the plane perpendicular to the chain axis (uniaxial orientation). These assumptions are justified for the following reasons: First, electron micrographs indicated that the microfibril angle in ramie fibers and the fiberlike aggregates of Valonia cellulose is very small. Second, it is unlikely that there would be any preferred lateral orientation in the fiberlike aggregates extracted from Valonia. Third, Raman spectra of ramie cross sections indicated that the cellulose is oriented randomly in the plane perpendicular to the chain axis (see Chapter III).

The transformation between laboratory fixed coordinates (L) and molecule based coordinates (m) is given by:

$$\underline{\alpha}(L) = \underline{\Phi\alpha}(m)\Phi t \qquad (6)$$

where Φ = the transformation matrix between coordinate systems m and L

Φt = the transpose of Φ

$\underline{\alpha}(m)$ = the derived polarizability tensor expressed in molecule based coordinates

$\underline{\alpha}(L)$ = the derived polarizability tensor expressed in laboratory based coordinates

If β is defined as the angle between x and Y and Θ as the angle between z and X, then the transformation matrix, Φ, can be written as:

$$\Phi = \begin{bmatrix} -\sin\Theta\sin\beta & -\sin\Theta\cos\beta & \cos\Theta \\ \cos\beta & \sin\beta & 0 \\ \cos\Theta\sin\beta & \cos\Theta\cos\beta & \sin\Theta \end{bmatrix} \quad (7)$$

In the scattering geometry shown in Fig. 2a, the intensities are proportional to α^2_{XX}. The relationship between α^2_{XX} and $\alpha(m)$ was derived from Eq. (6) and (7) by assuming that $\alpha(m)$ is symmetric and averaging overall values of β:

$$\alpha^2_{XX} = 1/8[2(\alpha_{xx}+\alpha_{yy})^2 + (\alpha_{xx}-\alpha_{yy})^2 + 4\alpha^2_{xy}]\sin^4\Theta + [(\alpha_{xx}+\alpha_{yy})\alpha_{zz}+2\alpha^2_{yz}]\sin^2\Theta\cos^2\Theta + \alpha^2_{zz}\cos^4\Theta \quad (8)$$

Equation (8) can be rearranged to yield:

$$\alpha^2_{XX} = B + (C-2B)\cos^2\Theta + (B-C+A)\cos^4\Theta \quad (9)$$

where $A = \alpha^2_{zz}$

$B = 1/8[2(\alpha_{xx} + \alpha_{yy})^2 + (\alpha_{xx}-\alpha_{yy})^2 + 4\alpha^2_{xy}]$

$C = [(\alpha_{xx}+\alpha_{yy})\alpha_{zz} + 2\alpha^2_{xz} + 2\alpha^2_{yz}]$

Since the intensities are proportional to α^2_{XX}, Eq. (9) defines the relationship between the band intensities and the angle between the electric vector of the incident light and the fiber axis.

The intensity maxima were found by setting the first derivative of Eq. (9) equal to zero:

$$-4(B-C+A)\cos^3\Theta\sin\Theta - 2(C-2B)\sin\Theta\cos\Theta = 0 \quad (10)$$

Equation (10) has the following roots:

$$\Theta_m = 0 \tag{11}$$

$$\Theta_m = 90 \tag{12}$$

$$\Theta_m = \arccos[-(C-2B)/2(B-C+A)]^{1/2} \tag{13}$$

The roots given by Eq. (11)-(12) can be either maxima or minima, since the first derivative of Eq. (9) is zero in either case. Maxima were distinguished from minima by evaluating the second derivative of Eq. (9):

$$\begin{aligned} \alpha^2_{XX}/(d\Theta)^2 = &-4(B-C+A)(-3\cos^2\Theta+\cos^4\Theta) \\ &- 2(C-2B)(-\sin^2\Theta+\cos^2\Theta) \end{aligned} \tag{14}$$

When the values of Θ_m given by Eq. (11)-(13) are substituted into Eq. (14), the second derivative takes on the following values:

$$[d^2I/(d\Theta)^2]_{\Theta = 0^\circ} = -4(B-C+A) -2(C-2B) \tag{15}$$

$$[d^2I/(d\Theta)^2]_{\Theta = 90^\circ} = 2(C-2B) \tag{16}$$

$$[d^2I/(d\Theta)^2]_{\Theta = x} = -4(C-2B)-2(C-2B)^2/(B-C+A) \tag{17}$$

where $x = \arccos[-(C-2B)/2(B-C+A)]^{1/2}$

Equations (15)-(17) show that the relative values of C-2B and B-C+A determine the location of the maxima and minima.

In summary, the intensity maxima were found by recording spectra from oriented fibers. The angle between the electric vector of the incident light and the fiber axis was varied from 0 to 90 degrees in 15 degree increments. Equation (9) was fitted to the observed intensities using linear regression. The estimates of the parameters (C-2B) and (B-C+A) were substituted into Eq. (13), and (15)-(17) to determine the locations of the maxima and minima.

EXPERIMENTAL

CELLULOSE SAMPLES

Algal Celluloses

Algal celluloses were chosen for the study of the Raman spectra of celluloses because of their high crystallinities and because pure cellulose can be isolated by mild purification methods. In addition, algae can be cultured in the laboratory making it easy to obtain fresh material. Finally, by growing the algae in heavy water it is possible to produce deuterium substituted cellulose. Two types of algae were investigated. The first species, Valonia macrophysa, is a green single-celled marine algae. The second species, Cladophora glomerata, is a green filamentous fresh water algae.

We obtained a living sample of Valonia macrophysa from the Culture Collection of Algae.* The algae were grown in enriched synthetic seawater. The recipe for the synthetic seawater was kindly provided by Dr. Raymond Legge at the University of Texas. Its preparation is described in Appendix I. The seawater was enriched with 5 mL of Provasoli's ES enrichment for seawater.[30] The preparation of the enrichment solution is also described in Appendix I. This level of enrichment, which is one-fourth of the normal level, was suggested by researchers at the University of Texas as being more suitable for Valonia. The pH of the medium was adjusted with either 1N hydrochloric acid or 1N sodium hydroxide until a value of 7.8 was reached. The medium was filtered through a Millipore filter (0.22 micron pore size) to reduce the contamination with other microorganisms.

*University of Texas at Austin, Department of Botany, Austin, Texas 78712. The culture was designated in the UTEX catalog as Valonia (Ginnani), LB 1977 V. macrophysa Kutz.

The growing conditions employed were suggested by Dr. John A. West (University of California, Berkeley). The culture vessels were either 170 x 90 mm crystallizing dishes or 2000 mL Erlenmeyer flasks. Each vessel contained approximately 50 algae and 500 mL of medium. The vessels were covered with Saran wrap to keep out airborne contaminants. The medium was changed every 2-3 weeks.

temperature	22°C
light intensity	200-300 footcandles (white fluorescent bulbs + purple fluorescent grow lights)
photoregime	16 hours light + 8 hours dark

In order to obtain pure cellulose from Valonia, it is necessary to remove the other components. A study was conducted to assess the ability of various extraction methods to produce pure cellulose from Valonia. The purity of the cellulose was measured by carbohydrate analysis and visually by the whiteness of the cellulose. The details of the study are given in Appendix II. The following procedure produced the purest cellulose from Valonia:

1. Extract in a Soxhlet extractor with 95% ethanol for four hours followed by chloroform-methanol (50:50, V:V) for 8 hours.
2. Wash with methanol, then water to remove residual solvent.
3. Boil in 1% NaOH for 6 hours under nitrogen, changing the liquor twice.
4. Wash with water until washings are neutral.
5. Soak in 0.05N HCl for 8-12 hours.
6. Wash with water until neutral.
7. Bleach with sodium chlorite at 70°C for 3 hours; liquor consists of 150 mL water, 1.5 g sodium chlorite, and 0.5 mL glacial acetic acid.[31]

8. Wash with water until neutral.

9. Wash with DTPA solution several times, soaking the Valonia for 15 minutes each time; DTPA solution consists of 2 g diethylenetriaminepentaacetic acid (DTPA) dissolved in 1 L of water at pH 9.0.

10. Wash with water until neutral.

The purified Valonia contained a mixture of intact cell wall fragments and fibrillated material. Fiberlike aggregates of Valonia cellulose were prepared for examination with the microprobe by pulling on the cell wall material with forceps. Although there are no macroscopic fibers present in the Valonia cell wall, apparently the microfibrils can be aligned to form fiberlike aggregates by applying tension to the water-swollen cell wall. The aggregates range in length from 2-3 mm up to around 2 cm depending on how much tension is applied. The longer the aggregate is, the thinner it will be. Generally, the aggregates break before they get over 1 cm long. In the rest of the thesis, these fiberlike aggregates of Valonia cellulose will be referred to as fibrillar aggregates.

The fibrillar aggregates were laid across small washers (1/4 inch diameter) and allowed to air-dry. The adhesion between the fibrillar aggregate and the washer applied enough tension to the aggregate to keep it straight during drying. Once the fibrillar aggregates were dry, they were glued to the washer with Duco cement. The washers holding the fibrillar aggregates were then glued to a metal microscope slide which had rows of 1/8 inch diameter holes drilled in it. This device was used because ordinary glass slides cause extraneous peaks in the Raman spectra.

Valonia samples were also examined in the form of pellets. To prepare a pellet, the purified material was freeze dried. Pellets were pressed in a standard laboratory pellet press. The pressure was approximately 5000 psi (gage).

Valonia samples were characterized by carbohydrate analysis, x-ray diffraction, Raman spectroscopy, and electron microscopy. Carbohydrate analyses of *Valonia* cellulose were performed by Mr. Arthur Webb (IPC) according to a TAPPI method.[32] Diffraction patterns were recorded from purified pellets of *Valonia* cellulose. The electron micrographs were taken from the *Valonia* fibrillar aggregates.

Another type of algae, *Cladophora glomerata*, was grown in our laboratory by Ms. Rebecca E. Whitmore. The medium and growing conditions were based on a study by Graham *et al.*[33] The recipe for the medium is listed in Appendix I. The algae was grown in either one liter Erlenmeyer flasks or in small fish tanks, depending on the volume of algae desired. Filtered air, which was humidified by first bubbling it through water, was bubbled through the medium continuously.

light intensity	300-400 footcandles
photoregime	16 hours light 8 hours dark
temperature	14°C

The *Cladophora* cellulose was purified by the same procedure used to purify *Valonia* cellulose.

Deuterated Algal Celluloses

In an effort to obtain deuterated cellulose, we attempted growing *Valonia* in D_2O. Dr. H. L. Crespi at Argonne Laboratories has successfully adapted many species of algae to growing in D_2O.[34] We consulted with Dr. Crespi and appreciate the helpful advice he gave us. The *Valonia* were adapted to D_2O by gradually replacing the H_2O in the synthetic seawater with equal volumes of D_2O. We started the adaptation with 60% (volume basis) D_2O. The normal level of ES

enrichment (in water) was used. We found that the algae adapted more quickly to D_2O if the light intensity was reduced. We did this by wrapping several layers of cheese cloth around the flasks so that the light intensity was approximately 1/4 the original value. The medium was changed about once a month and the D_2O-H_2O mixture was recovered from the salts by distillation to conserve D_2O. The concentration of the recycled D_2O-H_2O mixture was monitored by measuring specific gravity.

When the algae started growing well in 60% D_2O (after about 6 weeks), the D_2O concentration was increased to 80%. The next step in the adaptation procedure was 90%. Finally the algae were placed in 99% D_2O. Although the Valonia had been growing in 90% D_2O fairly well, they died in the 99% D_2O after a couple of months. Since it took approximatly 6 months to reach the stage where the Valonia was growing well in 90% D_2O and our attempts to deuterate other types of algae were looking more promising, we abandoned our efforts to grow Valonia in D_2O.

The procedure used to adapt the Cladophora to D_2O was the same as the procedure for Valonia described above. Since a significant proportion of the medium came from the stock solutions, it was necessary to make the macrosalts, sodium silicate, nitrate, and phosphate stocks using D_2O instead of H_2O. Furthermore, the air bubbled through the medium was dried with Drierite and then bubbled through D_2O before it was bubbled through the medium. These precautions cut down on the contamination of the medium with hydrogen.

The Cladophora adapted much more readily to D_2O than Valonia. This is probably because the Cladophora grew much more quickly than the Valonia did in normal medium. It still took approximately one year for the Cladophora to start growing in 99% D_2O.

Purification of the deuterated Cladophora was done following the Valonia procedure except that the bleaching steps (Steps 7 and 8) were omitted. These steps were omitted because the amount of deuterated material remaining after the previous steps was small and we did not wish to risk losing any more material. Secondly, the deuterated material tended to fragment more readily and a bleaching step would have broken the cell wall apart too much.

The Cladophora fibers were stretched across copper specimen support grids commonly used in the electron microscope (3.05 mm diameter, Polaron Inc.). The grids had covers which helped hold the fibers in place and were coated with a thin layer of an adhesive. The grids themselves were mounted on the metal microscope slide described above.

The deuterated Cladophora cellulose was characterized by x-ray diffraction and electron microscopy. Electron micrographs of deuterated Cladophora cellulose were compared with normal Cladophora cellulose to determine effects of deuteration on morphology. Insufficient material was available for any kind of carbohydrate analysis.

Ramie Cellulose

Ramie (Boehmeria nivea) fibers were chosen for the study of the Raman spectra of celluloses because they have a high cellulose content, are easily purified, and the cellulose chains are parallel to the fiber axis.[1-2] Furthermore, the fibers are large and easily manipulated. The original source of the ramie is a sample used by Bruce Dimick in his thesis work.[35]

The ramie fibers had been previously purified by the following procedure:[35]

1. Removal of debris with carding combs and forceps.
2. Extraction with chloroform for 18 hours in a Soxhlet extractor.
3. Extraction with 95% ethanol for another 18 hours.
4. Boiling for 8 hours in 1% NaOH under nitrogen.

The drying method was not listed. The ramie was purified further for this study by washing it with DTPA as described for Valonia. The material was then freeze-dried.

In order to obtain straight fibers, the freeze-dried ramie was rewetted and dried under tension using the apparatus shown in Fig. 3. This device was designed by Dr. Carl Jentzen.[36] The fiber is mounted in the jaws and then the tub is filled with water until the fiber is submerged. Tension is applied to the fiber through the spring and thumb-screw. When the water was drained out, the tension on the fiber was adjusted so that the fiber remained straight as it dried. The dried fibers were then mounted on washers as described for Valonia.

The ramie cellulose was characterized by carbohydrate analysis, x-ray diffraction, Raman spectroscopy and electron microscopy. Scanning electron micrographs were recorded from whole fibers and fibers which we tore in half longitudinally to reveal the microfibril angle.

Bacterial Cellulose

Bacterial cellulose was chosen for our study of the Raman spectra of cellulose because we had a fully deuterated sample available to us. The sample was kindly provided by Dr. H. L. Crespi at Argonne Laboratories. It was produced by growing Acetobacter xylinum in a deuterated growth medium.[34] Acetobacter produces extracellular cellulose.

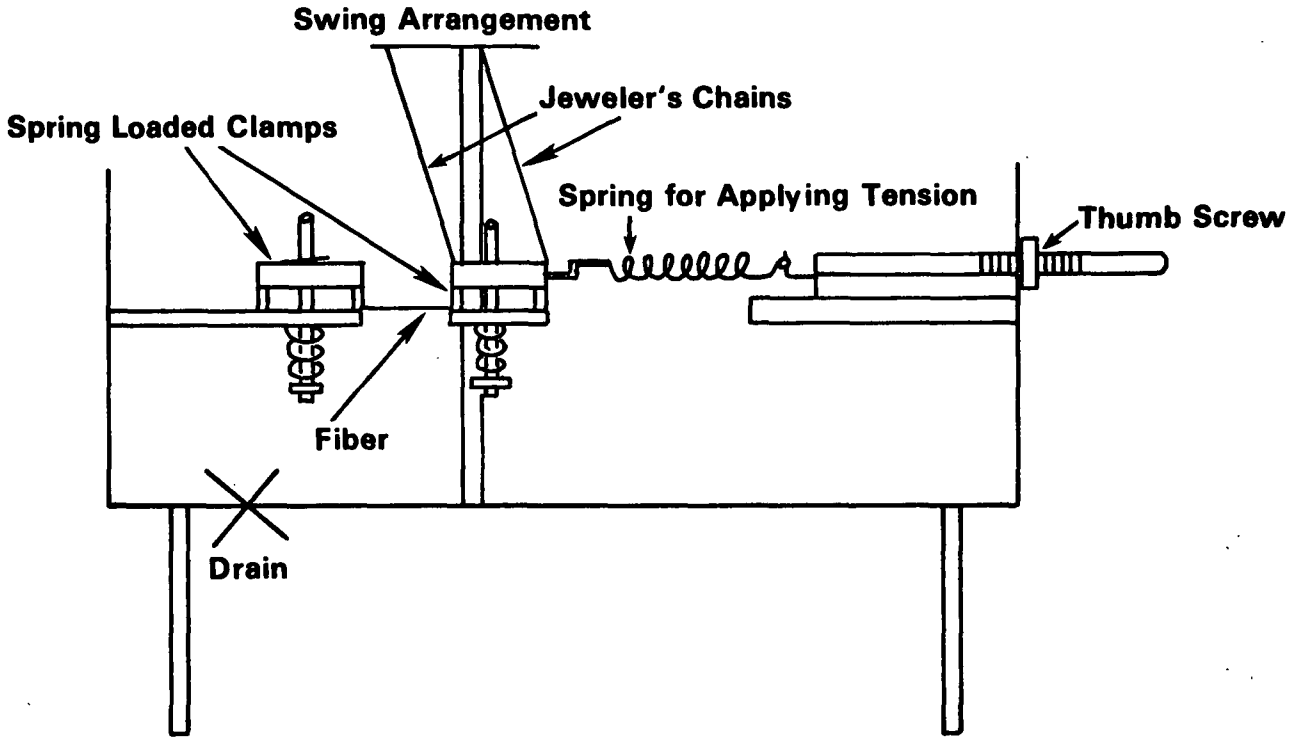

Figure 3. Apparatus for drying fibers under tension.

A portion of the deuterated bacterial cellulose pellicle was cut into small pieces, purified by the procedure outlined for Valonia cellulose, freeze-dried and pelletized. The Raman spectrum of this sample had a very high level of fluorescence. Therefore, another portion of the pellicle was purified by a modified procedure. The new procedure was the same through Step 8. The residue from Step 8 was added to boiling 2.5N HCl and boiled for 15 minutes under nitrogen. The residue was collected on a fine fritted glass funnel, washed with distilled water until the pH was neutral, and then DTPA washed and freeze-dried. It was hoped that the acid hydrolysis would reduce the fluorescence by removing more of the metal ions. The deuterated bacterial cellulose was characterized by x-ray diffraction.

INSTRUMENTAL

X-Ray Diffraction

Diffractograms were recorded from Valonia, Cladophora, ramie, and deuterated bacterial celluloses using a Phillips ADP 3720 diffractometer equipped with a powder pattern type goniometer and theta compensating slits. Nickel filtered CuKα radiation was used. The x-ray tube was operated at 45 KV and 40 ma. Two theta was scanned from 8 to 30°. The scan speed was 0.02° 2 theta per second; the sample interval was 0.02° 2 theta; and the sample time 1.00 second.

Electron Microscopy

Scanning electron micrographs were recorded from samples of Valonia, Cladophora, and ramie celluloses by Mrs. Hilkka Kaustinen.

Raman Microprobe

A diagram of the Raman microprobe system is shown in Fig. 4. It consists of a Jobin Yvon Ramaonor HG2S monochromator system coupled with a Nachet optical microscope. Exciting light is provided by the 514.5 nm line of an argon ion laser. The data acquisition system consists of a photomultiplier detector and a Tracor Northern TN1500 digital signal analyzer. The scanning motor in the monochromator is also computer controlled.

In order to record a spectrum with the microprobe, a sample is placed on the mechanical stage (label ms) and the image of the sample is viewed with white transmitted light on the view screen (label g). The domain of interest is brought into focus at the crosshair on the view screen. Then the laser (label 1) is switched on, the white light is turned off, and the mirror mL (label mL) is removed so that the image travels to the monochromator. The size of the domain from which spectra are recorded is determined by the resolving power of

the objective. In this investigation, a 40X (numerical aperture = 0.75) was used. This objective acquires data from a spot 2-3 microns in diameter. Although higher resolution objectives were available, the 40X provided adequate resolution and yielded a better signal to noise ratio than the higher powered objectives.

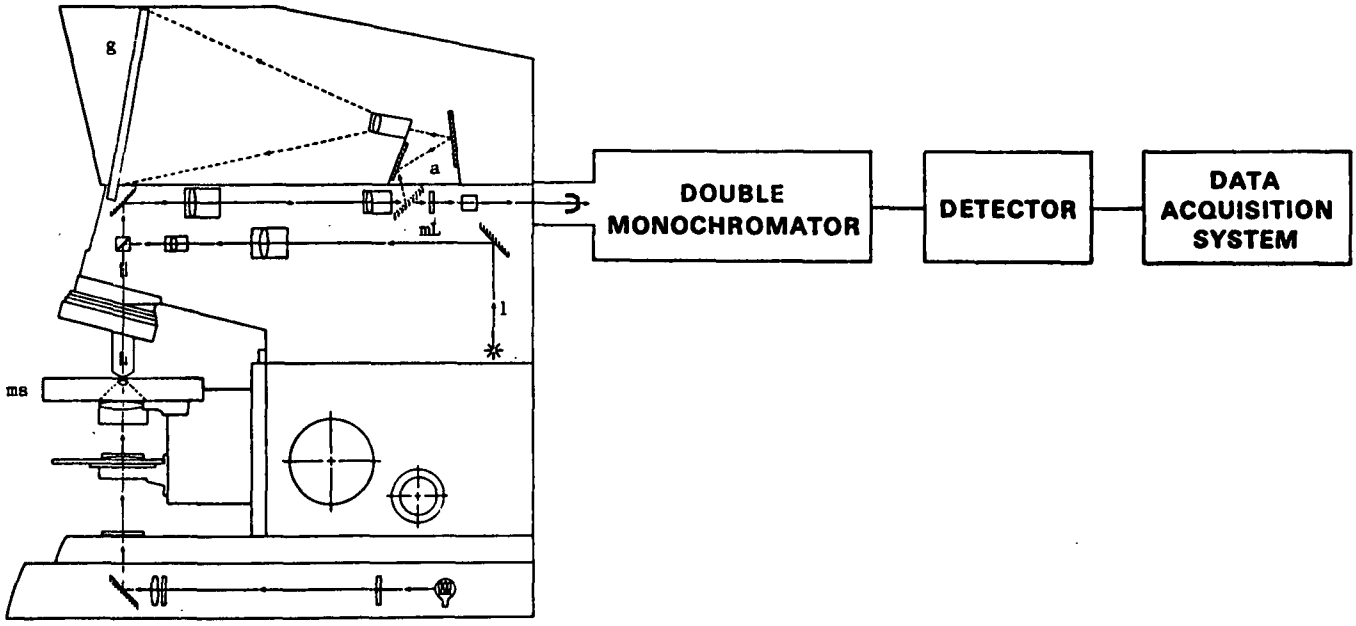

Figure 4. The Raman microprobe system.

As shown in Fig. 2a, the angle between the electric vector of the incident light and the fiber axis was varied from 0 to 90°. Since we wanted to compare the intensities in spectra recorded with different polarizations of the exciting light, special precautions were taken to avoid problems associated with the dichroism inherent in the microprobe system. First, we did not change the polarization of the incident light directly but instead used the rotating mechanical stage to rotate the sample relative to the plane of polarization of the incident light. The stage was aligned so that its axis of rotation coincided with the optical axis of the microscope. This was done by observing a micrometer slide and adjusting the stage so that it could be rotated without observing

any translation of the micrometer markings. The actual samples were carefully observed during rotation to check that no translation occurred. The samples remained in sharp focus during rotation, making it unlikely that any vertical translation had occurred. These precautions made it possible to rotate the sample without changing the domain being analyzed.

Second, a polarization scrambler was inserted in the path of Raman scattered light at the coupling between the microscope and the monochromator. The polarization of the scattered light analyzed by the spectrometer was determined by the polarization analyzer (label a). When polarized spectra were recorded, the analyzer was oriented so that the electric vector of the scattered light was parallel to the electric vector of the incident light. In depolarized spectra, the analyzer was rotated so that the electric vectors of the incident and scattered beams were perpendicular.

The acquisition time required for each spectrum was 8 hours. Multiple scans were recorded to reduce distortion of relative intensities due to power fluctuations during a single scan. Each scan required approximately 50 minutes (scan rate = 60 cm^{-1}/min). The laser power measured at the sample was approximately 7 mW. The power varied less than 3% between each spectrum in a set. The spectral slit width was 8 cm^{-1} (slit opening = 800 microns).

Conventional Raman Spectra

Conventional Raman spectra were recorded from the pelletized samples. These spectra were recorded using the conventional HG2S sample chamber. A 90° scattering geometry was used. Again multiple scans were recorded, each scan lasting approximately 50 minutes (scan rate = 60 cm^{-1}/min). The slit width and total acquisition time varied from sample to sample and will be listed on the figures. The laser power was approximately 150 mW.

EXPERIMENTAL RESULTS

CARBOHYDRATE ANALYSIS

The results of the carbohydrate analyses of purified Valonia macrophysa and ramie are given in Table 1.

Table 1. Carbohydrate analyses of purified Valonia and ramie celluloses.

Sample	Araban, %	Xylan, %	Mannan, %	Galactan, %	Glucan,[a] %
Valonia macrophysa[b]	0.6	0.2	1.0	1.2	92.6
Ramie[c]	0.2	0.6	0.6	--	100.9

[a]Percentages based on moisture free weight of the sample.
[b]Based on duplicate determinations.
[c]Based on single determination.

X-RAY DIFFRACTOGRAMS

The x-ray diffractograms recorded from pellets of purified Valonia macrophysa, ramie, deuterated bacterial cellulose, and the deuterated Cladophora glomerata grown in 90% D_2O are given in Fig. 5-8.

SCANNING ELECTRON MICROGRAPHS

A scanning electron micrograph (SEM) of a fibrillar aggregate from Valonia is shown in Fig. 9. Figure 10 is an SEM of a ramie fiber; Fig. 10a shows the fiber surface and Fig. 10b shows the interior of the fiber. A micrograph of Cladophora glomerata grown in H_2O is given in Fig. 11a and Cladophora grown in 99% D_2O is shown in Fig. 11b.

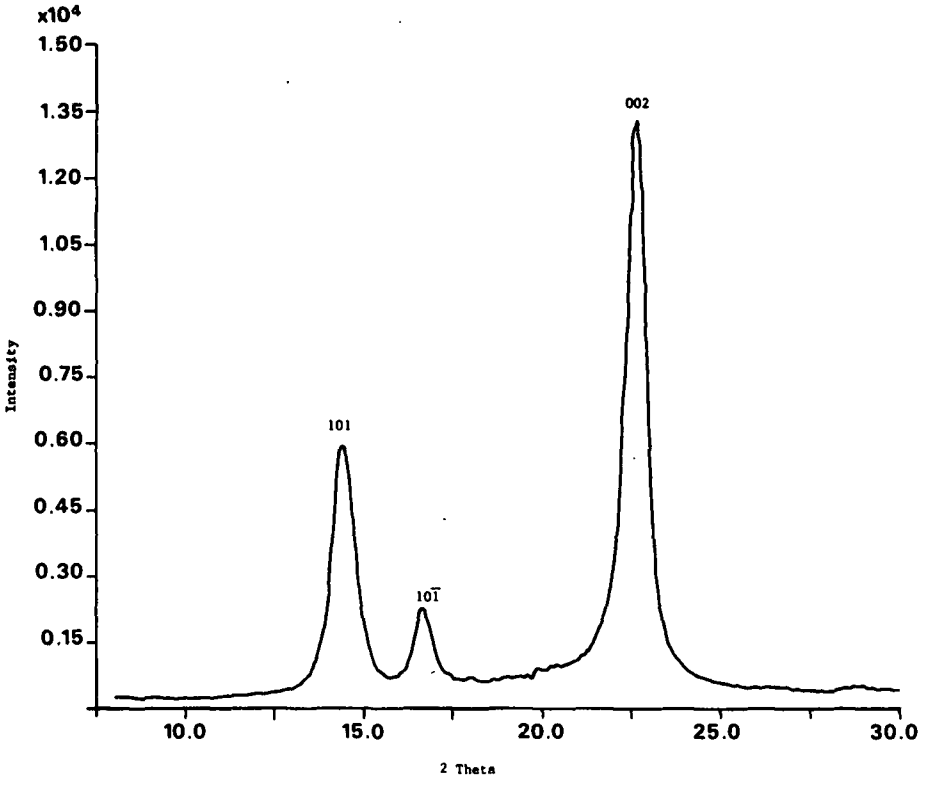

Figure 5. X-ray diffractogram of Valonia macrophysa.

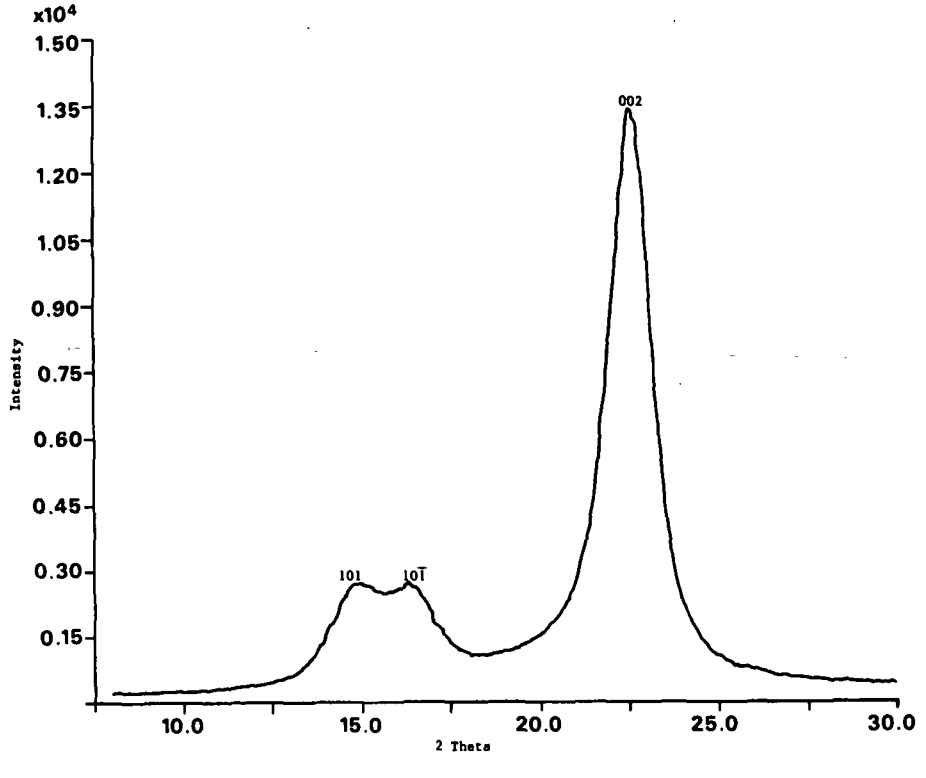

Figure 6. X-ray diffractogram of ramie.

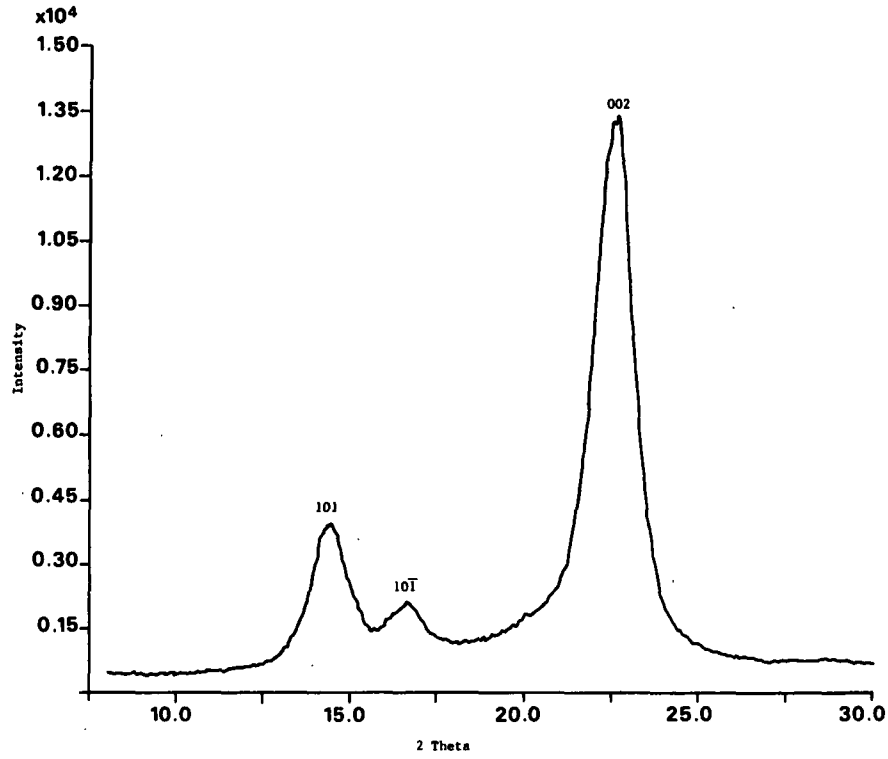

Figure 7. X-ray diffractogram of deuterated bacterial cellulose.

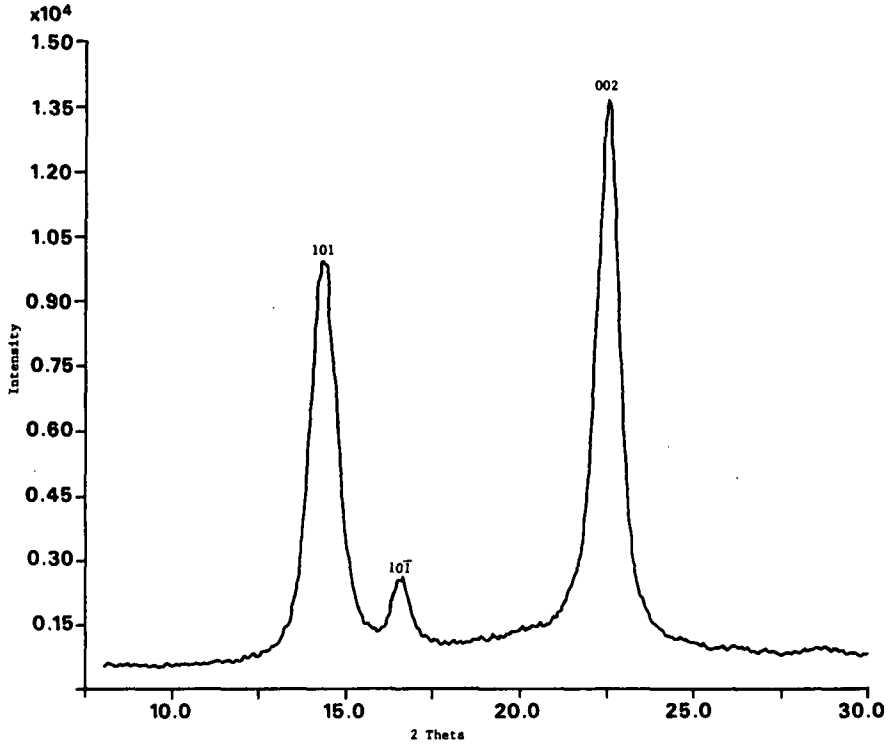

Figure 8. X-ray diffractogram of cellulose from Cladophora glomerata grown in 90% D_2O.

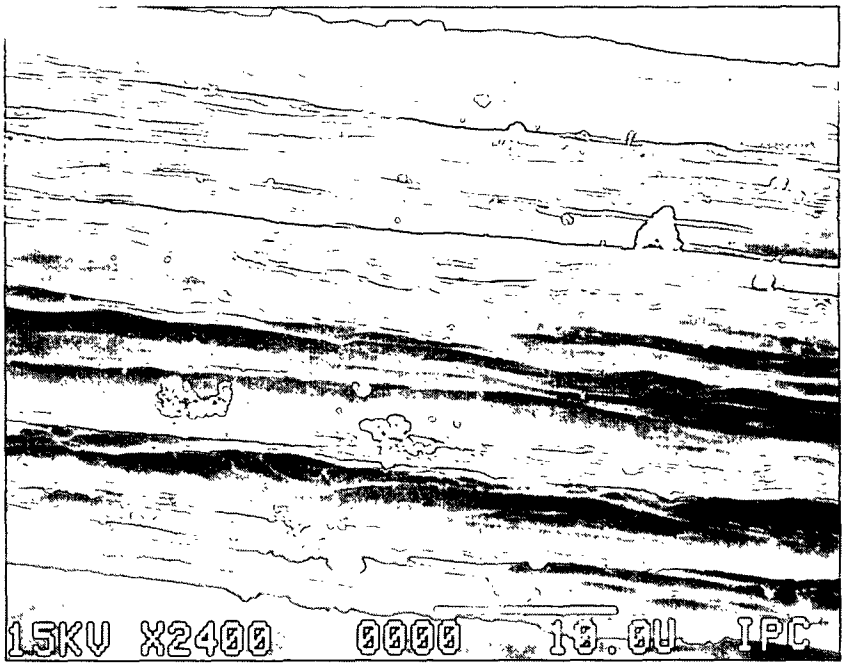

Figure 9. Scanning electron micrograph of a Valonia fibrillar aggregate.

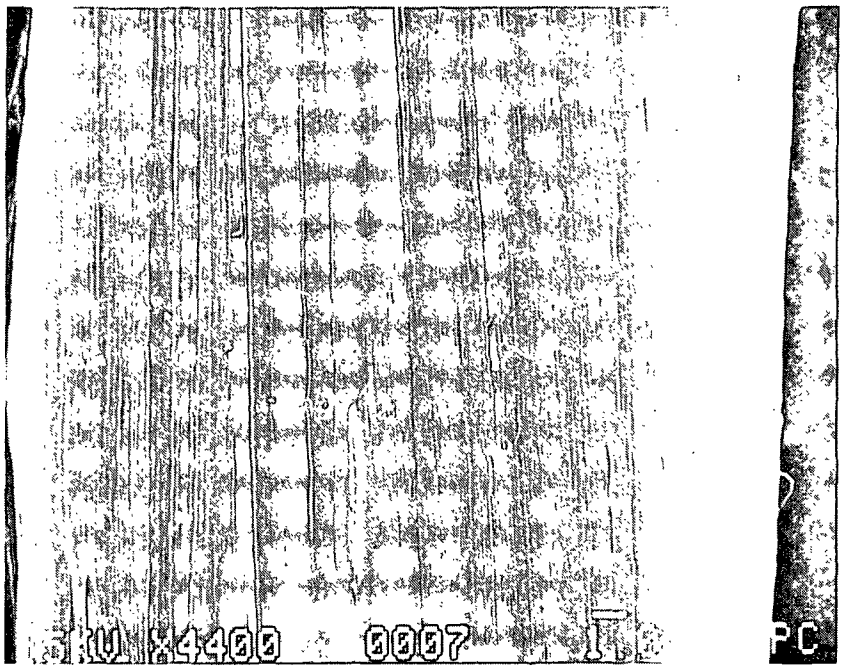

a) surface view

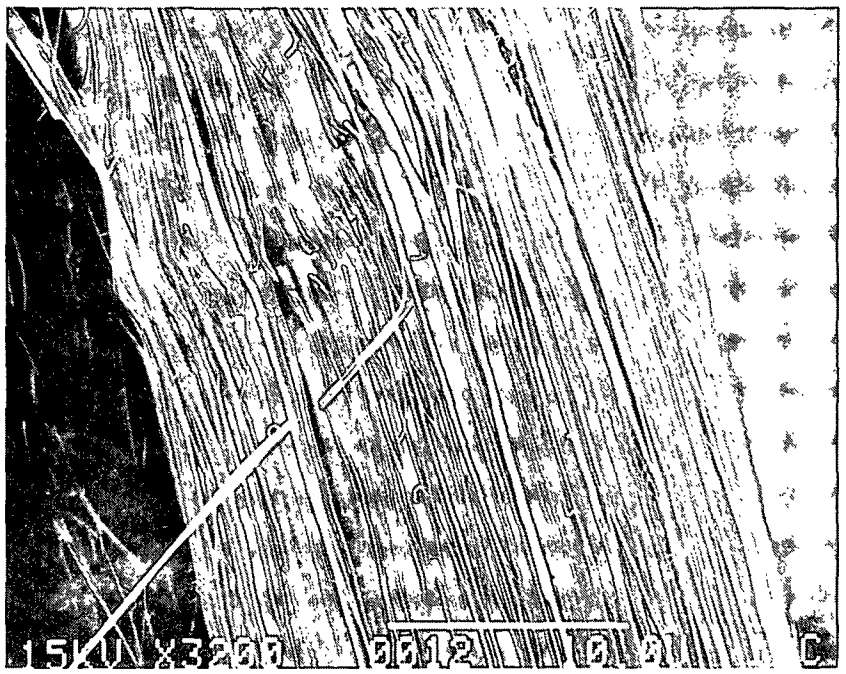

b) longitudinal section

Figure 10. Scanning electron micrographs of ramie fiber.

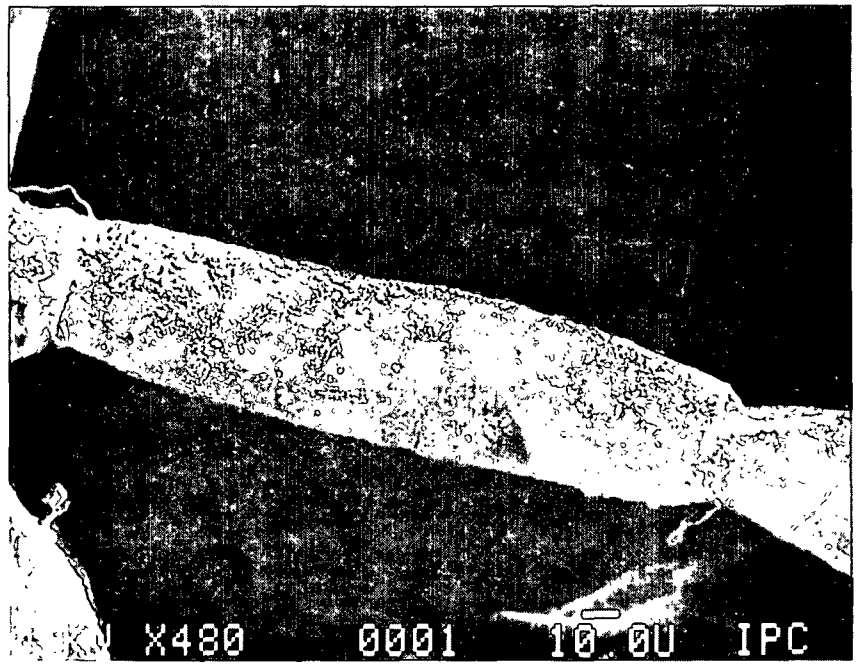

a) from H_2O

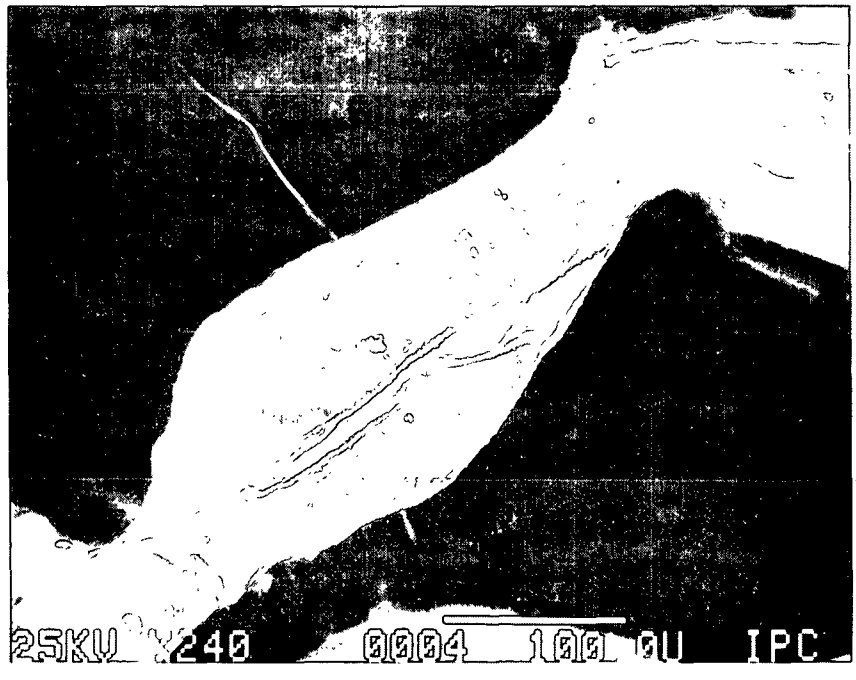

b) from D_2O

Figure 11. Scanning electron micrographs of Cladophora glomerata.

RAMAN SPECTRA

Figure 12 shows a conventional Raman spectrum from a pellet of Valonia macrophysa. The band frequencies observed in this spectrum are compared with the frequencies in the Raman spectrum of Valonia ventricosa reported by Blackwell et al.[28] in Table 2.

Polarized Raman microprobe spectra of a Valonia fibrillar aggregate and a ramie fiber in which the angle between the electric vector and the fiber axis was varied from 0 to 90° in 15° increments are shown in Fig. 13 and 14, respectively. Figure 15 compares polarized and depolarized spectra of a Valonia fibrillar aggregate recorded with the incident electric vector parallel and perpendicular to the fiber axis. In Table 3, the ratios of the depolarized intensities with the incident electric vector parallel and perpendicular to the fiber axis are given.

Figure 16 is a conventional Raman spectrum of acid hydrolyzed deuterated bacterial cellulose. Polarized Raman microprobe spectra of a Cladophora glomerata fiber grown in D_2O are shown in Fig. 17. These spectra were recorded with the electric vector of the incident light both parallel and perpendicular to the fiber axis.

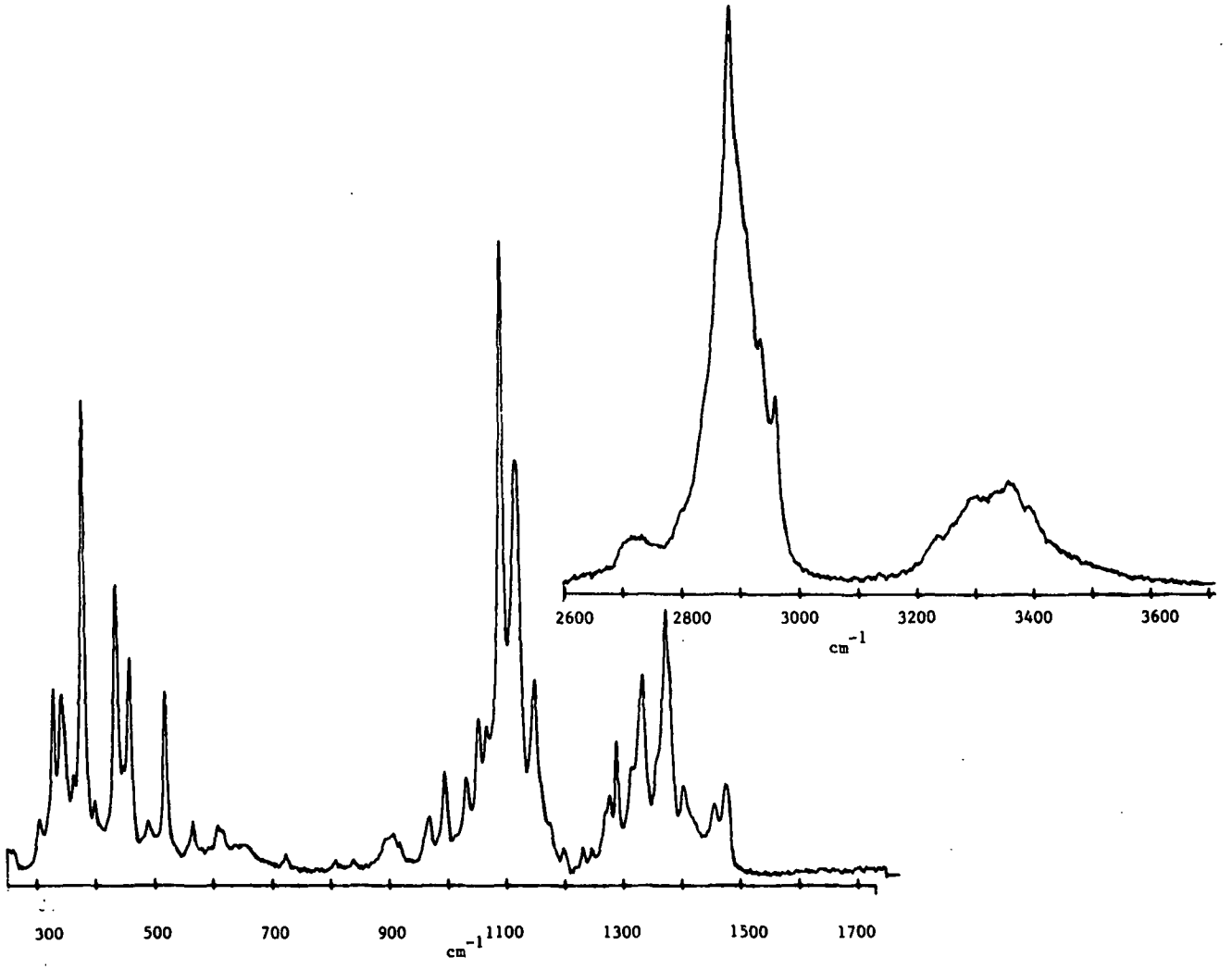

Figure 12. Conventional Raman spectrum of a Valonia macrophysa pellet. (Slit width = 100 microns, acquisition time = 28 hours.)

Table 2. Observed band frequencies in the conventional Raman spectrum of *Valonia macrophysa*.

Frequencies from Present Study (cm^{-1})	Frequencies from Blackwell *et al.*[28] (cm^{-1})	Frequencies from Present Study (cm^{-1})	Frequencies from Blackwell *et al.*[28] (cm^{-1})
261 sh[a]	277 vw	1176 sh	1174 w
306 w	303 w	1201 w	1204 vw
331 m	330 m	1234 w	1234 vw
345 m	346 w	1239 w	1249 vw
364 sh	366 vw	1272 sh	
380 st	378 st	1279 m	1277 w
400 w	394 vw	1292 m	1293 m
436 st	438 st	1318 sh	1319 vw
449 sh		1337 m	1337 st
459 m	462 st	1359 sh	1359 vw
489 w		1376 st	1377 st
495 sh		1383 sh	
519 m	524 m	1405 m	1407 m
556 sh		1420 sh	
566 w	568 w	1425 sh	1432 vw
609 w	611 w	1457 m	1454 w
618 sh		1477 m	1479 m
639 vw	639 w	2723 w	
657 vw		2804 sh	
724 vw	726 vw	2842 sh	2850 w
809 vw		2864 sh	2867 w
840 vw		2885 vs	2889 m
895 sh		2902 sh	2907 m
908 w	910 w	2915 sh	2920 w
920 sh		2940 m	2932 m
963 sh		2964 m	2972 w
971 w	971 w	3238 w	3235 w
997 m	997 m		3277 m
1015 sh			3295 m
1034 m	1035 w	3302 m	3307 m
1056 m	1057 w	3339 m	3339 m
1070 m	1071 w	3360 m	3354 m
1095 vs	1090 vs		3369 m
1120 st	1122 vs		3374 w
1152 m	1152 m	3395 m	3398 w

[a] vw = very weak, w = weak, m = medium, st = strong, vs = very strong, sh = shoulder.

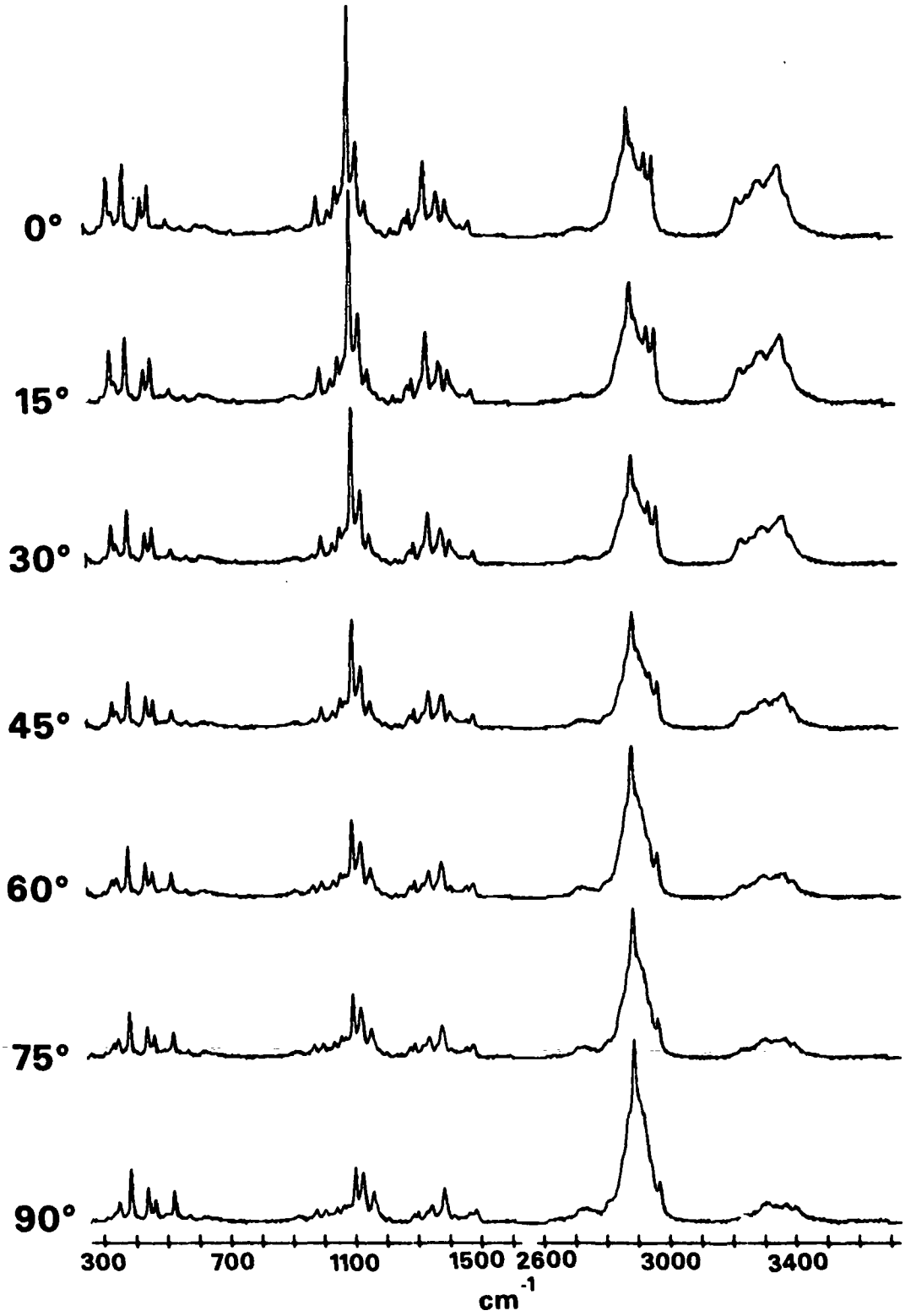

Figure 13. Polarized Raman spectra of a Valonia fibrillar aggregate. θ was varied from 0 to 90°.

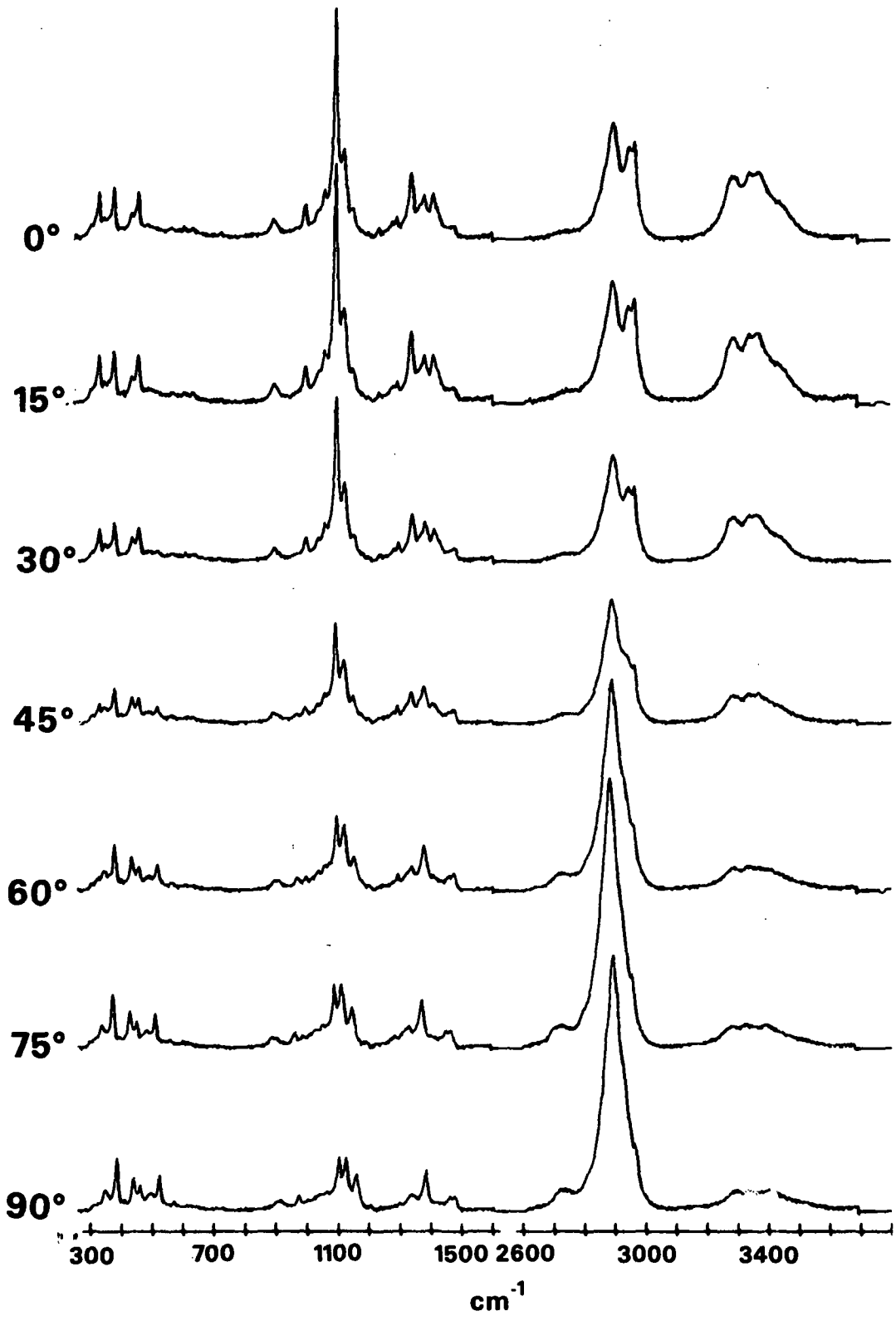

Figure 14. Polarized Raman spectra of a ramie fiber. θ was varied from 0 to 90°.

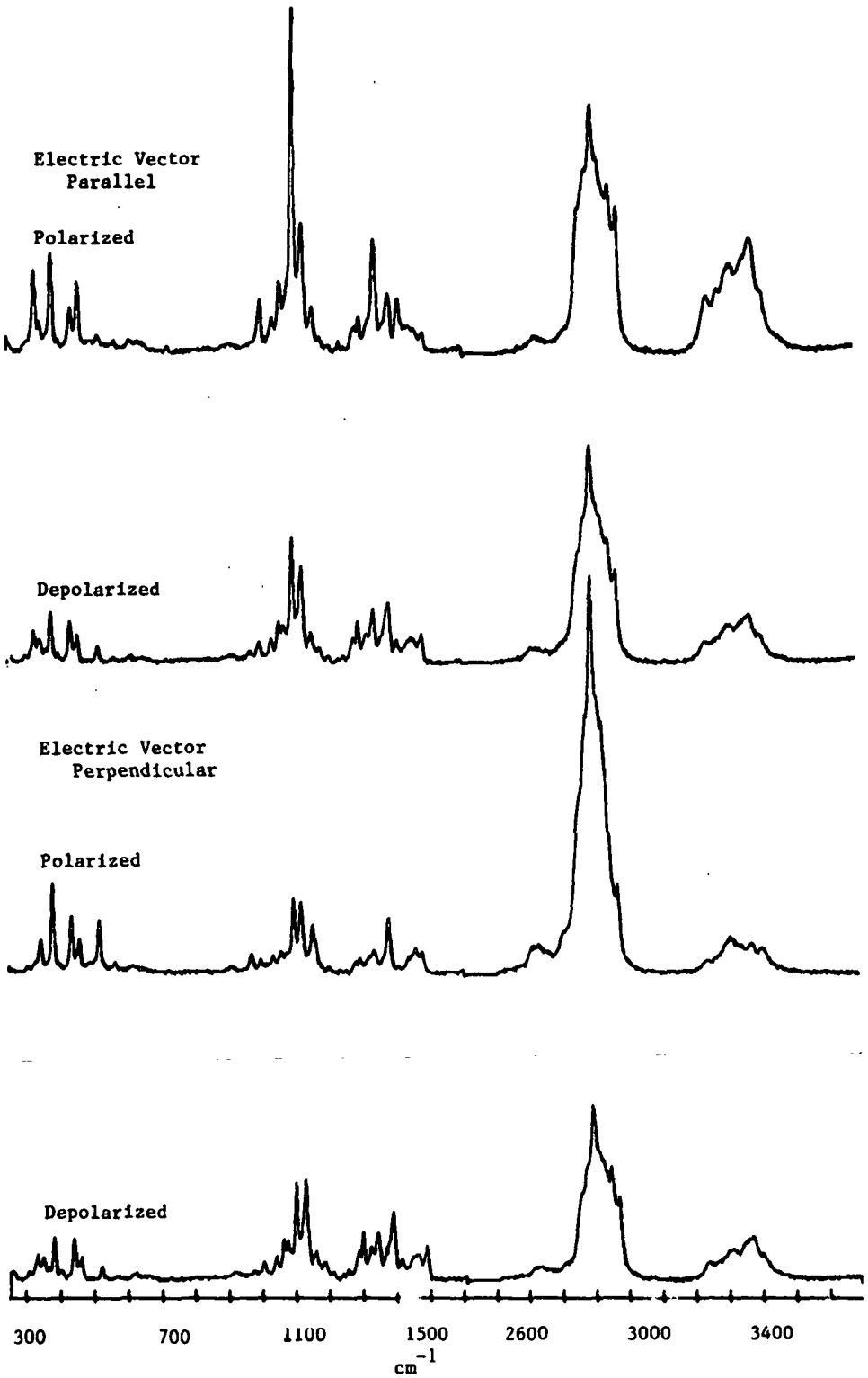

Figure 15. Comparison of polarized and depolarized spectra of a Valonia fibrillar aggregate.

Table 3. Ratios of depolarized intensities with the incident electric vector parallel and perpendicular to the fiber axis.

Frequency (cm^{-1})	Ratio of Depolarized Intensity	Frequency (cm^{-1})	Ratio of Depolarized Intensity
331	1.26	1477	0.91
344	1.03	1481	0.85
381	1.17	2848	1.30
437	1.00	2868	1.29
459	1.28	2885	1.25
520	1.22	2904	1.25
913	1.00	2941	1.10
968	1.14	2965	1.12
997	1.21	3231	1.16
1034	1.03	3239	1.16
1057	1.00	3266	1.18
1071	0.95	3291	1.20
1095	1.28	3299	1.28
1118	1.01	3302	1.20
1123	0.96	3307	1.27
1152	1.07	3334	1.16
1279	0.84	3345	1.08
1292	0.87	3356	1.09
1334	1.08	3361	1.16
1337	1.13	3366	1.13
1378	0.89	3390	1.17
1406	1.09	3395	1.12
1455	0.96		

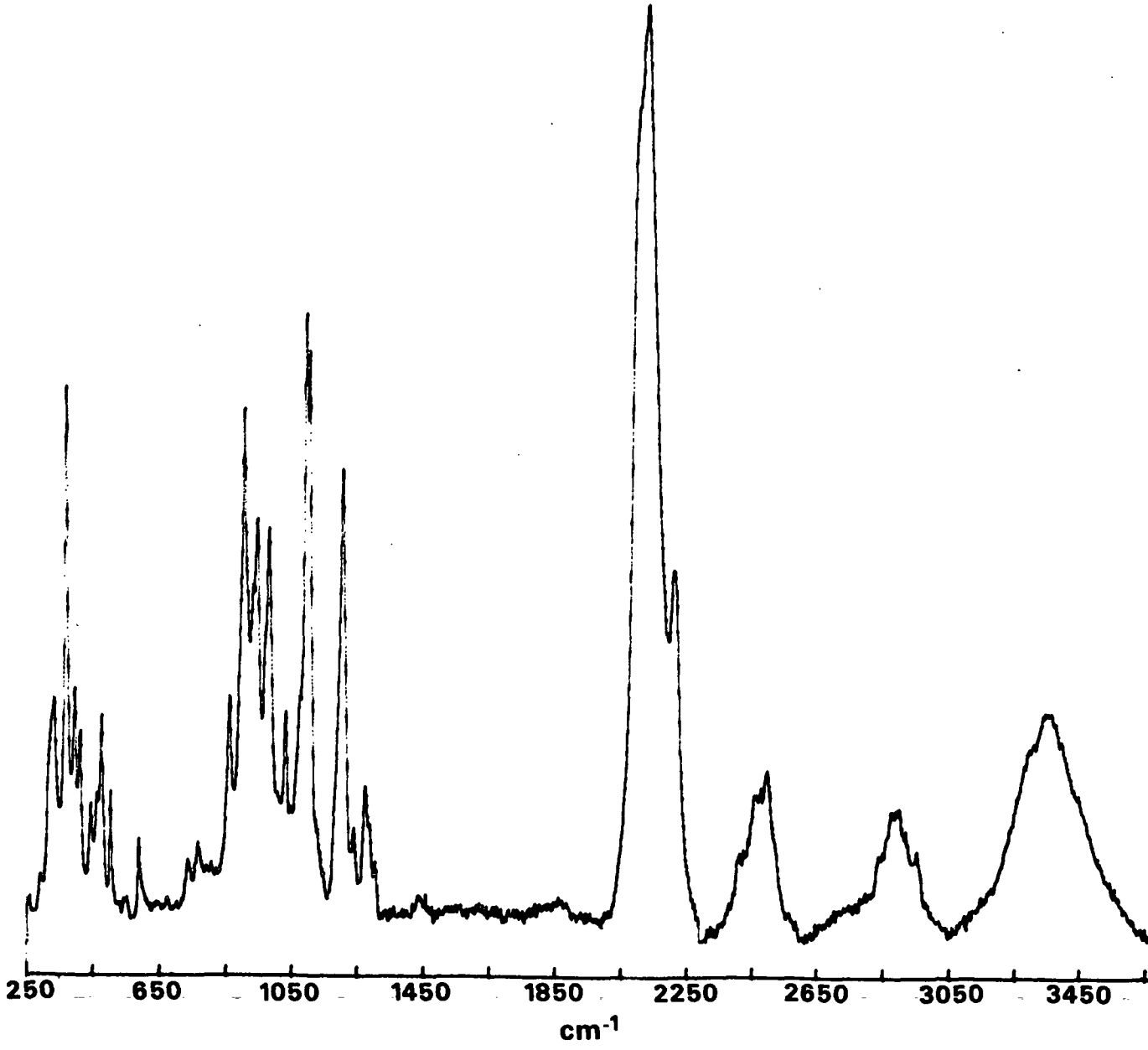

Figure 16. Conventional Raman spectrum of acid hydrolyzed deuterated bacterial cellulose. (Slits = 300 microns; acquisition time = 20 hours.)

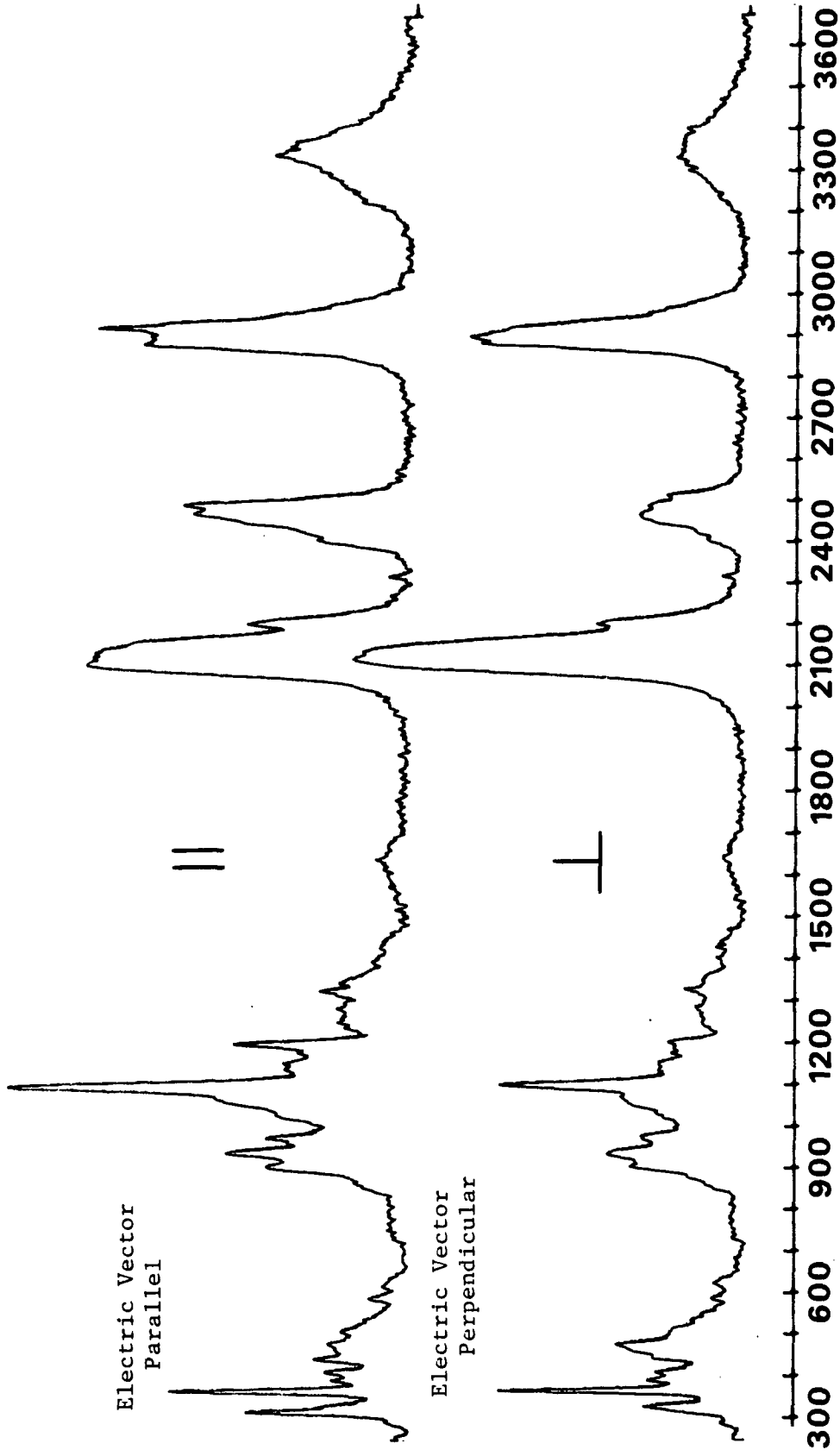

Figure 17. Polarized Raman spectra of a deuterated Cladophora fiber.

COMPUTATIONS

REGRESSION ANALYSIS

The intensity data from the spectra in Fig. 13 and 14 were analyzed by a multiple linear regression technique. The BMDP5R-polynomial regression program* was used to fit Eq. (9) to the observed data by fitting the parameters B, C-2B, and B-C+A. The parameter estimates, the 90% confidence intervals for the parameter estimates, and the multiple correlation coefficients (R^2 values) are summarized in Appendix III. Not all of the observed bands were analyzed because some bands were too weak or poorly resolved to obtain reliable intensity measurements.

In order to remove intensity variations due to fluorescence decay, it was necessary to subtract the background fluorescence from the raw spectra. The fluorescence curve was approximated by a superposition of 5 straight lines having different slopes. The straight lines were subtracted from the original spectra using the TN-1500 computer. The superposition of straight lines provided an adequate approximation of the small fluorescence background in the spectra. After the fluorescence had been subtracted, the baseline shapes of all the Valonia and ramie spectra were the same.

Almost every band in the spectra shown in Fig. 13 and 14 is sensitive to the polarization of the incident light to some extent. It was impossible to find a peak which was insensitive to polarization that could be used as an internal standard. Therefore, it was necessary to analyze the intensities without normalizing the spectra. Due to the precautions taken to minimize extraneous

*BMDP Statistical Software, Inc., 1964 Westwood Blvd. Suite 202, Los Angeles, California, 90025. Program version: April, 1985.

intensity variations, the lack of a suitable internal standard was not serious. The laser power was monitored and was found to drift less than plus or minus 3% in 8 hours. Furthermore, the spectra recorded with different polarizations of the incident light were run in a random order to minimize any time dependence in the intensities.

In the derivation of Eq. (9), it was assumed that true intensities were being measured. Band intensities are found by taking the area under the peaks. Since many of the bands in Fig. 13 and 14 overlap, area measurements were difficult. Therefore, peak heights instead of true intensities were used in the analysis. Peak heights are proportional to true intensities.

PLOTS

The peak heights predicted by the fitted equations and the experimentally determined peak heights were plotted against the angle between the incident electric vector and the fiber axis. The plots were used to assess the quality of the least squares fits and to classify the polarization sensitivity of the bands. Representative plots are given in Fig. 18. The rest of the plots are included in Appendix III.

INTENSITY MAXIMA AND MINIMA

The angles between the electric vector of the incident light and the fiber axis which corresponded to intensity maxima and minima were located by determining the angles where the first derivative of Eq. (9) is equal to zero. Equations (11)-(13) give the values of θ where the first derivative is equal to zero. The maxima were distinguished from the minima by substituting the values of C-2B and B-C+A into the expressions for the second derivative given in Eq.

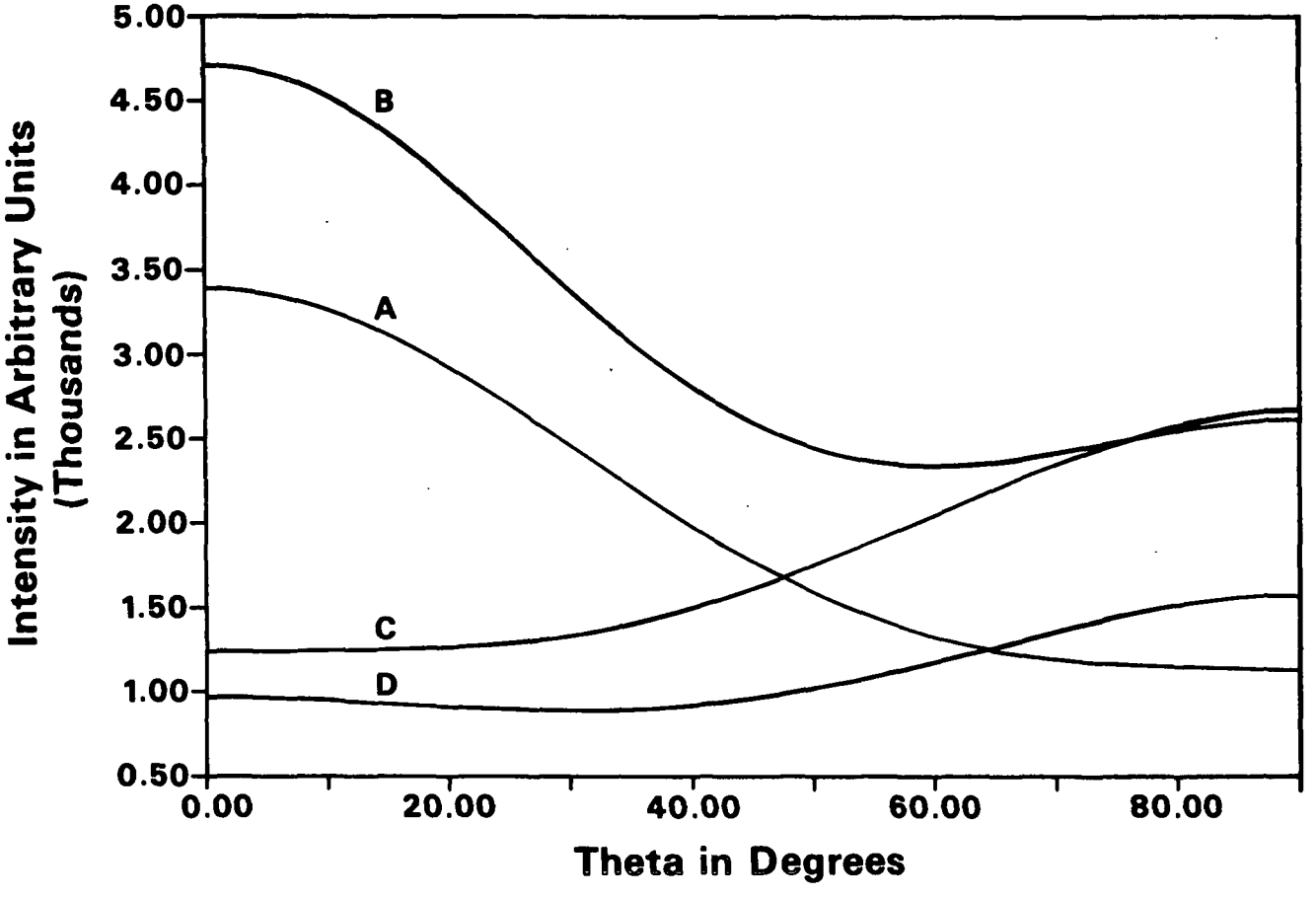

Figure 18. Plots of intensity vs. theta for four different classes of bands. A) A_0 mode, B) B_0 mode, C) A_{90} mode, D) B_{90} mode.

(15)-(17). The θ_m values are maxima when the second derivative is negative and minima when the second derivative is positive. The intensity maxima and minima from the spectra of the ramie fiber and the Valonia fibrillar aggregate are summarized in Table 4.

Since the locations of the maxima and minima depend upon the relative values of C-2B and B-C+A, the error in the maxima and minima will be proportional to the errors in C-2B and B-C+A. Error estimate for the maxima and minima were calculated by substituting 90% confidence intervals for C-2B and B-C+A into Eq. (13) and (15)-(17). The error limits obtained in this manner are also summarized in Table 4.

Table 4. Intensity maxima and minima determined from the spectra of the Valonia fibrillar aggregate and the ramie fiber.

Valonia			Ramie		
Frequency (cm^{-1})	Maximum (deg)	Minimum (deg)	Frequency (cm^{-1})	Maximum (deg)	Minimum (deg)
- limit	0	90	- limit	0	90
331	0	90	331	0	90
+ limit	0	90	+ limit	90[a]	34
- limit	0[a]	70	- limit	0[a]	72
344	0[a]	51	344	90[a]	38
+ limit	90	0	+ limit	90	0
			- limit	0[a]	74
			349	--[b]	45
			+ limit	90	0
- limit	0[a]	74	- limit	0[a]	63
381	0[a]	55	380	90[a]	43
+ limit	90	0	+ limit	90	0
- limit	0	90[d]	- limit	0[a]	78
437	0[a]	46	437	90[a]	17
+ limit	90	0	+ limit	90	0
- limit	0	90	- limit	0[a]	81
459	0[a]	77	458	0[a]	60
+ limit	0[a]	59	+ limit	90[a]	26

Table 4 (Contd.). Intensity maxima and minima determined from the spectra of the Valonia fibrillar aggregate and the ramie fiber.

Valonia			Ramie		
Frequency (cm^{-1})	Maximum (deg)	Minimum (deg)	Frequency (cm^{-1})	Maximum (deg)	Minimum (deg)
	- limit 90[a]	29		- limit 90[a]	19
520	90	0	519	90	0
	+ limit 90	0		+ limit 90	0
				- limit 0[a]	90
			894	0[a]	68
				+ limit 90[a]	43
				- limit 0	90
			900	0[a]	58
				+ limit 90	0
	- limit 0[a]	79		- limit 0	90
913	0[a]	49	910	0[a]	47
	+ limit 90	0		+ limit 90	0
	- limit 0[a]	72		- limit 90[a]	35
968	90[a]	19	969	90[a]	30
	+ limit 90	0		+ limit 90	0
	- limit 0	90		- limit 0	90
997	0	90	995	0[a]	77
	+ limit 0	90		+ limit 90[a]	20
	- limit 0	90		- limit 0	90
1034	0	90	1037	0	90
	+ limit 90	0		+ limit 90	0
	- limit 0	90		- limit 0	90
1057	0	90	1057	0	90
	+ limit 0	90		+ limit 90	0
	- limit 0	90			
1071	0	90			
	+ limit 0[a]	56			
	- limit 0	90		- limit 0	90
1095	0	90	1095	0	90
	+ limit 0	90		+ limit 90[a]	36
	- limit 0	90		- limit 0	90
1118	0[a]	61	1117	0[a]	73
	+ limit 0	90		+ limit 0	90

Table 4 (Contd.). Intensity maxima and minima determined from the spectra of the *Valonia* fibrillar aggregate and the ramie fiber.

Valonia			Ramie		
Frequency (cm^{-1})	Maximum (deg)	Minimum (deg)	Frequency (cm^{-1})	Maximum (deg)	Minimum (deg)
	- limit 0	90		- limit 0	90
1123	0	90	1121	0	90
	+ limit 0	90		+ limit 90	0
	- limit 0[a]	73		- limit 0[a]	74
1152	0[a]	50	1151	90[a]	36
	+ limit 90	0		+ limit 90	0
	- limit 0	90		- limit 0	90
1279	0	90	1275	0	90
	+ limit 0[d]	90		+ limit 0[d]	90
	- limit 0	90		- limit 0	90
1292	0	90	1291	18	90[c]
	+ limit 0[d]	90		+ limit 60	0[c]
	- limit 0	90		- limit 0	90
1334	0	90	1331	0[a]	81
	+ limit 0	90		+ limit 90	0
	- limit 0	90		- limit 0	90
1337	0	90	1337	0	90
	+ limit 0	90		+ limit 90	0
	- limit 0[a]	84		- limit 0	90
1378	0[a]	56	1378	90[a]	44
	+ limit 90	0		+ limit 90[d]	0
	- limit 0	90		- limit 0	90
1406	0	90	1407	0	90
	+ limit 0	90		+ limit 90	0
	- limit 0	90		- limit 0	90
1455	90[a]	37	1456	90[a]	34
	+ limit 90[d]	0		+ limit 90[d]	0
				- limit 0	90
			1460	90	0
				+ limit 90[d]	0
	- limit 0	90		- limit 0	90
1477	90	0	1475	90	0
	+ limit 90[d]	0		+ limit 90[d]	0

Table 4 (Contd.). Intensity maxima and minima determined from the spectra of the Valonia fibrillar aggregate and the ramie fiber.

Valonia				Ramie			
Frequency (cm^{-1})		Maximum (deg)	Minimum (deg)	Frequency (cm^{-1})		Maximum (deg)	Minimum (deg)
	- limit	0	90				
1481		27	90[c]				
	+ limit	90	0				
	- limit	0[a]	71				
2848		90[a]	32				
	+ limit	90	0				
	- limit	0[a]	64		- limit	90[a]	32
2868		90[a]	35	2866		90[a]	22
	+ limit	90	0		+ limit	90	0
	- limit	0[a]	63		- limit	90[a]	33
2885		90[a]	34	2889		90[a]	24
	+ limit	90	0		+ limit	90	0
	- limit	0[a]	64				
2904		90[a]	36				
	+ limit	90	0				
	- limit	0[a]	77		- limit	0[a]	69
2941		0[a]	57	2943		90[a]	43
	+ limit	90[a]	18		+ limit	90	0
	- limit	0	90		- limit	0	90
2965		0[a]	64	2963		0[a]	54
	+ limit	90	0		+ limit	90	0
	- limit	0	90				
3231		0[a]	67				
	+ limit	90	0				
	- limit	0	90				
3239		0	90				
	+ limit	0[a]	75				
	- limit	0	90				
3266		0	90				
	+ limit	0[a]	64				
	- limit	0	90		- limit	0	90
3291		0[a]	82	3286		0[a]	74
	+ limit	0[a]	75		+ limit	90[a]	23

Table 4 (Contd.). Intensity maxima and minima determined from the spectra of the *Valonia* fibrillar aggregate and the ramie fiber.

Valonia			Ramie		
Frequency (cm^{-1})	Maximum (deg)	Minimum (deg)	Frequency (cm^{-1})	Maximum (deg)	Minimum (deg)
- limit	0	90			
3299	0[a]	75			
+ limit	0[a]	67			
- limit	0	90			
3302	0[a]	74			
+ limit	0[a]	57			
- limit	0	90			
3307	0[a]	76			
+ limit	0[a]	60			
- limit	0	90	- limit	0	90
3334	0	90	3335	0[a]	71
+ limit	0[a]	71	+ limit	90[a]	27
- limit	0	90			
3345	0	90			
+ limit	90	0			
- limit	0	90			
3356	0	90			
+ limit	0	90			
- limit	0	90	- limit	0	90
3361	0	90	3363	0[a]	77
+ limit	0	90	+ limit	90[a]	33
- limit	0	90			
3366	0	90			
+ limit	0	90			
- limit	0	90			
3390	0	90			
+ limit	0[a]	65			
- limit	0	90	- limit	0	90
3395	0[a]	78	3402	0[a]	61
+ limit	0[a]	67	+ limit	90	0
			- limit	0	90
			3429	0[a]	62
			+ limit	90[a]	28

[a]Curve has two maxima; the number given is the location of the highest maximum.
[b]Curve has two maxima; the maxima are equal in height.
[c]Curve has two minima; the number given is the location of the lowest minimum.
[d]For at least one of the 90% confidence extremes a maximum occurred between 0 and 90°.

DISCUSSION

SAMPLE CHARACTERIZATION

Valonia macrophysa

The carbohydrate analysis of purified Valonia macrophysa (see Table 1) showed that the cellulose is predominantly glucan (93%). Araban, xylan, mannan, and galactan together comprise about 3% of the cellulose. In principle, pure cellulose should be 100% glucan. There is, however, approximately a 2-3% error associated with the carbohydrate analysis method. Therefore, the level of impurities in the Valonia cellulose is quite small.

Figure 5 shows that the x-ray diagram of Valonia macrophysa cellulose is consistent with x-ray diagrams of native Valonia cellulose reported in the literature,[37-40] and with other patterns of Valonia recorded in our own laboratory. The d-spacings calculated for the 101, $1\bar{0}1$, and 002 planes were 6.11, 5.30, and 3.91 Å, respectively. These are reasonable values for native cellulose. The diffraction peaks are quite narrow, suggesting that there is a high degree of lateral order in the Valonia cellulose crystallites. The larger intensity of the 101 peak relative to the $1\bar{0}1$ peak (see Fig. 5) indicates a slight preferential orientation of the 101 planes parallel to the surface of the cellulose. This orienting tendency has been reported in the literature for Valonia as well as other algal celluloses.[1,2,38]

The Raman spectrum of a pellet of Valonia macrophysa (see Fig. 12) cellulose is very similar to the spectrum of Valonia ventricosa reported by Blackwell et al.[28] Our tabulated frequencies (see Table 2) match their frequencies quite well in the region below 1500 cm^{-1}. In the CH and OH stretching regions (2800-

3600 cm^{-1}), their frequencies differ somewhat from ours. The discrepancies are probably due to the large extent of band overlap.

The scanning electron micrograph of a fibrillar aggregate extracted from the purified Valonia cell wall (see Fig. 9) shows that the fibrils are oriented parallel to the axis of the aggregate. The fibrils in the aggregate are less than 5 μm in diameter, and the aggregate itself is approximately 30 μm in diameter. Although the fibrillar aggregate in the micrograph is not the same one used to record Raman spectra, it is representative of the aggregates extracted from the Valonia cell wall.

Ramie

The carbohydrate analysis of purified ramie fibers (see Table 1) showed that the ramie cellulose contains almost pure glucan (101%). The araban, xylan, and mannan added up to about 1.5%. No galactan was detected in the sample. The analysis indicated that the isolated ramie cellulose was somewhat purer than the Valonia cellulose.

The x-ray diagram of purified ramie cellulose (see Fig. 6) is consistent with x-ray diagrams of native cellulose in the literature.[37-40] The d-spacings for the 101, $10\bar{1}$, and 002 planes are 6.05, 5.36, and 3.95 Å, respectively. These values are within the experimental error of the d-spacings reported in the literature for cellulose I. The d-spacings differ slightly from Valonia d-spacings, but the size of these differences is not greater than the normal spread of d-spacing values among native celluloses. The peaks in the ramie diagram are much broader than the peaks in the Valonia diagram, suggesting that the lateral dimensions of the ramie crystallites are smaller. Other studies have also found that ramie crystallites are much smaller than Valonia

crystallites.[1,41-42] The relative peak heights of the 101 and $10\bar{1}$ planes show that ramie crystallites do not exhibit a tendency to orient with the 101 plane parallel to the pellet surface.

Atalla and coworkers[43] reported polarized Raman spectra of a ramie fiber recorded with the electric vector of the incident light parallel and perpendicular to the fiber axis using a conventional Raman spectrometer. Although the spectra in Fig. 15 were recorded with the microprobe, the spectra recorded with electric vector parallel and perpendicular to the fiber axis are very similar to the spectra reported by Atalla et al.

In the literature, it has been reported by several workers that ramie has a fibril angle of approximately 5°.[1,2] Therefore, the cellulose chains are almost parallel to the fiber axis. The scanning electron micrographs of the ramie cell wall in Fig. 10a and b are consistent with these reports. The SEM's show that the cell wall consists of fibrils less than 1 micron in diameter which lie parallel to each other and parallel to the fiber axis.

Deuterated Celluloses

The x-ray diagram of deuterated bacterial cellulose and deuterated Cladophora cellulose (see Fig. 7 and 8) exhibit normal native cellulose patterns.[37-40] The d-spacings were d_{101} = 6.12, $d_{10\bar{1}}$ = 5.33, and d_{002} = 3.94 Å for deuterated bacterial cellulose and d_{101} = 6.19, $d_{10\bar{1}}$ = 5.35, and d_{002} = 3.95 Å for deuterated Cladophora cellulose. The difference between these d-spacings and the d-spacings for nondeuterated bacterial and Cladophora celluloses is quite small. In the deuterated cellulose diagrams, the diffraction peaks are slightly broader, indicating that the lateral dimensions of the crystallites are somewhat smaller in the deuterated celluloses than in the nondeuterated celluloses.

Although the effects of deuteration on the x-ray patterns of the cellulose are small, scanning electron micrographs of Cladophora filaments harvested from H_2O and from D_2O (see Fig. 11a-b) show that deuteration has a noticeable effect on cell morphology. The nondeuterated cells are more compact and appear to have more material attached to their surfaces, whereas the deuterated cells are more voluminous and the cell wall appears disrupted and less ordered. It is interesting that deuteration can have what seems to be a very small effect on the cellulose structure but still have such a noticeable effect on the morphology of the cells. Perhaps deuteration mainly disrupts the structure of the materials that hold the cellulose microfibrils together without much affecting the structure of the microfibrils themselves.

In summary, the samples of purified Valonia macrophysa and ramie appear to contain small levels of impurities. The impurities were not detected, however, in either the x-ray diagrams or in the Raman spectra. Therefore, these celluloses are pure enough for the purposes of this thesis. The x-ray patterns further indicate that the ramie and Valonia contain the cellulose I lattice. Electron microscopy showed that the cellulose microfibrils in both Valonia fibrillar aggregates and ramie fibers are preferentially oriented parallel to the fiber axis. The x-ray patterns of deuterated Cladophora and bacterial celluloses indicate the normal cellulose I lattice. Electron micrographs suggested, however, that deuteration has a significant effect on the morphology of Cladophora cells. Since it is mainly important in the assignment work that the cellulose I lattice remain intact, the effects of deuteration on morphology should not preclude the use of the deuterated materials.

INTENSITY MAXIMA AND MINIMA

Evaluation of the Model

The spectra of the Valonia fibrillar aggregates and ramie fibers in Fig. 13 and 14 clearly demonstrate the strong dependence of the band intensities on the angle between the incident electric vector and the chain axis. All of the bands appear to exhibit some sensitivity to the polarization of the incident light.

The R^2 values and plots of intensity vs. θ (see Appendix III) show that Eq. (9) adequately accounts for the observed intensity variation. The average R^2 values for the Valonia and ramie data are 0.91 and 0.87, respectively. Those bands with lower R^2 values are usually either weakly sensitive to θ or are poorly resolved. When the sensitivity of the intensities to θ is small, extraneous sources of intensity variation cause scatter in the data. In the case of poorly resolved bands, the intensities are scattered due to low accuracy in the intensity measurements.

For some bands, the parameters C-2B and B-C+A were insignificant at the 90% level (see Appendix III). This is presumably due to either scatter in the intensity data or low sensitivity of the intensities to the polarization of the incident light. For other bands, just one of the parameters C-2B or B-C+A is significant. In these cases, the significant parameter is usually much larger than the insignificant one. Since the $\cos^2\theta$ and $\cos^4\theta$ terms are not independent, the errors in C-2B and B-C+A are correlated. When one of the parameters is much larger than the other, the magnitude of the error is determined by the larger parameter, thereby overestimating the error in the smaller parameter. Thus the smaller parameter is insignificant unless the error in the larger parameter is very small. For all the bands, the precision is reduced by the small number of

degrees of freedom available to estimate the error. This problem could be reduced by collecting more data points on the intensity vs. θ curves.

The lack of precision in the estimates of C-2B and B-C+A carries over into the calculation of the intensity maxima and minima. Table 4 shows that the error windows for the maxima and minima are as large as 90° in some cases.

Another estimate of the uncertainty in the maxima and minima can be obtained by comparing the Valonia and ramie data. Below 3000 cm^{-1} the ramie and Valonia band frequencies match quite closely. Hence, it is likely that the same vibrations occur in this region of the spectra in both celluloses. Above 3000 cm^{-1}, the Valonia band frequencies differ significantly from the ramie band frequencies, suggesting different vibrational modes and/or structures. The structural implications of the differences and similarities between the Valonia and ramie spectra will be discussed in the next chapter. Since the modes below 3000 cm^{-1} are most likely the same, the maxima and minima calculated from the Valonia and ramie data can be compared in this region.

For the 331, 459, 520, 913, 968, 1034, 1057, 1095, 1118, 1123, 1279, 1337, 1406, 1455, 1477, 2868, 2885, and 2965 cm^{-1} modes the Valonia and ramie data are in agreement regarding the number of maxima and minima and their locations. In the case of the 997 and 1334 cm^{-1} modes, both the Valonia and ramie data indicate that the bands are most intense when the electric vector is parallel to the chain axis, but the ramie data exhibit multiple maxima whereas the Valonia data show only one maximum. The Valonia data for these bands have very high R^2 values and narrow confidence intervals, whereas the ramie data are more scattered and less precise. The maxima and minima calculated from the Valonia data lie within the 90% confidence intervals calculated from the ramie data. Therefore,

the Valonia data provide a more reliable model of the dependence of the 997 and 1334 cm^{-1} modes on θ.

For the 344, 381, 437, 1152, 1378, and 2941 cm^{-1} modes, both the Valonia and ramie data indicate two maxima. The two data sets are inconsistent, however, regarding the values of θ corresponding to the largest intensities. For the 1378 cm^{-1} band, the Valonia data exhibit two maxima while the ramie data have two minima. Both the Valonia and ramie confidence intervals are broad for these bands. Therefore, it is difficult to determine which data set more accurately represents the locations of the maxima and minima.

The 349, 894, 900, and 1460 cm^{-1} bands observed in the ramie spectra were not resolved in the Valonia spectra. The 1071, 1481, 2848, and 2904 cm^{-1} bands observed in the Valonia spectra were not resolved in the ramie spectra. For these bands, only the 90% confidence limit can be used to assess the reproducibility of the maxima and minima.

One of the assumptions made in the derivation of Eq. (9) was that the derived polarizability tensor relative to the molecule base coordinate system, $\alpha(m)$, is symmetric. If $\alpha(m)$ is symmetric and the orientation distribution in the plane perpendicular to the chain axis is also symmetric, then $\alpha(L)$ will be symmetric. Figure 15 shows depolarized spectra of a Valonia fibrillar aggregate recorded with the incident electric vector parallel and perpendicular to the fiber axis. The depolarized intensities observed with the incident electric vector parallel to the chain are proportional to α^2_{ZX} whereas the intensities are proportional to α^2_{XZ} when the incident vector is perpendicular. If $\alpha(L)$ is symmetric, then α^2_{ZX} equals α^2_{XZ}. Table 3 gives the ratios of the depolarized intensities recorded with the incident electric vector parallel and

perpendicular to the fiber axis. Since the ratios are not equal to one for many of the bands, $\alpha(L)$ is not perfectly symmetric in several cases.

The source of the asymmetry in $\alpha(L)$ could be either $\alpha(m)$ or the orientation distribution in the plane perpendicular to the chain axis. We have recorded other sets of depolarized spectra and found that the amount of asymmetry in $\alpha(L)$ varies from sample to sample. If the source of the asymmetry were in $\alpha(m)$, then the asymmetry in $\alpha(L)$ should be constant from sample to sample. Therefore, the source of asymmetry appears to be in the distribution of crystallite orientations in the plane perpendicular to the chain axis, although we cannot rule out the possibility of asymmetry in $\alpha(m)$. It may be that there are not enough crystallites to establish a truly random distribution of orientations in the small domains where the microprobe acquires spectra. This hypothesis is supported by the fact that the amount of asymmetry indicated by depolarized spectra recorded with the conventional Raman system is much less than with the microprobe system.

It appears that the assumptions made in the derivation of Eq. (9) are not fully justified. If we do not assume random crystallite orientation and symmetry in the derivation however the form of Eq. (9) remains the same, but the constants are different. Furthermore, the amount of asymmetry indicated in Table 3 is generally not very large and Eq. (9) is able to fit the observed intensities very well. Therefore, Eq. (9) provides an adequate model for the interpretation of band intensity data.

Classification of the Bands

The bands can be divided into two broad groups based on the relationship between the band intensities and, θ, the angle between the incident electric vector and fiber axis. The bands in the first group exhibit a single maximum

and minimum in the intensity vs. θ plots. Sample plots for this group are given in Fig. 18, curves a and c. This group will be designated group A. The bands in the second group exhibit maxima at both 90 and 0°, and a single minimum between 0 and 90°. This group is illustrated by curves b and d in Fig. 18. It will be referred to as group B.

Within groups A and B the bands can be further categorized by whether they are most intense when θ is 0 or 90°. The bands that are most intense when θ equals 0° will be designated by a 0 subscript. This group is illustrated by curves a and b in Fig. 18. Those bands that are most intense when θ equals 90° will be designated by a subscript, 90. These bands are exemplified by curves c and d.

In Table 5, the bands in the spectra of Valonia and ramie have been classified into the four categories. The bands for which the ramie and Valonia data suggest differing classifications are denoted by question marks. In the case of the 997 and 1334 cm^{-1} bands, the Valonia data suggest the bands belong in the A_0 category while the ramie data suggest that they fall in the B_0 category. As mentioned in the previous section, the Valonia data for these bands appear to be more reliable due to the high R^2 value and narrow confidence limits. Therefore, the 997 and 1334 cm^{-1} bands were placed in the A_0 category.

Some of the observed bands did not fit into any of the four categories. A band at 349 cm^{-1} which was resolved only in the ramie spectra fell into the B category but its maxima were equal in height so it could not be assigned to either the B_0 or B_{90} categories. A band at 1481 cm^{-1} which was resolved only in the Valonia spectra appeared to have a single maximum between 0 and 90° and minima at 0 and 90°. Based on the ramie data, the 1292 cm^{-1} mode also appears

Table 5. Classification of bands based on the Valonia and ramie fiber spectra.

Band Frequency (cm^{-1})		Intensity
Valonia	Ramie	Classification
331	331	A_0
344	344	$B_?$
	349	$B_?$
381	380	$B_?$
437	437	$B_?$
459	458	B_0
520	519	A_{90}
	894	B_0
	900	B_0
913	910	B_0
968	969	B_{90}
997	995	A_0
1034	1037	A_0
1057	1057	A_0
1071		A_0
1095	1095	A_0
1118	1117	B_0
1123	1121	A_0
1152	1151	$B_?$
1279	1275	A_0
1292	1291	?
1334	1331	A_0
1337	1337	A_0
1378	1378	$B_?$
1406	1407	A_0
1455	1456	B_{90}
	1460	A_{90}
1477	1475	A_{90}
1481		a
2848		B_{90}
2868	2866	B_{90}
2886	2889	B_{90}
2904		B_{90}
2941	2943	$B_?$
2965	2963	B_0
3231		B_0
3239		A_0
3266		A_0
3291	3286	B_0
3299		B_0
3302		B_0
3307		B_0
3334	3335	$?_0$
3345		A_0
3356		A_0
3361	3363	$?_0$
3366		A_0
3390		A_0
3395	3402	B_0
	3429	B_0

[a]Band exhibits two minima at 0 and 90° and a single maximum between 0 and 90°.

to have a maximum between 0 and 90°, but the Valonia data suggest that it is an A_0 band. Since the confidence intervals are quite broad for all of these bands, it is difficult to tell whether they truly fall outside the four classes discussed above. The bands may, however, differ from the majority of the bands and involve some different types of motion.

In spite of the uncertainties associated with the intensity data, most of the bands could be successfully classified into the A_0, B_0, A_{90}, and B_{90} categories. The classifications provide information about the relative magnitudes of the elements in the derived polarizability tensor and thereby can reveal the overall direction of the vibrational motions.

For A_0 bands, there is a single maximum at 0° and a single minimum at 90°. Therefore, the second derivative of Eq. (9) must be negative at 0° and positive at 90°. When these conditions are substituted into Eq. (15) and (16), we find that C must be less than 2A and greater than 2B. These conditions further imply that A is greater than B. Since B is less than A, α_{zz} must be the predominant diagonal component of the derived polarizability tensor in the molecule associated with the vibrational coordinate. Therefore, the largest change in the polarizability is parallel to the chain axis.

Conversely, the A_{90} bands have a single maximum at 90° and a single minimum at 0°. In this case Eq. (15) and (16) dictate that C is greater than 2A and less than 2B, and that B is greater than A. If α_{xx}, α_{yy}, or α_{xy} are large in magnitude compared to the other tensor components, B will be larger than A or C. The magnitude of these components would be large only when the largest change in polarizability associated with the vibrational coordinate is perpendicular to the chain axis.

The B group of bands is the most difficult to interpret because there are different ways for multiple maxima to come about. In this case, Eq. (15) and (16) indicate that both A and B are large relative to C. This can occur only when α_{zz} and either α_{xx}, α_{yy}, or α_{xy} are nonzero. Furthermore, either one or two of the diagonal components must be negative or α_{zz} and α_{xy} must be very large relative to α_{xx}, α_{yy}, α_{yz}, and α_{xz}.

Another way in which a band could have two maxima is if the band was due to two or more degenerate modes. Two vibrational modes are degenerate when they occur at the same frequency. If one of the degenerate modes was an A_0 type motion and the other an A_{90} type motion, the resultant band might exhibit more than one intensity maximum. Normal coordinate calculations done on cellobiose and cellotetraose[18] showed that many of the bands are very closely spaced. Therefore, it is plausible that there could be accidentally degenerate modes in the spectrum of cellulose. In support of this hypothesis is the observation that some of the bands in the Valonia and ramie spectra shifted position slightly as the polarization of the incident light was changed.

Regardless of whether the B bands result from degenerate modes or negative tensor components, the intensity maxima reveal the direction in which the major change in polarizability occurs. For B_0 bands, the change in polarizability associated with the vibration must be parallel to the chain axis, while in the case of B_{90} bands the change in polarizability must be perpendicular to the chain axis.

In summary the study of the relationships between the band intensities and θ has allowed the bands to be classified into four groups. The band classifications yield information about the directional nature of the vibrations. In

addition, the intensity study has provided a more thorough characterization of the bands than has been possible in previous studies. This information will be useful in future microprobe studies of native tissues.

SPECTRA OF DEUTERATED CELLULOSES

The extent of deuteration was estimated by comparing the intensities of the OH* (3200-3500 cm^{-1}), OD (2400-2600 cm^{-1}), CH (2800-3000 cm^{-1}), and CD (2000-2300 cm^{-1}) stretching bands. The ratio of the OD and OH stretching intensities was used to measure the extent of hydroxyl deuteration and the ratio of the CD and CH stretching intensities the extent of carbon deuteration. It was necessary to correct the ratios for the different scattering activities of CD stretching relative to CH stretching and OD stretching relative to OH stretching. A CD/CH correction factor was obtained by comparing the CD and CH stretching intensities in the spectrum of an equimolar mixture of deuterated and normal chloroform. The correction factor was 0.86, which shows that CH stretching is inherently more intense than CD stretching. The OD/OH stretching correction factor was obtained from the spectrum of an equimolar mixture of normal and heavy water. In this case, OD stretching is more intense than OH stretching, as indicated by the correction factor of 1.2.

In the spectrum of deuterated bacterial cellulose (see Fig. 16), the corrected CD/CH ratio is 6.27 and the corrected OD/OH ratio is 0.307. These ratios indicate that there are 6.27 deuteriums for every hydrogen attached to the carbon atoms and 0.307 OD groups for every OH group. The much lower degree of deuterium substitution at the hydroxyl groups may be due to deuterium-hydrogen

*O = oxygen, H = hydrogen, D = deuterium, C = carbon.

exchange reactions during the purification procedures. Hydroxyl protons are labile enough to undergo exchange in protonated solvents, whereas much more drastic conditions must be employed to cause exchange of the hydrogens attached to carbon.

The spectra of the Cladophora fiber (see Fig. 17) show that the Cladophora is less deuterated at the carbon atoms but more deuterated at the hydroxyl groups than the bacterial cellulose. The corrected CD/CH ratio is 1.59 in the spectrum recorded with the incident electric vector parallel to the fiber axis and 2.06 in the spectrum recorded with incident electric vector perpendicular to the fiber axis. The OD/OH ratios are 0.79 and 0.68 depending on whether the incident electric vector is parallel or perpendicular to the fiber axis, respectively.

The discrepancies between the extents of deuteration measured in the Cladophora spectra with the incident electric vector parallel and perpendicular to the fiber could arise from errors in the measurements. Alternatively, these discrepancies might reflect preferential deuteration of some sites in the cellulose. This explanation is supported by the fact that the shapes of the CD band relative to the CH band and the OD band relative to the OH band are different. If the distribution of deuterium is random, then the shape of the CD stretching band should be the same as the CH stretching band and the OD shape should be the same as the OH shape.

In the spectrum of deuterated bacterial cellulose, the shape of the CD stretching band differs from the shape of the CD band in the deuterated Cladophora spectra and the shape of the CH band in nondeuterated cellulose. Since the

bacterial and Cladophora celluloses are deuterated to different extents, it would appear that the band shapes are dependent on the extent of deuteration. The shape of the CD band in the deuterated bacterial cellulose spectrum, however, is not the same as the normal CH band shape even though the bacterial cellulose is almost entirely carbon-deuterated. If selective deuteration is the only factor responsible for different CH and CD band shapes, the CD band shape in fully deuterated cellulose should be the same as the normal CH band shape. Therefore, there may be other factors affecting the CD and CH band shapes.

Another factor which could influence the CD and CH band shapes is Fermi resonance. Fermi resonance occurs when the overtone of one mode of a group lies close in frequency to the fundamental of another mode of the same group. The overtone, which would normally be very weak, resonates with the fundamental, thereby gaining intensity. Only the overtones of the modes between 1420 and 1500 cm^{-1} are set up for Fermi resonance with the CH modes (2840-3000 cm^{-1}), whereas the CD modes (2020-2280 cm^{-1}) could be in resonance with the modes in the 1010-1140 cm^{-1} region. Since there are more modes between 1010 and 1140 cm^{-1} in the deuterated cellulose spectrum than there are between 1420 and 1500 cm^{-1} in the nondeuterated cellulose spectrum, there are more opportunities for Fermi resonance in the CD stretching region. In the spectra in Fig. 16 and 17, the CD bands are broader than the CH bands, which is consistent with the hypothesis that more Fermi resonance occurs in the CD region than in the CH region.

Comparison of OD and OH stretching bands in the spectra of deuterated bacterial, deuterated Cladophora, and nondeuterated cellulose demonstrates that the OD stretching bands are narrower and sharper than the OH stretching bands.

There are no modes which have the proper frequency to be in Fermi resonance with the OH stretching band but there are a few modes which could resonate with the OD stretching band. Since the normal effect of Fermi resonance is to broaden bands, the OD stretching band should be broader if Fermi resonance is the cause of the different band shapes. The OD stretching band, however, is narrower than the OH band. Therefore, Fermi resonance does not offer a plausible explanation for the different band shapes.

Selective deuteration offers a likely explanation for the different shapes of the OH and OD stretching bands. Selective deuteration might occur either as a result of the biosynthetic processes or deuterium-hydrogen exchange reactions occurring during the purification. If selective deuteration resulted from the biosynthetic processes, then we would expect the shape of the OD stretching band to change as the cellulose became more deuterated. The OD band shape in the spectrum of deuterated bacterial cellulose appears the same as in the spectra of deuterated Cladophora indicating that the OD band shape does not depend strongly on the extent of deuteration. On the other hand, deuterium-hydrogen exchange reactions would occur predominantly in the disordered regions of the cellulose structure. In the deuterated cellulose spectra, the OD stretching band would result from OD groups embedded in the crystalline regions which were not accessible to exchange, while the OH stretching would result from a mixture of crystalline and amorphous OH groups. Therefore, the OH bands would be broader than the OD bands.

In summary, the different extents of deuteration observed in the Cladophora spectra recorded with different polarizations of the incident light and the different band shapes in the deuterated and nondeuterated spectra provide some interesting insights into the nature of the vibrations as well as the deuteration

processes. The study of the CH and CD bands suggested the possibility of selective deuteration during biosynthesis and that Fermi resonance occurs in the the C-H and C-D stretching regions. The study of the OH and OD bands indicated that selective deuterium-hydrogen exchange reactions occurred during the purification of the celluloses.

The residual hydrogen in the deuterated celluloses together with their complex band patterns make it difficult to fully determine the effects of deuteration. For most bands, however, it was possible to determine whether the effect of deuteration was large or small. This information yields a qualitative measure of the contribution of hydrogen motions to the vibrational modes.

Two criteria were used to sort out the deuteration sensitivity of the bands. First, the normal coordinate calculations done by Wells[17] on fully deuterated β-D-glucose were used. Many of the vibrations in cellulose and glucose are expected to be very similar. Therefore, the frequency pattern and potential energy distribution calculated for fully deuterated glucose provides an approximate model for the frequency pattern and types of motion which occur in the spectrum of deuterated cellulose.

Second, a comparison was made of the sensitivities of the band intensities to the polarization of the incident light in the spectra of deuterated and nondeuterated cellulose. The modes that contain little contribution from hydrogen should have the same sensitivity to the polarization of the incident light in spectra of deuterated cellulose as in spectra of nondeuterated cellulose. Furthermore, isolated group vibrations that involve hydrogen will have the same sensitivity to the polarization of the incident light in the deuterated and nondeuterated cellulose spectra. Therefore, the sensitivity of the bands to the polarized exciting light is useful information for correlating bands in the

spectra of deuterated and nondeuterated celluloses. The deuteration sensitivities of several of the bands in the Raman spectrum of cellulose were determined based on the evidence discussed above and are summarized in Table 6.

Table 6. Deuteration sensitivities of the bands in the Raman spectrum of cellulose.

Frequency, cm^{-1}	Deuteration Sensitivity	Frequency, cm^{-1}	Deuteration Sensitivity
331	weak	1455	strong
344	weak	1477	strong
381	weak	1481	strong
437	weak	2848	strong
459	weak	2868	strong
520	weak	2885	strong
913	?	2904	strong
968	?	2941	strong
997	?	2965	strong
1034	?	3231	strong
1057	?	3239	strong
1071	weak	3266	strong
1095	weak	3291	strong
1118	weak	3299	strong
1123	weak	3302	strong
1152	?	3307	strong
1279	?	3334	strong
1292	?	3345	strong
1318	strong	3356	strong
1334	strong	3361	strong
1337	strong	3366	strong
1361	strong	3390	strong
1376	strong	3395	strong
1406	strong		

In the region between 250 and 550 cm^{-1}, the spectra of deuterated Cladophora and bacterial celluloses are very similar to spectra of nondeuterated cellulose. The bands in the deuterated cellulose spectra are shifted by 5 to 40 cm^{-1} relative to their positions in the spectra of nondeuterated cellulose. There are more bands in the deuterated Cladophora and bacterial cellulose spectra than in the nondeuterated cellulose spectra. The band frequencies in the deuterated

cellulose spectra do not match any of the frequencies in the nondeuterated cellulose spectra. Therefore, it is unlikely that the extra bands are residual bands due to incomplete deuteration. The normal coordinate calculations also predict more modes in the 250 to 550 cm^{-1} region of deuterated glucose spectrum than in the nondeuterated glucose spectrum. Thus, the new bands in the deuterated cellulose spectra may arise from new modes in the region due to deuteration. Alternatively, it is possible that some of the modes in the nondeuterated cellulose spectra are degenerate modes which are split in the spectra of deuterated celluloses.

The peak positions, relative intensities, and sensitivities of the peaks to the polarization of the incident light suggest a one-to-one correspondence between the 381, 344, and 331 cm^{-1} peaks in the nondeuterated cellulose spectra and the 371, 335, and 317 cm^{-1} peaks in the spectrum of deuterated bacterial cellulose. There are six bands between 390 and 520 cm^{-1} in the spectrum of deuterated bacterial cellulose which could be correlated with the 437, 459, and 520 cm^{-1} modes in the spectrum of nondeuterated cellulose. Based on the sensitivity of the bands to the polarization of the incident light, it appears that the 520 cm^{-1} mode in normal cellulose could be correlated with either the 398 or 479 cm^{-1} modes in deuterated bacterial cellulose. The 459 and 437 cm^{-1} mode in normal cellulose could be correlated with either the 398, 414, or 446 cm^{-1} modes in deuterated bacterial cellulose. For the 507 and 465 cm^{-1} modes in deuterated bacterial cellulose, it is difficult to determine the sensitivity of the bands to the polarization of the incident light. Therefore, it is difficult to discern which bands in the normal cellulose spectrum these bands might be correlated with.

In the 550 to 850 cm^{-1} region of the Raman spectrum of nondeuterated cellulose, the peaks are weak and widely spaced. This general trend is also observed in the Raman spectra of deuterated celluloses. Five bands are resolved in the spectrum of nondeuterated cellulose and four bands are resolved in the spectrum of deuterated bacterial cellulose. The normal coordinate calculations on glucose and fully deuterated glucose also predict more widely spaced bands in this region and about the same number of bands in the nondeuterated and deuterated glucose spectra.

Since the bands are weak, the sensitivity of the bands to the polarization of the incident light could not be determined. The deuteration sensitivity of the bands appears to be small but the bands are difficult to sort out without the intensity data. The normal coordinate calculations also predict only minor changes in the region due to deuteration.

In the 850 to 1250 cm^{-1} region of the Raman spectra of deuterated celluloses, the pattern of bands differs markedly from the pattern observed in nondeuterated cellulose spectra. Most significant are the differences in the 850-1000 cm^{-1} and 1150-1250 cm^{-1} regions. The normal coordinate calculations for fully deuterated glucose also predict many new bands in these regions. It is difficult to establish any one-to-one correlations between the bands in the nondeuterated cellulose spectrum and the new bands in the spectrum of deuterated cellulose, however.

According to the glucose normal coordinate calculations, the modes originally in the 850-1250 cm^{-1} region before deuteration should not be shifted significantly by deuteration. Consistent with this prediction are the 1095, 1118, 1071, and 1123 cm^{-1} modes in normal cellulose which appear to be shifted only

slightly in the spectrum of deuterated bacterial cellulose. Furthermore, these bands exhibit the same sensitivity to the polarization of the incident light relative to fiber axis in the deuterated Cladophora spectra as in the non-deuterated cellulose spectra. For the other bands originally in the 850-1250 cm^{-1} region it is difficult to determine the effect of deuteration due to overlap with the new bands in the region.

The bands in the 2800-3600 region are strongly sensitive to deuteration. The group of bands centered at 2900 cm^{-1} which is due to CH and CH_2 stretching shifts down to 2100 cm^{-1} in the spectra of deuterated Cladophora and bacterial celluloses. The CD and CD_2 stretching bands appear to exhibit the same dependence on the polarization of the incident light relative to the fiber axis as the CH and CH_2 stretching bands. Most of the CD stretching bands in the Cladophora spectra were more intense when the incident electric vector was perpendicular to the fiber axis. The shoulder at 2215 cm^{-1}, however, was more intense when the incident electric vector was parallel to the fiber axis. In the CH stretching region, all of the bands except the shoulder at 2965 cm^{-1} are also more intense with the incident electric vector perpendicular to the fiber axis. The shoulder resolved at 2965 cm^{-1} is more intense in the spectra recorded with the incident electric vector parallel to the fiber axis. Therefore, it appears that the 2965 and 2215 cm^{-1} peaks correspond to the same mode. The other bands in the CH and CD stretching regions are difficult to correlate due to the different shapes of the CH and CD bands.

The O-H stretching bands between 3200 and 3500 cm^{-1} are shifted down to the 2400 to 2600 cm^{-1} region in the deuterated cellulose spectra. The deuterated Cladophora spectra show that the O-D bands have the same sensitivity to the polarization of the incident light relative to the fiber axis as the O-H bands.

Both the O-H and O-D bands are more intense with the incident electric vector parallel to the fiber axis. As with the C-H bands, it is difficult to correlate the O-H and O-D bands because of the different band shapes.

Although there are several reports in the literature of vibrational spectra recorded from hydroxyl-deuterated cellulose,[44] there are very few reports of spectra recorded from carbon-deuterated cellulose because of the difficulties associated with preparing it. Dechant,[45-46] however, has recorded infrared spectra from carbon-deuterated bacterial cellulose. In the CH and CD stretching region, Dechant's results are similar to ours. He proposed that selective deuteration must occur in the biosynthesis of the deuterated cellulose. Dechant also observed that the group of bands between 1000 and 1200 cm^{-1} in the spectra of normal cellulose are affected very little by deuteration. This is consistent with our results. In the other regions of the spectra, however, Dechant's results are difficult to compare with our own because the residual OH groups affect IR and Raman spectra to different extents. In infrared spectra, OH vibrations are more intense than CH vibrations due to the greater dipole moment of the OH bond. Conversely, CH modes are more intense in Raman spectra because the CH bonds are more polarizable. Therefore, the effect of the residual OH groups in the deuterated bacterial cellulose will be greater in Dechant's IR spectra than in our Raman spectra.

Neutron scattering spectra provide information which complements the spectra from deuterated celluloses, since they reveal the frequencies where the hydrogen motions occur. In neutron scattering experiments, only the motions of the hydrogen atoms are seen, since the scattering cross section of hydrogen is extremely large compared to other atoms. Due to this selection rule, neutron spectra

are essentially plots of the density of states for phonons involving hydrogen *vs.* phonon frequency.

Kaji, *et al.*[47] recorded neutron inelastic scattering spectra of ramie cellulose which cover the 0 to 2000 cm^{-1} region. In the 1200-1500 cm^{-1} region, they observed a strong broad peak with its maximum intensity at 1350 cm^{-1}. This is consistent with our results since the peaks in the 1200 to 1500 cm^{-1} region are very sensitive to deuteration. The neutron spectra were devoid of any strong peaks in the 900-1200 cm^{-1} region, which is consistent with the low deuteration sensitivity of the bands in this region.

In the region below 500 cm^{-1}, the neutron spectra exhibit a fine structure which corresponds quite closely to the Raman spectra of cellulose in this region, suggesting that these modes contain hydrogen motions. This is in contrast to the small deuteration sensitivity of these peaks. A possible explanation for this discrepancy is that modes can involve hydrogen motion without distortion occurring in the CH bonds. Since the potential energy distributions are expressed in internal coordinates, hydrogen motions will not contribute unless distortion of the CH bonds occurs. Displacement drawings for the modes below 500 cm^{-1} in glucose show that the modes involve displacements of almost all of the hydrogens even though the potential energy distributions contain very small contributions from CH internal coordinates. Therefore, very little distortion of the CH bonds is occurring. This explains the low deuteration sensitivity of the bands.

BAND ASSIGNMENTS

Assignments of the cellulose vibrational spectrum in the literature have traditionally assumed that the vibrational motions can be described in terms of

simple group motions. The normal coordinate analyses demonstrated that this is a poor assumption. In the region below 1500 cm^{-1}, only the internal motions of the CH_2OH group can be adequately approximated as group motions. The rest of the modes are delocalized motions involving more than one group or site in the molecule. The assignments in this thesis are descriptions of the predominant motions contributing to the bands and the directional character of the vibrations. Normal coordinate calculations done by Carlson[18] for the cellodextrins were used to identify the internal coordinates involved in each region of the cellulose vibrational spectrum. Cellodextrins equal to or larger than cellotetraose have spectra which are very similar to the spectrum of cellulose II. Therefore, similar vibrations must occur in cellulose and cellotetraose, and the normal coordinate analysis of cellotetraose will provide a good basis for understanding the cellulose spectrum.

Since the crystal structure of cellotetraose is unknown, it is necessary to use assumed structures in the normal coordinate analyses. Carlson conducted normal coordinate analyses using two different assumed structures. The structures differed in the values of the dihedral angles about the glycosidic linkages. In the first structure, referred to as the cellobiose type structure, the dihedral angles were all assumed to be the same as in the crystal structure of cellobiose. In the second structure, referred to as the methyl-β-cellobioside structure, the dihedral angle in the crystal structure of methyl-β-cellobioside was adopted.

Bar graphs showing the frequency distributions and potential energy distributions calculated for the cellobiose and methyl-β-cellobioside type structures are given in Fig. 19 and 20, respectively. In making the graphs, the internal coordinates were divided into four categories. The positions of the bars along

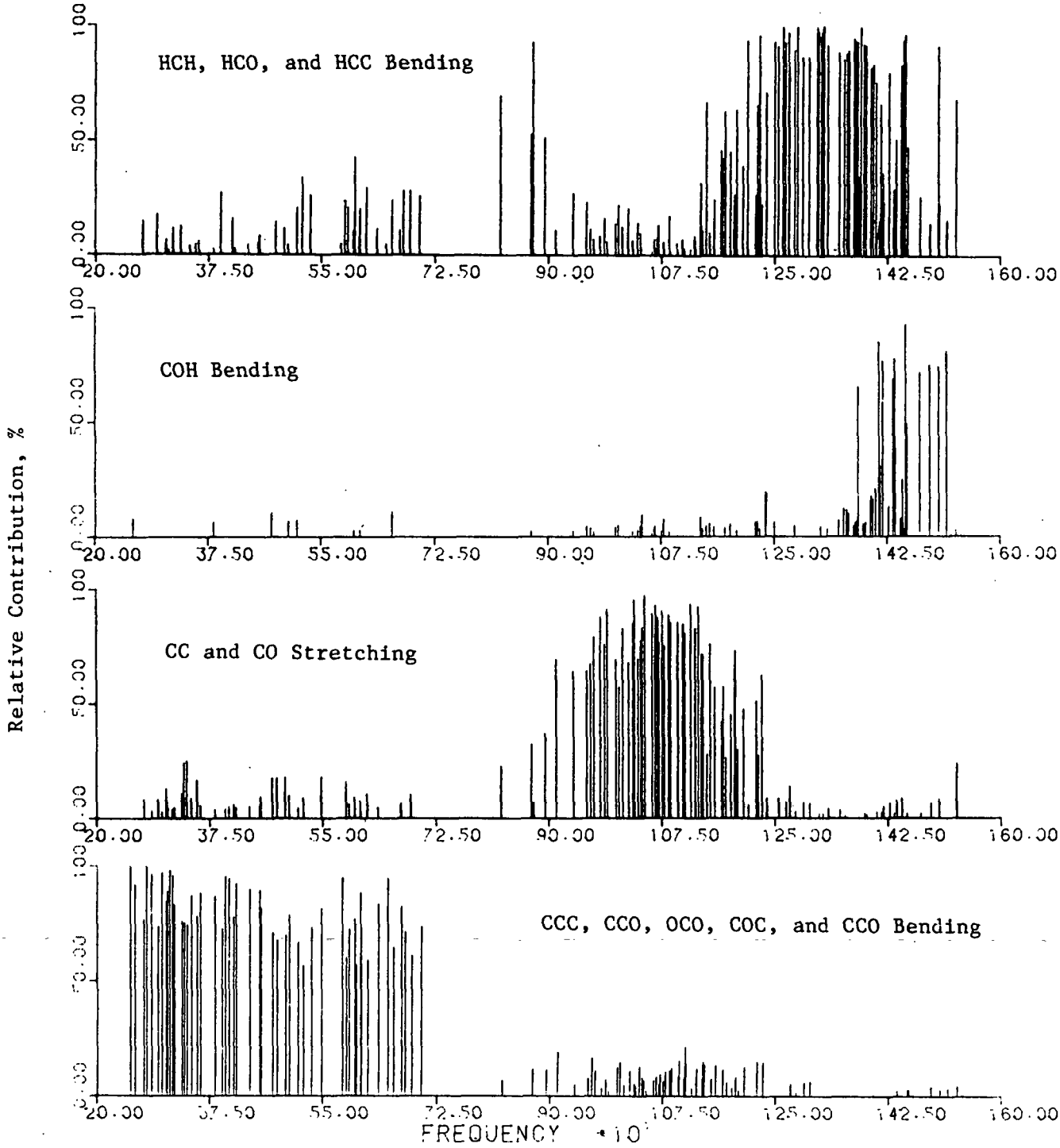

Figure 19. Potential energy distributions for cellotetraose calculated using the cellobiose type structure.

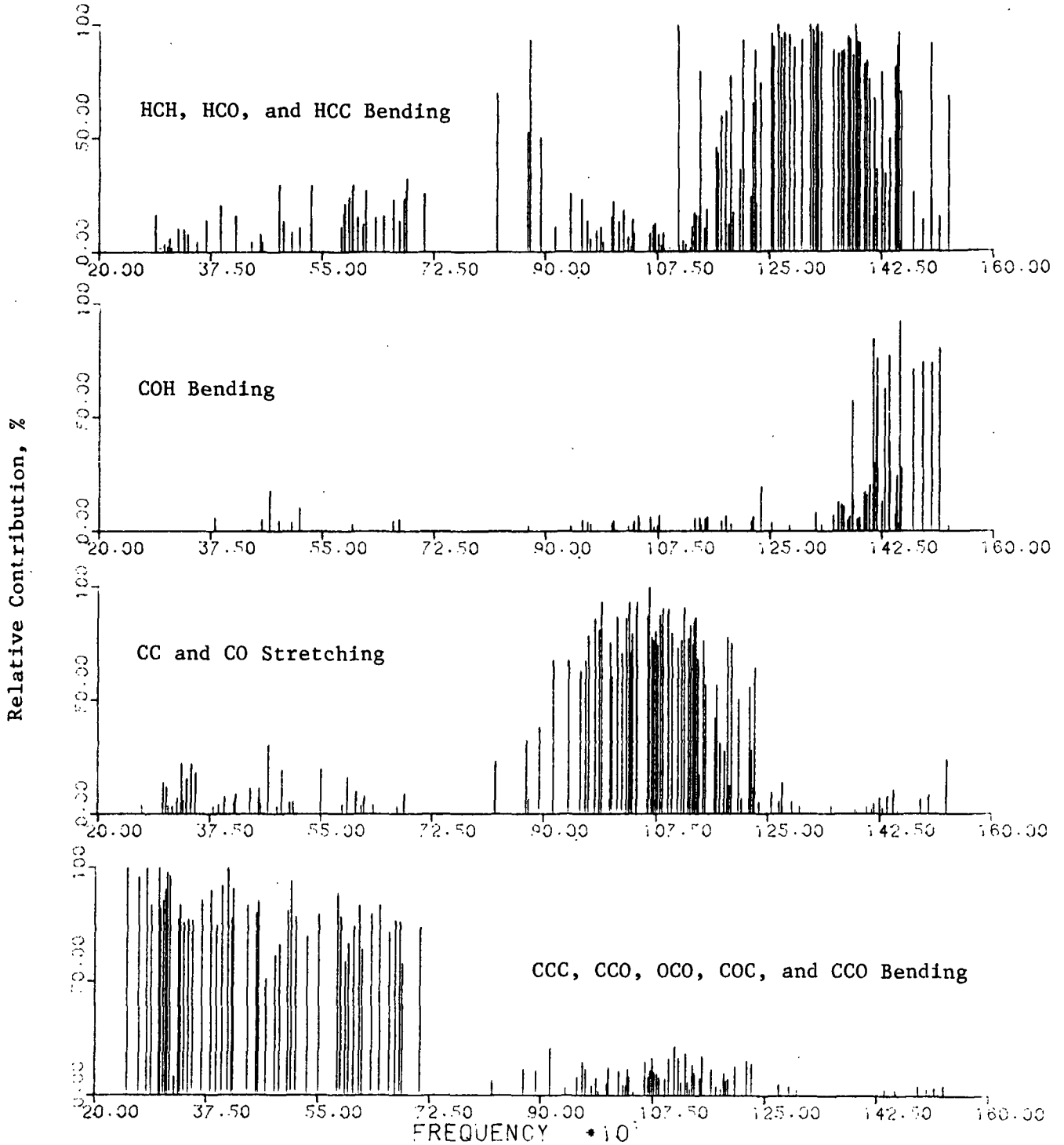

Figure 20. Potential energy distributions for cellotetraose calculated using the methyl-β-cellobioside type structure.

frequency axis indicate the calculated frequencies. The height of the bars in each of the internal coordinate categories is proportional to the contribution of that group of internal coordinates to the potential energy distribution.

The figures show that the frequency and potential energy distributions are quite similar for the different cellotetraose structures. In both cases, the number of calculated modes greatly exceeds the number of bands actually observed in the infrared and Raman spectra of either cellotetraose or cellulose. If we consider an isolated chain, cellotetraose has over 200 vibrational degrees of freedom. Since the assumed cellotetraose structures possess no symmetry, all of the vibrational degrees of freedom are potentially both infrared and Raman active. Cellulose also possesses a large number of potentially infrared and Raman active vibrational modes. In the infrared and Raman spectra of cellulose and cellotetraose, however, only about 60 to 70 modes are observed. One possible explanation for the discrepancy between the number of potentially active modes and the number of modes actually observed is that even though all the modes are allowed by the infrared and Raman selection rules, satisfaction of the selection rules is a necessary but not a sufficient condition for there to be IR or Raman activity. It is possible for a mode to be allowed by the selection rules but still be too weak to be observed in the spectra.

Another possible explanation for the discrepancy between the number of observed and predicted bands is that some of the bands may be accidentally degenerate. In the cellodextrin calculations, it was found that the bands became very closely spaced as the number of glucose units in the chain increased. In the case of the disaccharides some of the modes, which were isolated within one of the two rings, would have a complement at a very close

frequency involving similar motions in the neighboring ring. These modes were spaced closely enough to combine to form one observable band.

Eventually, as the number of glucose units increases even further, the infrared and Raman band intensities will be determined by the density of vibrational states as a function of frequency. Figures 21 and 22 are histogram plots of the vibrational state density as a function of frequency based on the cellotetraose normal coordinate calculations. Figure 21 was based on the cellobiose type structure and Fig. 22 was based on the methyl-β-cellobioside type structure. The histograms imitate the frequency distributions and intensity patterns in the vibrational spectra of cellotetraose and cellulose. Therefore, many of the bands observed in the cellulose vibrational spectrum may actually arise from a composite of vibrational modes having approximately the same frequencies.

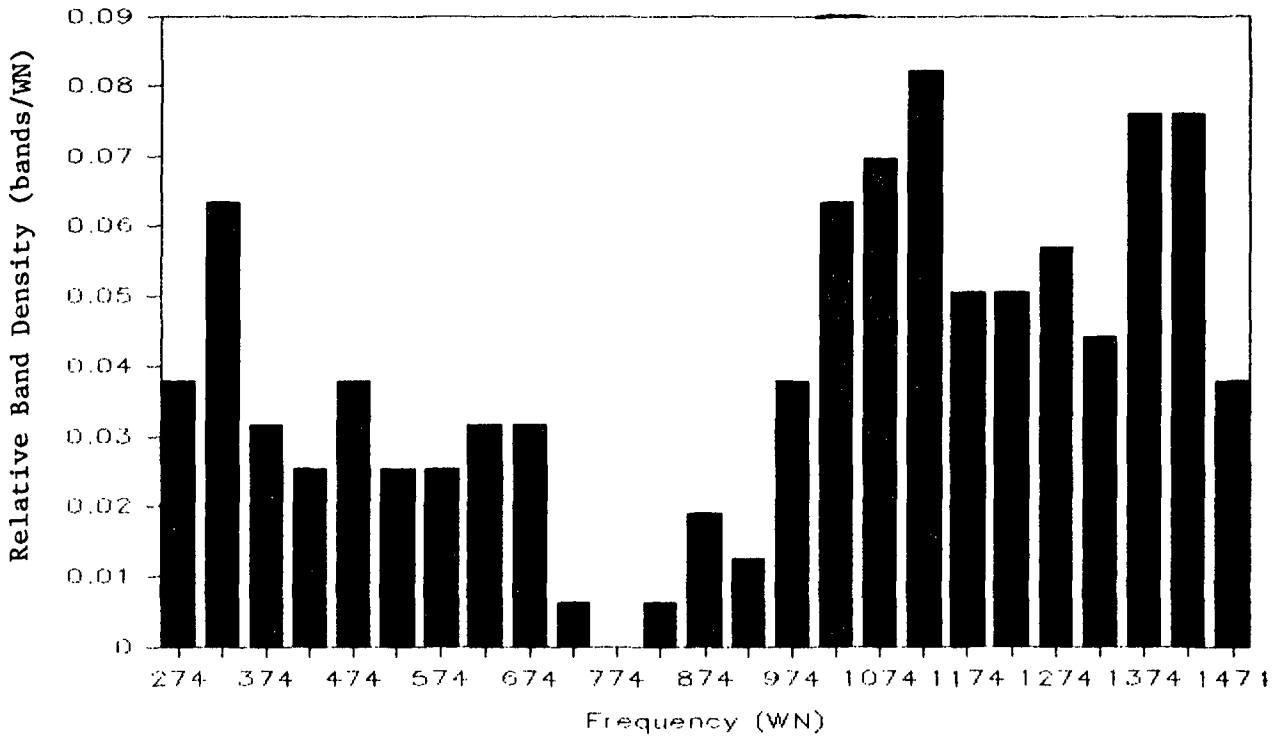

Figure 21. Frequency distribution calculated for cellotetraose using the cellobiose type structure.

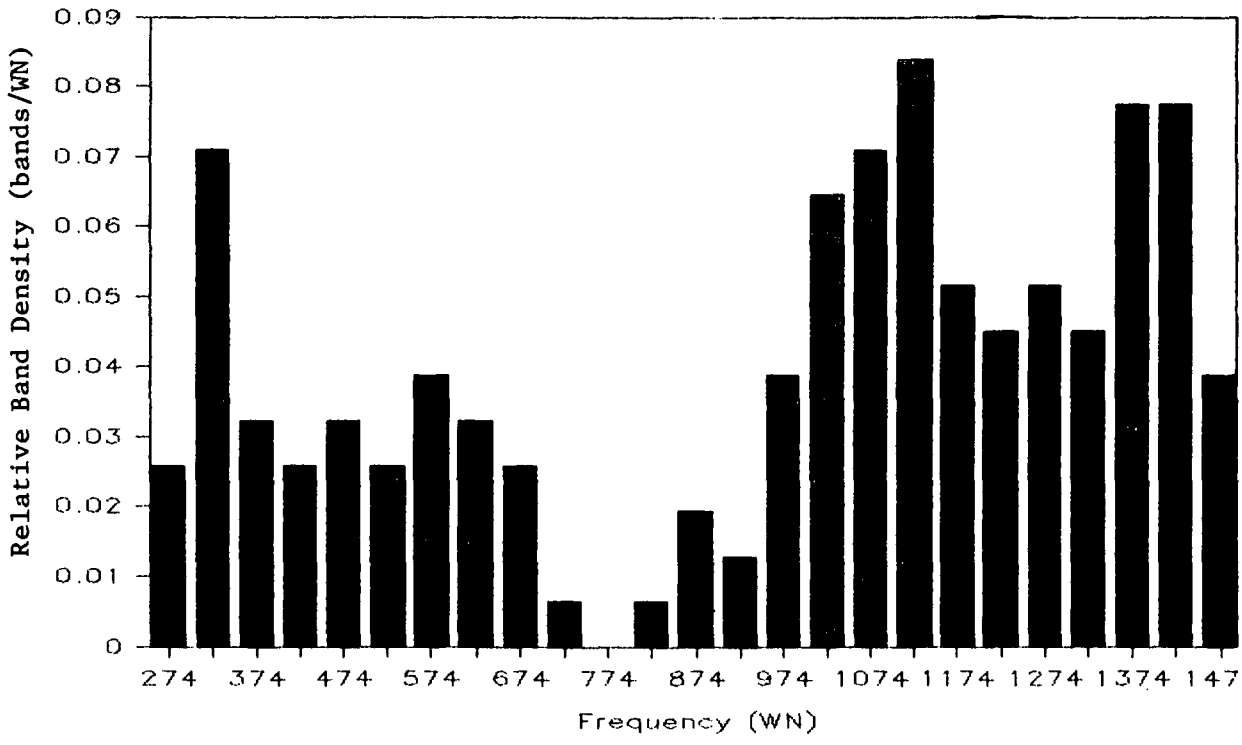

Figure 22. Frequency distribution calculated for cellotetraose using the methyl-β-cellobioside type structure.

When the histograms for the cellobiose and methyl-β-cellobioside structures are compared, the major differences show up below 700 cm^{-1}. Thus the frequency distribution below 700 cm^{-1} is most sensitive to the conformation of the glucose units about the glycosidic linkages. Except for some small differences between 1200 and 1300 cm^{-1}, the frequency distributions for the different conformations of cellotetraose are identical above 700 cm^{-1}. This suggests that to a large extent, the frequency distributions are determined by the structure of the pyranose rings rather than the way the rings are hooked together. In cellulose, the conformation of the linkages alternates between the cellobiose and methyl-β-cellobioside types. Therefore, neither structure by itself is truly representative of cellulose.

In the interpretation of the Raman spectrum of cellulose that follows, the potential energy distributions in Fig. 19 and 20 will be used as a basis for understanding the vibrational motions in cellulose. Even though neither structure is truly representative of cellulose, the potential energy distributions are not very sensitive to the conformation of the linkage and therefore either distribution provides an adequate model for understanding the motions. Since we suspect that at least some of the observed bands are actually composites of more than one vibrational mode, only the general types of motion will be discussed. The assignments have been divided into six regions for convenience.

250-550 cm^{-1} Region

In the region between 250 and 550 cm^{-1}, several closely spaced, medium intensity bands were observed in the Raman spectra of Valonia and ramie celluloses (see Fig. 12-14). A similar pattern has been observed in the infrared spectra of native celluloses.[18,24-28] The potential energy distributions are to a large extent delocalized, indicating that the vibrational modes are quite complex. Displacement drawings based on the normal coordinate calculations for the disaccharides[18] show that almost every atom in the molecule participates in these modes.

The predominant motions are skeletal bending modes involving the CCC, COC, OCC, and OCO internal coordinates (See Fig. 19-20). Small amounts of methine bending (CCH and OCH) and skeletal stretching (CC and CO) also contribute in the region. Torsional motions, which are out-of-plane bending about the CO and CC bonds, become significant below 300 cm^{-1}. The small sensitivity of the bands to deuteration is consistent with the small contribution of the C-H coordinates in the potential energy distributions.

According to the classifications in Table 5, the bands at 331, 459, and 520 cm^{-1} are types A_0, B_0, and A_{90}, respectively. The 344, 381, and 437 cm^{-1} all belong to the B category but their distribution in groups B_0 and B_{90} is uncertain due to the disagreement between the Valonia and ramie data. Since the 331 and 459 cm^{-1} modes are most intense when the incident electric vector is parallel to the chain axis, these modes are skeletal bending modes where the change in polarizability is parallel to the chain axis. The accordionlike bending motion depicted in Fig. 23a is a plausible representation of these modes. Since the 459 cm^{-1} band falls in the B category, it may actually be a composite of a motion in which the change in polarizability is parallel to the chain axis and a motion where the change in polarizability is perpendicular to the chain axis. Alternatively, some of the polarizabilities may decrease during the vibration. The 520 cm^{-1} mode is most intense when the incident electric vector is perpendicular to the chain axis. The bending motion shown in Fig. 23b is consistent with the data for this mode.

Very few band assignments are available in the literature for the 250-550 cm^{-1} region. Cael, et al.[21] performed a normal coordinate analysis on cellulose which included the modes in this region. Their analysis is approximate in nature since they did not refine their force constants and used a simplified structural model for cellulose. They assumed that the cellulose chain possesses a twofold helix conformation. Others have questioned the twofold helix assumption.[39,48-51] The symmetry of the twofold helix requires that the vibrations in the cellulose chain arise from a single glucose residue. In spite of the assumptions made by Cael, et al., their potential energy distributions qualitatively predict the same types of motion for the 250-550 cm^{-1} region as the cellodextrin and hexose calculations.[17-18]

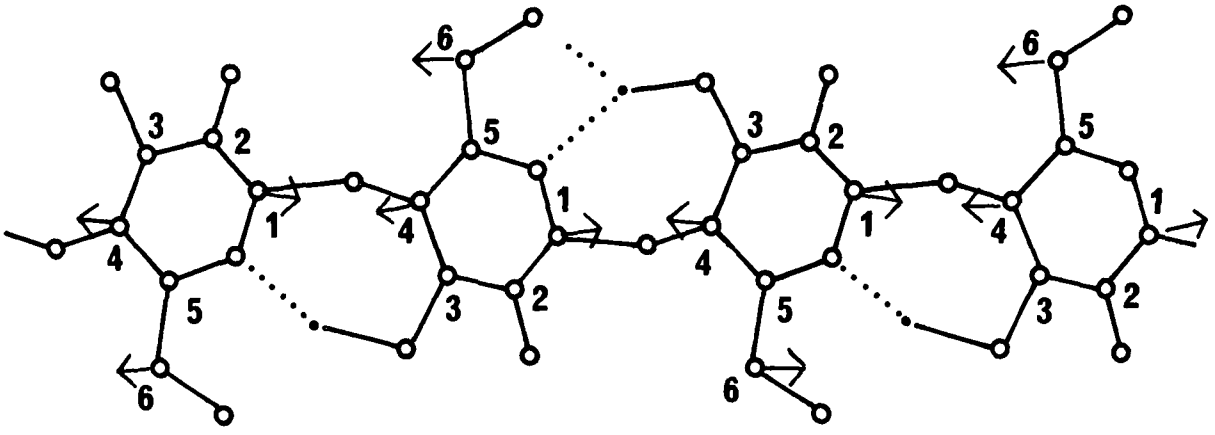

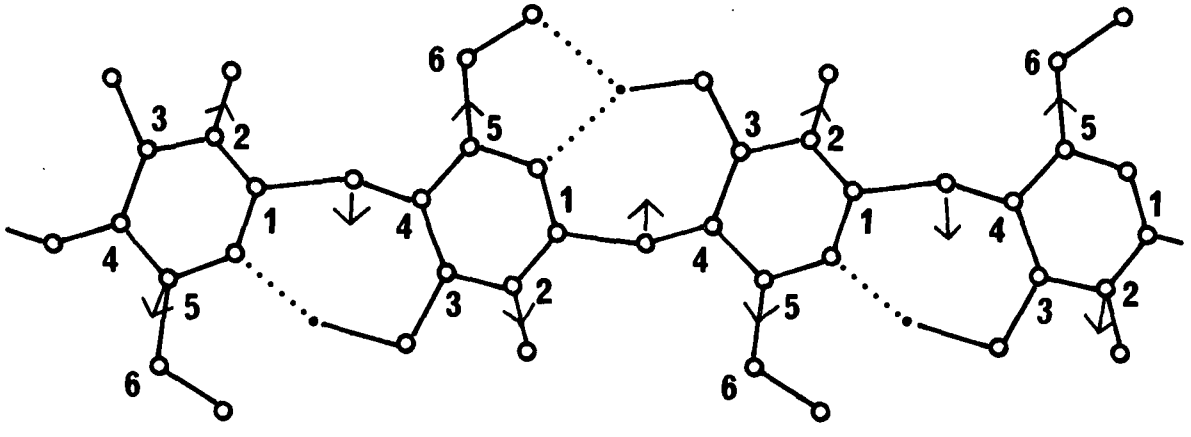

Figure 23. Plausible displacement drawings for skeletal bending modes. A) maximum change in polarizability parallel to chain axis, B) maximum change in polarizability perpendicular to the chain axis.

The histograms based on the two alternative structures for cellotetraose (see Fig. 21-22) show that the frequency distributions below 700 cm^{-1} are sensitive to the dihedral angles at the glycosidic linkages. Raman spectra of various types of cellulose[50-51] have shown that the Raman spectra are very sensitive to the polymorphic form of the cellulose. The observed spectral differences are very similar to the differences observed in the frequency

distributions for the alternate structures of cellotetraose. This has reinforced the conclusion that celluloses I and II possess different conformations of the glycosidic linkages.[50-51]

550-950 cm^{-1} Region

In the region between 550 and 950 cm^{-1} of the Raman spectra of Valonia and ramie celluloses (see Fig. 12-14), the bands are weak and widely spaced. The region between 750 and 800 cm^{-1} is devoid of any significant features. Infrared spectra of native celluloses differ from the Raman spectra between 550 and 750 cm^{-1} in that several medium intensity peaks are observed.[18,24-28] Between 750 and 850 cm^{-1}, the IR spectra are also devoid of any significant features. Both the Raman and IR spectra possess a weak, poorly-resolved cluster of bands at approximately 900 cm^{-1}.

The potential energy distributions for cellotetraose (see Fig. 19-20) indicate that between 550 and 750 cm^{-1} the predominant internal coordinates are CCC, COC, OCO, and CCO bending and OH out-of-plane bending. The OH bending modes are observed in infrared spectra but are absent in Raman spectra because of the large dipole moment associated with the OH bond. No bands are calculated between 750 and 800 cm^{-1}, which is consistent with the observed frequency pattern. A cluster of peaks is calculated around 900 cm^{-1} that involves HCC and HCO bending localized at the C6 positions.

The deuteration sensitivities of the bands in the Raman spectrum between 550 and 850 cm^{-1} were small. This observation is consistent with the dominance of the CCC, COC, OCO, and CCO internal coordinates in this region of the Raman spectrum. Since the peaks around 900 cm^{-1} involve primarily methine bending coordinates, these bands should be strongly deuteration sensitive. We were

unable to identify a peak in the appropriate region of deuterated cellulose spectra which could correspond to the 900 cm^{-1} band. New peaks are shifted into the region around 900 cm^{-1} by deuteration so that it is difficult to tell if the 900 cm^{-1} band is still present. It appears that the 900 cm^{-1} band is shifted by much less than would be the case if this was a pure CH mode.[52] Therefore, it is likely that the bands around 900 cm^{-1} are more delocalized than predicted by the cellotetraose calculations.

Carlson and Wells[17-18] showed that the frequency and potential energy distributions for the bands around 900 cm^{-1} are sensitive to the rotational position of the CH_2OH group.[17-18] In β-D-glucose where the conformation at C6 differs from the conformation assumed for cellotetraose, the bands around 900 cm^{-1} are more delocalized motions involving CC and CO stretching in addition to methine bending at C6. If the conformation of the hydroxymethylene groups in cellulose differs from that assumed for cellotetraose, the bands around 900 cm^{-1} might be more delocalized motions, which would be more consistent with the deuterated cellulose spectra.

In assigning the modes around 900 cm^{-1}, several empirical observations are useful. The band at 900 cm^{-1} is more intense in the spectra of ramie than in Valonia (see Fig. 13-14). This is the most significant difference between the ramie and Valonia spectra below 3000 cm^{-1}. A comparison of the spectra of ramie, cotton, bacterial, algal, and amorphous celluloses suggested that the intensity of the 900 cm^{-1} band is related to the lateral size of the cellulose crystallites. The intensity of the 900 cm^{-1} band was also found to correlate in some instances with the intensity of the broad upfield shoulders for the C4 and C6 carbons in the solid state ^{13}C NMR spectra of native celluloses.[53] The broad shoulders arise from cellulose chains on the crystallite surfaces and in the

amorphous regions. These results suggest that the intensity of the 900 cm^{-1} band is proportional to the amount of disorder in the cellulose. Since the likely sites of disorder in the cellulose molecules are the glycosidic linkages, the C6 positions, and the hydroxyl groups, the 900 cm^{-1} band must somehow be involved with these sites.

In the literature, the assignment of the 900 cm^{-1} band is also controversial. Blackwell[28] assigned the band as a methine deformation at the C1 positions since the modes in this region had been reported to be correlated with the configuration at the anomeric carbon. Liang and Marchessault[25] assigned the mode as an antisymmetric ring stretching motion analogous to the ring modes observed in the spectra of tetrahydropyran. In the normal coordinate analysis for cellulose done by Cael, et al.,[21] the 900 cm^{-1} modes are delocalized ones involving COH, HCC, and HCO bending in the ring as well as at C6. The difference between their potential energy distribution and ours results from the different structure they used and their choice of a lower OH bending constant. Based on Cael's results, the 900 cm^{-1} band should be strongly deuteration sensitive, which contradicts the Raman spectra of deuterated celluloses.

In the 550 to 750 cm^{-1} region, Liang and Marchessault[26] and Blackwell, et al.[28] assigned the CH_2 rocking mode between 740 and 745 cm^{-1}. In the normal coordinate calculations on the hexoses, Wells[17] argues against their assignment based on the weak Raman intensity around 750 cm^{-1}, and the complexity of the potential energy distributions precludes any of the bands in this region as being assigned as CH_2 rocking.

Liang and Marchessault[26] assigned the modes in the infrared spectra at 663 and 700 cm^{-1} as OH out-of-plane bending modes. This assignment is consistent

with the low Raman intensity of the 663 and 700 cm^{-1} bands. Normal coordinate calculations indicate that OH out-of-plane bending modes tend not to couple with other internal coordinates.[11-18] Carlson found that the modes in this region were very temperature sensitive.[18] Since OH out-of-plane bending modes would be sensitive to hydrogen bonding, the assignment is consistent with the temperature sensitivity of the bands.

950-1180 cm^{-1} Region

In the region between 950 and 1180 cm^{-1}, several closely spaced intense bands are observed in both the Raman spectra of Valonia and ramie celluloses (see Fig. 12-14) and in the infrared spectra of native celluloses reported in the literature.[18,24-28] The frequency distributions (see Fig. 21-22) show that the band density in the 950 to 1180 cm^{-1} region is very high. The potential energy distributions (see Fig. 19-20) are dominated by CC and CO stretching. Small amounts of HCC, HCO, and skeletal atom bending also contribute to the bands. The motions are highly coupled, often involving coupling between the glucose rings.

The high Raman and infrared intensities of the bands are consistent with the large band density and dominance of CC and CO stretching motions predicted by the normal coordinate calculations. It is difficult to determine the deuteration sensitivities because many new bands appear in the region due to deuteration. The 1071, 1095, 1118, and 1123 cm^{-1} exhibit very little sensitivity to deuteration which is consistent with the negligible contribution of CH, CH_2, and OH coordinates in the region.

The 997, 1034, 1057, 1095, and 1123 cm^{-1} modes all fall in the A_0 category (refer to Table 5). The band at 1118 cm^{-1} is a B_0 mode. Since these bands are

most intense when the electric vector of the incident light is parallel to the fiber axis, they must result from CC and CO stretching motions which are parallel to the chain axis. A plausible displacement drawing for an A_0 type skeletal stretching modes is shown in Fig. 24a. The 968 cm^{-1} peak is a B_{90} mode. It must result from skeletal stretching motions that are predominantly perpendicular to the chain axis. A plausible displacement drawing for a B_{90} skeletal stretching mode is shown in Fig. 24b. In addition to 1118 and 968 cm^{-1} band, the band at 1152 also belongs in the B category. The ramie and Valonia data are not consistent, however, as to whether the 1152 cm^{-1} band is a B_0 or B_{90} mode. The directionality of the 1152 cm^{-1} mode is, therefore, uncertain.

In the group frequency literature,[24-28] the modes between 950 and 1180 cm^{-1} have been assigned as CO stretches and as various ring modes in analogy with tetrahydropyran. Although these types of motion are consistent with the potential energy distributions, the normal coordinate calculations show that the modes are highly coupled and therefore are not very well approximated as group modes or by analogies with tetrahydropyran.

In the normal coordinate calculations for cellulose done by Cael et al.[21] the modes between 950 and 1180 cm^{-1} were shown to be complex mixtures of CC and CO stretching, skeletal atom bending, C-H bending, and O-H bending. Their results agree qualitatively with our own.

1180-1500 cm^{-1} Region

Between 1180 and 1270 cm^{-1} the Raman and infrared spectra of Valonia and ramie cellulose exhibit only weak and widely spaced bands.[18,24-28] The potential energy distributions indicate that the 1180 to 1270 cm^{-1} region is a transition region (see Fig. 19-20). Below 1180 cm^{-1}, CC and CO stretching coordinates

dominate the potential energy distributions, while above 1270 cm^{-1}, HCC, HCO, HCH, and COH bending coordinates are most significant. Between 1180 and 1270 cm^{-1}, the modes involve significant amounts of skeletal stretching as well as methine bending.

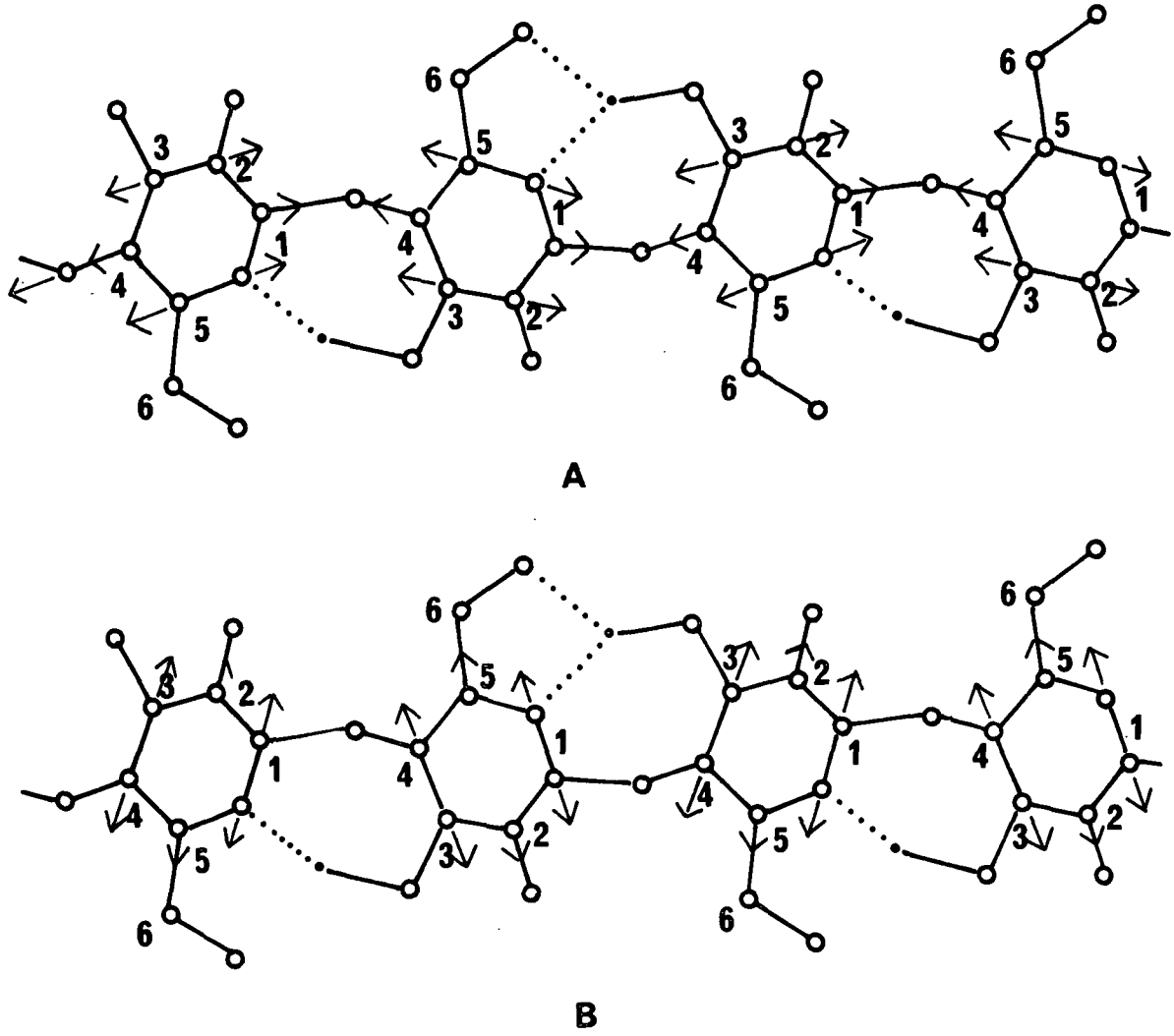

Figure 24. Plausible displacement drawings for skeletal stretching modes.
A) maximum change in polarizability parallel to chain axis,
B) maximum change in polarizability perpendicular to chain axis.

In the group frequency literature,[24-28] bands in the 1180 to 1270 cm^{-1} region have been assigned as OH in-plane bending. The cellotetraose calculations show that the bands are delocalized and that OH bending is not the predominant internal coordinate. Cael's calculations for cellulose agree with the

cellotetraose calculations in that the modes are delocalized but his OH bending frequencies are lower than ours. Cael's calculations predict a higher proportion of OH bending and are more comparable to the group frequency assignments.

Between 1200 and 1300 cm^{-1}, differences are observed in the cellotetraose frequency distributions based on the cellobiose and methyl-β-cellobioside type structures (see Fig. 21-22). Therefore, the frequency distribution is sensitive to the conformation of the glycosidic linkages in this region. The differences in the frequency distributions correspond closely with the differences observed in the spectra of celluloses I and II. A medium intensity band is observed in the Raman spectrum of cellulose II at 1261 cm^{-1} that is not observed in the spectrum of cellulose I. This observation lends support to the proposal that celluloses I and II possess different molecular conformations. The sensitivity of the bands to conformation may arise from the nature of the potential energy distributions. Since the 1180 to 1270 cm^{-1} region is a transition region, many different types of internal coordinates contribute to the modes, thereby increasing the amount of delocalization.

In the 1270 to 1500 cm^{-1} region several closely spaced medium intensity bands are observed in both the Raman and infrared spectra of native celluloses. The bands are strongly sensitive to deuteration. The normal coordinate calculations for cellotetraose also predict a high density of bands in the region (see Fig. 21-22). The predominant internal coordinates in the potential energy distributions (see Fig. 19-20) are CCH, OCH, COH, and HCH bending. Between 1430 and 1500 cm^{-1} the major internal coordinate is HCH bending; from 1430 to 1350 cm^{-1} it is COH bending; and from 1350 to 1270 cm^{-1} it is HCC and HCO bending. Except for the internal modes of the CH_2OH groups, the motions are quite delocalized.

The dominance of C-H and O-H bending coordinates is consistent with the strong deuteration sensitivity of the bands.

The Raman bands at 1279, 1334, 1337, and 1406 cm^{-1} are all A_0 modes. Since these modes are most intense when the electric vector of the incident light is parallel to the chain axis, they must result primarily from HCC and HCO bending motions where the change in polarizability is parallel to the chain axis. Although COH bending coordinates also contribute to the potential energy distributions above 1300 cm^{-1}, OH bending is very weak in Raman spectra, so the intensities will be dominated by the motions of CH groups. A plausible drawing of a CH bending mode in which the motions are parallel to the chain axis is shown in Fig. 25.

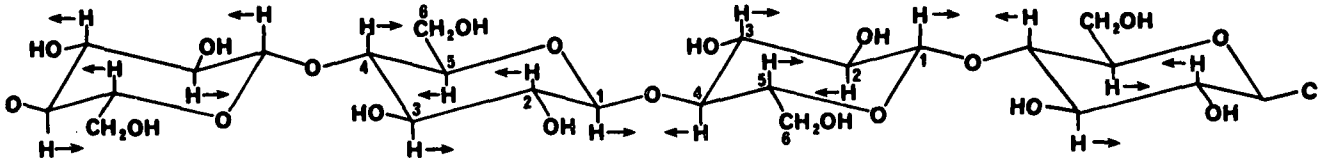

Figure 25. Plausible displacement drawing for a methine bending mode. The maximum change in polarizability is parallel to the chain axis.

The Raman bands at 1455 and 1479 cm^{-1} fall in the B_{90} and A_{90} categories, respectively. The potential energy distributions show that these bands are HCH bending modes which contain a small proportion of COH bending. The bands are most intense when the electric vector of the incident light is perpendicular to the fiber axis. Therefore, the vibrations must be oriented so that the change in polarizability accompanying the vibrations is also perpendicular to the chain

axis as shown in Fig. 26. This can only occur in the so-called gt and tg rotational conformations for the methylene groups.[54] In the gt conformation, the C6-O6 bond is gauche to the C5-O5 bond and trans to the C4-C5 bond, whereas in the tg conformation it is trans to the C5-O5 bond and gauche to the C4-C5 bond. As the tg conformation has not been observed in crystalline carbohydrates,[54] the gt conformation is most likely.

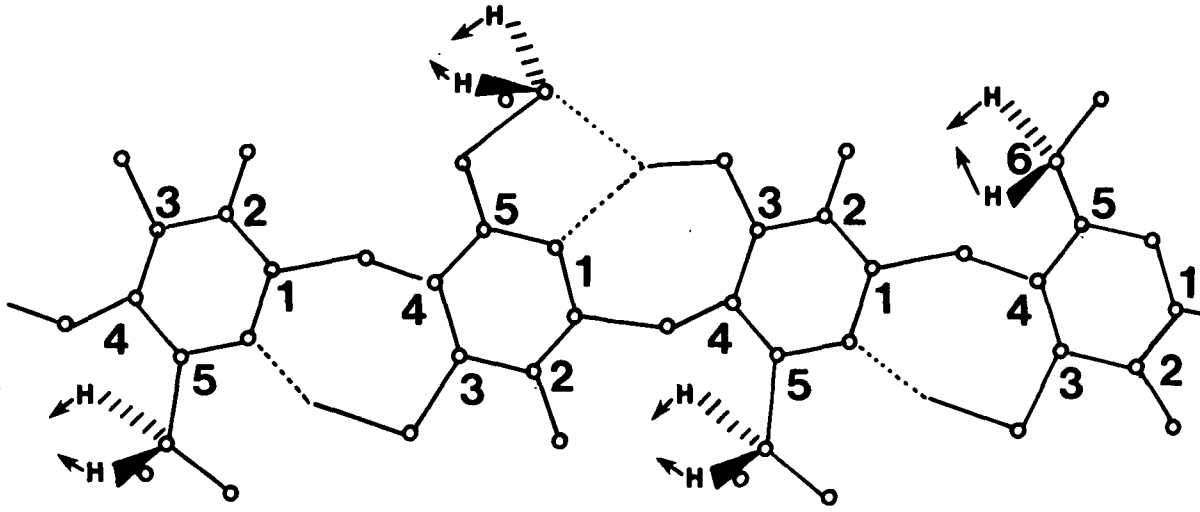

Figure 26. Plausible displacement drawing for a methylene bending mode. The maximum change in polarizability is perpendicular to the chain axis.

Since the HCH bending modes approximate group vibrations, it should be possible to identify a DCD bending band in the spectra of deuterated celluloses. In the normal coordinate calculation for deuterated glucose, a relatively pure DCD bending motion is predicted at 1034 cm^{-1}. A peak is observed in the spectrum of deuterated bacterial cellulose at 1034 cm^{-1} that is consistent with this prediction. Since the spectrum of nondeuterated cellulose also contains a peak at this frequency, it is difficult to tell whether the peak in the spectrum of deuterated cellulose is indeed due to DCD bending. Almost every peak appears to shift at least slightly as a result of deuteration. Thus, it is unlikely that the 1034 cm^{-1} peak would be totally unshifted by deuteration.

In the group frequency literature, the band at 1430 cm^{-1} has been assigned as the methylene bending mode. As mentioned above, the cellotetraose calculations predict methylene bending between 1450 and 1480 cm^{-1}. This assignment is supported by the fact that the Raman intensity at 1430 cm^{-1} is extremely weak, whereas two clearly resolved bands appear between 1450 and 1480 cm^{-1}. The multiple bands coalesce to form a single peak in the Raman spectrum of cellulose II. Cael, et al.[21] calculated the methylene bending mode around 1430 cm^{-1}. The discrepancy between Cael's calculations and our own reflects the different HCH and OH bending constants that were used.

Tsuboi[24] assigned the methylene wagging mode to the band at 1250 cm^{-1}, whereas Liang and Marchessault[26] and others[27-28] favor the band at 1320 cm^{-1}. Wells' calculations for the hexoses[17] show that either the band at 1335 or 1360 cm^{-1} is consistent with the methylene wagging assignment. Blackwell[28] assigned the band at 1293 cm^{-1} as CH_2 twisting. This calculation is quite reasonable in view of Wells' calculations.

The rest of the modes in this region have been assigned as either CH or OH bending modes in the group frequency literature. Although the normal coordinate calculations predict CH and OH bending as the predominant motions, except for the internal modes of the methylene group the modes are highly coupled.

2800-3000 cm^{-1} Region

Between 2800 and 3000 cm^{-1}, the Raman spectra of Valonia and ramie contain several closely spaced, very intense bands. In the infrared spectra, the band structure is very similar but the bands are not as intense.[18,24-28] The bands are strongly deuteration sensitive. The normal coordinate calculations predict that the CH and CH_2 stretching vibrations occur in this region. These modes are

isolated from the other motions in the molecule and, therefore, behave as group vibrations.

The 2868 and 2885 cm^{-1} bands fall into the B_{90} category in both the Raman spectra of ramie and Valonia. The 2965 cm^{-1} band is a B_0 band in both sets of spectra. Although it is difficult to assign the bands in this region due to the overlapping of the bands and the possibility of Fermi resonance, the most intense band at 2885 cm^{-1} is most likely due to the methine protons. The methine CH bonds are perpendicular to the chain axis and, hence, would result in stretching bands that are most intense when the electric vector of the incident light is perpendicular to the chain axis. Also, there are more methine protons than CH_2 protons so that the methine stretch should be the most intense CH band.

The CH_2 group should exhibit both symmetric and antisymmetric stretching bands. The antisymmetric stretching band will be at higher frequency than the symmetric stretching band. Since the symmetric methylene bending mode is most intense with the incident electric vector perpendicular to the fiber axis, the symmetric methylene stretch is also expected to be most intense in the perpendicular mode. In contrast, the antisymmetric stretch should be most intense in the parallel mode. The 2965 cm^{-1} band is most intense when the incident electric vector is parallel to the fiber axis and is a plausible frequency for a CH_2 antisymmetric stretching mode.

The 2941 cm^{-1} band is also at approximately the right frequency for CH_2 antisymmetric stretching. This band was classified as a B_0 mode based on Valonia data and as a B_{90} mode based on the ramie data. Since the 2941 cm^{-1} band is more clearly resolved in the Valonia spectra, the Valonia data provide a more reliable classification for this mode. Therefore, the 2941 cm^{-1} mode

appears to have the proper sensitivity to the polarization of incident light for a CH_2 antisymmetric stretching mode. It is likely then that both the 2941 and 2965 cm^{-1} bands are CH_2 antisymmetric modes. This assignment is supported by the observation of two distinct CH_2 bending peaks between 1450 and 1480 cm^{-1}. In addition, adjacent methylene groups are thought to be nonequivalent in the cellulose I and equivalent in cellulose II.[50-51] The spectra of cellulose II exhibit a single peak in the antisymmetric methylene stretching and methylene bending regions.

Since there are several modes other than the methine stretching band that are most intense when the incident electric vector is perpendicular to the chain axis, the symmetric CH_2 stretching mode is more difficult to identify. As mentioned above, the 2868 cm^{-1} band is a B_{90} mode. The 2848 and 2904 cm^{-1} bands were classified as B_{90} bands based on the Valonia data, but they were not resolved in the ramie spectra. Since the symmetric CH_2 stretching frequency is usually at least 100 cm^{-1} lower than the antisymmetric stretching frequency, either or both of the 2848 and 2868 cm^{-1} bands are most likely the CH_2 symmetric stretching modes.

In previous studies, Tsuboi[24] resolved three CH bands in infrared spectra recorded from ramie cellulose. The most intense band at 2907 cm^{-1} exhibited perpendicular dichroism. This band was assigned to the methine CH stretching vibrations. Two parallel bands at 2853 and 2967 cm^{-1} were assigned as the symmetric and antisymmetric CH_2 stretching modes, respectively. Liang and Marchessault[25] recorded spectra from more crystalline specimens of Valonia and bacterial celluloses and were able to resolve 7 CH bands. They assigned the parallel band at 2853 as the symmetric CH_2 stretch and the perpendicular band at 2945 cm^{-1} as the antisymmetric stretch. The rest of the bands were assigned to

methine stretching including the parallel band at 2970 cm^{-1}. Blackwell, et al.[28] recorded infrared and Raman spectra from Valonia cellulose. Their assignments agree with those given by Liang and Marchessault.

3200-3500 cm^{-1} Region

Between 3200 and 3500 cm^{-1}, the Raman spectra of Valonia and ramie contain several closely spaced medium intensity bands. In the infrared spectra of native celluloses, the band frequencies are similar but the bands are much more intense.[18,24-28] The bands are strongly deuteration sensitive. The normal coordinate calculations predict that the O-H stretching vibrations occur in this region. As was the case with the CH motions, the OH motions are isolated from the other internal motions of the cellulose molecule. Hydroxyl stretching motions, however, can couple with lattice modes due to their involvement in intermolecular hydrogen bonds. Since normal coordinate calculations are based on an isolated molecule approximation, they cannot predict the coupling of lattice modes with internal modes in this region.

All of the bands were found to be most intense when the electric vector of the incident light was parallel to the fiber axis, suggesting that the O-H groups are oriented predominantly parallel to the chain axis. The bands are not clearly resolved, however, so it is possible that some of the bands might be more intense with the electric vector perpendicular to the chain axis. In the literature, the bands in this region have also been assigned as OH stretching vibrations.

The frequencies of the OH stretching bands in the spectra of Valonia differ significantly from those in the spectra of ramie. These differences are related to the different hydrogen bonding patterns found in Valonia and ramie celluloses, which will be discussed in the next chapter.

CONCLUSIONS

This study has generated new information for interpreting the vibrational spectrum of cellulose. Spectra of deuterated celluloses allowed the OH and CH vibrations to be identified. Prior normal coordinate analyses of cellulose model compounds together with the spectra of deuterated cellulose enabled us to identify the types of vibrational motion responsible for most of the bands. We found good agreement between the predictions of the model compound studies and the OH and CH motions identified by the study of deuterated celluloses. Although our assignments agree qualitatively in most cases with the motions predicted by traditional group frequency assignments, the vibrational motions are much more complex than was recognized in the group frequency assignments.

The relationships between the band intensities and the polarization of the incident light indicated the direction of the major change in the polarizability associated with the vibrational modes. For many of the bands, this study revealed the direction of the motions relative to the chain axis. The intensity study together with the study of deuterated celluloses provides a more thorough characterization of the Raman spectrum of cellulose than has been possible in previous studies.

The data establishes a basis for future Raman microprobe studies of native tissues. In our study of cellulose polymorphy described in Chapter II, the assignments were used to identify the structural differences between cellulose polymorphs. In Chapter III, the directional character of the vibrations was used to study cellulose orientation. In future Raman microprobe studies of woody tissues, the spectra will contain a complex composite of bands from cellulose, hemicellulose, and lignin. The information generated in this study will

simplify the interpretation of these composite spectra by helping us to identify those bands which are associated solely with the cellulose component.

CHAPTER II. POLYMORPHY IN CELLULOSE FIBERS

INTRODUCTION

Cellulose exists in at least four polymorphic forms, each of which yields a distinct x-ray pattern.[38-39,48] The two forms that are most common are celluloses I and II. Cellulose I, which is generally referred to as native cellulose, is found in the cell walls of many plants and is produced by some bacteria and aquatic animals. Cellulose II is prepared by mercerizing native cellulose or by regenerating cellulose from solution.

Although celluloses I and II have been studied extensively, the basic structures and differences between the polymorphs are not fully understood. In the present study, Raman spectroscopy was used as a tool to study polymorphy in cellulose fibers. The Raman spectra of fibers having different polymorphic compositions were compared. The differences observed in the Raman spectra were found to provide insight into the structures of the celluloses.

BACKGROUND

The two major polymorphic forms of cellulose, cellulose I and cellullose II, have been studied using a variety of different techniques. Based primarily on x-ray diffractometric evidence, Blackwell et al.,[55-56] Sarko et al.,[57-58] and others[39-40,48] proposed structures for cellulose I and cellulose II in which it is assumed that cellulose possesses a twofold screw axis of symmetry parallel to the cellulose chain axis. This assumption severely restricts the conformations of the cellulose backbone because each anhydroglucose residue must be rotated by 180° relative to adjacent residues. The only conformational degree of freedom left is the rotational positions of the methylene groups. In these models, the conformation of the cellulose backbone is the same in cellulose I and cellulose II. The differences between the polymorphs lie in the way the chains are packed into lattices, the hydrogen bonding patterns, and the rotational conformations of the methylene groups.

The evidence for the twofold screw axis is not conclusive and several researchers have questioned the validity of this assumption.[39,48-51] The backbone conformations possessing the twofold screw conformation are thought to be sterically unfavorable because of repulsive interactions between the methine hydrogens attached to the carbons involved in the glycosidic linkage.[39,48,50,59-60]

Based on Raman and NMR spectroscopic evidence and conformational energy calculations, Atalla[50-51] proposed a model in which cellulose I and cellulose II possess different backbone conformations. In this model, adjacent anhydroglucose units are nonequivalent. Therefore, the cellulose chain does not possess the twofold helix conformation assumed in earlier models. The glucosidic linkages alternate between small left-handed and right-handed departures from the

twofold helix conformation such that anhydrocellobiose is the repeat unit instead of anhydroglucose.

The differences between the conformations of cellulose I and cellulose II are centered at the glycosidic linkages and the methylene positions as shown in Fig. 27. In cellulose I, adjacent methylene groups are nonequivalent, whereas the methylenes are all approximately equivalent in cellulose II. Secondly, the degree of nonequivalence between adjacent anhydroglucose units is greater in cellulose II than in cellulose I. The nonequivalence of the methylenes in cellulose I and the greater degree of nonequivalence between anhydroglucose units in cellulose II is a result of different hydrogen bonding patterns in cellulose I and cellulose II. In cellulose I every other C-6 hydroxyl participates in a bifurcated intramolecular hydrogen bond, whereas all of the hydrogen bonds in cellulose II are isolated.

The conversion of cellulose I to cellulose II involves the removal of the C-6 hydroxyl from the bifurcated intramolecular hydrogen bond. This allows the glycosidic linkages to relax into more distinct positions and permits the methylene groups to move into approximately equivalent positions. This model has been gaining acceptance among cellulose scientists as the most plausible model for the differences between celluloses I and II.

The question of polymorphy within the cellulose I family has not received as much attention as the differences between celluloses I and II. Evidence has been reported, however, that the structure of native cellulose varies depending on the source. Early x-ray studies of cotton, ramie, linen, algal cellulose, and bacterial cellulose detected significant differences in the unit cell parameters.[62] Based on electron diffractograms, Honjo and Watanabe[63] and

others[49,64-65] concluded that the unit cell of algal cellulose is larger and has lower symmetry than the commonly accepted cell for cellulose I. Marrinan and Mann[66-67] and later Liang and Marchessault[25] observed that the infrared spectra of algal and bacterial cellulose differ from the spectra of ramie.

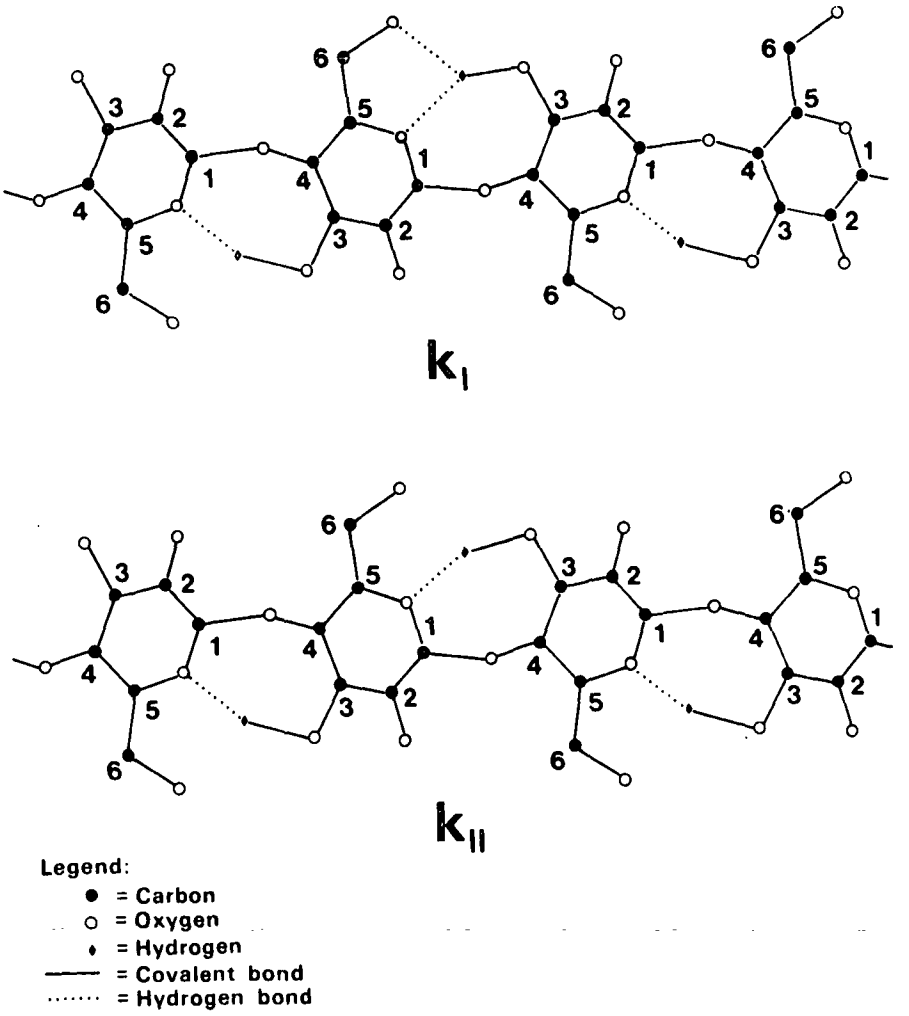

Figure 27. The different molecular conformations proposed for celluloses I and II.

More recently, Atalla and VanderHart[53,68] have studied the solid-state ^{13}C NMR spectra of several forms of native cellulose. They concluded that native celluloses appeared to be a composite of two distinct crystalline forms of

cellulose called I_α and I_β. The proportions of I_α and I_β in the composite varies depending on the source of the cellulose. In algal and bacterial cellulose, the I_α form dominates whereas the I_β form dominates in ramie, cotton, and wood pulp. These results are consistent with the data from diffractometry and infrared spectroscopy in that algal and bacterial cellulose are similar to each other but different from other native celluloses.

The structural differences between I_α and I_β are not understood yet. Atalla[68] compared the Raman spectra of various native celluloses with different I_α to I_β ratios. He also compared the native cellulose spectra with the spectrum of cellulose II. The spectra of the native celluloses are all similar to each other in the region most sensitive to cellulose conformation. The spectrum of cellulose II is quite different in this region. Therefore, Atalla concluded that celluloses I_α and I_β have the same conformation but are packed in different lattices. In cellulose II, both the conformation and lattice are different from that of cellulose I.

Other workers[69-70] have interpreted these differences in the NMR spectra in alternative ways. They believe that the differences within the cellulose I family are derived from the size of the unit cells. Valonia contains a larger 8 chain unit cell, whereas ramie contains a mixture of the 8 chain unit cell and the smaller Meyer and Misch unit cell.[70] Therefore, the interpretation of the NMR spectra remains controversial.

EXPERIMENTAL

CELLULOSE SAMPLES

The cellulose I samples that were compared were Valonia fibrillar aggregates and ramie fibers. The source and preparation of these celluloses are described in the previous chapter. The cellulose I samples were compared with a cellulose II sample prepared by mercerizing ramie fibers. The preparation procedure for mercerized ramie fibers is as follows:

1) An aqueous solution of 30% sodium hydroxide was prepared by dissolving 30 grams of sodium hydroxide in 70 grams of distilled water in a polyethylene beaker under nitrogen. The beaker was cooled in an ice bath. After the sodium hydroxide had dissolved, nitrogen was bubbled through the solution for an additional 10 minutes. The sodium hydroxide solution was used immediately after it was prepared.

2) The sodium hydroxide solution was added to the ramie fiber in a glove bag under nitrogen. 0.2 Gram of fiber was placed in a polyethylene bottle and 30 milliliters of sodium hydroxide solution was added. The bottle was sealed and placed inside a glass jar which was also sealed. The fiber slurry was stored at room temperature.

3) After 25 hours, the sodium hydroxide solution was filtered off on a coarse glass filter funnel and the fibers were washed with 2 liters of distilled water.

4) The sample was washed with DTPA and distilled water and then freeze-dried.

5) Fibers were prepared for the microprobe by rewetting and then drying under tension as described in the previous chapter. The fibers were mounted on small washers with Duco cement.

INSTRUMENTAL

X-Ray Diffraction

The acquisition of x-ray patterns from purified Valonia and ramie cellulose is described in the previous chapter. A diffractogram was recorded from

mercerized ramie using the same sample preparation and instrumental settings that were used to record diffractograms from the Valonia and native ramie samples.

Raman Microprobe

A series of spectra were recorded from the Valonia fibrillar aggregate and the native ramie, and mercerized ramie fibers in which the angle between the electric vector of the incident light and the fiber axis was varied from 0 to 90° in 15 degree increments. The acquisition of the spectra from the Valonia fibrillar aggregates and native ramie fibers is described in the previous chapter. The spectra from the mercerized ramie fibers were recorded using the same basic procedures, but some modifications were necessary because the mercerized fibers were very prone to burning under the laser beam. First, the laser power incident on the sample was reduced to 1-2 mW. Second, a stream of nitrogen was directed on the sample. Since the laser power was so low, it was necessary to increase the acquisition time from 8 to 12 hours. The spectra were noisier than the Valonia and native ramie spectra but still were acceptable.

EXPERIMENTAL RESULTS

X-RAY DIFFRACTOGRAMS

The x-ray diffractograms of Valonia and native ramie celluloses are shown in Fig. 5 and 6, respectively, in the previous chapter. The x-ray diffractogram of mercerized ramie is shown in Fig. 28.

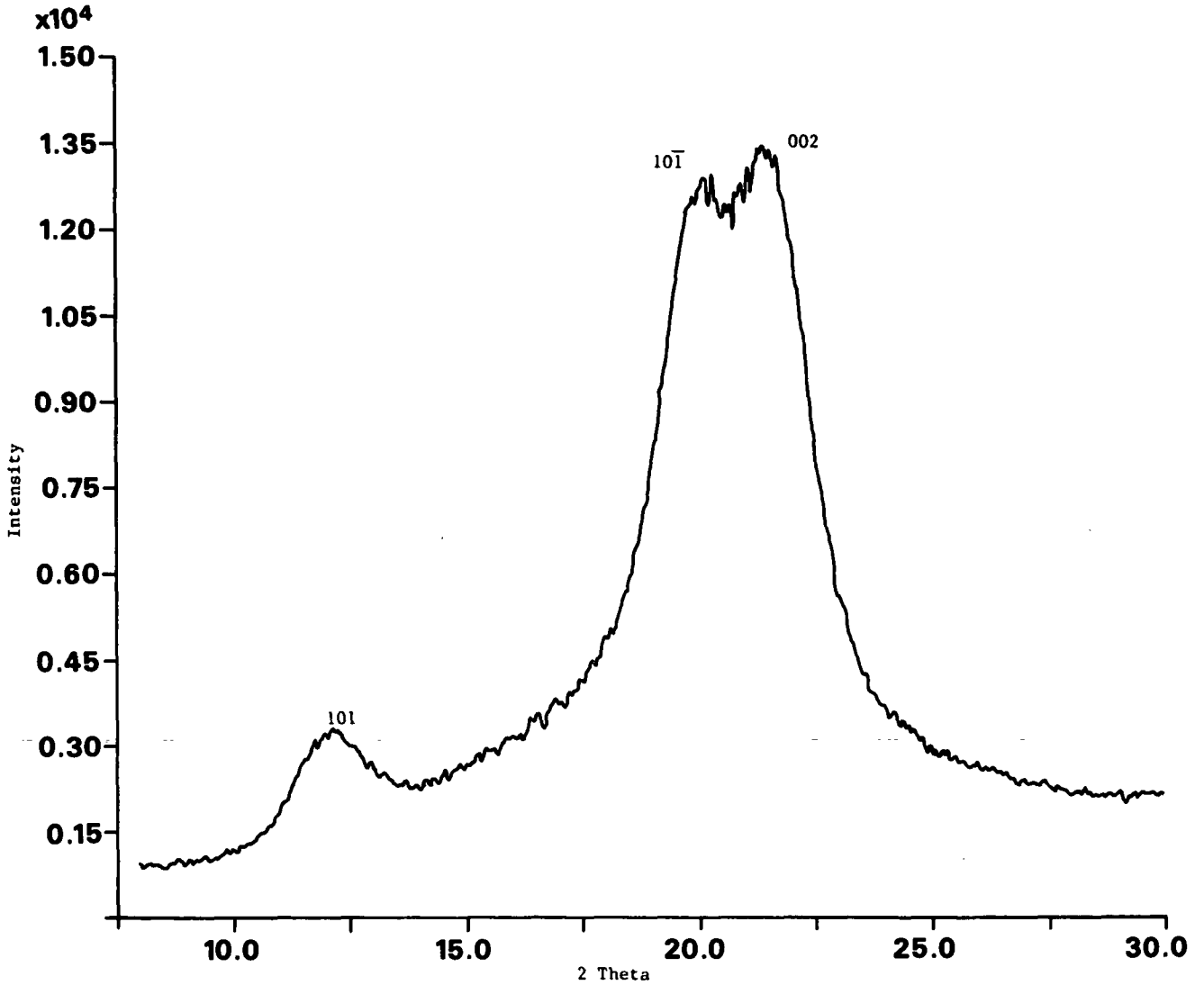

Figure 28. X-ray diffractogram of mercerized ramie.

RAMAN SPECTRA

Raman spectra of the Valonia fibrillar aggregate and the native ramie fiber in which the angle between the incident electric vector and the fiber axis was varied from 0 to 90° are shown in Fig. 13 and 14, respectively. The Raman spectra of a mercerized ramie fiber in which the angle between the incident electric vector and the fiber axis was varied are shown in Fig. 29.

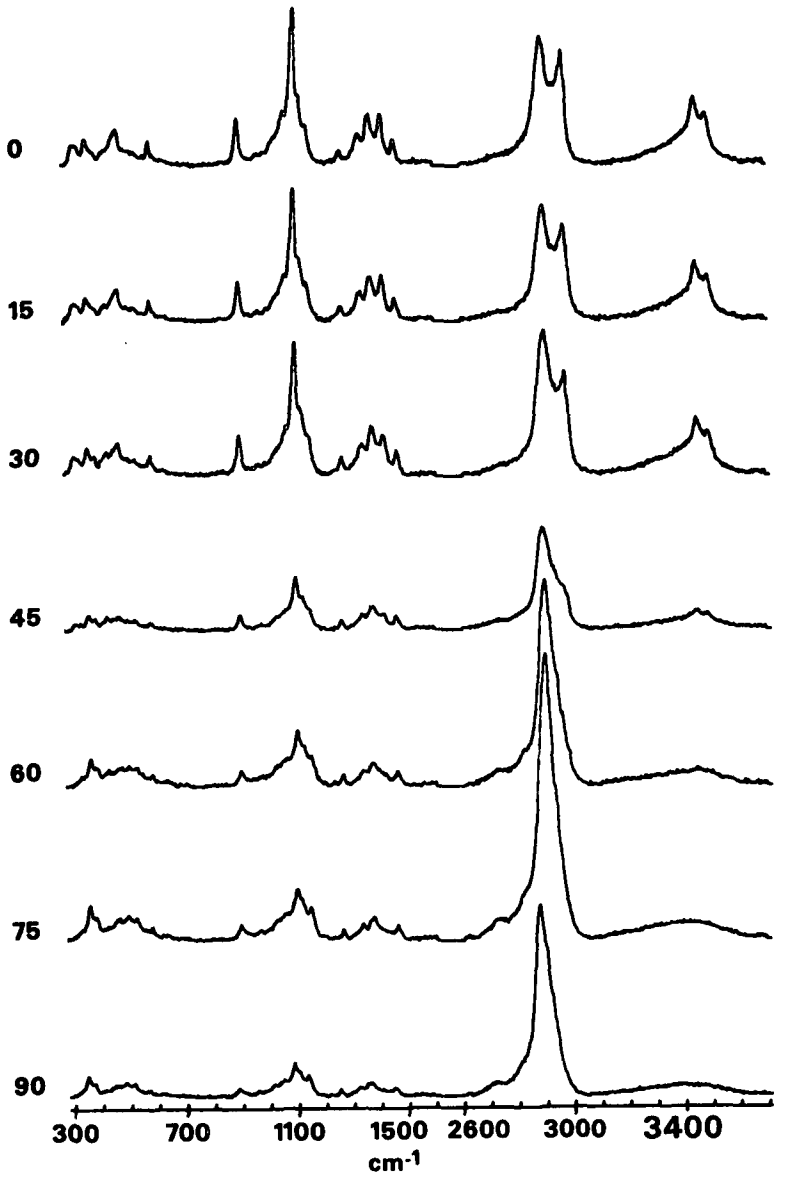

Figure 29. Polarized Raman spectra of a mercerized ramie fiber. θ was varied from 0 to 90°.

DISCUSSION

SAMPLE CHARACTERIZATION

Native cellulose samples were characterized by carbohydrate analysis, x-ray diffraction, electron microscopy, and Raman spectroscopy as discussed in the previous section. The characterization methods showed that the samples were pure cellulose I in which the molecules are oriented parallel to the fiber axis.

The d-spacings calculated from the x-ray pattern of mercerized ramie (see Fig. 28) are: d_{101} = 7.27 Å, $d_{10\bar{1}}$ = 4.51 Å, and d_{002} = 4.12 Å. These values are consistent with values reported in the literature.[37-40] The relative heights of the $10\bar{1}$ and 002 diffraction peaks indicate that although the sample is not completely converted to cellulose II, the degree of conversion is high. Since the diffraction peaks are broad, the lateral dimensions of the cellulose II crystallites must be small. Furthermore, the curved background suggests that a substantial amount of amorphous cellulose is present.

The Raman spectra recorded from the mercerized ramie fiber (see Fig. 29) exhibit the same bands as spectra of cellulose II reported in the literature.[50-51] Therefore, the spectra in Fig. 29 are representative of the cellulose II polymorph. Similar to the cellulose I spectra, the bands in the spectrum of mercerized ramie are strongly dependent on the angle between the incident electric vector and the chain axis.

COMPARISON OF CELLULOSE FIBERS

Cellulose polymorphy was studied by comparing the Raman spectra of the Valonia fibrillar aggregate and the native ramie, and mercerized ramie fibers with the electric vector of the incident light parallel and perpendicular to the

fiber axis (see Fig. 30-31). As discussed above, the mercerized ramie is predominantly cellulose II while the Valonia and native ramie are cellulose I. Solid state ^{13}C NMR spectra indicate that the I_α form predominates in Valonia while the I_β form predominates in ramie.[53,68] Therefore, the structural differences between both celluloses I_α and I_β and celluloses I and II can be studied by investigating the differences in the Raman spectra of these celluloses. In principle, cellulose II can also be prepared from Valonia cellulose but only cellulose II from ramie was examined due to the resistance of Valonia cellulose to mercerization.[71-72]

The spectra were divided into two regions. The region below 1600 cm^{-1} (Fig. 30) is most sensitive to the conformation of the cellulose backbone (especially below 700 cm^{-1}). The higher frequency region, above 2700 cm^{-1} (Fig. 31), is more sensitive to hydrogen bonding. In the low frequency region (Fig. 30), there are only minor differences between the spectra of native ramie and Valonia. The peaks in the Valonia spectra are narrower and better resolved. The reason for this is probably the larger size of the crystallites in Valonia cellulose.[41-42] When the crystallites are larger, the environment of the molecules is more homogeneous. Therefore the vibrational energy of the molecules is more uniform, resulting in narrower bands.

The most significant difference between the two native cellulose spectra in the low frequency region is that the intensity of the peak at 913 cm^{-1} is greater in the ramie spectra. This peak is also more intense in the spectrum of bacterial cellulose than in the Valonia spectra.[68] Since bacterial cellulose has approximately the same I_α and I_β ratio as Valonia[53], the intensity of this peak does not appear to be related to structural differences between I_α and I_β.

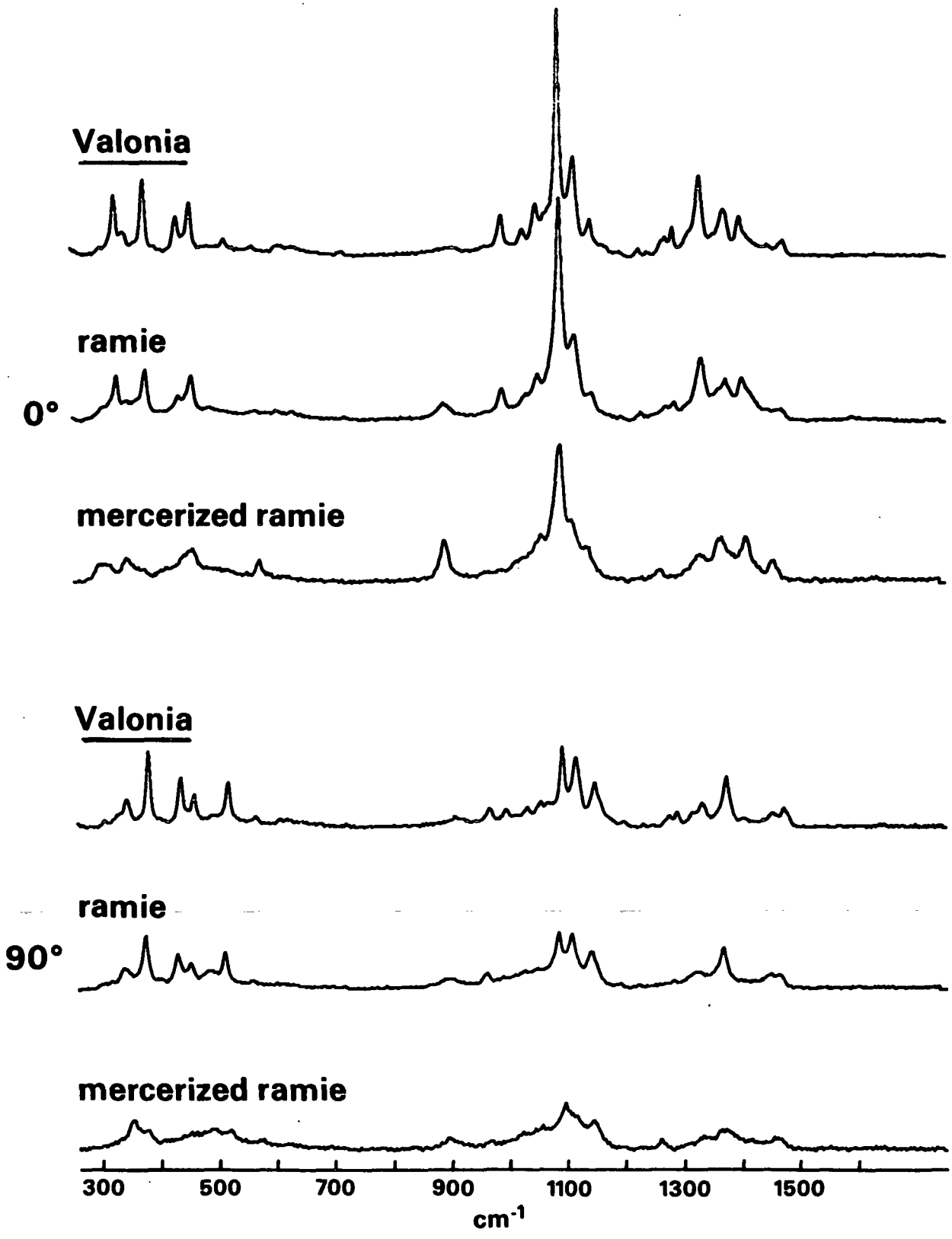

Figure 30. Comparison of the Raman spectra of Valonia, ramie, and mercerized ramie (low frequency region).

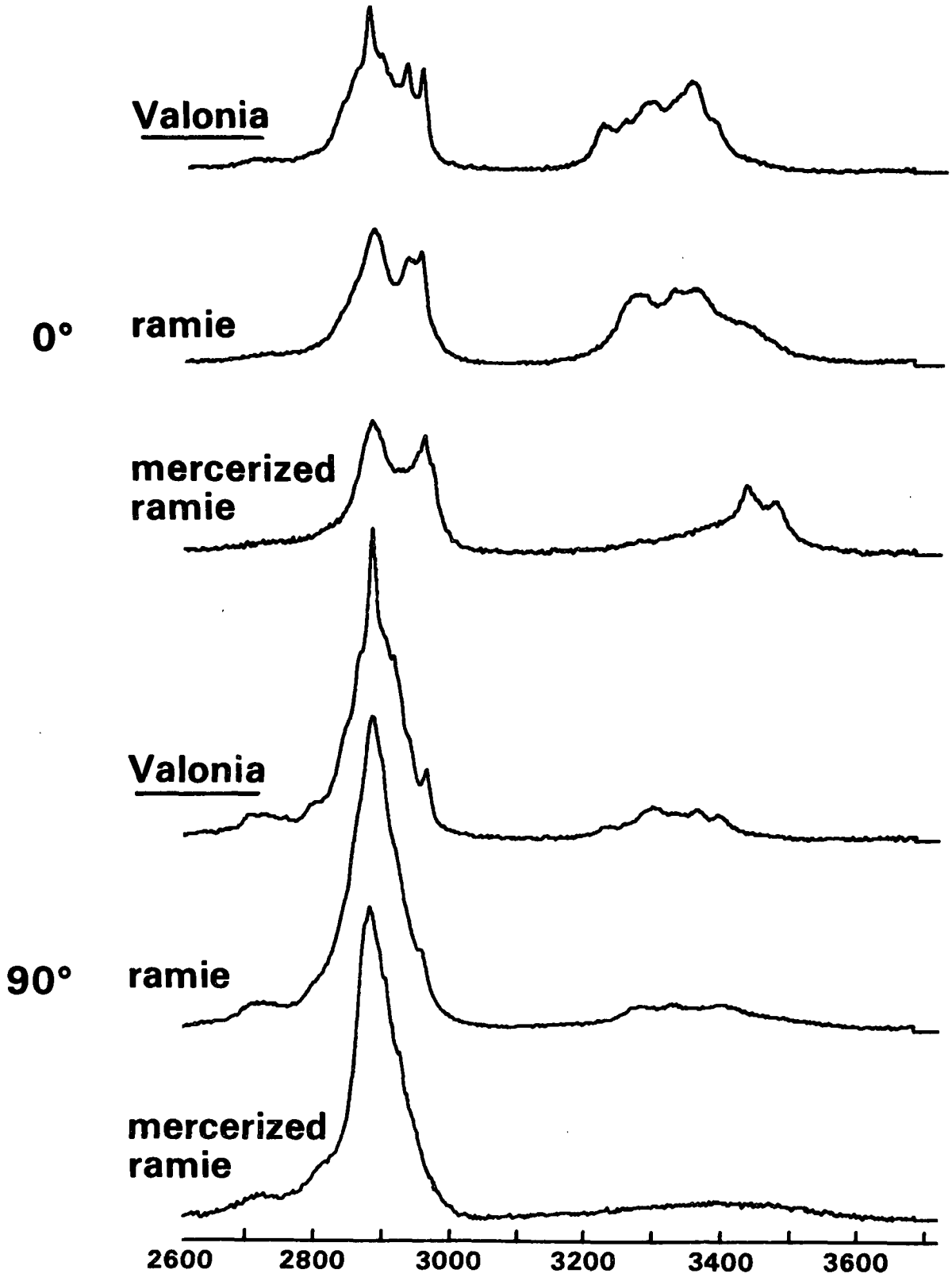

Figure 31. Comparison of the Raman spectra of Valonia, ramie, and mercerized ramie (high frequency region).

As mentioned in the previous chapter, the intensity of 913 cm^{-1} appears to be inversely related to the size of the crystallites. It is very weak in the spectra of Valonia, which has very large crystallites, but it is stronger in the spectra of ramie and bacterial cellulose, which both have smaller crystallites.[41-42]

The differences between the spectra of ramie and Valonia are quite small compared to the differences between native cellulose and cellulose II (see Fig. 31). Below 700 cm^{-1}, the band frequencies, the number of peaks, and the dependence of the band intensities on θ in the cellulose II spectra differ significantly from the cellulose I spectra. In the previous chapter, it was shown that the region below 700 cm^{-1} is most sensitive to the conformation of the cellulose backbone. Therefore, the differences between the spectra of cellulose I and cellulose II provide evidence for different backbone conformations in these polymorphs.

The spectral differences which are indicative of conformational change are not observed in the spectra of ramie and Valonia. Since ramie and Valonia have different I_α to I_β ratios, it would appear that cellulose I_α and I_β must have the same molecular conformations.

In the C-H stretching region (Fig. 31, 2700-3000 cm^{-1}), the primary difference between the spectra of ramie and Valonia is the broadness of the peaks. As found in the low frequency region, the peaks in the ramie spectra are broader, presumably due to the smaller size of the ramie crystallites. In the spectra of mercerized ramie, only one antisymmetric CH_2 stretching peak is observed (2930-2970 cm^{-1}), whereas two distinct peaks are observed in the spectra of the native celluloses. The splitting of the methylene stretching peak in the cellulose I spectra probably reflects the nonequivalence of adjacent methylene groups.

Conversely, the equivalent methylenes in cellulose II result in a single methylene stretching band. In both the native and mercerized cellulose spectra, the intensities of C-H stretching bands appear to exhibit the same dependence on θ.

In the O-H stretching region (3200-3600 cm^{-1}), however, significant differences are observed in the spectra of all three celluloses. These differences are most prominent in the spectra recorded with the electric vector parallel to the fiber axis (Fig. 31a-c). The frequencies as well as the broadness of the peaks vary in this region. The spectra of Valonia cellulose have peaks between 3230 and 3270 cm^{-1} that are not observed in the ramie spectra. The spectra of native ramie on the other hand, have peaks above 3400 cm^{-1} that are not observed in the Valonia spectra. The spectrum of mercerized ramie recorded with the electric vector parallel to the fiber axis has two sharp peaks at frequencies above those observed in the native celluloses. These band patterns observed in the O-H stretching regions are consistent with the patterns observed in infrared spectra of Valonia, ramie, and mercerized cellulose reported in the literature.[25,67]

The differences in the O-H region between Valonia, ramie, and mercerized ramie suggest that the hydrogen bonding patterns are different in each of these celluloses. Since ramie and Valonia contain different ratios of cellulose I_α to cellulose I_β, the results imply that celluloses I_α and I_β possess different hydrogen bonding patterns. Furthermore, the peaks between 3230 and 3270 cm^{-1} which are present in the Valonia spectra but not in the ramie spectra suggest that cellulose I_α contains stronger hydrogen bonds than cellulose I_β. This hypothesis is consistent with the fact the Valonia cellulose is much more resistant to mercerization than ramie cellulose.[1,71-72]

CONCLUSIONS

A comparison of the Raman spectra of Valonia, ramie, and mercerized ramie indicates that the conformation of the cellulose backbone is similar in Valonia and ramie, but is different in mercerized ramie. The hydrogen bonding patterns, however, are different in Valonia and native ramie as well as in mercerized ramie. The results imply that cellulose I_α and cellulose I_β have similar molecular conformations, but have distinct hydrogen bonding patterns. In cellulose II, the molecular conformation as well as hydrogen bonding pattern differs from that in cellulose I.

CHAPTER III. MOLECULAR ORIENTATION IN CELLULOSE FIBERS

INTRODUCTION

Molecular orientation influences the physical and chemical properties of fibers. The basic cellulosic building blocks in the plant cell wall are fibrils.[1,2] Within the threadlike fibrils, the cellulose chains are oriented parallel to the fibril axis. The fibrils are oriented parallel to each other and at a particular angle to the fiber axis in the bulk of the cell wall. Much less is known about the orientation of cellulose in the plane perpendicular to the chain axis, since this orientation has not been thoroughly studied except in the case of the algae.

In the present study, cellulose orientation in the plane perpendicular to the chain axis was studied with the Raman microprobe. Spectra recorded with different polarizations of the incident light relative to the sample morphology were compared. Since band intensities depend on the orientation of the electric vector of the incident light relative to the molecules, these spectra provide information about cellulose orientation.

BACKGROUND

In algal celluloses, the evidence from x-ray and electron diffraction indicates that the cellulose is arranged nonrandomly in the plane perpendicular to the chain axis.[1-2,73-79] Early on, Preston[1,75] conducted a detailed study of the architecture in the cell wall of Valonia ventricosa using x-ray diffraction and electron microscopy. The Valonia cell wall was found to have a highly ordered multilayered structure. Preston termed the basic cellulosic units in the wall microfibrils. These microfibrils are rectangular crystallites of cellulose, approximately 200 Å wide and 120 Å thick.

Preston found that the microfibrils are aligned parallel to each other within a given layer of the Valonia cell wall. The fibrils in adjacent layers lie at roughly right angles. Occasionally a third orientation of the fibrils was observed which was 45° to the two predominant fibril orientations. This cross-fibrillar type of cellulose orientation has been found to be very common in the algae.[1]

To account for the x-ray data, Preston proposed the model shown in Fig. 32 in which there are two distinct orientations of the microfibrils in the plane perpendicular to the microfibril axis.[1] The microfibrils are oriented relative to each other so that the 002 planes in one set of microfibrils are perpendicular to the 002 planes in the other set. In both sets of microfibrils, the 101 planes are oriented preferentially parallel to the cell wall surface.

Revol and Goring[79] recently confirmed Preston's model. Based on an electron diffraction study of single microfibrils in the Valonia cell wall, they concluded that the crystallites within a single microfibril are all oriented the same way. The microfibrils therefore approximate single crystals. The 002

planes in adjacent microfibrils within the same layer of the cell wall are perpendicular to each other. Since the orientation of the 002 planes alternates from microfibril to microfibril, the type of cellulose orientation found in Valonia will be referred to as alternating orientation.

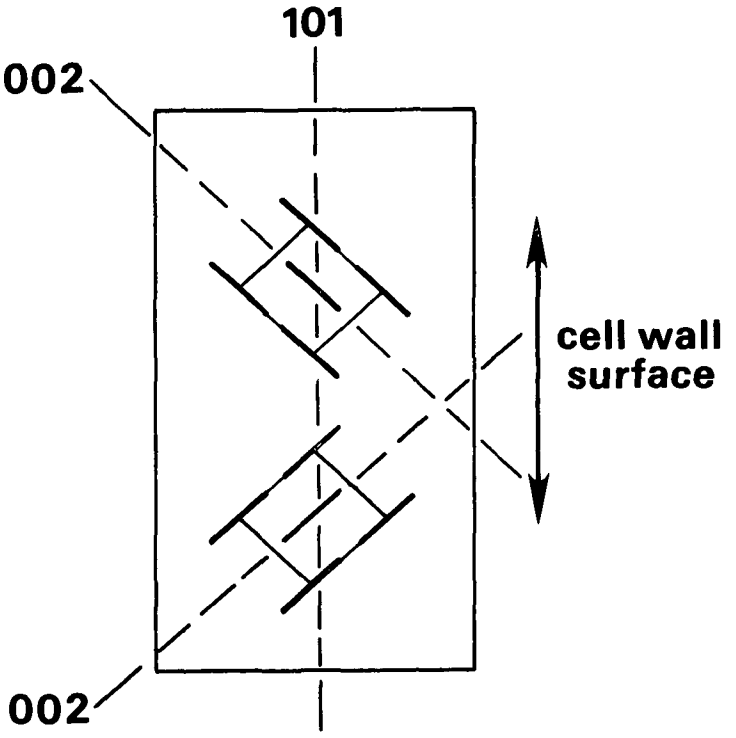

Figure 32. The alternating crystallite orientation found in algal celluloses.[1]

Measurements of cellulose orientation in fibers from higher plants have yielded conflicting results. Revol, et al.[80] studied the orientation of cellulose crystallites in spruce and birch wood cell walls by electron and x-ray diffraction. They concluded that the cellulose crystallites are arranged randomly in the plane perpendicular to the fiber axis.

Tanaka and coworkers[81-83] used x-ray diffraction to study the three-dimensional orientation distribution of cellulose crystallites in tension, compression, and normal wood. In tension wood, the cellulose crystallites were oriented with the chain axes nearly parallel to the fiber axis. The crystallites appeared to be oriented randomly in the plane perpendicular to the fiber axis. In normal wood, the chain axes are oriented at an angle to the fiber axis. The crystallites exhibited a small degree of preferred orientation in the plane perpendicular to the chain axis. In compression wood, the angle between the chain axes and the fiber axis is larger and the degree of preferred orientation in the plane perpendicular to the fiber axis is larger. The authors hypothesized that the orientation is influenced by the amount of uniaxial stretching that occurs during fiber growth.

The interpretation of the x-ray diagrams from wood is complicated by the fact that many fibers lie in the beam. The domains being analyzed may contain more than one cell type. Furthermore, the cross sectional shape of the fibers is in between circular and rectangular. These morphological factors can influence the x-ray patterns. Therefore, the x-ray studies are not conclusive.

Atalla et al.[43] recorded Raman spectra of individual cotton fibers using polarized light. In these experiments, the domain from which spectra were recorded included the entire fiber cross section. A point was found along the fiber axis where the skeletal stretching intensity with the incident electric vector parallel to the fiber axis was equal to the intensity with the vector perpendicular. This indicated that the fibril angle was approximately 45°. It was observed that even though the fibril angle was 45°, the C-H stretching intensity was still greater in the spectrum recorded with the electric vector

perpendicular to the fiber axis. Therefore, there appears to be a preferred orientation of the C-H bonds perpendicular to the fiber axis.

Atalla reasoned that if the C-H bonds are preferentially oriented perpendicular to the cell wall surface, the average C-H orientation over the circumference of the cell wall would be perpendicular to the fiber axis. The methines can be oriented perpendicular to the cell wall surface only if the cellulose is oriented nonrandomly in the plane perpendicular to the chain axis. In the unit cell of native cellulose, the methine C-H bonds are approximately perpendicular to the 002 plane. If the methine C-H bonds are oriented perpendicular to the cell wall surface, then the 002 planes must be parallel to the cell wall surface. Therefore, the cellulose orientation suggested by the Raman spectra of cotton fibers differs from the alternating orientation in the algae where the 101 planes are parallel to the cell wall surface.

In summary, the cellulose orientation in higher plant fibers is not well understood. Various diffraction studies of wood provide conflicting evidence about the cellulose orientation in the plane perpendicular to the chain axis. Raman studies of cotton suggest the orientation in this plane is nonrandom but that the orientation differs from that found in algal celluloses. Further study is deemed necessary to resolve these controversies.

THEORY

In order to investigate the cellulose orientation in the plane perpendicular to the fiber axis, spectra were recorded from ramie cross sections. The experiment is illustrated in Fig. 33. The angle between the electric vector of the incident light and the cell wall surface, θ, was varied from 0 to 90° in 45° increments. In this section, the relationship between the band intensities and θ will be derived for three different types of cellulose orientation. These are random orientation, alternating orientation, and orientation of the methines perpendicular to the cell wall surface. A comparison of the observed intensities with the intensities derived for each type of orientation will then be used to determine the cellulose orientation.

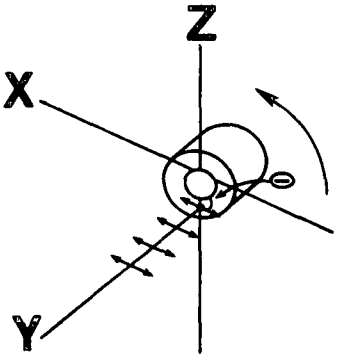

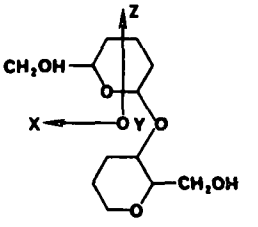

Figure 33. Diagram of cross section experiment and coordinate system definitions. XYZ = laboratory system, xyz = molecule based system.

We define xyz as the molecule based coordinate system and XYZ as the laboratory based coordinate system (see Fig. 33). The chain axis is parallel to the z axis, the methines are parallel to the y axis, and the plane of the anhydroglucose rings is parallel to the x axis. The Y coordinate axis is parallel to the z axis and δ is the angle between X and x. In the experiment depicted in Fig. 33, the incident beam is along the Y direction and the electric vectors of the incident and scattered beams are in the X direction. Therefore, the intensities will be proportional to the scattering activity, α^2_{XX}.

The dependence of the intensities on θ is found by relating α^2_{XX} to α_{xy}, the tensor components in the molecule based coordinate system. This is done by inserting the proper transformation matrix, Φ, into Eq. (6). For the coordinate systems described above, Φ will be given by:

$$\Phi = \begin{bmatrix} -\cos\delta & -\sin\delta & 0 \\ 0 & 0 & 1 \\ -\sin\delta & \cos\delta & 0 \end{bmatrix} \tag{18}$$

When Φ is substituted into Eq. (6), the following equation results for α^2_{XX}:

$$\begin{aligned} \alpha^2_{XX} = {} & \alpha^2_{xx}\cos^4\delta + 4\alpha_{xx}\alpha_{xy}\cos^3\delta\sin\delta + 2\alpha_{xx}\alpha_{yy}\cos^2\delta\sin^2\delta \\ & + 4\alpha^2_{xy}\cos^2\delta\sin^2\delta + 4\alpha_{xy}\alpha_{yy}\sin^3\delta\cos\delta + \alpha^2_{yy}\sin^4\delta \end{aligned} \tag{19}$$

In general, the angle δ depends both on the orientation of the molecules in XZ plane and on θ. If the cellulose orientation is random, however, δ will be independent of θ and take on all possible values between 0 and 360°. In this case the scattering activity, α^2_{XX}, is found by averaging Eq. (19) over all possible values of δ:

$$\alpha^2_{XX} = 1/8[2(\alpha_{xx} + \alpha_{yy})^2 + (\alpha_{xx} - \alpha_{yy})^2 + 4\alpha^2_{xy}] \quad (20)$$

The value of α^2_{XX} is independent of θ. Therefore, the intensities observed when the incident electric vector is parallel, perpendicular, and 45° to the cell wall surface should all be equal if the cellulose orientation is random in the XZ plane.

If the orientation of the cellulose crystallites alternates as shown in Fig. 32, δ will depend on both θ and orientation of the crystallites. When θ is either 0 or 90°, the incident electric vector is oriented at 45° relative to the plane of the anhydroglucose rings in both sets of crystallites. The scattering activity, α^2_{XX}, is determined by averaging Eq. (19) over all values of δ where the angle between the incident electric vector and the plane of the anhydroglucose rings is 45°:

$$\alpha^2_{XX} = 1/4[\alpha_{xx} + \alpha_{yy})^2 + 4\alpha^2_{xy}] \quad (21)$$

When θ is 45°, the incident electric vector will be parallel to the plane of the anhydroglucose rings in one set of crystallites and perpendicular to the ring planes in the other set of crystallites. The value of α^2_{XX} is determined by averaging Eq. (19) over all values of δ where the electric vector is either parallel or perpendicular to the ring planes:

$$\alpha^2_{XX} = 1/2(\alpha^2_{xx} + \alpha^2_{yy}) \quad (22)$$

Therefore, in the case of alternating orientation, the intensities recorded with the incident electric vector either parallel or perpendicular to the cell wall surface will be equal. In general, the intensities recorded with the electric vector at 45° to the wall surface will differ from the parallel and perpendicular intensities. Only when the scattering activities given by Eq.

(21) and (22) are equal can the intensities in all three modes be equal:

$$4\alpha^2_{xy} = 1/4(\alpha_{xx} - \alpha_{yy})^2 \tag{23}$$

Although Eq. (23) might be satisfied for some of the bands, it is unlikely that all intensities could be equal in the parallel, perpendicular and 45° modes if alternating orientation was present in the XZ plane.

If the methines are preferentially oriented perpendicular to the cell surface as appears to be the case in cotton fibers, δ will again depend on θ. When θ is 0°, the incident electric vector is parallel to the plane of the anhydroglucose rings. The value of α^2_{XX} is determined by averaging Eq. (19) over all values of δ where the electric vector is parallel to the ring planes. Similar arguments are used to derive α^2_{XX} when θ is 45 and 90°:

$$\theta = 0°;\ \alpha^2_{XX} = \alpha^2_{xx} \tag{24}$$

$$\theta = 45°;\ \alpha^2_{XX} = 1/4[(\alpha_{xx} + \alpha_{yy})^2 + 4(\alpha_{xy} + \alpha_{yy} + \alpha_{xx})\alpha_{xy}] \tag{25}$$

$$\theta = 90°;\ \alpha^2_{XX} = \alpha^2_{yy} \tag{26}$$

Thus, in the case of radial methine orientation, the intensities when θ is 0, 45, and 90° should all be different.

In summary, the cross section spectra can be used to distinguish different types of cellulose orientation in the plane perpendicular to the fiber axis. In the case of random orientation, the intensities will be the same for each orientation of the incident electric vector. For alternating orientation, the intensities recorded with the incident electric vector parallel and perpendicular to the cell wall will be equal, but intensities recorded with vector at 45° will be different. If the methines are oriented perpendicular to the cell wall surface, the intensities recorded with the electric vector parallel, perpendicular, and at 45° to wall will each be different.

EXPERIMENTAL

CELLULOSE SAMPLES

Ramie cross sections were prepared from freeze-dried ramie fibers that were purified by the procedure given in Chapter I. The sections were prepared by Mrs. Hilkka Kaustinen using the following method:

1) A bundle of fibers was pulled through a plastic straw in order to orient the fibers. Then the fibers were left in the straw and embedded in Spurr's resin.

2) Eight to ten microns thick cross sections were cut with the ultramicrotome.

3) The sections were mounted on albuminized microscope slides.

4) The resin was removed with Poly Solv.[a]

A sample of long-staple cotton was obtained from Dr. Victor Gentile. This sample had been purified by a procedure similar to that used for purifying algal celluloses[84] (see Chapter I). Spectra were recorded from both freeze-dried fibers and from fibers which were dried under tension using the device shown in Fig. 4 as described in Chapter I. Since the freeze-dried fibers are not constrained during the drying process, they will be referred to as freely dried fibers. The fibers were mounted on small washers using Duco cement.

INSTRUMENTAL

Raman spectra were recorded from ramie cross sections with the microprobe as outlined in Chapter I. A few modifications were made in the Chapter I procedures. An 80X objective (numerical aperture = 0.9), which has an approximately 1 micron resolution, was used. The laser power incident on the sample was

[a]Polysciences, Inc.

approximately 9 mW, and the acquisition time was 2 hours. Only spectra in which the electric vector of the scattered light was parallel to the electric vector of the incident light were recorded.

Raman spectra of individual cotton fibers were recorded with the conventional Raman spectrometer in the backscattering mode. The fiber was mounted so that its axis was perpendicular to the slits. An analyzer was used so that only the portion of the scattered light polarized parallel to the incident light was received by the monochromator. The laser power incident on the sample was 100 mW. The spectral slit width was 8 cm^{-1}. In the spectra of the freely dried fibers the acquisition time was 4 hours. The acquisition time for the tension-dried fibers was 2 hours. Other parameters were set as described in Chapter I.

The cotton fiber spectra were recorded from a domain where the average fibril angle is 45°. This was done by translating the fiber perpendicular to the slits until a region was found where the intensity ratio of the 1095 cm^{-1} peak to the 1123 cm^{-1} peak was equal, with the incident electric vector either parallel or perpendicular to the fiber axis.

EXPERIMENTAL RESULTS

Raman microprobe spectra of a ramie cross section recorded with the electric vector of the incident light parallel, perpendicular, and at 45° to the cell wall surface are shown in Fig. 34. Conventional Raman spectra from freely dried and tension-dried cotton fibers are shown in Fig. 35 and 36, respectively. The spectra were recorded with the electric vector of incident light parallel and perpendicular to the fiber axis. Each of the spectra contained a small amount of background fluorescence which was removed by the method described in Chapter I.

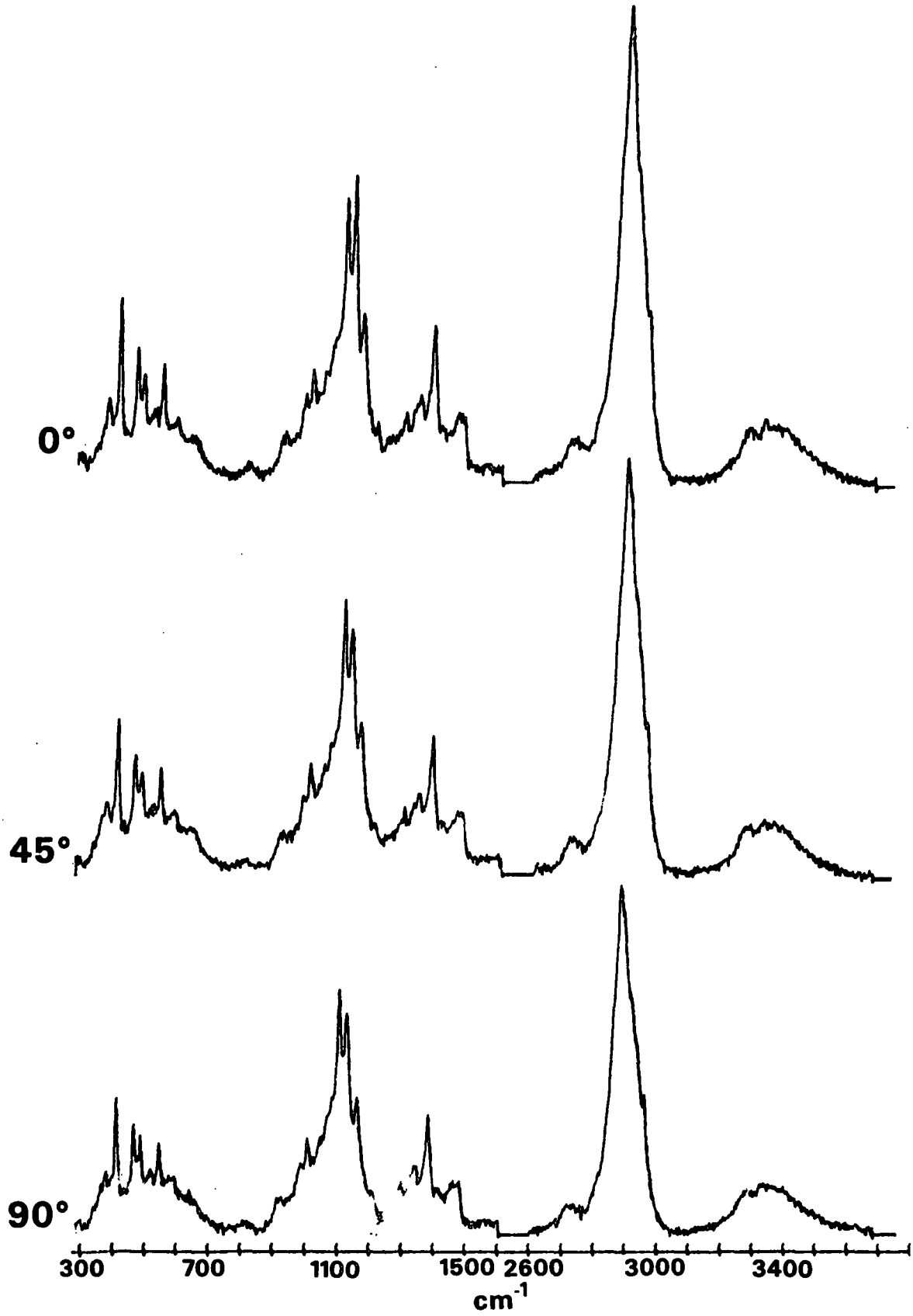

Figure 34. Polarized Raman spectra of a ramie cross-section. θ was varied from 0 to 90°.

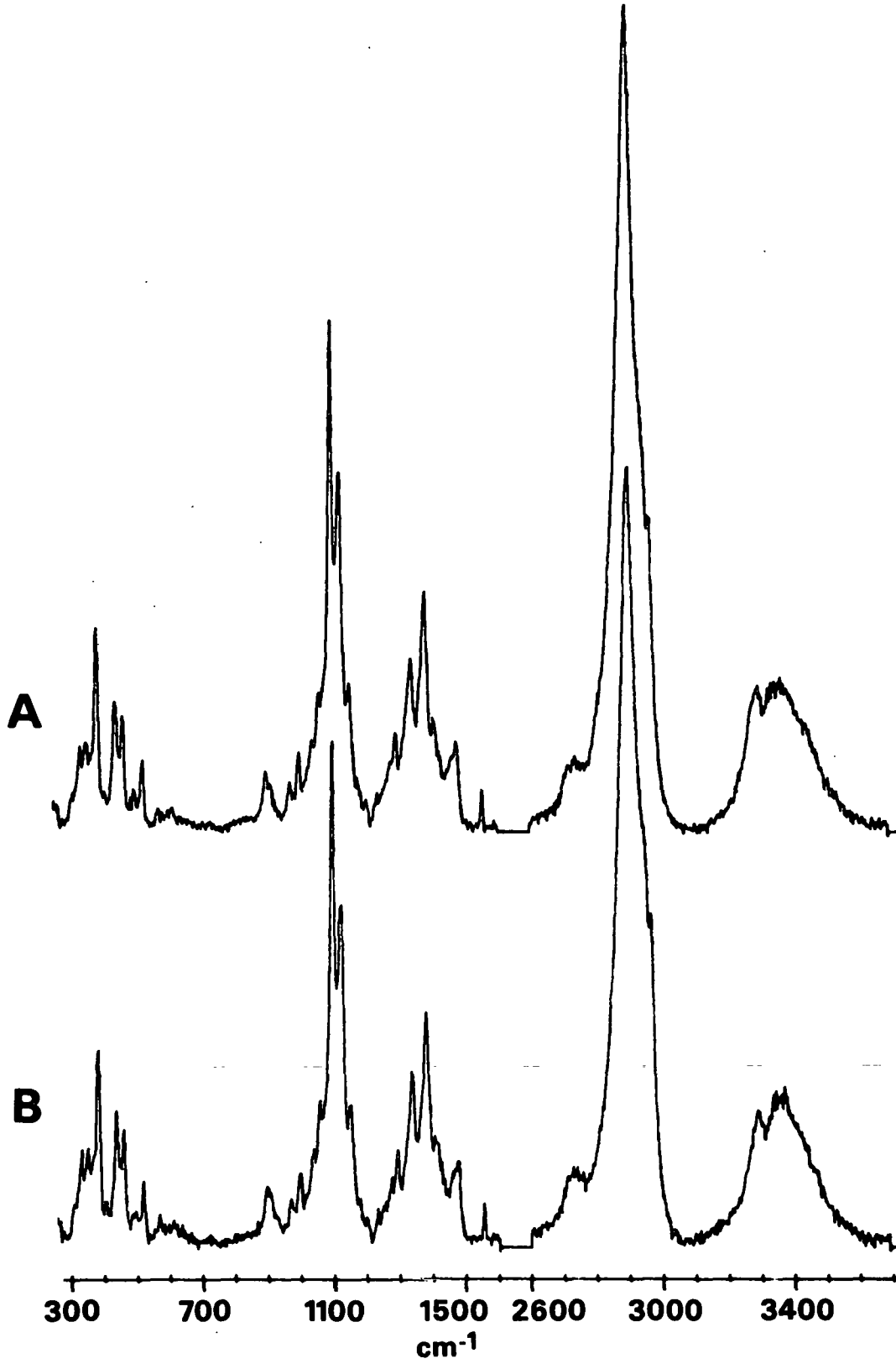

Figure 35. Polarized Raman spectra of a freely dried cotton fiber. A) electric vector parallel to fiber axis; B) electric vector perpendicular to fiber axis.

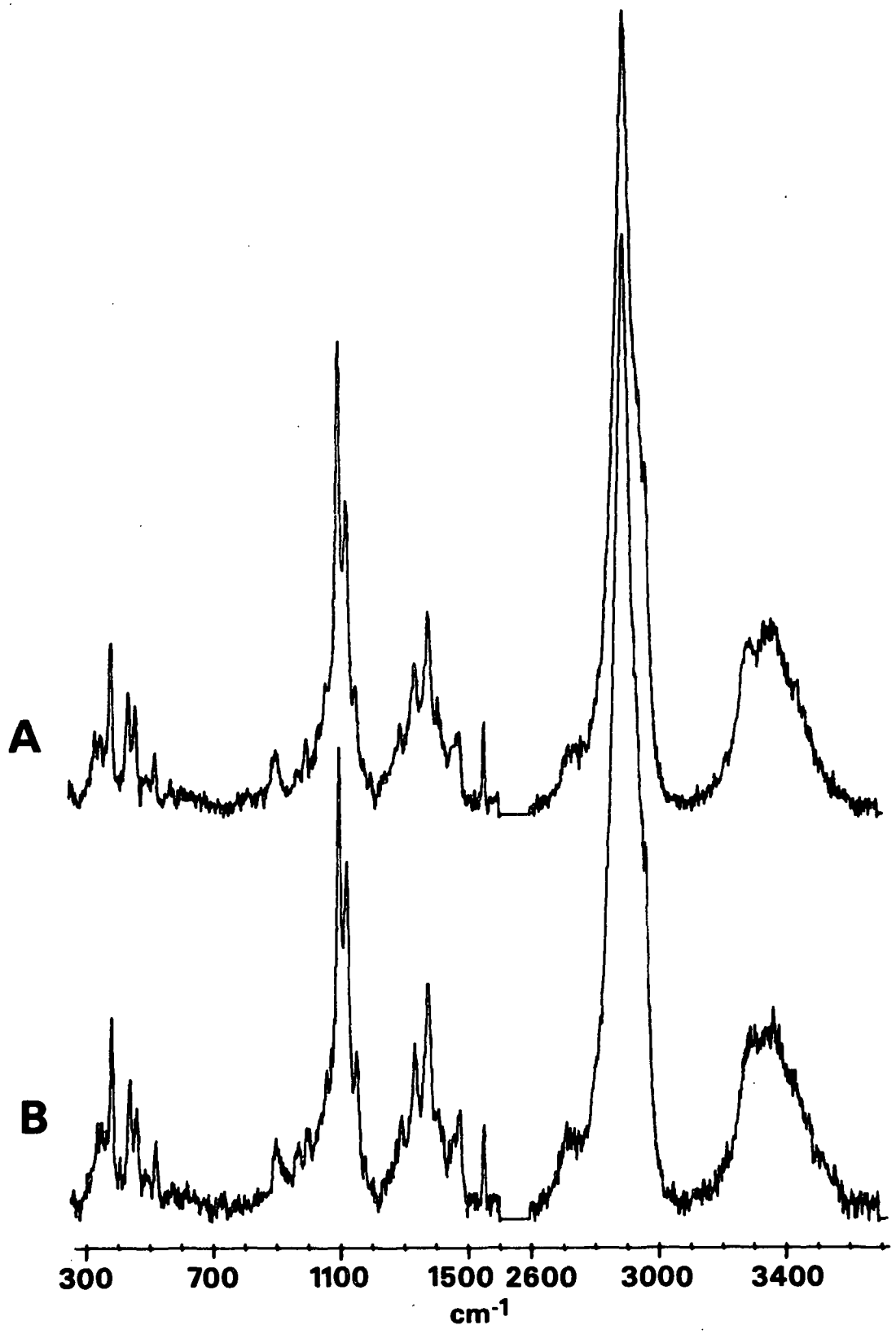

Figure 36. Polarized Raman spectra of a tension dried cotton fiber. A) electric vector parallel to fiber axis; B) electric vector perpendicular to fiber axis.

DISCUSSION

If the cellulose orientation in the plane perpendicular to the chain axis is anisotropic, the intensities will differ in the cross section spectra recorded with different polarizations of the incident light. With the exception of the 1095 and 1123 cm^{-1} bands, the relative peak intensities in the cross section spectra did not vary noticeably as the angle between the incident electric vector and the cell wall surface was changed (see Fig. 34).

The variation in the relative intensities of the 1095 and 1123 cm^{-1} bands indicates some degree of anisotropy in the cellulose orientation. These variations are not consistent, however, with either alternating cellulose orientation or orientation of the methines perpendicular to the cell wall surface. If alternating orientation was present, the intensities observed with the incident electric vector parallel to the cell wall surface should be equal to the intensities with the vector perpendicular to the wall [refer to Eq. (21) and (22)]. This pattern is not observed in Fig. 34. If the methines were oriented perpendicular to the cell wall surface, we would expect the ratio of the methine stretching band (2889 cm^{-1}) to the skeletal stretching band (1095 cm^{-1}) to be greater with incident electric vector perpendicular than with the vector parallel. This is because the methine intensity should be greater when the electric vector is parallel to the bond than when it is perpendicular [$\alpha_{yy} > \alpha_{xx}$ in Eq. (24)-(26)]. In Fig. 34, however, the opposite trend is observed. The ratio of the methine stretch to the skeletal stretch is largest when the electric vector is parallel to the cell wall surface.

The variation in the relative intensities of the 1095 and 1123 cm^{-1} bands may be due to a sectioning artifact. If the plane of sectioning was not

perpendicular to the chain axis, the chain axes would be tilted relative to the plane of the section. The 1095 cm^{-1} band is very sensitive to the angle between the incident electric vector and the chain axis. It is most intense when the electric vector of the incident light is parallel to the chain axis. If the chains were tilted, the incident electric vector would be aligned more parallel to the chain axis when the electric vector is perpendicular to the wall surface. Therefore, the relative intensity of the 1095 cm^{-1} band would increase as the electric vector is rotated from 0 to 90°, as is observed in Fig. 34. This explanation is further supported by the fact that the variation in the 1095 cm^{-1} band intensity has not been consistently observed in other cross section spectra. The degree of tilting must be small, since other bands did not vary noticeably.

The insensitivity of the bands in the cross section spectra to the polarization of the incident light relative to the cell wall surface is consistent with the random orientation model. The spectra suggest that in higher plant fibers the cellulose is oriented randomly in the plane perpendicular to the fiber axis. Similar results have been obtained in spectra recorded from other cross section specimens.

There are some anomalies, however, in the cross section spectra. The intensities of the 1095 cm^{-1}, 1123 cm^{-1}, and OH stretching bands are significantly larger than they are in the spectra of whole ramie fibers recorded with the electric vector perpendicular to the fiber axis (see Fig. 14). The cross section spectra are similar to spectra recorded from pellets where the cellulose orientation is random. Therefore, some scrambling of the polarization of the incident light may have occurred or the orientation may have been randomized by the sectioning process. We are not certain, however, that the cross section spectra should look the same as the whole fiber spectra where the electric

vector is perpendicular. In the whole fiber spectra, the beam was perpendicular to the fiber axis, whereas in the cross section spectra, the beam was parallel to the fiber axis. The differences between the cross section and whole fiber spectra may be caused by the different beam orientations. Further studies will be necessary to sort these things out.

The cross section spectra are consistent with the conclusions by Revol, et al.[80] in their study of cellulose orientation in wood. These results are not consistent, however, with the Raman spectra of cotton fibers reported by Atalla et al.[43] which suggested the methines are oriented perpendicular to the cell wall surface. Therefore, we attempted to reproduce the cotton spectra recorded in the earlier study.

We recorded spectra of cotton fibers (Fig. 35) under the same conditions employed in the earlier study. The relative intensity of the skeletal band at 1095 cm^{-1} is the same for both parallel and perpendicular orientations of the incident electric vector. Since the 1095 cm^{-1} is most intense when the electric vector is parallel to the fiber axis, the average fibril angle in the region where the spectra were recorded must be 45°. Contrary to the earlier results, the methine intensity when the electric vector was parallel to the fiber axis was equal to the intensity when the electric vector was perpendicular. Therefore, the spectra in Fig. 35 suggest that the methines are oriented randomly in the plane perpendicular to the chain axis. These results are consistent with the ramie cross section spectra.

The fiber used to record the spectra in Fig. 35 was freeze-dried. Apparently the fibers used in the earlier study were dried under tension. Therefore, we recorded spectra from a tension-dried cotton fiber (see Fig. 36). Again, a

region was found where the average fibril angle was 45°. The methine intensity in these spectra was greater when the incident electric vector was perpendicular to the fiber axis. These results are consistent with the earlier study. Therefore, it appears that the tension applied to fibers during drying can affect the cellulose orientation. In the fiber dried under tension, the cellulose is oriented nonrandomly in the plane perpendicular to the chain axis while the orientation is random in the freely dried fiber.

The Raman spectra of freely dried cotton fibers and ramie cross sections suggest that the cellulose is oriented randomly in the plane perpendicular to the chain axis. Since the Raman sees an average of many microfibrils, it is not possible to tell if the cellulose orientation within a single microfibril is nonrandom. Cellulose crystallites have been shown to have the 101 plane oriented parallel to their surfaces.[85-86] In microfibrils from algal celluloses, the 101 plane is also oriented parallel to the surface. In higher plants, it may be that the crystallites are oriented randomly in a single microfibril; or perhaps the crystallites are oriented nonrandomly in the microfibrils, but the microfibrils are oriented randomly in the lateral direction. Drying apparently affects the cellulose orientation. It is not known whether tension-drying or free-drying more closely resembles the orientation found in the native state.

In summary there are many questions remaining regarding cellulose orientation in plant fibers. The answers to these questions will provide insight into the biosynthesis and mechanical properties of the cell wall.

CONCLUSIONS

Spectra recorded from ramie cross sections and freely dried cotton indicate that the cellulose is oriented randomly in the plane perpendicular to the chain axis. In tension-dried cotton fibers, however, the cellulose is oriented non-randomly in the lateral direction. Apparently, the drying method can influence the cellulose orientation. Further study is suggested to sort out the factors influencing cellulose orientation and the interpretation of the cross section spectra.

ACKNOWLEDGMENTS

I wish to acknowledge some of the many contributions by others to the completion of this thesis. Dr. Rajai Atalla, who served as the chairman of my thesis advisory committee, provided guidance, encouragement and friendship throughout the course of the thesis. Dr.'s Umesh Agarwal, Harry Cullinan, John Litvay, and Norman Thompson also served on my committee and have been very helpful. Ms. Mary Block and Ms. Hilkka Kaustinen took the electron micrographs and helped me with sample preparation methods. Mr. Art Webb performed the carbohydrate analyses. Ms. Becky Whitmore grew the deuterated algae and Mr. Clark Woitkovich helped me to learn how to use the Raman spectrometer. I also wish to thank Dr. H. L. Crespi at Argonne Labs for providing the sample of deuterated bacterial cellulose and for helping us to grow deuterated algae.

I would like to thank The Institute of Paper Chemistry and its member companies for making this research possible and for providing financial assistance throughout my stay at the Institute.

Last but not least, I wish to thank my family, especially my wife Meg, for their sacrifice, support, and encouragement.

REFERENCES

1. Preston, R. D., Physical Biology of Plant Cell Walls, Chapman and Hall, 1974.

2. Frey-Wyssling, A., The Plant Cell Wall, Gebruder Borntraeger, Berlin, Stuttgart, 1976.

3. Long, D. A., Raman Spectroscopy, McGraw Hill, New York, 1977.

4. Dhamelincourt, P.; Wallart, F.; Leclercq, M.; N'Guyen, A. T.; Landon, D. O., Anal. Chem. 51(3):414-21A(1979).

5. Rosasco, G. J., Advances in Infrared and Raman Spectroscopy, R. J. H. Clark and R. E. Hester, eds., Heyden, London, 1980, Vol. 3, Chap. 4.

6. Andersen, M. E.; Muggli, R. Z., Anal. Chem. 53:1772-7(1981).

7. Wilson, E. B.; Decius, J. C.; Cross, P. C., Molecular Vibrations, McGraw-Hill, New York, 1955.

8. Woodward, L. A., Introduction to the Theory of Molecular Vibrations and Vibrational Spectroscopy, Oxford-Clarendon Press, Oxford, 1972.

9. Herzberg, G., Infrared and Raman Spectra of Polyatomic Molecules, Van Nostrand Press, New York, 1945.

10. Zbinden, R., Infrared Spectroscopy of High Polymers, Academic Press, New York, 1964.

11. Pitzner, L. J. An investigation of the vibrational spectra of the 1,5-anhydropentitols. Doctoral Dissertation, Appleton, WI, The Institute of Paper Chemistry, Jan., 1973. 402 p.

12. Pitzner, L. J.; Atalla, R. H., Spectrochim. Acta 31A:911-29(1975).

13. Watson, G. M. An investigation of the vibrational spectra of the pentitols and erythritol. Doctoral Dissertation, Appleton, WI, The Institute of Paper Chemistry, June, 1974. 178 p.

14. Edwards, S. L. An investigation of the vibrational spectra of the pentose sugars. Doctoral Dissertation, Appleton, WI, The Institute of Paper Chemistry, Jan., 1976. 245 p.

15. Williams, R. M. An investigation of the vibrational spectra of the inositols. Doctoral Dissertation, Appleton, WI, The Institute of Paper Chemistry, June, 1977. 377 p.

16. Williams, R. M.; Atalla, R. H., J. Phys. Chem. 88:508-19(1984).

17. Wells, H. A. An investigation of the vibrational spectra of glucose, galactose, and mannose. Doctoral Dissertation, Appleton, WI, The Institute of Paper Chemistry, Jan., 1977. 431 p.

18. Carlson, K. P. An investigation of the vibrational spectra of the cellodextrins. Doctoral Dissertation, Appleton, WI, The Institute of Paper Chemistry, Jan., 1979. 153 p.

19. Vasko, P. D.; Blackwell, J.; Koenig, J. L., Carbohyd. Res. 23:407-16(1972).

20. Cael, J. J.; Koenig, J. L.; Blackwell, J., Carbohyd. Res. 32:79-91(1974).

21. Cael, J. J.; Gardner, K. H.; Koenig, J. L.; Blackwell, J. J., Chem. Phys. 62:1145-53(1975).

22. Pray, H. L. Normal coordinate analysis of the planar vibrations of cellulose. Doctoral Dissertation, Memphis, TN, University of Tennessee, March, 1972. 150 p.

23. Krimm, S. Infrared spectra of high polymers. Advances in Polymer Science, Springer-Verlag, Berlin 2:51(1960/1961).

24. Tsuboi, M., J. Polymer Sci. 25:159-71(1957).

25. Liang, C. Y.; Marchessault, R. H., J. Polymer Sci. 37:385-95(1959).

26. Liang, C. Y.; Marchessault, R. H., J. Polymer Sci. 39:269-78(1959).

27. Higgins, H. G.; Stewart, C. M.; Harrington, K. J., J. Polymer Sci. 51: 59-84(1961).

28. Blackwell, J.; Vasko, P. D.; Koenig, J. L., J. Appl. Physics 41:4375-9 (1970).

29. Synder, R. G., J. Mol. Spectry. 37:353-65(1971).

30. Starr, R. C., J. Phycology 14(Suppl.):47-100(1978).

31. Browning, B. L., Methods in Wood Chemistry. Wiley Interscience, New York, 2:295(1967).

32. Borchardt, L. G.; Piper, C. V., Tappi 53(2):257-61(1970).

33. Graham, J. M.; Auer, M. T.; Canale, R. P.; Hoffmann, J. P., J. Great Lakes Res. 8(1):100-11(1982).

34. Crespi, H. L. Biosynthesis with deuterated microorganisms. Technical Committee Meeting on Modern Trends in the Biological Applications of Stable Isotopes. Leipzig, Germany, Dec. 6-10, 1976:1-15.

35. Dimick, B. E. The importance of the structure of alkali metal hydroxide solutions in decrystallizing cellulose I. Doctoral Dissertation, Appleton, WI, The Institute of Paper Chemistry, 1976. 185 p.

36. Jentzen, C. A. The effects of stress applied during drying on some of the properties of individual pulp fibers. Doctoral Dissertation, Appleton, WI, The Institute of Paper Chemistry, 1964. 129 p.

37. Tripp, V. W.; Conrad, C. M. Instrumental analysis of cotton cellulose and modified cotton cellulose. R. T. O'Connor, ed., Marcel Dekker, New York, 1972:339-77.

38. Howsmon, J. A.; Sisson, W. A., Cellulose and Cellulose Derivatives, E. Ott, H. M. Spurlin, and M. W. Grafflin, eds., Interscience, New York 1(4B):231-347(1954).

39. Jones, D. W., Cellulose and Cellulose Derivatives, N. M. Bikales and S. Segal, eds., Wiley-Interscience, New York 4(13C):117(1971), (and the references therein).

40. Ellefsen, O.; Tonnesen, B. A., Cellulose and Cellulose Derivatives, N. M. Bikales and S. Segal, eds., Wiley-Interscience, New York 4(13C.2):151 (1971).

41. Neiduszynski, I.; Preston, R. D., Nature 225:273-4(1970).

42. Boylston, E. K.; Hebert, J. J., J. Appl. Polymer Sci. 25:2105-7(1980).

43. Atalla, R. H.; Whitmore, R. E.; Heimbach, C. J., Macromolecules 13:1717 (1980).

44. Mann, J., Cellulose and Cellulose Derivatives, N. M. Bikales and S. Segal, eds., Wiley-Interscience, New York 4(13B):89(1971).

45. Correns, E.; Dechant, J., Faserforsch. Textiltech. 19:393-7(1968).

46. Dechant, J., Faserforsch. Textiltech. 19:491-9(1968).

47. Kaji, K.; Kanaya, T.; Inoue, K.; Kitamaru, R.; Sakurada, I., Cellulose Chem. Technol. 19:321-30(1985).

48. Tonnesen, A.; Ellefsen, O., Cellulose and Cellulose Derivatives, N. M. Bikales and S. Segal, eds., Wiley-Interscience, New York 4(13F):265(1971).

49. Hebert, J. J.; Muller, L. L., J. Appl. Polymer Sci. 18:3373-7(1974).

50. Atalla, R. H., Appl. Polymer Symp. 28:659-69(1976).

51. Atalla, R. H. Spectroscopic studies of polymorphy in cellulose: a new structural model. Proceedings of the International Symposium on Wood and Pulping Chemistry, Stockholm, June, 1981. SPCI Rept. No. 38(1):57(1981).

52. Krimm, S., J. Chem. Phys. 32:1780-3(1960).

53. VanderHart, D. L.; Atalla, R. H., Macromolecules 17:1465-72(1984).

54. Sundaralingam, M., Biopolymers 6:189-213(1968).

55. Gardner, K. H.; Blackwell, J., Biopolymers 13:1975-2001(1974).

56. Kolpak, F. J.; Blackwell, J., Macromolecules 9(2):273-8(1976).

57. Sarko, A.; Muggli, R., Macromolecules 7(4):486-94(1974).

58. Stipanovic, A. J.; Sarko, A., Macromolecules 9(5):851-7(1976).

59. Rees, D. A.; Skerrett, R. J., Carbohyd. Res. 7:334-48(1968).

60. Hayashi, J.; Yamada, T.; Kimura, K., Appl. Polymer Symp. 28:713-27(1976).

61. Atalla, R. H.; Gast, J. C.; Sindorf, D. W.; Bartuska, V. J.; Maciels, G. E., J. Am. Chem. Soc. 102:3249(1980).

62. Wellard, H. J., J. Polymer Sci. 13:471-6(1954).

63. Honjo, G.; Watanabe, M., Nature 181:326-8(1958).

64. Fisher, D. G.; Mann, J., J. Polymer Sci. 42:189-94(1960).

65. Nieduszynski, I. A.; Atkins, E. D. T., Biochim. et Biophys. Acta 222:109-18(1970).

66. Marrinan, H. J.; Mann, J., J. Polymer Sci. 21:301-11(1956).

67. Mann, J.; Marrinan, H. J., J. Polymer Sci. 32:357-70(1958).

68. Atalla, R. H. Polymorphy in native cellulose: recent developments. Function and Biosynthesis of Plant Cell Walls, W. M. Dugger and S. Bartnicki-Garcia, eds., Am. Soc. Plant Physiologists, Rockville, MD, 1984:381.

69. Dudley, R. L.; Fyfe, C. A.; Stephenson, P. J.; Deslandes, Y.; Hamer, G. K.; Marchessault, R. H., J. Am. Chem. Soc. 105:2469-72(1983).

70. Cael, J. J.; Kwoh, D. L. W.; Bhattacharjee, S. S.; Patt, S. L., Macromolecules 18:819-21(1985).

71. Okajima, S.; Kai, A., J. Appl. Polymer Sci. 11:289-96(1967).

72. Chanzy, H. D.; Roche, E., J. Appl. Polymer Sci. 28:701-11(1976).

73. Goto, T.; Harada, H.; Saiki, H., J. Japan Wood Res. Soc. 19(10):463-8 (1973).

74. Revol, J.-F., Carbohyd. Polymers 2:123-34(1982).

75. Preston, R. D., Disc. Faraday Soc. 11:165-70(1951).

76. Schurz, J., Phyton 5(2):53-66(1955).

77. Tanaka, F.; Okamura, K., J. Polymer Sci. Polymer Phys. Ed. 15:897-906 (1977).

78. Okamura, K. Memoirs of the College of Agriculture, Kyoto Univ. 115:63-7 (1980).

79. Revol, J.-F.; Goring, D. A. I., Polymer 24:1547-50(1983).

80. Revol, J.-F.; Gancet, C.; Goring, D. A. I., Wood Sci. 14(3):120-6(1982).

81. Tanaka, F.; Takaki, T.; Okamura, K.; Koshijima, T., Wood Res. 66:17-22 (1980).

82. Tanaka, F.; Koshijima, T., J. Japan Wood Res. Soc. 29(1):1-7(1983).

83. Tanaka, F.; Koshijima, T., Wood Sci. Technol. 18:177-86(1984).

84. Gentile, V. Effects of physical structure on the alkaline degradation of hydrocellulose. Doctoral Dissertation, Appleton, WI, The Institute of Paper Chemistry, June, 1986. 110 p.

85. Ranby, B. G. The fine structure of cellulose fibers. Fundamentals of Papermaking Fibers. Bolam ed., Technical Sec. British Paper and Board Manufacturers Association, London, 1958. p. 55-82.

86. Mukherjee, S. M.; Sikorski, J.; Woods, H. J., J. Textile Inst. 43(4):T196-201(1952).

87. Preston, R. D.; Cronshaw, J., Nature 181:248-50(1950).

88. Cronshaw, J.; Myers, A.; Preston, R. D., Biochim. Biophys. Acta 27:89-103(1958).

APPENDIX I

RECIPES FOR ALGAL GROWTH MEDIA

MEDIA FOR VALONIA

Synthetic Seawater

The recipe for synthetic seawater was obtained from Dr. Raymond Legge at the University of Texas at Austin Botany Department. The following salts were added to 1 liter of distilled water:

NaCl	27.18 g
$MgCl_2 \cdot 6H_2O$	6.09 g
$MgSO_4 \cdot 7H_2O$	5.74 g
$CaCl_2 \cdot 2H_2O$	1.49 g
K_2SO_4	0.86 g
$NaHCO_3$	0.20 g
NaBr	0.086 g
$SrCl_2 \cdot 6H_2O$	0.024 g
H_3BO_3	0.027 g
NaF stock solution	10 mL

The NaF stock solution was prepared by dissolving 0.2 g of NaF in a volumetric flask and diluting to a final volume of 1 liter.

Provasoli's ES Enrichment for Seawater

Provasoli's ES enrichment for seawater[30] was made by the following formula:

glass distilled water	224 mL
$NaNO_3$	1.40 g
$CH_2OHCH(OPO_3Na_2)CH_2OH \cdot 5H_2O$ (β-glycerophosphoric acid disodium salt)	0.200 g
Fe (as EDTA-1:1 molar)	100 mL
P II metals	250 mL
Vitamin B_{12} stock	4.0 mL
Thiamine stock	20.0 mL
Biotin stock	2.0 mL
Tris buffer	2.00 g

The enrichment solution was filter sterilized through a 0.22 micron filter. It was stored in a tightly sealed bottle in the cold room between uses. The stock solutions were prepared by the following methods:

Fe (as EDTA-1:1 molar)

0.351 g of $Fe(NH_4)_2(SO_4)_2 \cdot 6H_2O$ and 0.332 g of dibasic ethylenediaminetetraacetic acid 2 hydrate, $Na_2EDTA \cdot 2H_2O$, were dissolved in 500 mL of distilled water.

PII metal mix

H_3BO_3	0.114 g
$FeCl_3$ stock	10.0 mL
$MnSO_4$ stock	10.0 mL
$ZnSO_4$ stock	10.0 mL
$CoSO_4$ stock	1.0 mL
$Na_2EDTA \cdot 2H_2O$	0.111 g

The H_3BO_3 and $Na_2EDTA \cdot 2H_2O$ were dissolved in a small amount of distilled water in a volumetric flask. The stock solutions were added and the solution was diluted with distilled water to a final volume of 250 mL. The metal stock solutions had the following concentrations:

$FeCl_3$	0.294 g/L

Prepared by dissolving 0.49 g of $FeCl_3 \cdot 6H_2O$ in distilled water and diluting to a volume of 1.0 L.

$MnSO_4$	1.108 g/L

Prepared by dissolving 1.24 g of $MnSO_4 \cdot H_2O$ in distilled water and diluting to a volume of 1.0 L.

$ZnSO_4$	0.126 g/L

Prepared by dissolving 0.220 g of $ZnSO_4 \cdot 7H_2O$ in distilled water and diluting to a volume of 1.0 L.

$CoSO_4$	0.265 g/L

Prepared by dissolving 0.480 g of $CoSO_4 \cdot 7H_2O$ in distilled water and diluting to a volume of 1.0 L.

Vitamin B_{12}	0.010 g/L
Thiamine hydrochloride	0.100 g/L
Biotin	0.010 g/L

The vitamin stock solutions were filter sterilized through 0.22 micron filter. They were stored in tightly sealed bottles in the cold room.

MEDIA FOR CLADOPHORA

The medium used to grow Cladophora was based on a study by Graham et al.[33] The recipe was as follows:

Distilled water		967.8 mL
1.	macrosalts stock solution	10.0 mL
2.	sodium silicate stock solution	10.0 mL
3.	nitrate stock solution	5.0 mL
4.	D11 stock solution	1.0 mL
5.	C13 stock solution	0.1 mL
6.	B7 stock solution	0.1 mL
7.	phosphate stock solution	1.0 mL

The pH was adjusted to 6.0 and then the following substances were added:

8.	$NaHCO_3$	0.1 g
9.	vitamin stock solution	1.0 mL

The medium was filtered through a millipore filter (0.22 micron pore size) to remove any microorganisms which could compete with the algae. The stock solutions were prepared by the following recipes:

1. Macrosalts

$MgSO_4 \cdot 7H_2O$	10.0 g
KCl	3.0 g
Distilled water	1.0 L

2. Sodium silicate

$Na_2SiO_3 \cdot 9H_2O$	6.0 g
Distilled water	1.0 L

the pH was adjusted to 5.0 with concentrated HCl

3. Nitrate

$Ca(NO_3)_2 \cdot 4H_2O$	7.5 g
Distilled water	250.0 mL

4. D11

$Na_2EDTA \cdot 2H_2O$	12.5 g
$FeSO_4 \cdot 7H_2O$	5.0 g
H_3BO_3	1.00 g
$ZnSO_4 \cdot 7H_2O$	0.100 g
$MnSO_4 \cdot H_2O$	0.200 g
$Na_2MoO_4 \cdot 2H_2O$	0.025 g
$CuSO_4 \cdot 5H_2O$	0.023 g
Distilled water	1.0 L

1.0N NaOH was added to adjust the pH to 5.5. The salts after H_3BO_3 in the list were dissolved in a little water before adding them to the rest of the solution.

5. C13

$Al_2(SO_4)_3 \cdot 18H_2O$	0.06175 g
As_2O_3	0.0066 g
$CdCl_2$	0.0082 g
$SrCl_2$	0.0152 g
$HgCl_2$	0.0068 g
$PbCl_2$	0.0067 g
LiCl	0.0306 g
RbCl	0.0071 g
KBr	0.0074 g
KI	0.0065 g
NaF	0.011 g
Na_2SeO_4	0.0119 g
$BeSO_4 \cdot 4H_2O$	0.0982 g
Distilled water	1.0 L

The As_2O_3 was dissolved in concentrated HCl and diluted with distilled water before being added to the stock solution. All other salts were dissolved in a small amount of distilled water before they were added to the rest of the stock solution. The $PbCl_2$ had to be heated to get it to dissolve. The final pH of the stock solution was brought between 4 and 5 with 1.0N NaOH.

6. B7

NH_4VO_3	0.023 g
$CrK(SO_4)_2 \cdot 12H_2O$	0.096 g
$NiSO_4 \cdot 6H_2O$	0.045 g
$CoCl_2 \cdot 6H_2O$	0.040 g
$Na_2WO_4 \cdot 2H_2O$	0.018 g
$K_2TiO(C_2O_4)_2 \cdot 2H_2O$	0.0739 g
$SnCl_2 \cdot 2H_2O$	0.0190 g
Distilled water	1.0 L

The NH_4VO_3 was dissolved in a mixture of concentrated HNO_3 and water (1:1) and then diluted up to 800 mL with water. The $SnCl_2 \cdot 2H_2O$ was dissolved in concentrated HCl and then diluted before adding it to the rest of the stock solution. The other salts were all dissolved in small quantities of water separately before being added to the stock solution.

7. Phosphate stock

K_2HPO_4	1.5 g
Distilled water	100.00 mL

8. Vitamin stocks

The vitamin stock solution was prepared using the B_{12}, thiamine and biotin stock solutions prepared for the Valonia medium. The final stock solution was prepared by mixing 5.0 mL of thiamine stock, 44.5 mL of biotin stock, and 0.5 mL of B_{12} stock. The final stock solution was filter sterilized through a 0.22 micron filter and was stored in a sealed bottle in the cold room.

APPENDIX II

A STUDY OF PURIFICATION METHODS FOR ALGAL CELLULOSES

The ability of various extraction methods to purify algal celluloses was studied. The extraction methods examined were based on methods given in the literature,[28,31,88] and are listed below.

A) Acid chlorite bleach at 70-80°C for 4 hours as described in Browning[31]; wash with cold water until neutral and then freeze dry.

B) Extract with boiling 1% NaOH under nitrogen for 6 hours changing the liquor twice; soak in 0.05N HCl overnight; wash with water until neutral and then freeze dry.

C) Extract with 23% KOH at 25°C under nitrogen for 4 hours; soak in 0.05N HCl; wash with water until neutral and then freeze dry.

The starting material for these extractions was Cladophora glomerata which had been extracted with ethanol-chloroform, ethanol, boiling water, and freeze dried.

The purity of the extracted celluloses was measured by carbohydrate analyses. Table 7 summarizes the carbohydrate analyses of celluloses prepared by Methods A, B, and C and by combinations of Methods A, B, and C. The results show that Method B yields purer celluloses than either Methods A or C. The glucan content of the algae extracted by Method B was 97.8%, whereas the glucan contents of the algae extracted with Methods A and C were only 68-69%. Combining Methods A and C yielded a cellulose with glucan content almost as high as in the cellulose obtained by Method B alone. Combining Method B with Methods A and C did not result in a significant increase in the glucan content compared with Method B alone. Although the combination of Methods A and B did not yield an increase in the glucan content, the A + B combination yielded whiter cellulose. Since colored species can burn or fluoresce in the laser beam, completely white

samples are more suitable for Raman spectroscopy. Therefore, the combination of Methods A and B was used to purify algal celluloses for Raman spectroscopy.

Table 7. Summary of carbohydrate analyses for celluloses prepared by various extraction methods.

Extraction Methods Used	Araban, %	Xylan, %	Mannan, %	Galactan, %	Glucan,[a] %
Starting material	0.3	0.4	0.6	1.6	44.2
A	0.2	0.2	0.6	0.6	68.2
B	0.2	0.2	1.2	1.0	97.8
C	0.3	0.2	0.7	1.2	68.8
A+B	<0.1	0.2	1.0	0.6	89.6
A+C	0.1	0.2	1.4	1.0	93.1
B+C	<0.1	<0.1	1.2	1.0	96.2
A+B+C	<0.1	<0.1	1.2	1.0	94.0
95% Confidence Interval	±0.06	±0.08	±0.64	±0.59	±3.80

[a]Percentages based on moisture free weight of sample. All values are based on duplicate determinations.

APPENDIX III

ANALYSIS OF BAND INTENSITIES

Parameter Estimates
Confidence Intervals
Regression Coefficients
Plots of Intensity *vs.* Theta

Table 8. Analysis of the Raman band intensities in the Valonia spectra by linear regression [$I = B+(C-2B)\cos^2\theta + (B-C+A)\cos^4\theta$]. Summary of the estimated values for B, C-2B, and B-C+A; the 90% confidence intervals for B, C-2B, and B-C+A; and the multiple correlation coefficients (R squared values).

Freq (WN)	B	90% Conf. Interval	C-2B	90% Conf. Interval	B-C+A	90% Conf. Interval	R(Sqrd)
331	943.48	166.77	1383.85	915.86	2646.97	889.47	1.00
344	1717.11	90.64	-847.27	497.76	1068.60	483.39	0.91
381	4516.05	398.81	-3298.63	2190.20	4896.33	2126.95	0.94
437	2971.93	272.04	-880.09	1494.00	923.57	1450.93	0.32
459	2024.21	128.59	-264.36	706.16	2490.83	685.78	1.00
520	2651.27	253.09	-2753.29	1389.89	1343.87	1349.81	0.99
913	641.39	60.92	-390.72	334.53	446.82	324.90	0.73
968	1145.71	117.91	-848.83	647.55	474.52	628.88	0.88
997	1125.17	16.23	282.70	89.12	1983.41	86.55	1.00
1034	1291.10	103.69	250.84	569.41	627.41	553.00	0.98
1057	1669.07	154.10	1202.74	846.28	1369.78	821.89	1.00
1071	1641.87	167.36	881.375	919.11	954.225	892.60	0.99
1095	5207.46	410.18	2692.41	2252.46	12662.70	2187.65	1.00
1118	4586.74	1272.25	-3138.86	6986.78	6513.40	6785.30	0.85
1123	3737.73	278.14	2646.10	1527.51	1739.11	1483.47	0.99
1152	2717.87	186.48	-1496.63	1024.11	1786.23	994.58	0.84
1279	798.12	82.76	517.24	454.48	244.30	441.39	0.98
1292	1087.71	184.39	1338.14	1012.61	-164.89	983.41	0.96
1334	1561.81	134.71	1124.45	739.78	3214.82	718.44	1.00
1337	1531.67	204.94	1712.73	1125.48	3434.82	1093.03	1.00
1378	3090.84	216.50	-1253.23	1189.00	1964.90	1154.71	0.91
1406	672.20	114.02	865.00	626.17	1657.49	608.11	1.00
1455	924.43	154.93	-475.89	850.84	376.60	826.30	0.34
1477	1194.02	97.26	-134.79	534.13	31.86	518.74	0.43
1481	1003.64	139.97	640.42	768.69	-403.26	746.54	0.69
2848	5606.37	613.91	-4724.08	3371.54	3285.35	3274.33	0.83
2868	9410.35	935.44	-9718.59	5137.05	7265.69	4988.88	0.87
2885	15756.45	1513.36	-16287.86	8310.96	11822.32	8071.33	0.89
2904	10341.81	982.75	-10556.19	5396.94	8167.47	5241.31	0.87
2941	5267.83	409.73	-2991.37	2250.11	5071.29	2185.30	0.96
2965	3807.11	769.80	-2548.47	4227.54	6527.60	4105.59	0.95
3231	863.339	671.35	-1315.81	3686.87	4449.81	3580.48	0.94
3239	775.40	66.46	77.94	364.98	2436.15	354.32	1.00
3266	976.50	141.56	27.36	777.41	2658.08	754.98	1.00
3291	1567.43	52.65	-113.09	289.16	3243.57	280.81	1.00
3299	1694.72	90.75	-483.51	498.36	3753.20	483.99	1.00
3302	1793.32	192.96	-602.21	1059.69	3764.90	1029.14	1.00
3307	1748.83	169.81	-417.73	932.56	3650.68	905.65	1.00
3334	1516.80	149.47	281.65	820.84	3311.86	797.18	1.00
3345	1415.05	370.46	1697.24	2034.42	1918.66	1975.77	0.99
3356	1545.82	129.55	843.40	711.45	3847.42	690.94	1.00
3361	1568.91	208.17	905.44	1143.22	4003.86	1110.26	1.00
3366	1678.94	101.78	703.45	558.93	3934.68	542.81	1.00
3390	1238.20	127.60	11.07	700.77	2528.30	539.03	1.00
3395	1332.87	75.72	-216.49	415.83	2467.86	403.84	1.00
						Average Rsqr	0.91

Table 9. Analysis of the Raman band intensities in the ramie spectra by linear regression [$I = B+(C-2B)\cos^2\theta + (B-C+A)\cos^4\theta$]. Summary of the estimated values for B, C-2B, and B-C+A; the 90% confidence intervals for B, C-2B, and B-C+A; and the multiple correlation coefficients (R squared values).

Freq (WN)	B	90% Conf. Interval	C-2B	90% Conf. Interval	B-C+A	90% Conf. Interval	R(Sqrd)
331	860.50	388.13	958.50	2131.49	2924.29	2070.02	0.99
344	2274.82	260.81	-2006.74	1432.32	1605.77	1391.02	0.76
349	2069.64	197.88	-1446.02	1086.72	1435.85	1055.38	0.68
380	5487.61	547.80	-6943.65	3008.25	6559.11	2921.48	0.86
437	3606.48	404.61	-2523.70	2221.97	1375.84	2158.01	0.85
458	2611.07	334.57	-2162.13	1837.42	4256.00	1784.44	0.97
519	3570.94	192.92	-4985.59	1059.48	2343.26	1028.92	0.99
894	904.03	91.30	-360.20	501.40	1298.37	486.93	0.99
900	1015.55	118.15	-699.98	648.83	1330.22	630.11	0.96
910	1045.02	133.08	-699.30	730.83	752.15	709.76	0.58
969	1572.57	119.09	-1853.65	654.01	1244.30	635.17	0.96
995	1208.98	282.68	-268.41	1552.39	2539.11	1507.62	0.98
1037	1767.31	269.08	37.61	1477.73	1104.44	1435.18	0.93
1057	2078.59	404.04	824.68	2218.77	2090.36	2154.81	0.97
1095	5713.47	1891.30	1058.81	10386.46	17168.70	10086.92	0.99
1117	5757.87	894.95	-584.98	4914.69	3528.12	4773.12	0.89
1121	5177.30	944.05	2274.40	5184.38	1616.56	5034.93	0.92
1151	3851.99	458.68	-3315.08	2518.96	2513.76	2446.26	0.76
1275	609.49	160.61	934.80	882.01	7.55	856.57	0.96
1291	1005.98	189.28	2166.04	1039.48	-1204.01	1009.50	0.95
1331	1782.77	554.32	-204.35	3044.07	4033.02	2956.44	0.97
1337	1803.59	667.32	695.80	3664.69	4316.58	3558.95	0.98
1378	4365.55	693.35	-1790.04	3807.75	1755.39	3697.95	0.21
1407	1027.56	458.00	850.83	2515.12	2781.17	2442.63	0.98
1456	1516.64	299.44	-1024.74	1644.39	739.69	1596.97	0.46
1460	1566.43	204.26	-809.37	1121.73	372.29	1089.39	0.76
1475	1602.62	268.25	-318.26	1473.19	-47.41	1430.70	0.55
2866	17803.90	1820.58	-25777.00	9998.01	15074.90	9709.77	0.96
2889	27371.20	2911.89	-38928.10	15990.85	23162.10	15529.70	0.96
2943	10124.00	1260.57	-11319.40	6922.60	10545.30	6723.05	0.75
2963	7174.75	1181.64	-6410.36	6489.17	9426.20	6301.98	0.87
3286	2104.65	553.38	-832.69	3038.95	5242.51	2951.33	0.98
3335	2311.42	574.55	-1198.61	3155.36	5784.44	3064.32	0.98
3363	1995.92	556.60	-587.24	3056.65	5582.51	2968.60	0.98
3402	2250.30	460.70	-2133.03	2530.04	4523.10	2457.13	0.96
3429	1796.77	311.08	-1680.87	1708.35	3837.33	1659.08	0.97
						Average Rsqr	0.87

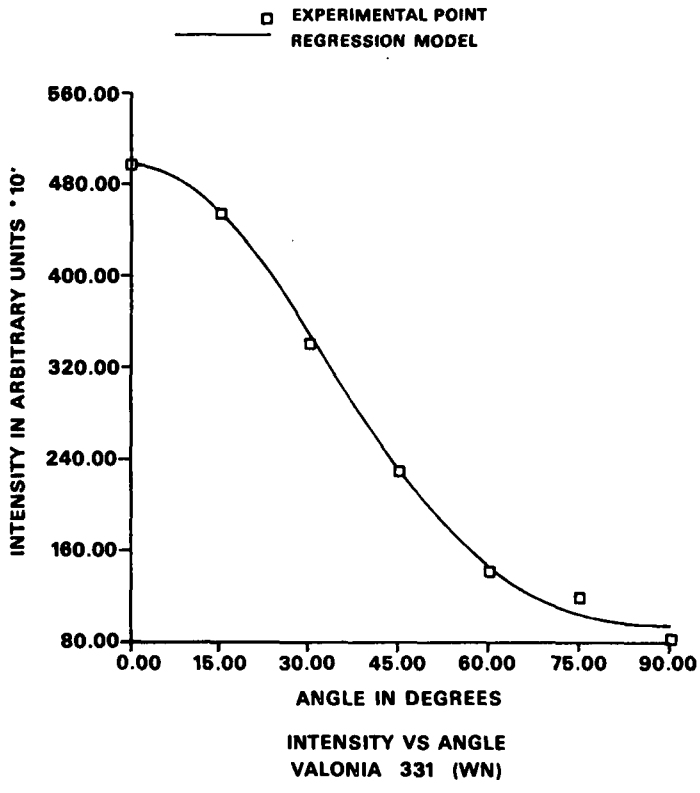

Figure 37. Intensity vs. angle - Valonia 331 (WN).

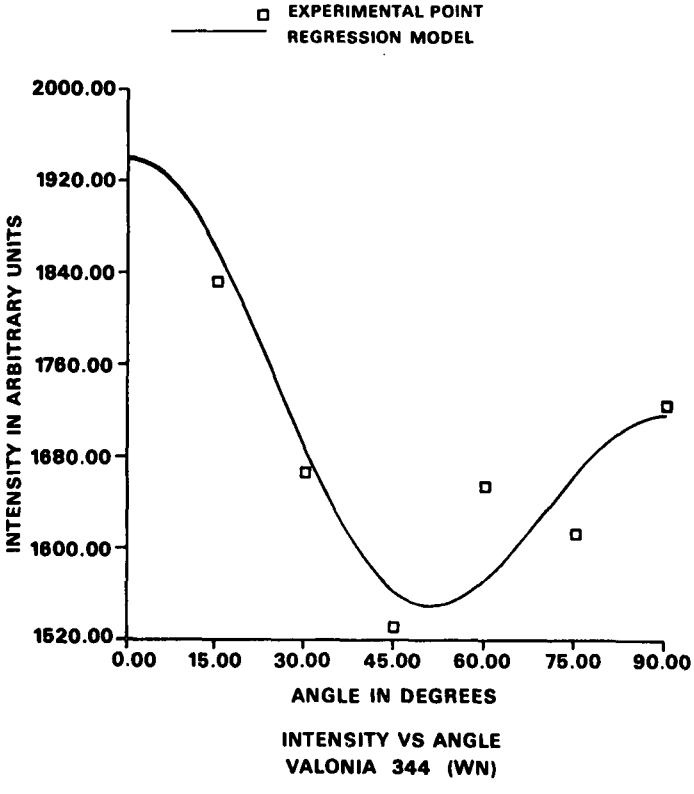

Figure 38. Intensity vs. angle - Valonia 344 (WN).

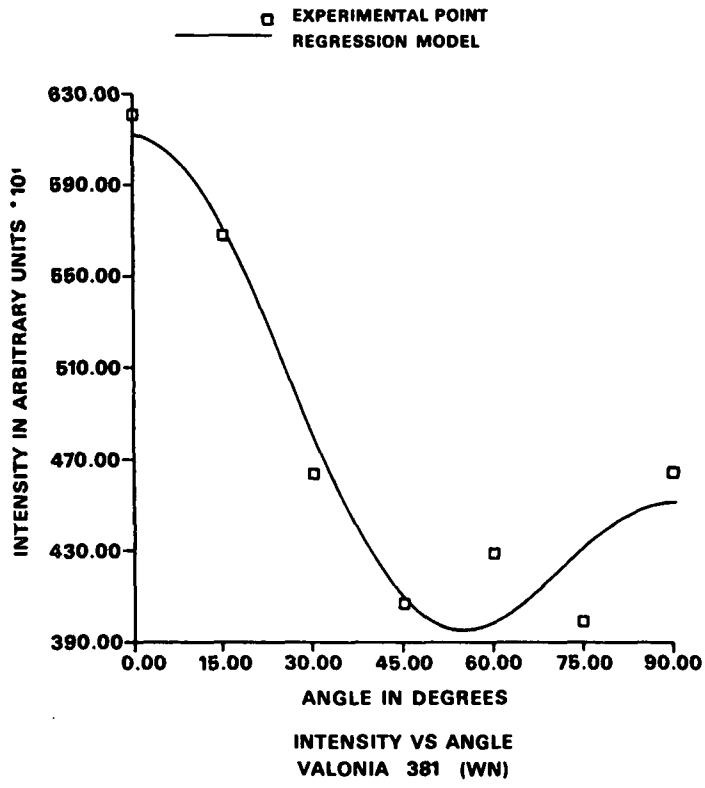

Figure 39. Intensity vs. angle - Valonia 381 (WN).

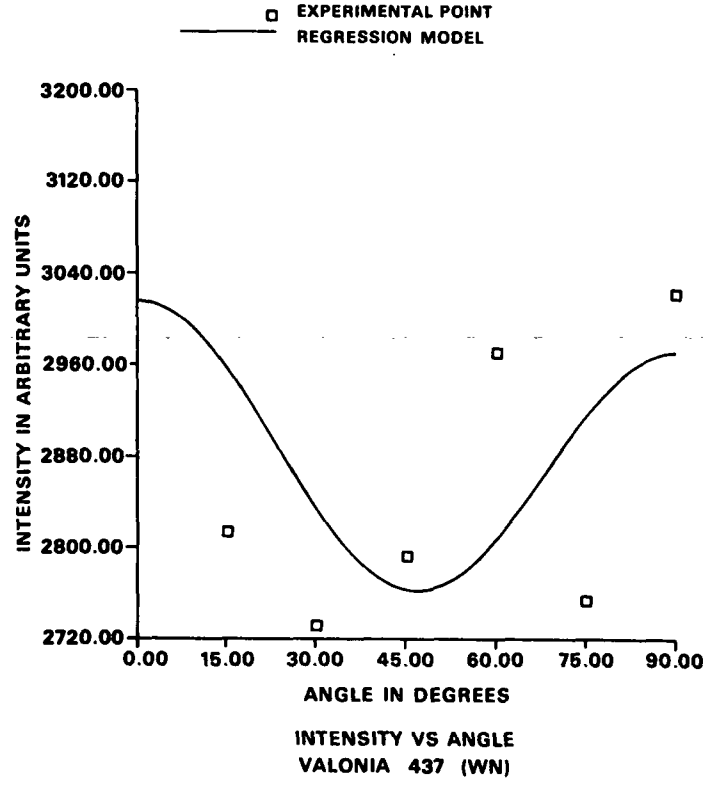

Figure 40. Intensity vs. angle - Valonia 437 (WN).

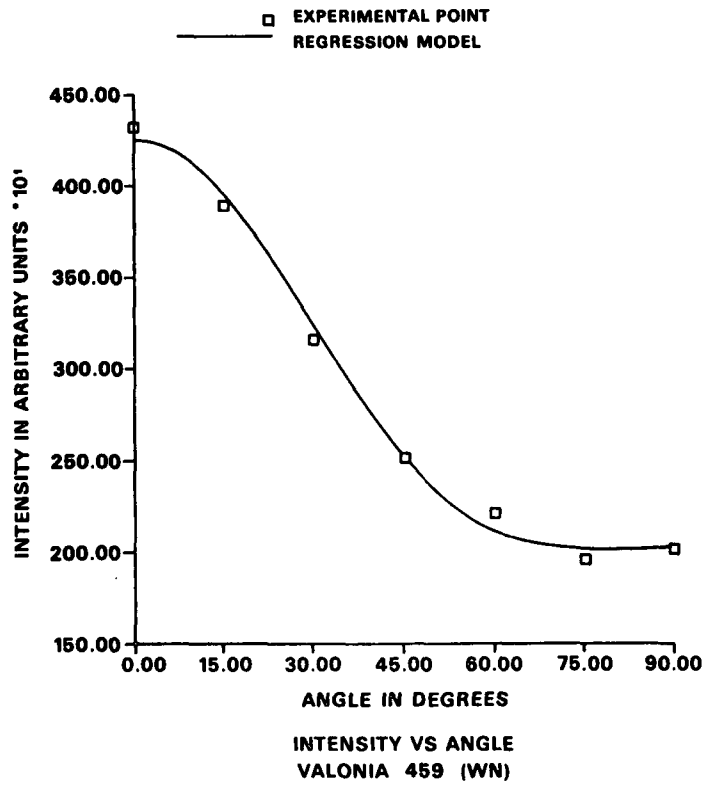

Figure 41. Intensity vs. angle - Valonia 459 (WN).

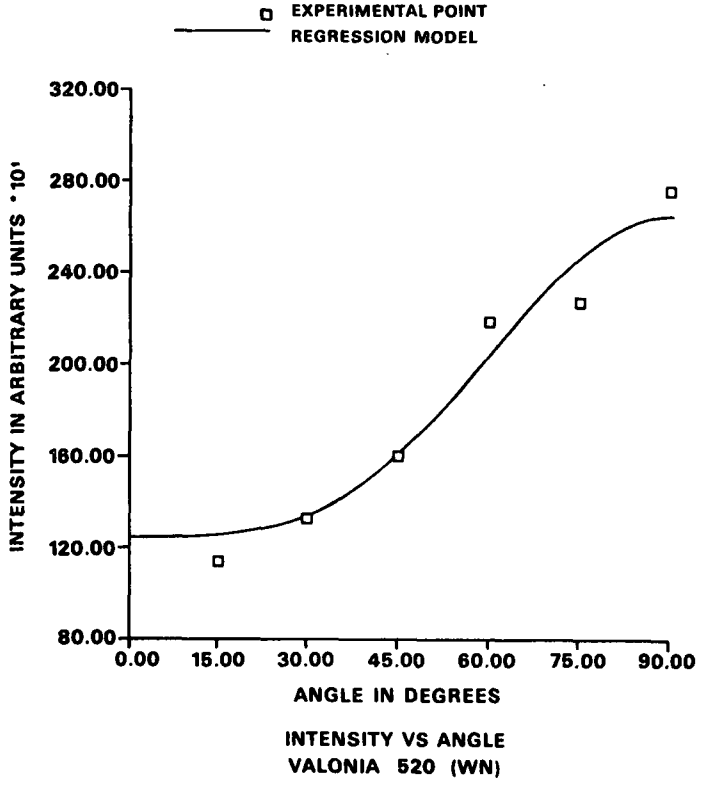

Figure 42. Intensity vs. angle - Valonia 520 (WN).

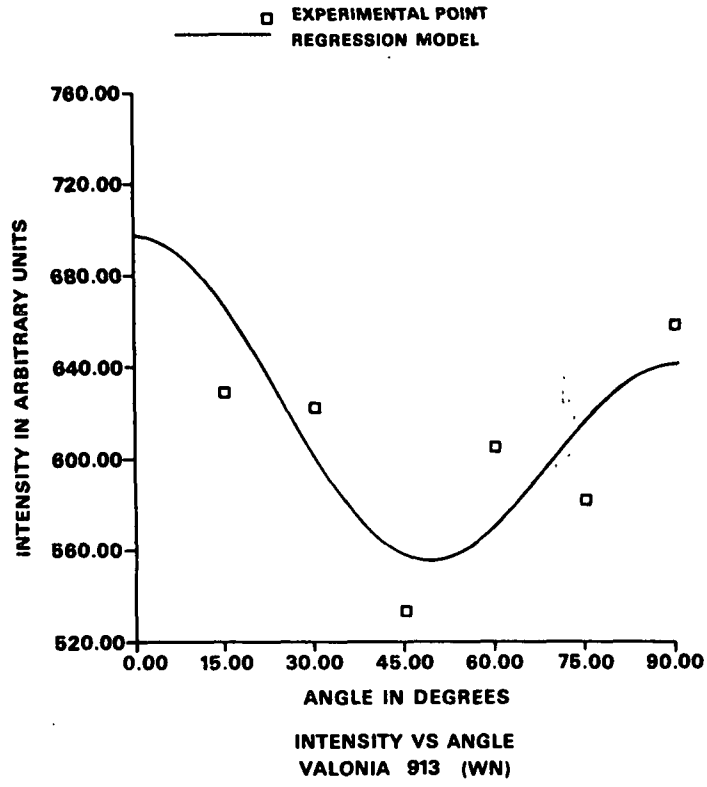

Figure 43. Intensity vs. angle - Valonia 913 (WN).

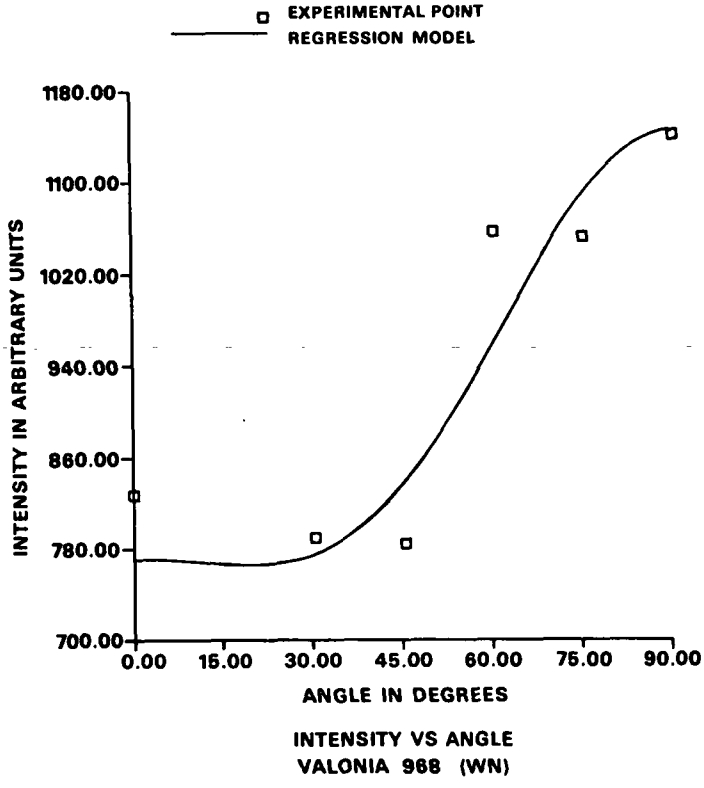

Figure 44. Intensity vs. angle - Valonia 968 (WN).

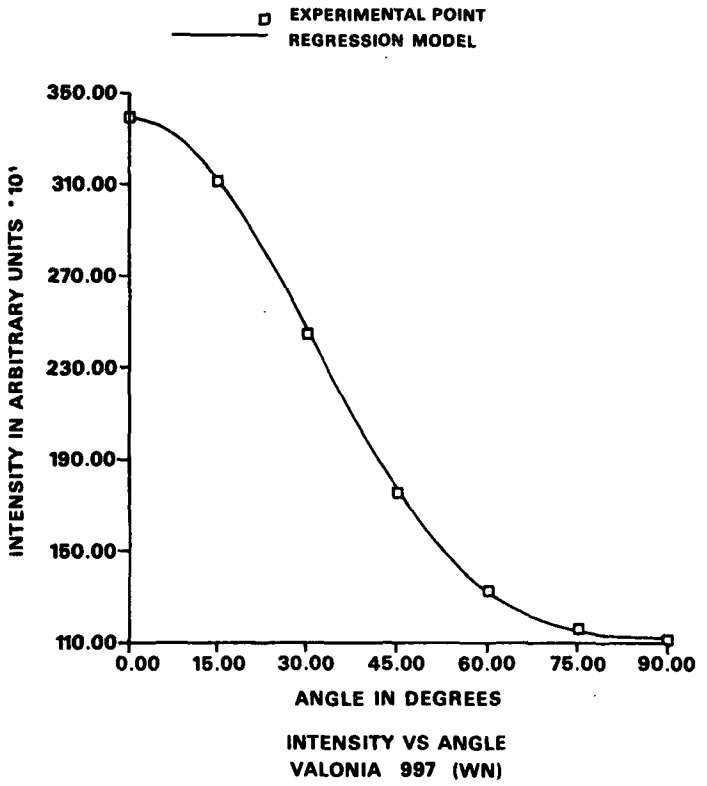

Figure 45. Intensity vs. angle - Valonia 997 (WN).

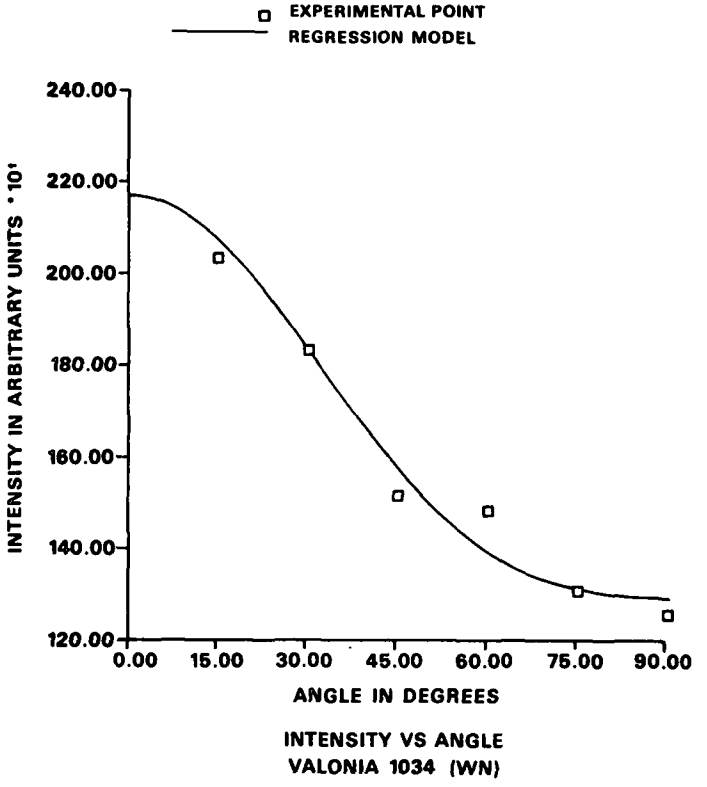

Figure 46. Intensity vs. angle - Valonia 1034 (WN).

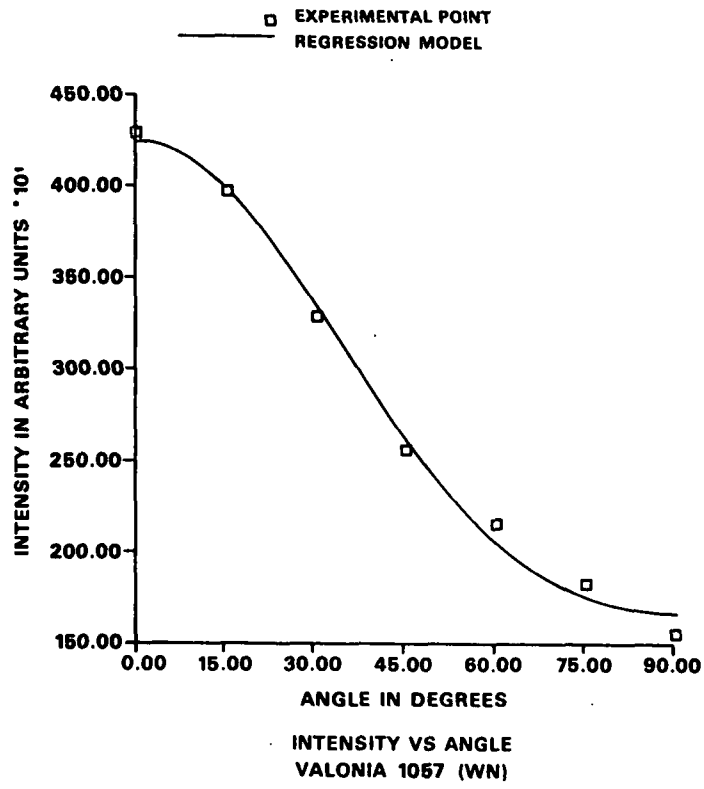

Figure 47. Intensity vs. angle - Valonia 1057 (WN).

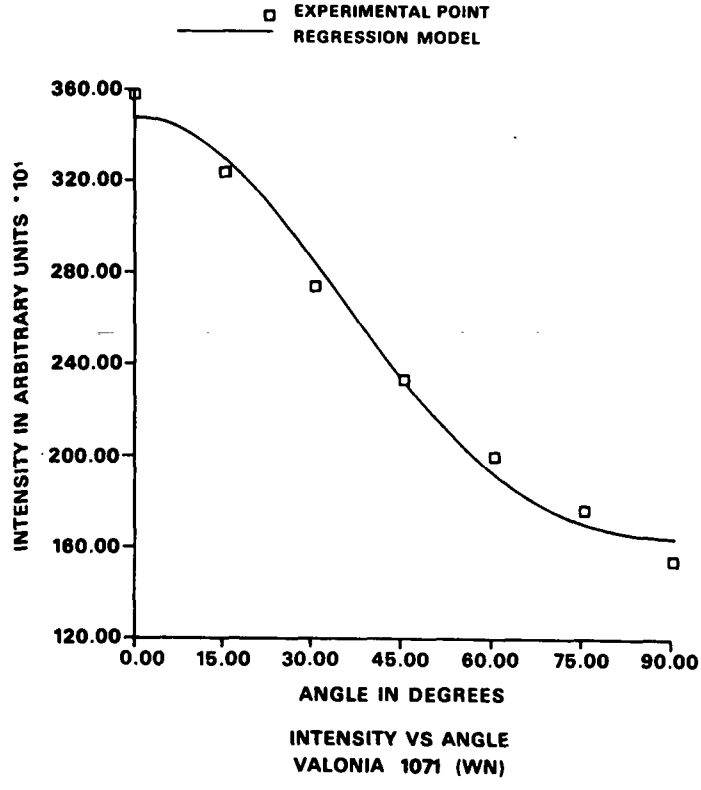

Figure 48. Intensity vs. angle - Valonia 1071 (WN).

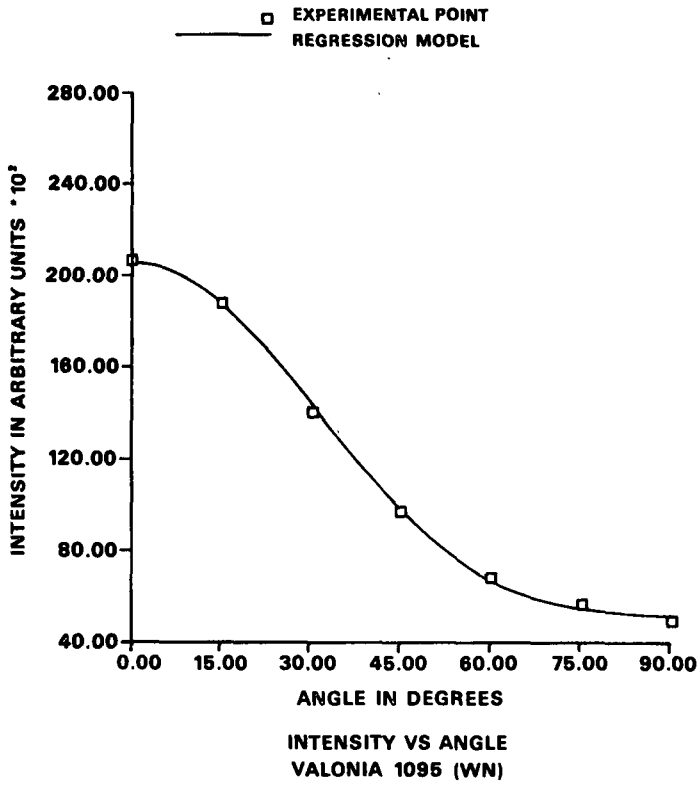

Figure 49. Intensity vs. angle - Valonia 1095 (WN).

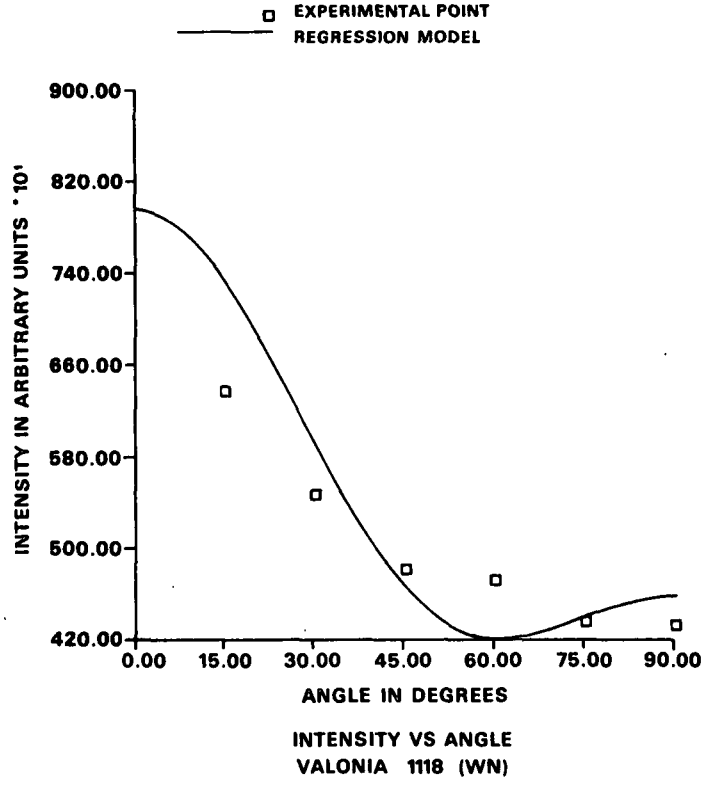

Figure 50. Intensity vs. angle - Valonia 1118 (WN).

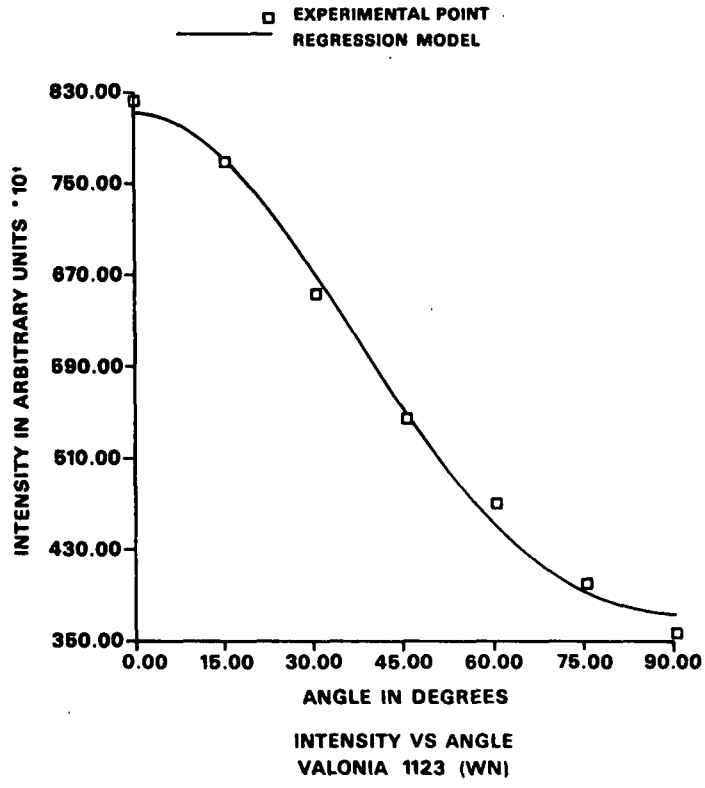

Figure 51. Intensity vs. angle - Valonia 1123 (WN).

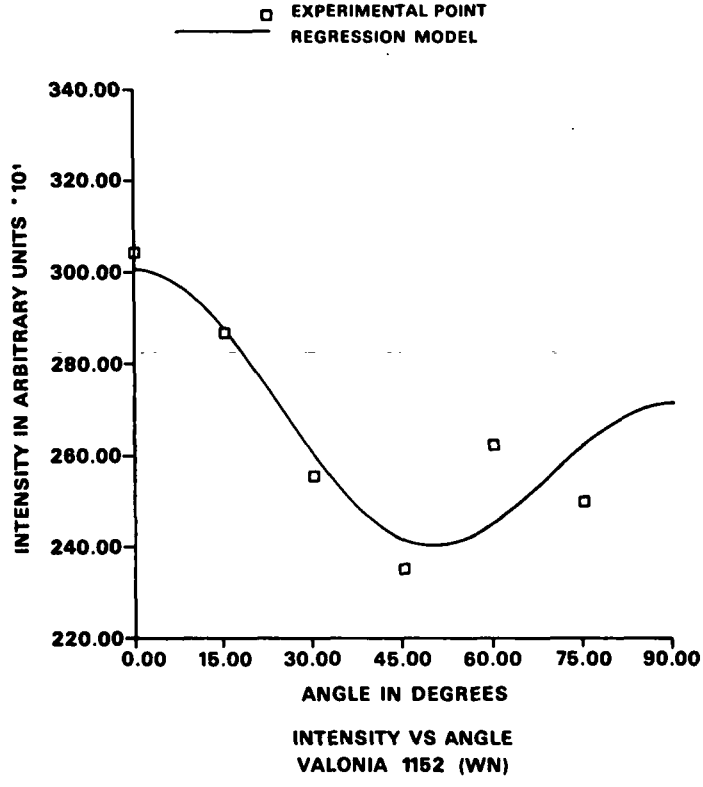

Figure 52. Intensity vs. angle - Valonia 1152 (WN).

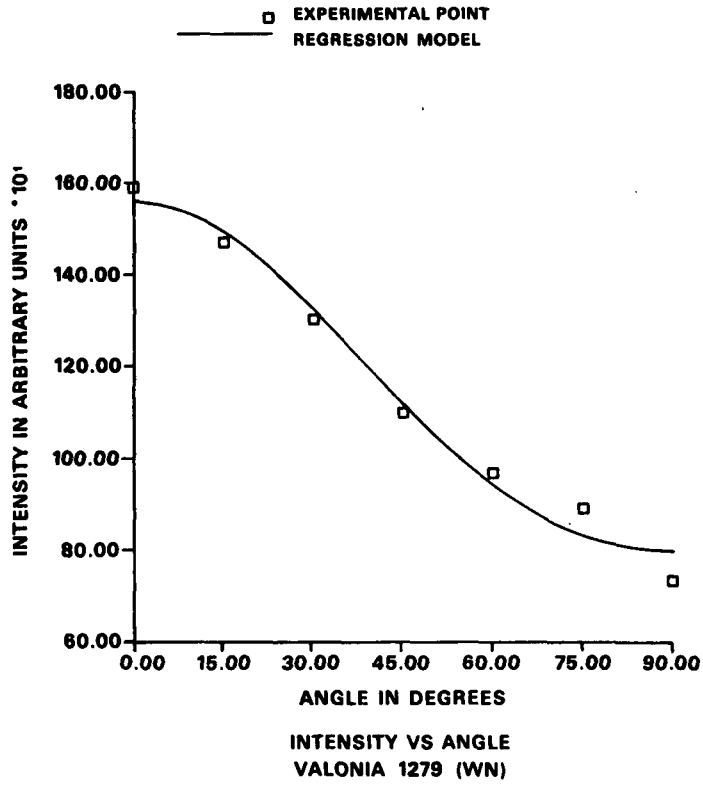

Figure 53. Intensity vs. angle - Valonia 1279 (WN).

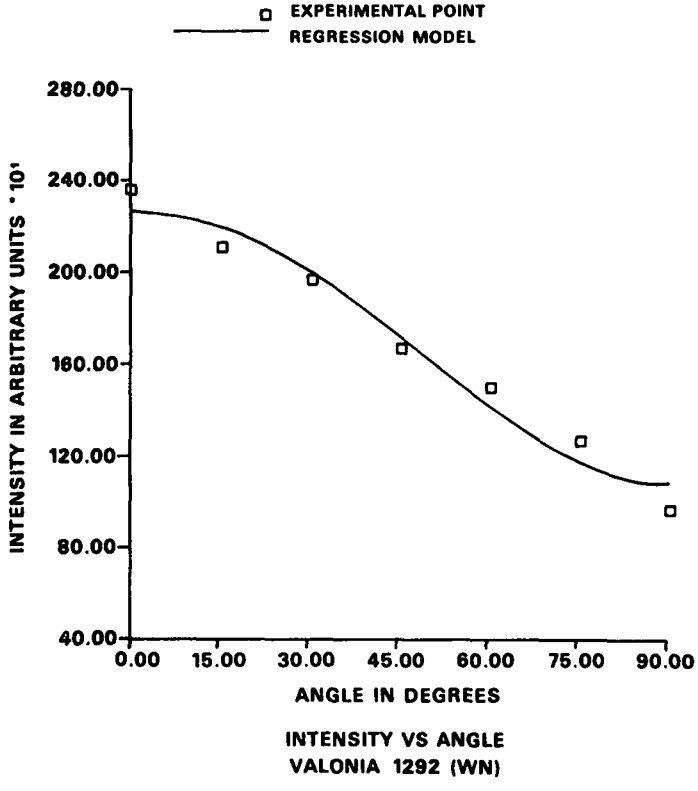

Figure 54. Intensity vs. angle - Valonia 1292 (WN).

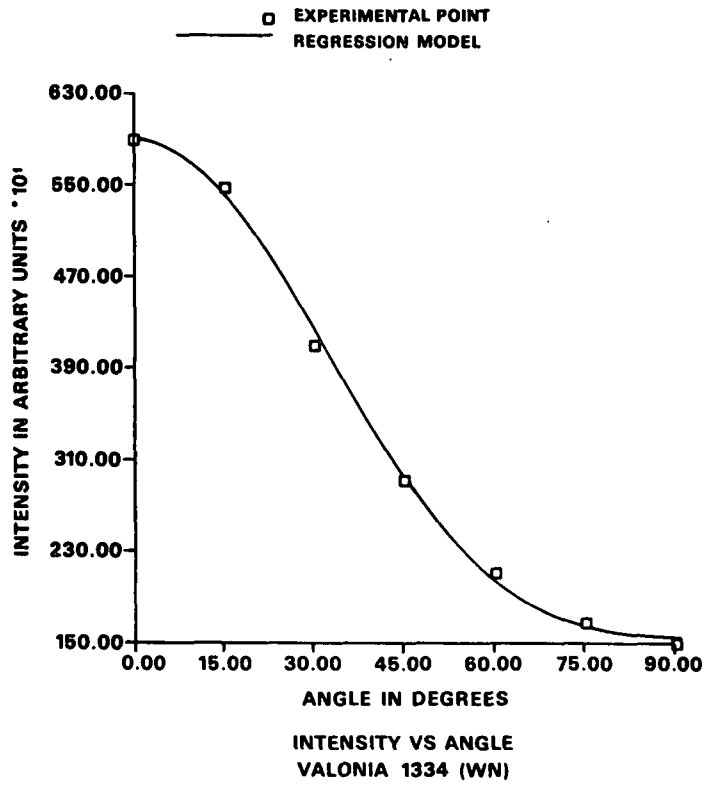

Figure 55. Intensity vs. angle - Valonia 1334 (WN).

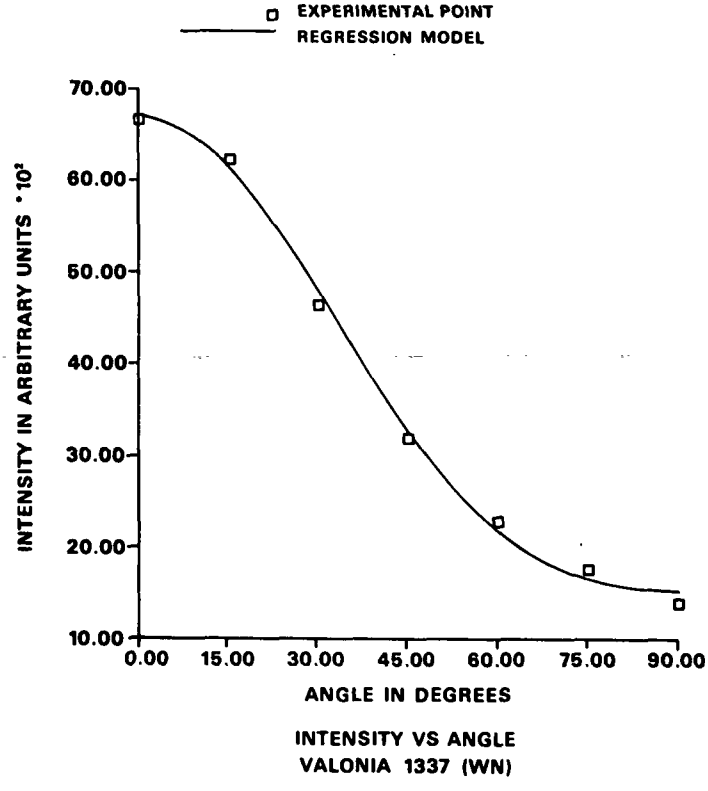

Figure 56. Intensity vs. angle - Valonia 1337 (WN).

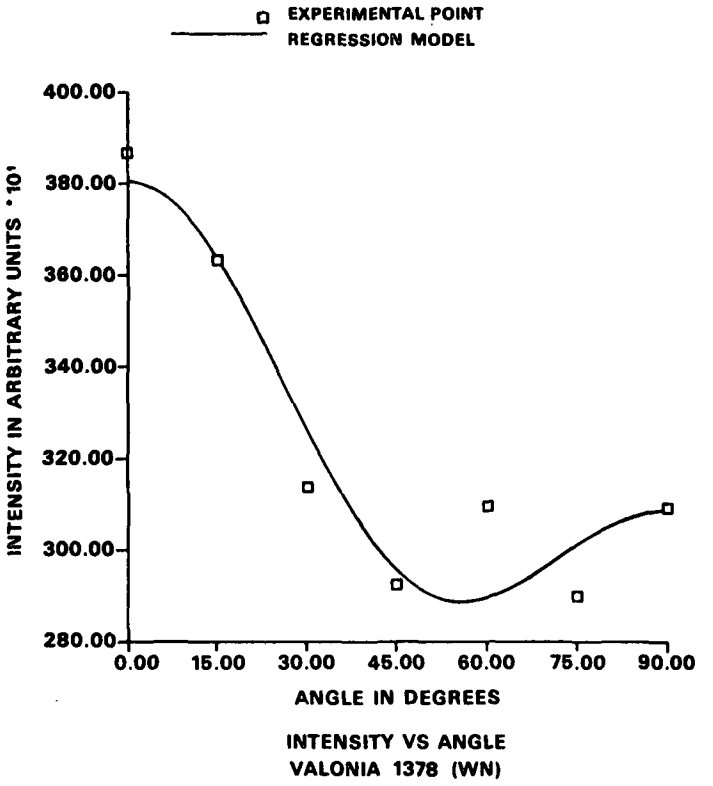

Figure 57. Intensity vs. angle - Valonia 1378 (WN).

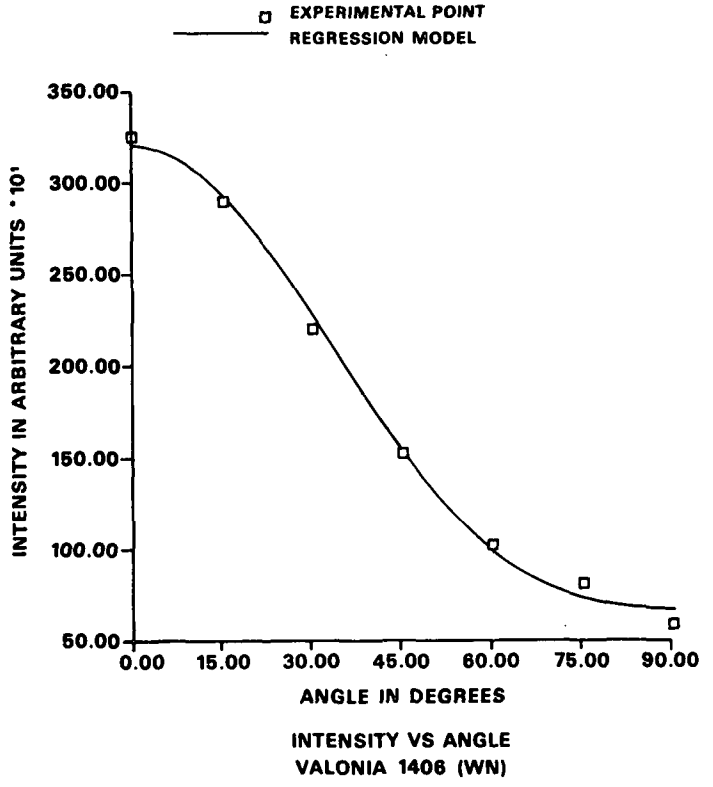

Figure 58. Intensity vs. angle - Valonia 1406 (WN).

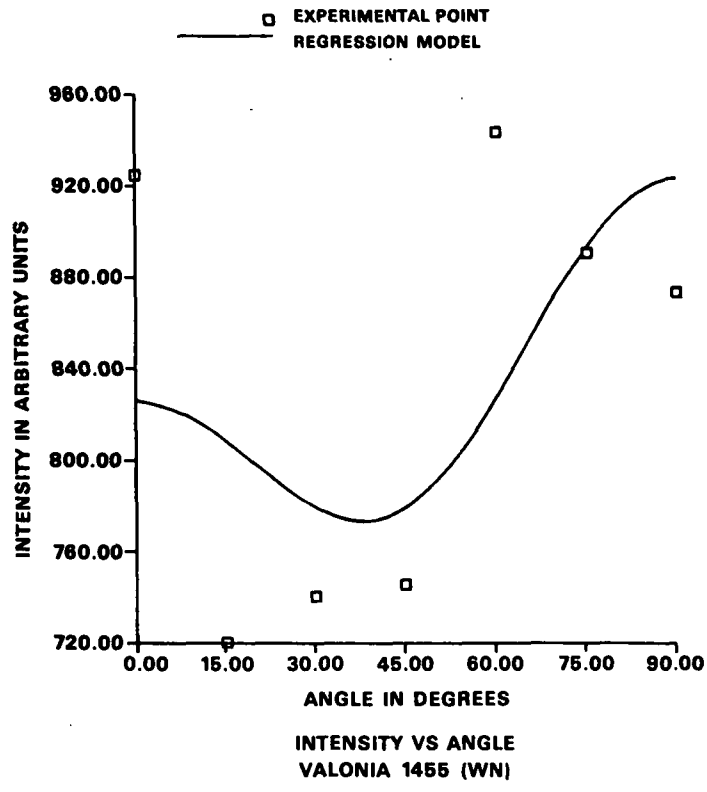

Figure 59. Intensity vs. angle - Valonia 1455 (WN).

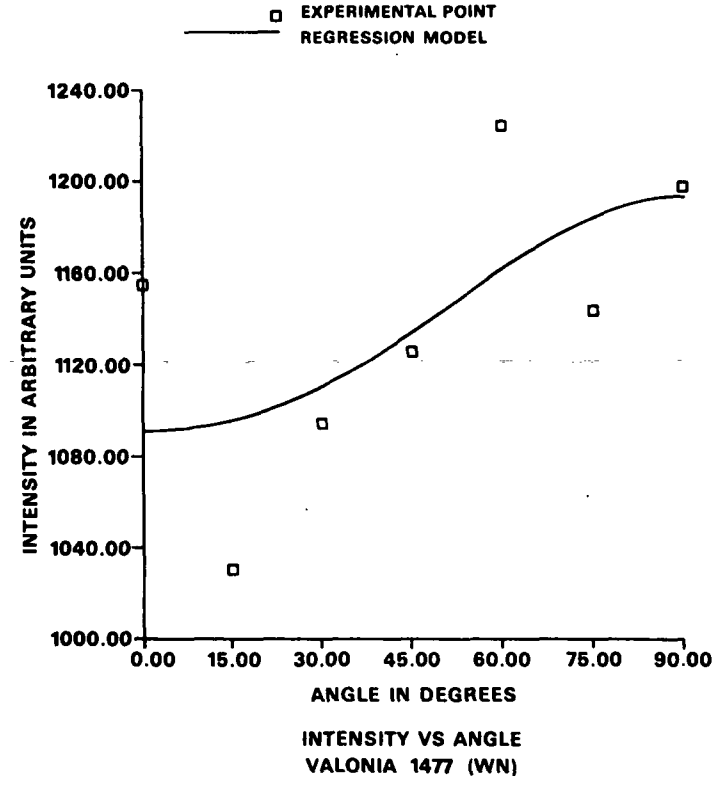

Figure 60. Intensity vs. angle - Valonia 1477 (WN).

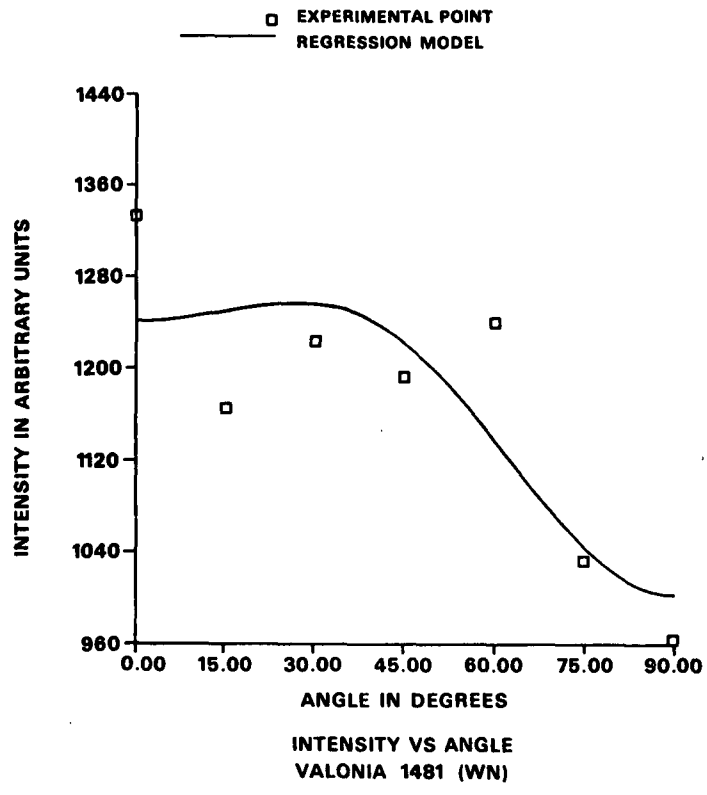

Figure 61. Intensity vs. angle - Valonia 1481 (WN).

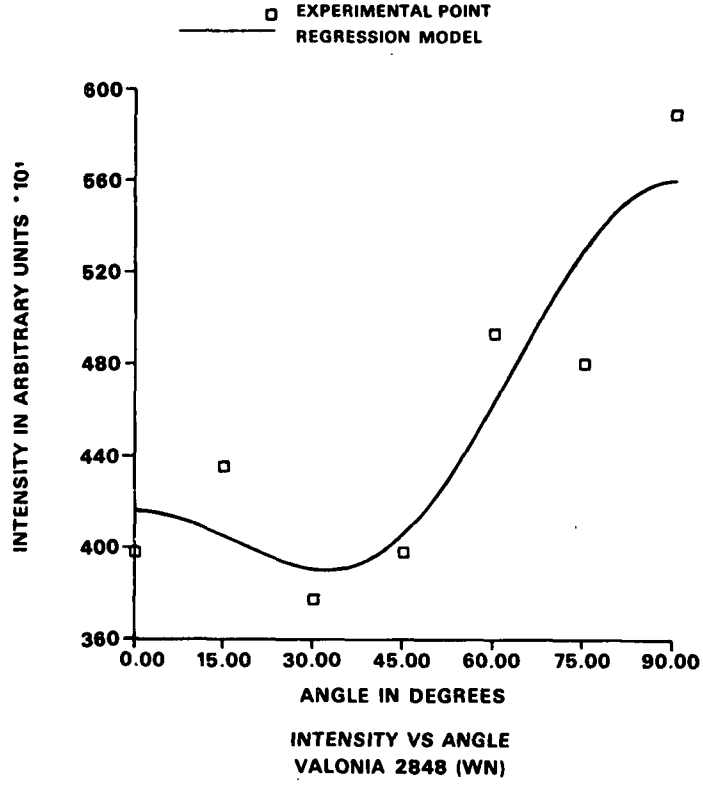

Figure 62. Intensity vs. angle - Valonia 2848 (WN).

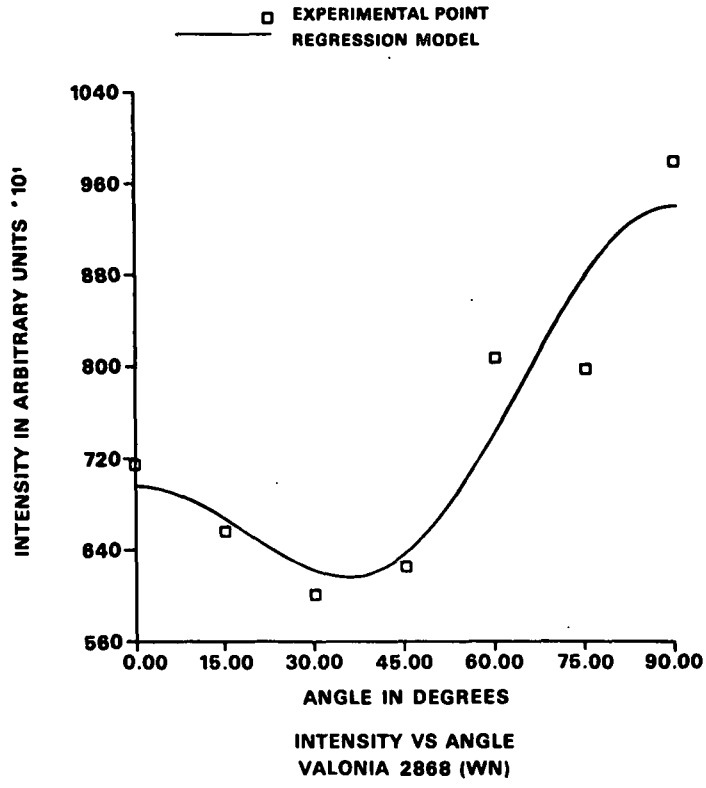

Figure 63. Intensity vs. angle - Valonia 2868 (WN).

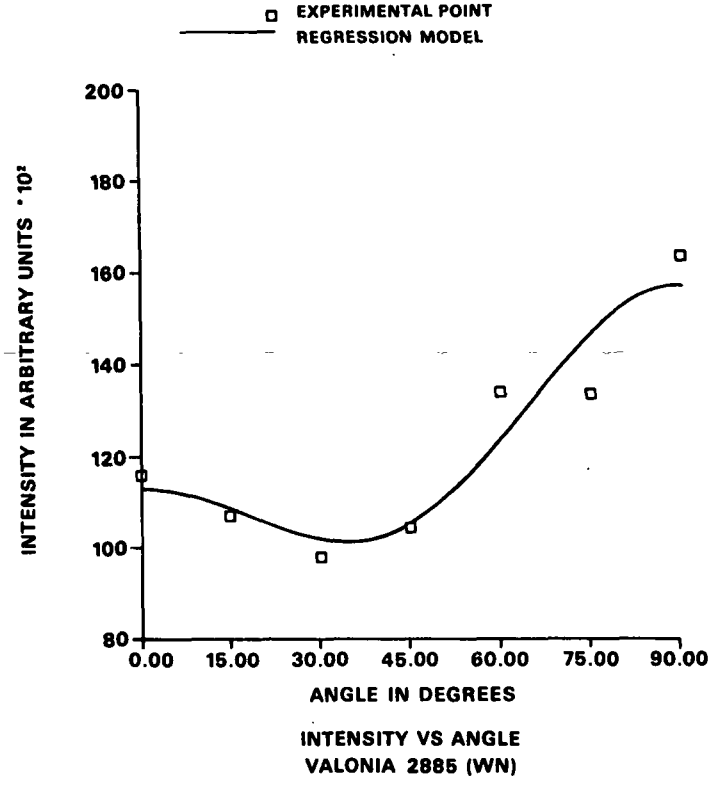

Figure 64. Intensity vs. angle - Valonia 2885 (WN).

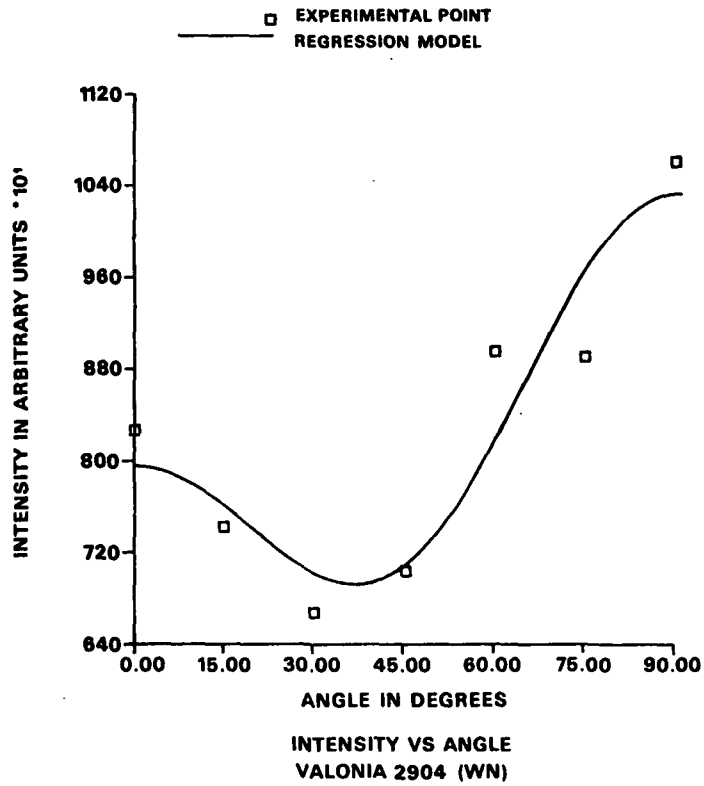

Figure 65. Intensity vs. angle - Valonia 2904 (WN).

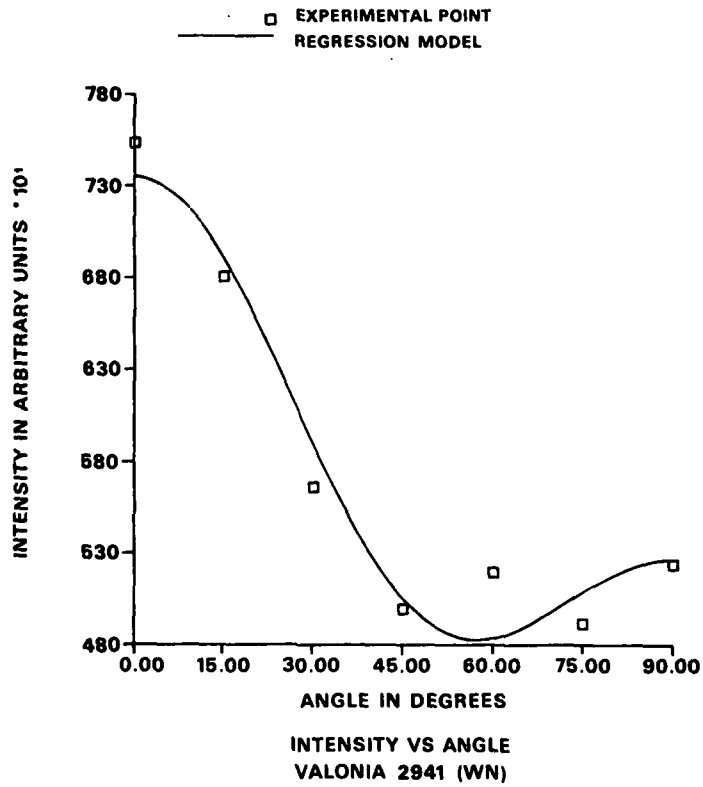

Figure 66. Intensity vs. angle - Valonia 2941 (WN).

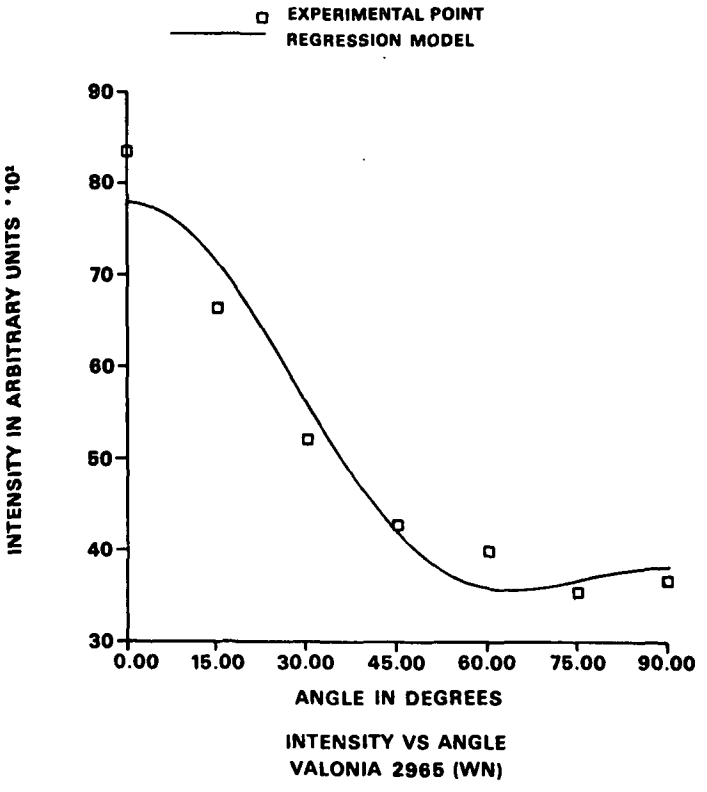

Figure 67. Intensity vs. angle - Valonia 2965 (WN).

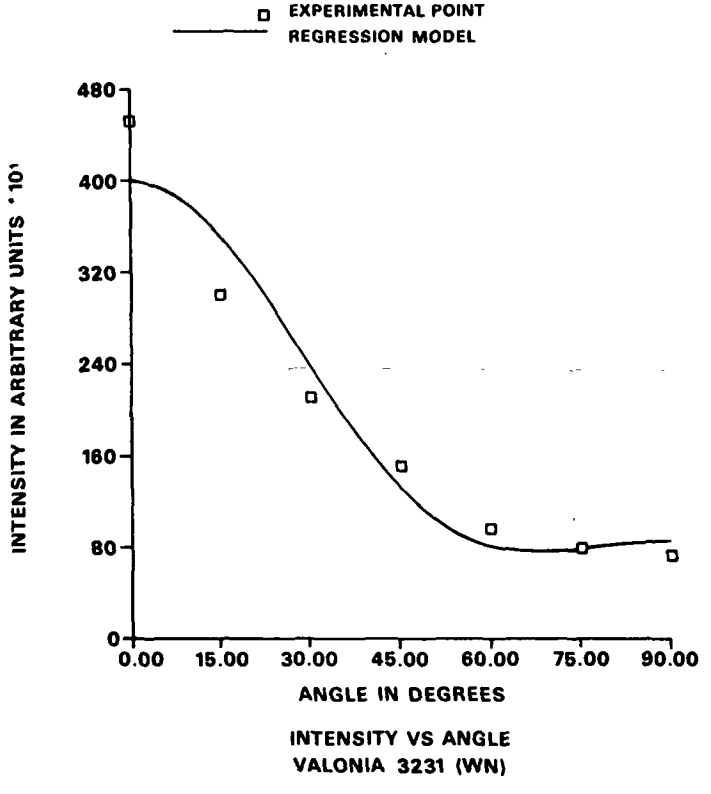

Figure 68. Intensity vs. angle - Valonia 3231 (WN).

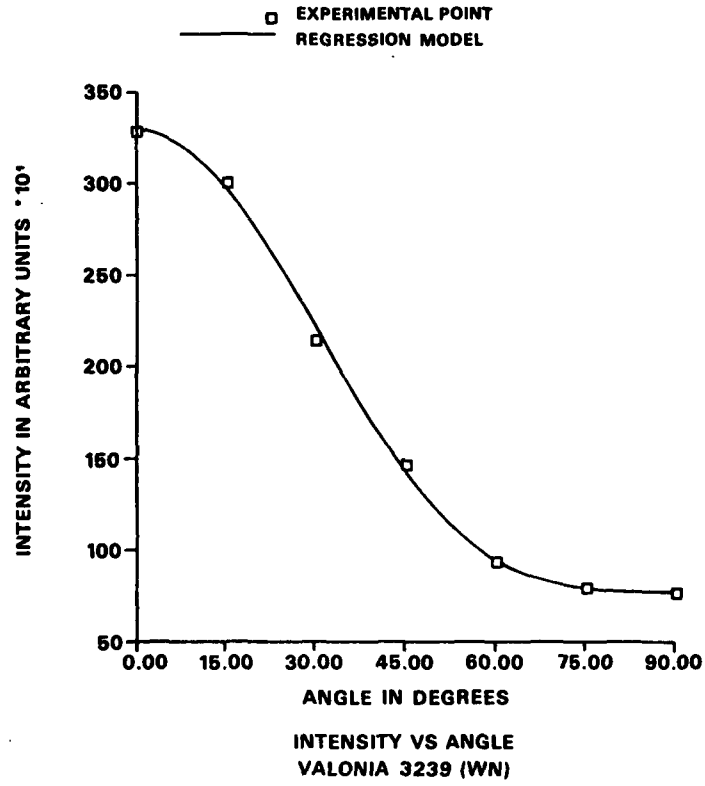

Figure 69. Intensity vs. angle - Valonia 3239 (WN).

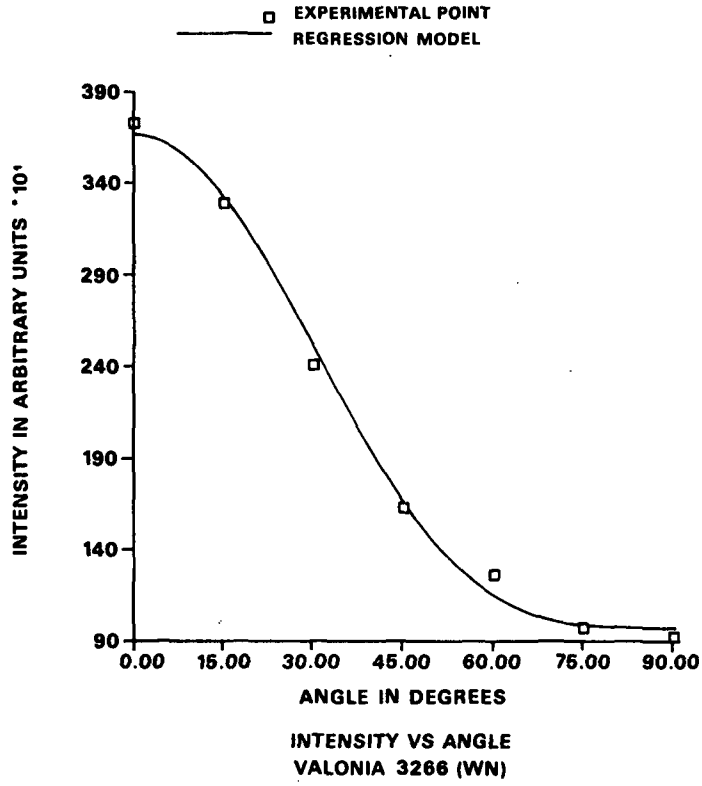

Figure 70. Intensity vs. angle - Valonia 3266 (WN).

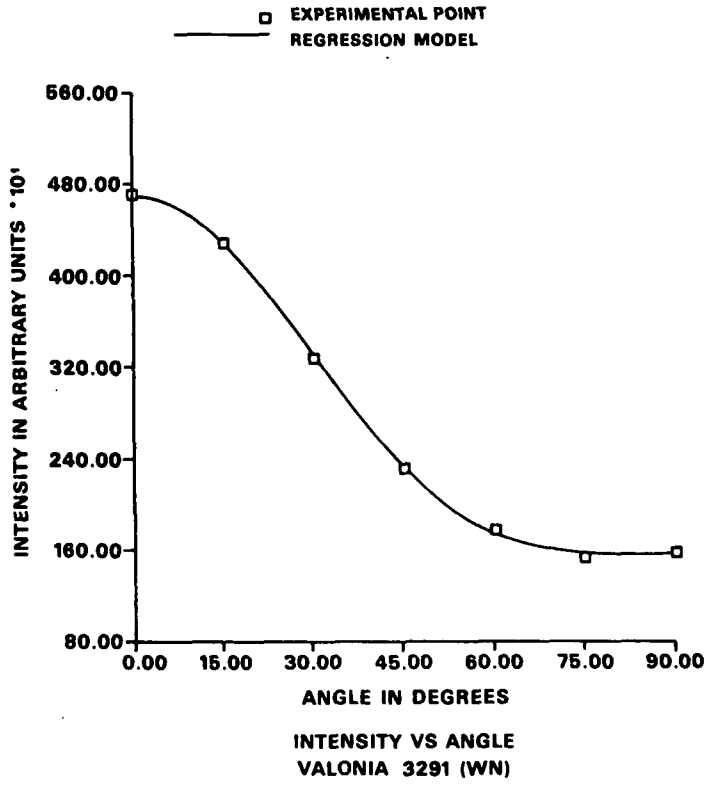

Figure 71. Intensity vs. angle - Valonia 3291 (WN).

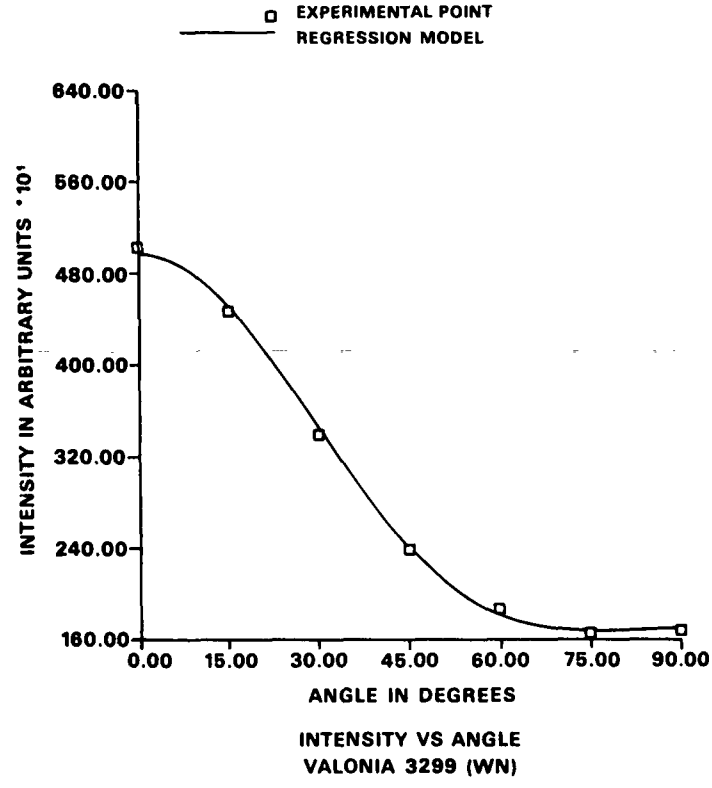

Figure 72. Intensity vs. angle - Valonia 3299 (WN).

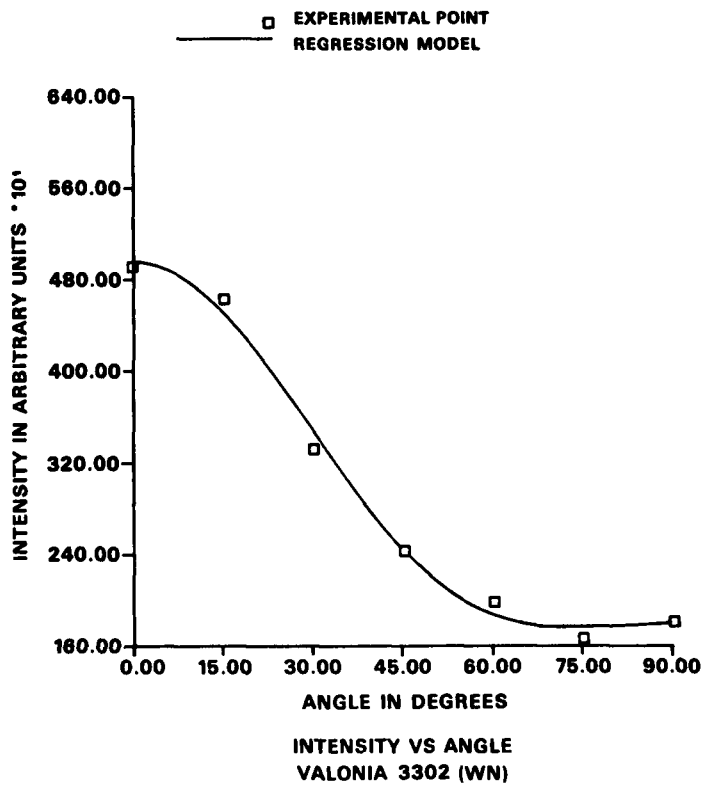

Figure 73. Intensity vs. angle - Valonia 3302 (WN).

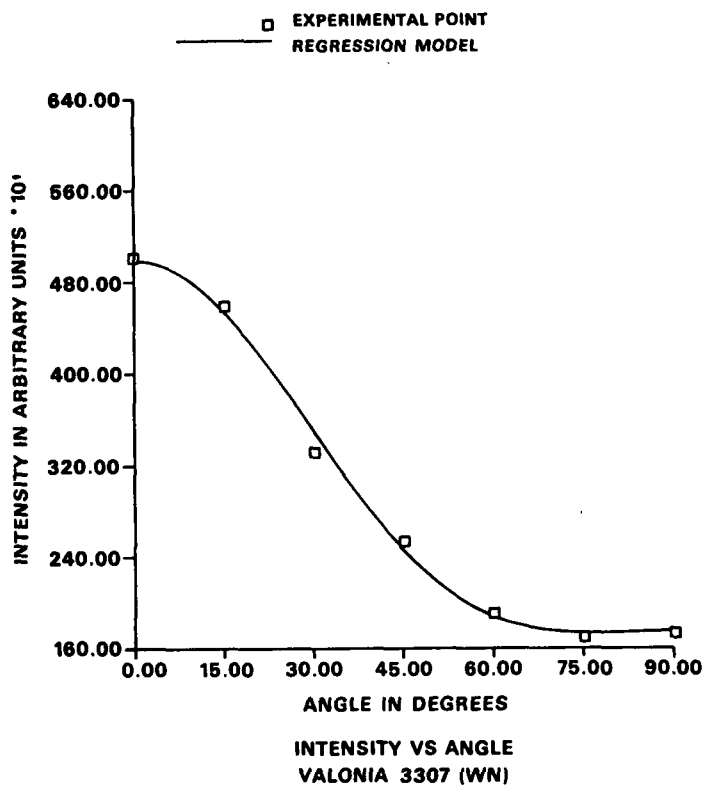

Figure 74. Intensity vs. angle - Valonia 3307 (WN).

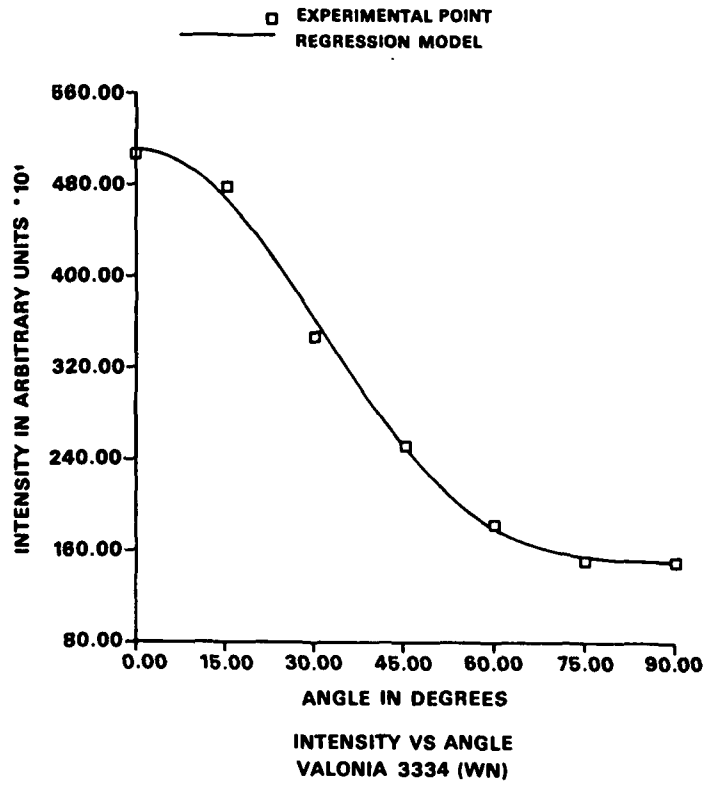

Figure 75. Intensity vs. angle - Valonia 3334 (WN).

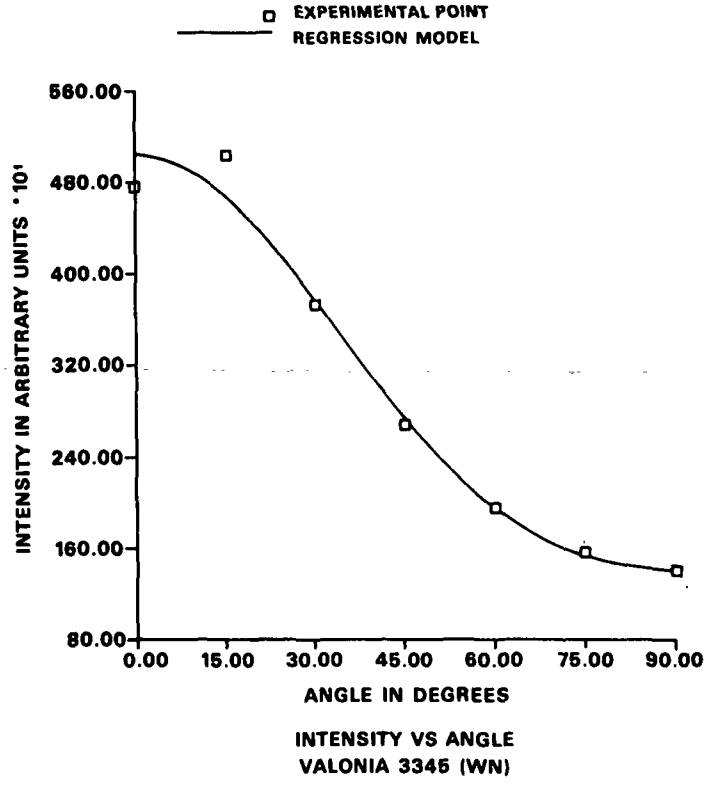

Figure 76. Intensity vs. angle - Valonia 3345 (WN).

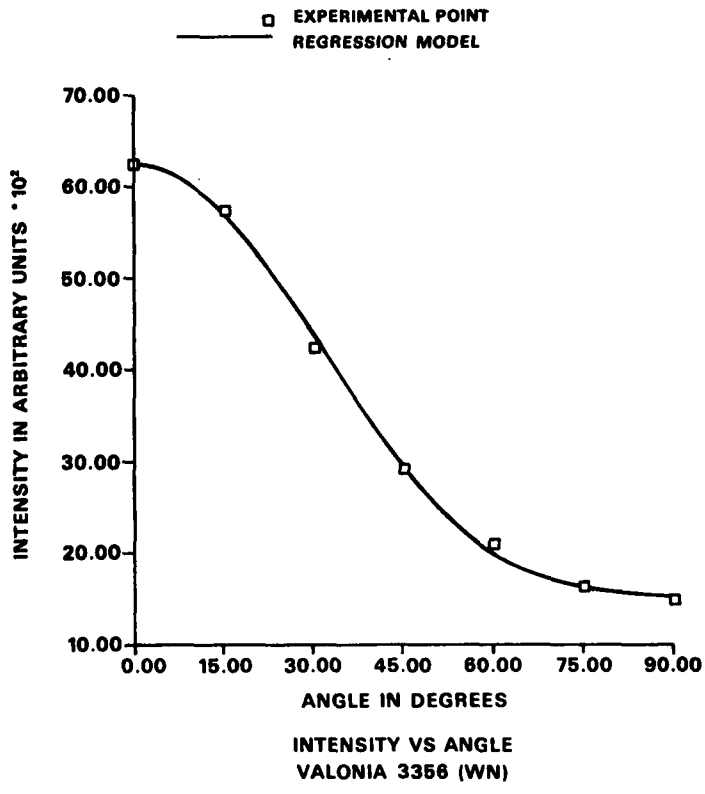

Figure 77. Intensity vs. angle - Valonia 3356 (WN).

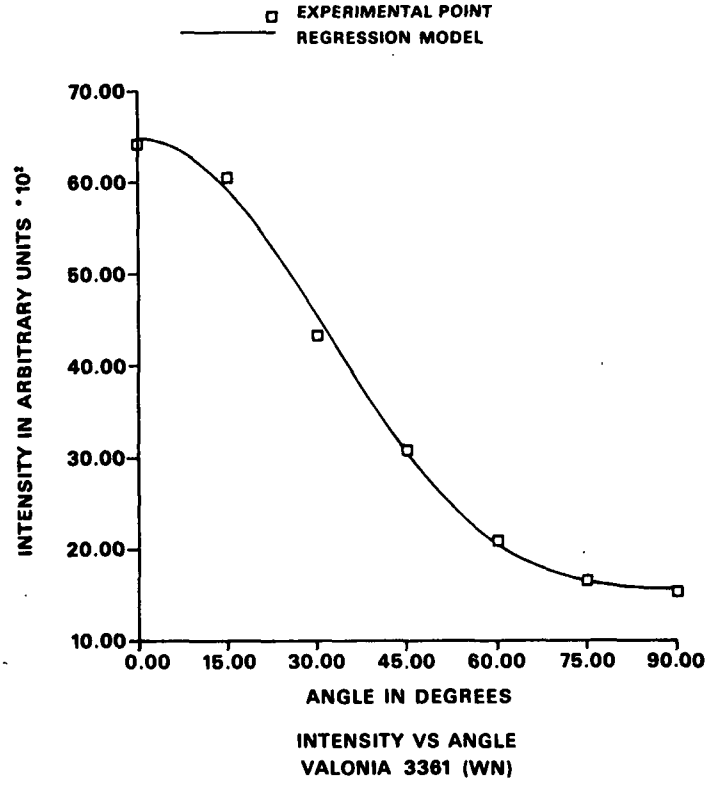

Figure 78. Intensity vs. angle - Valonia 3361 (WN).

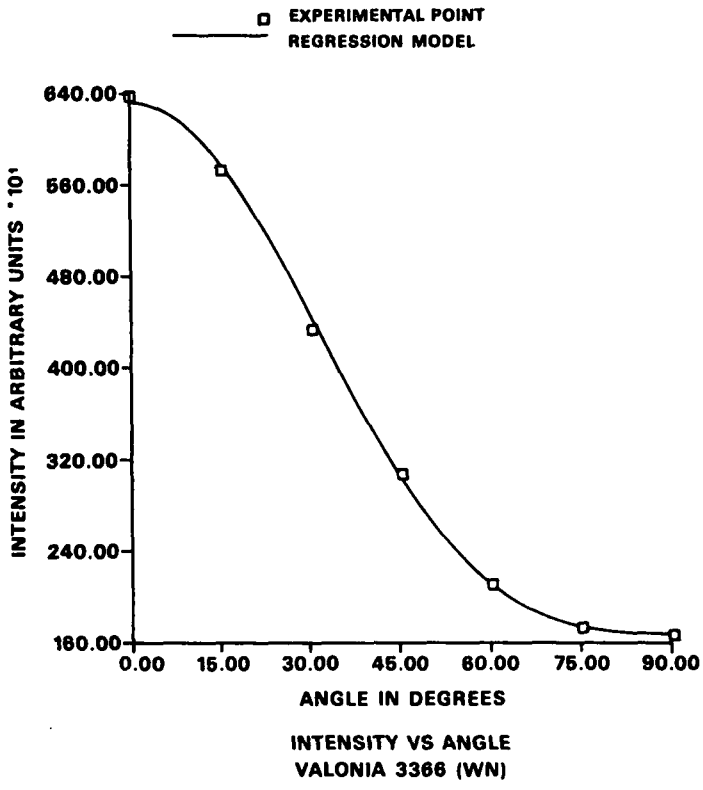

Figure 79. Intensity vs. angle - Valonia 3366 (WN).

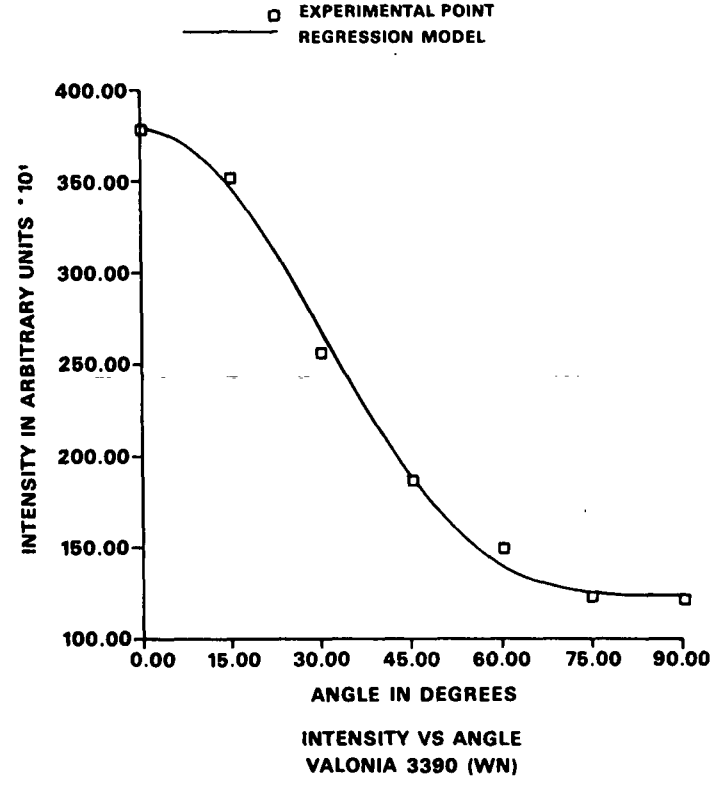

Figure 80. Intensity vs. angle - Valonia 3390 (WN).

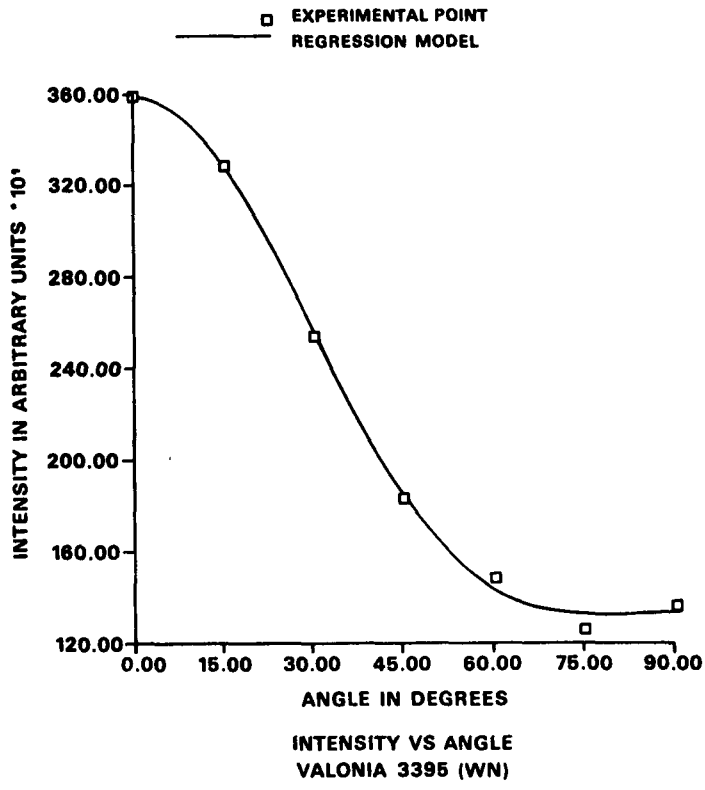

Figure 81. Intensity vs. angle - Valonia 3395 (WN).

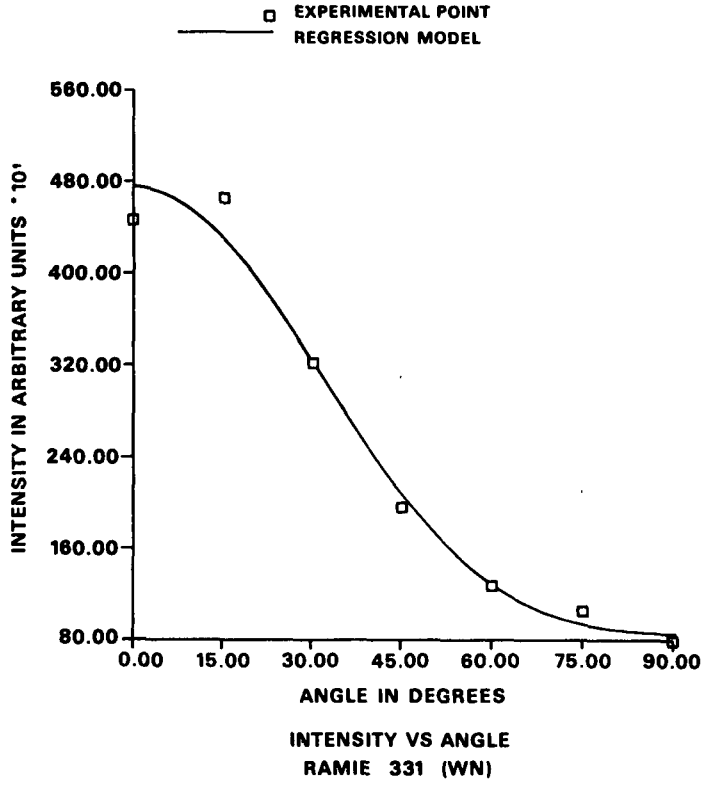

Figure 82. Intensity vs. angle - ramie 331 (WN).

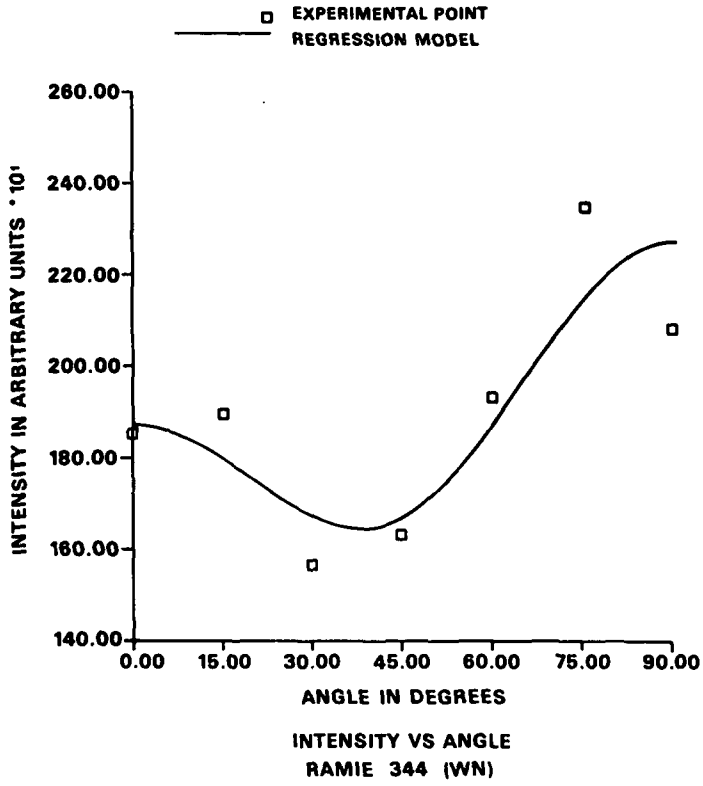

Figure 83. Intensity vs. angle - ramie 344 (WN).

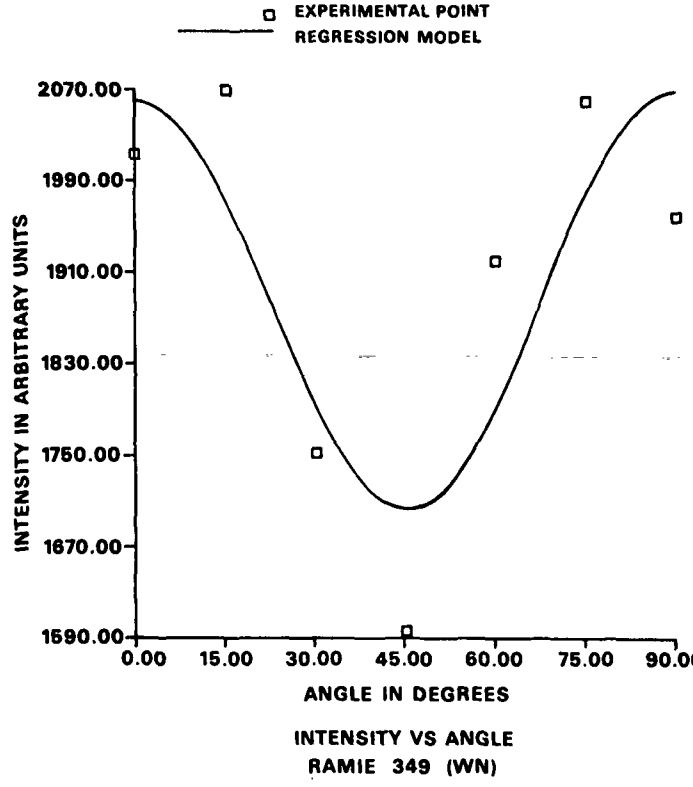

Figure 84. Intensity vs. angle - ramie 349 (WN).

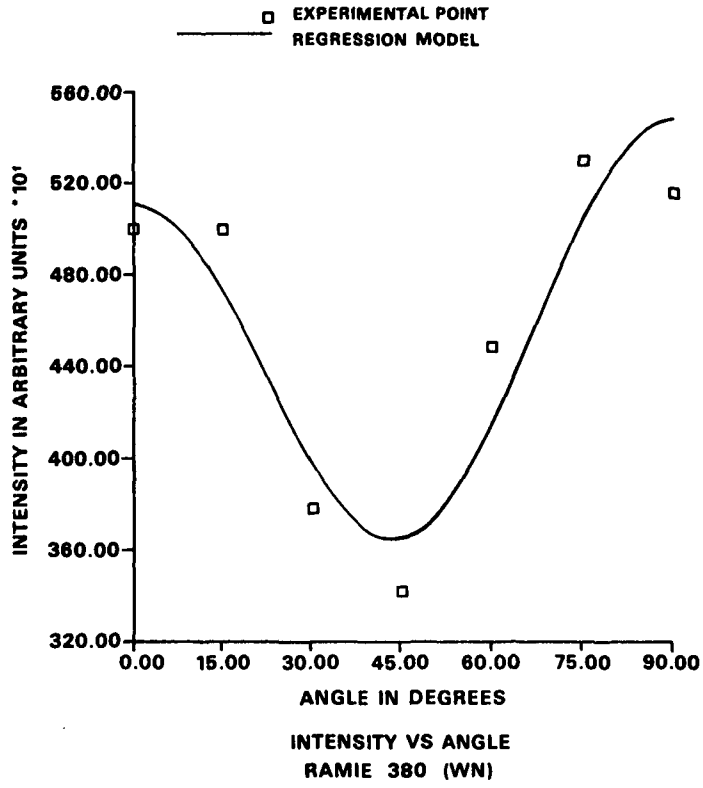

Figure 85. Intensity vs. angle - ramie 380 (WN).

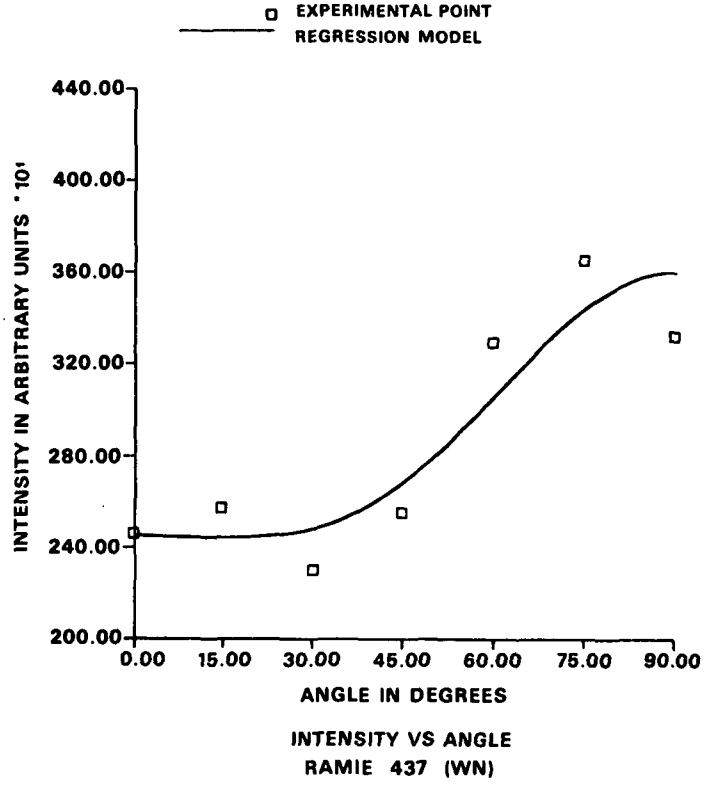

Figure 86. Intensity vs. angle - ramie 437 (WN).

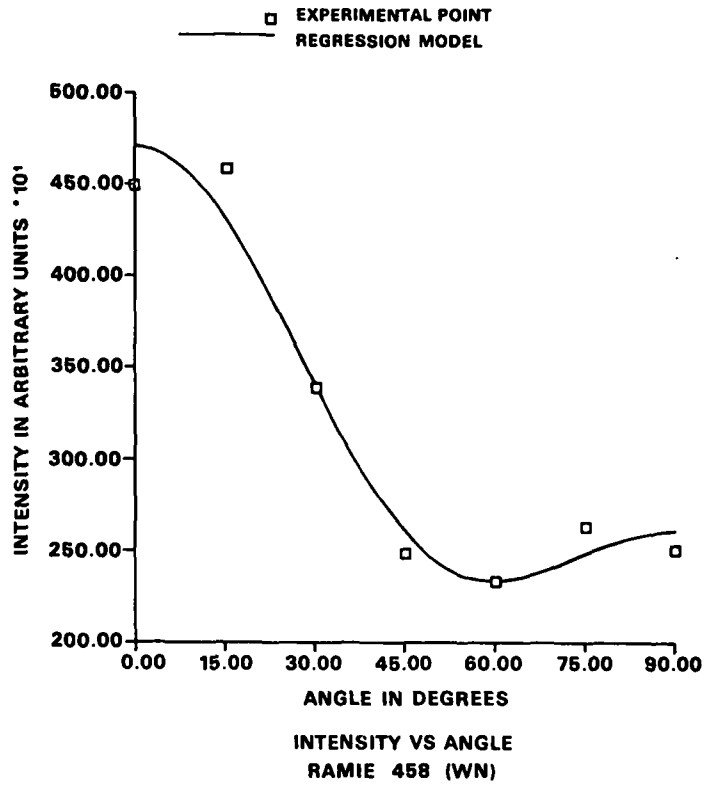

Figure 87. Intensity vs. angle - ramie 458 (WN).

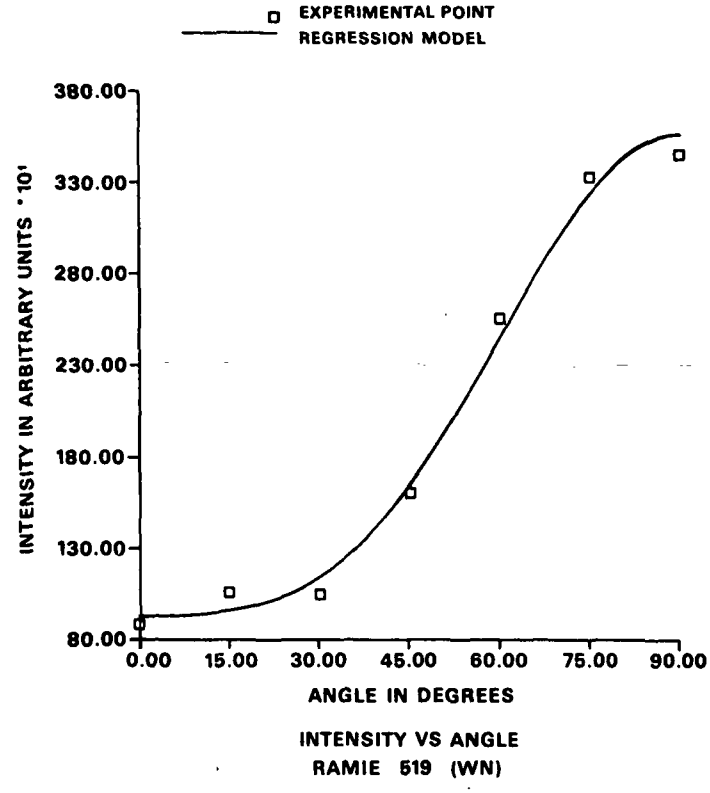

Figure 88. Intensity vs. angle - ramie 519 (WN).

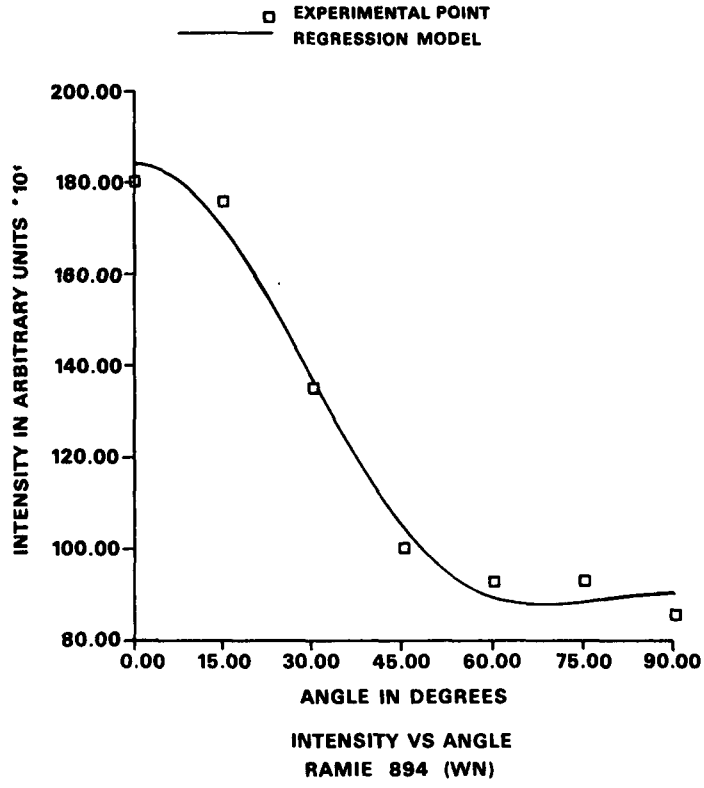

Figure 89. Intensity vs. angle - ramie 894 (WN).

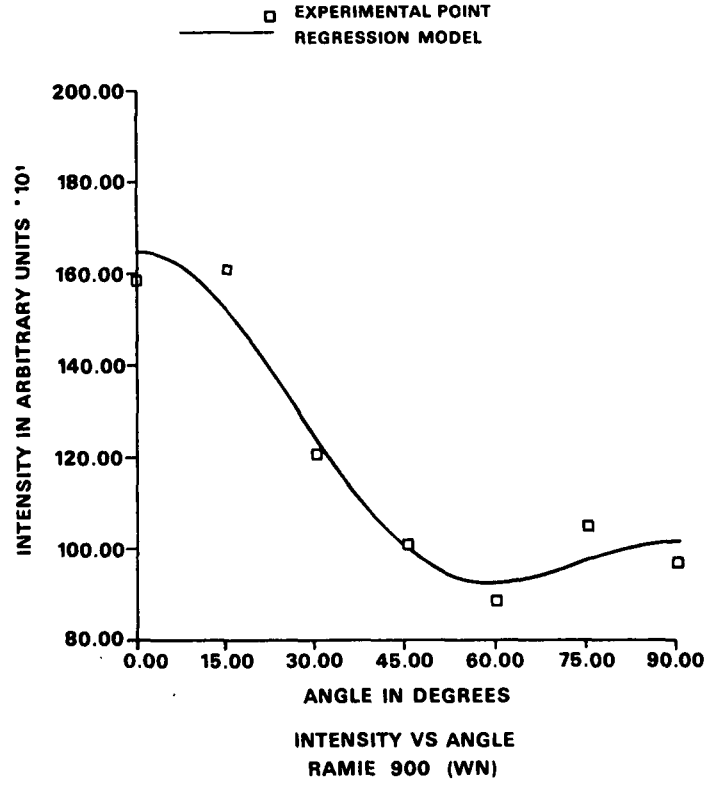

Figure 90. Intensity vs. angle - ramie 900 (WN).

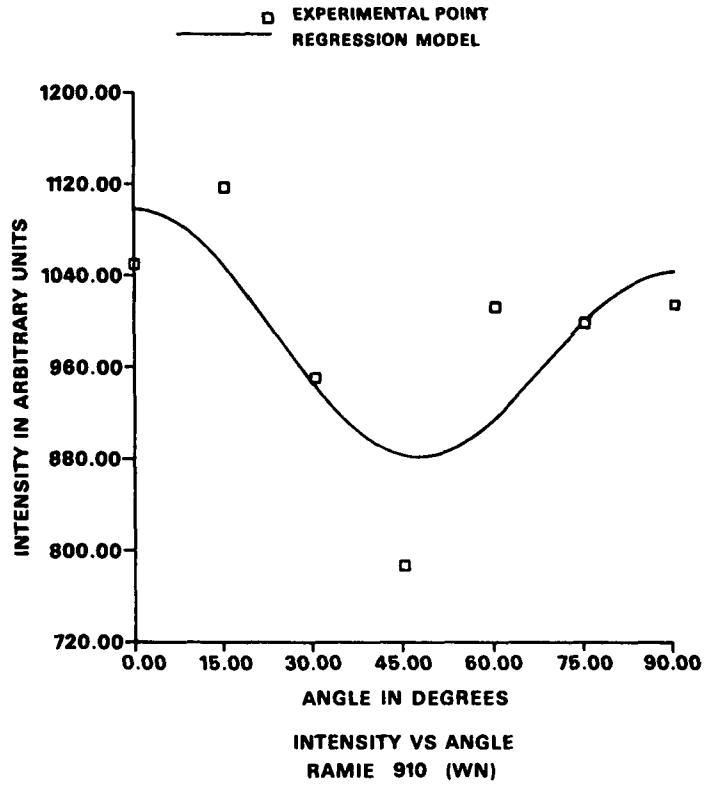

Figure 91. Intensity vs. angle - ramie 910 (WN).

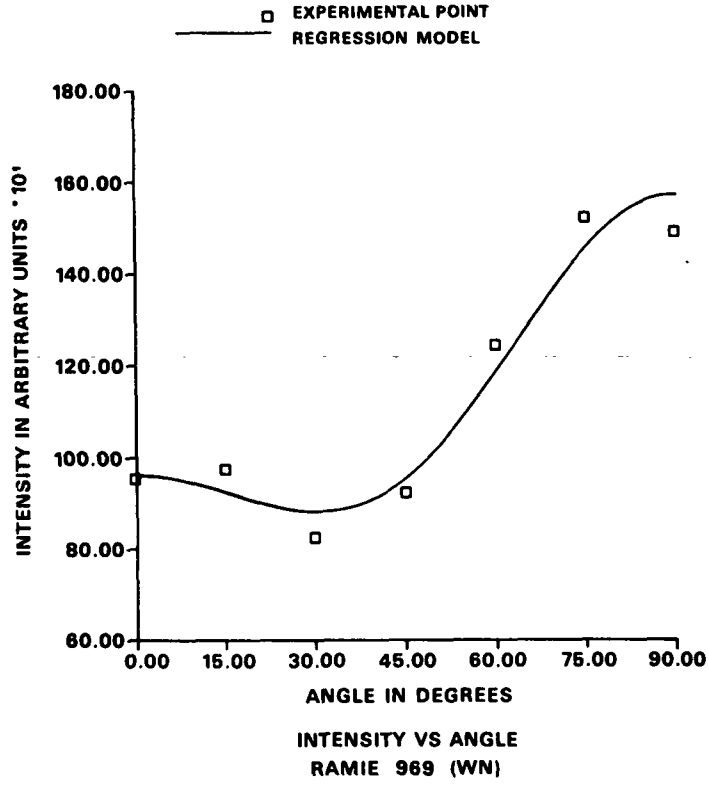

Figure 92. Intensity vs. angle - ramie 969 (WN).

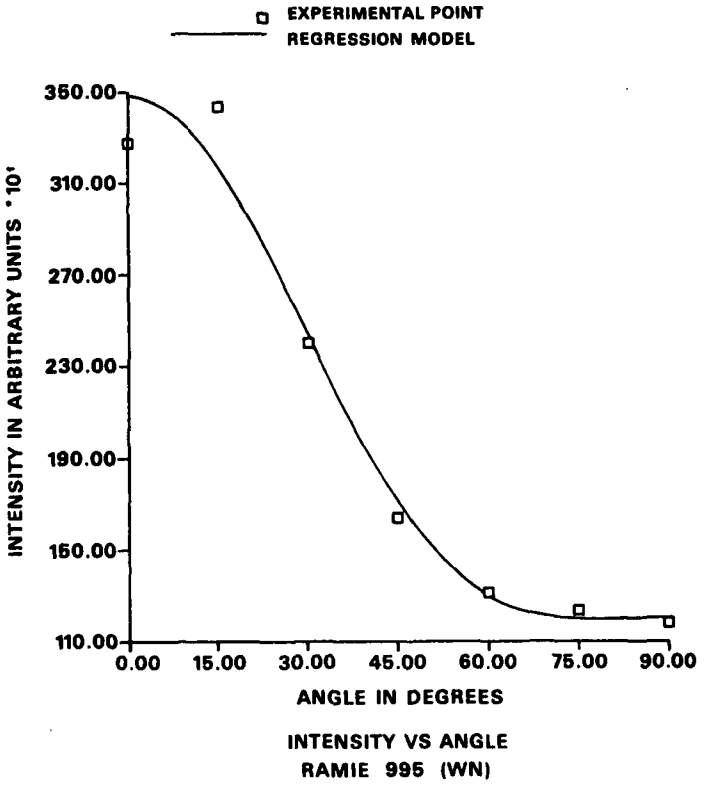

Figure 93. Intensity vs. angle - ramie 995 (WN).

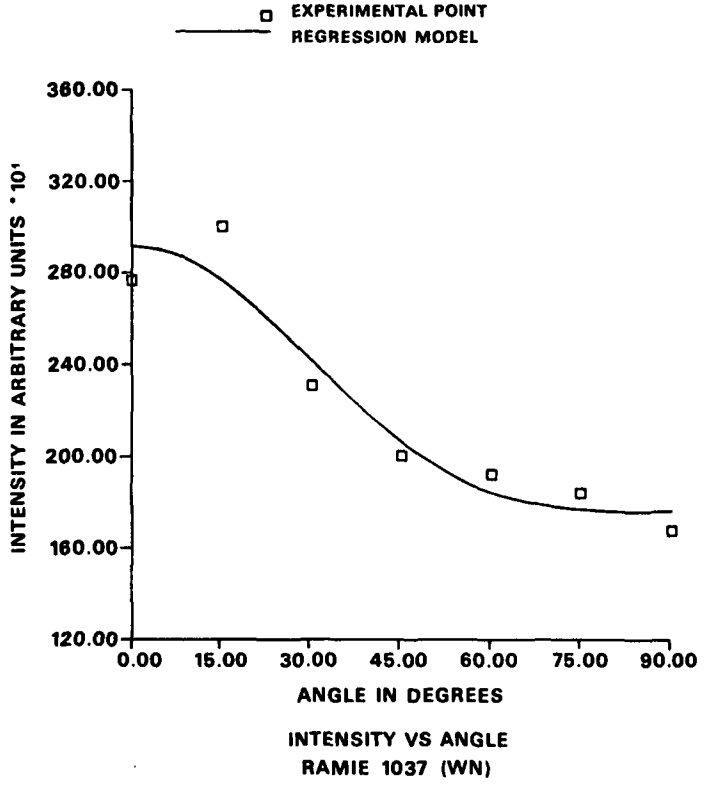

Figure 94. Intensity vs. angle - ramie 1037 (WN).

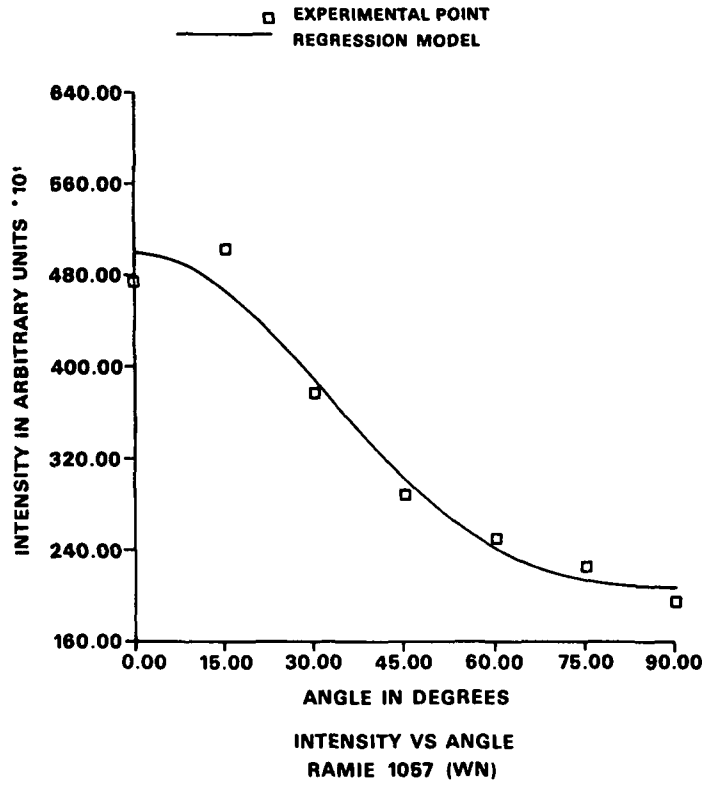

Figure 95. Intensity vs. angle - ramie 1057 (WN).

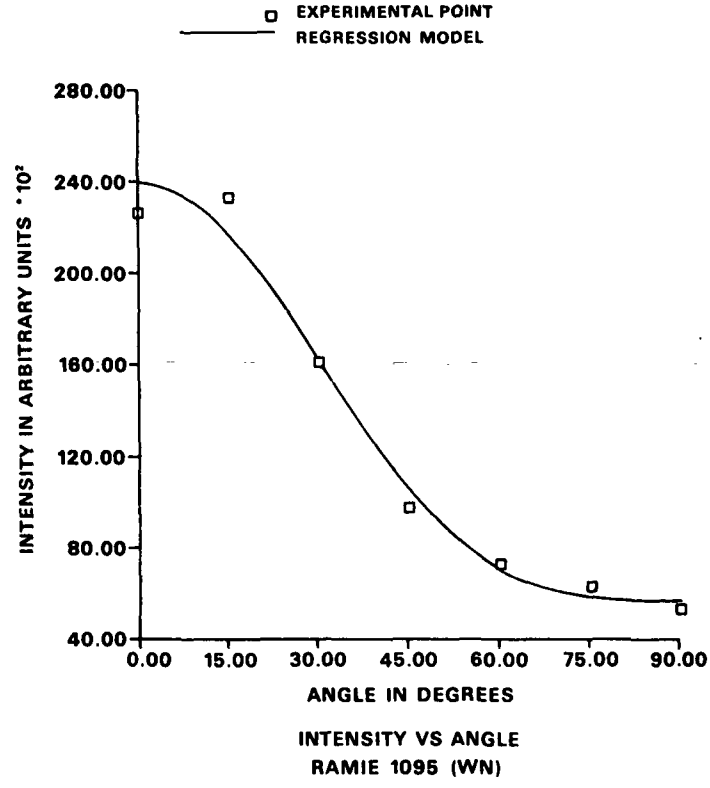

Figure 96. Intensity vs. angle - ramie 1095 (WN).

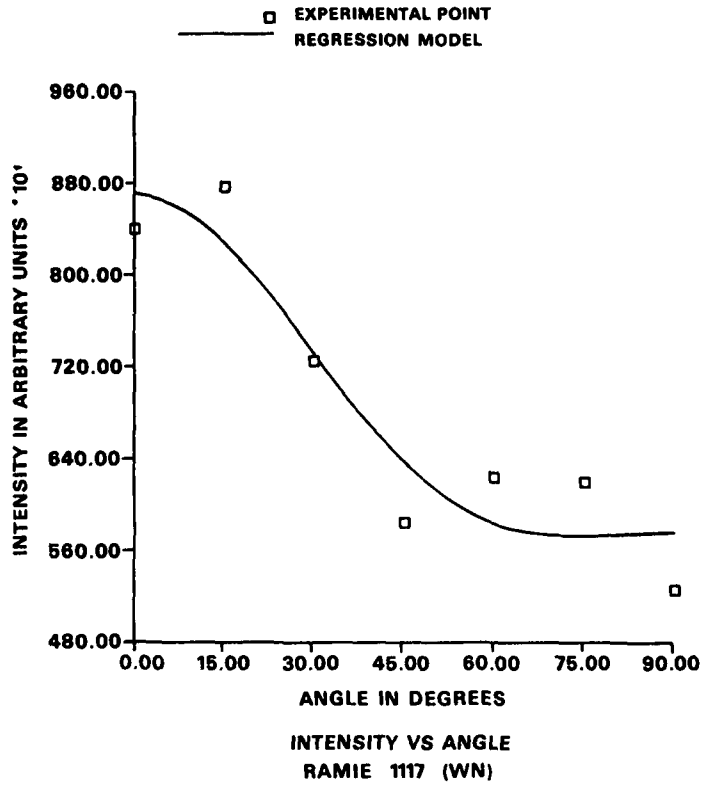

Figure 97. Intensity vs. angle - ramie 1117 (WN).

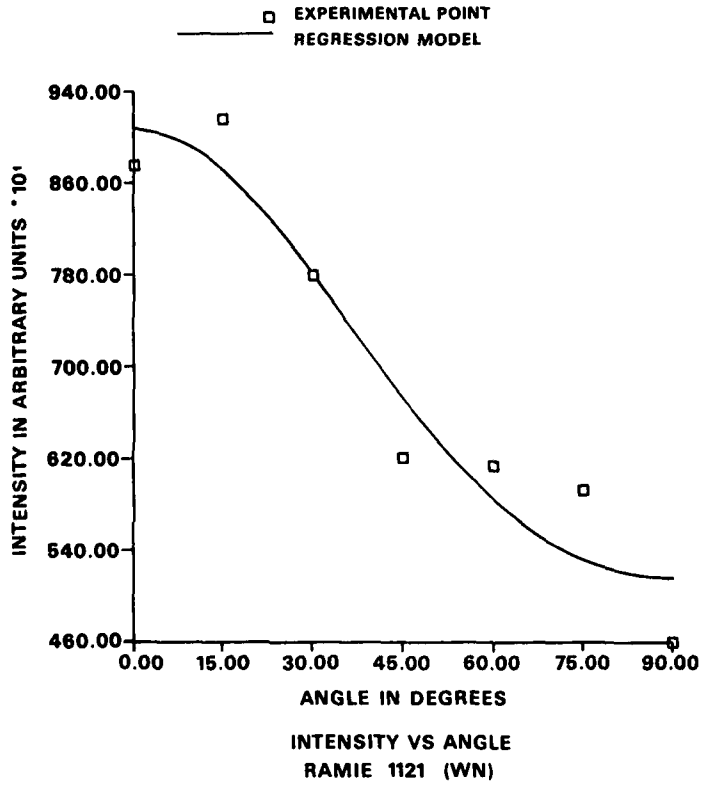

Figure 98. Intensity vs. angle - ramie 1121 (WN).

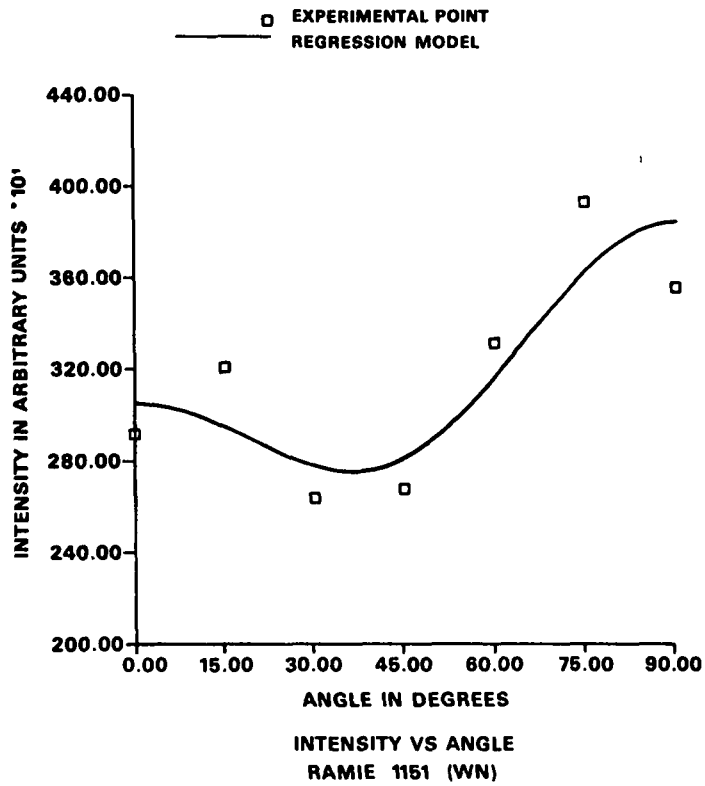

Figure 99. Intensity vs. angle - ramie 1151 (WN).

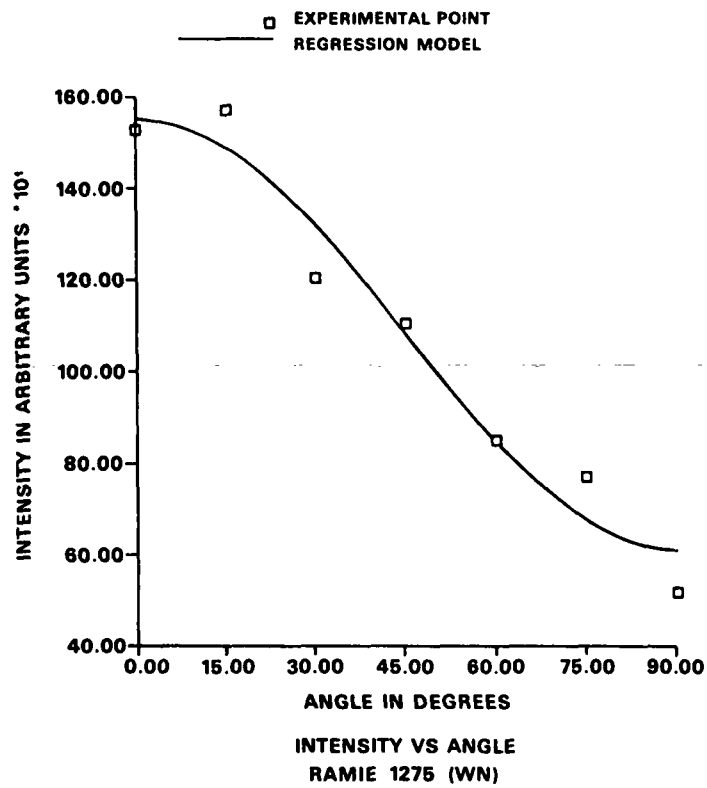

Figure 100. Intensity vs. angle - ramie 1275 (WN).

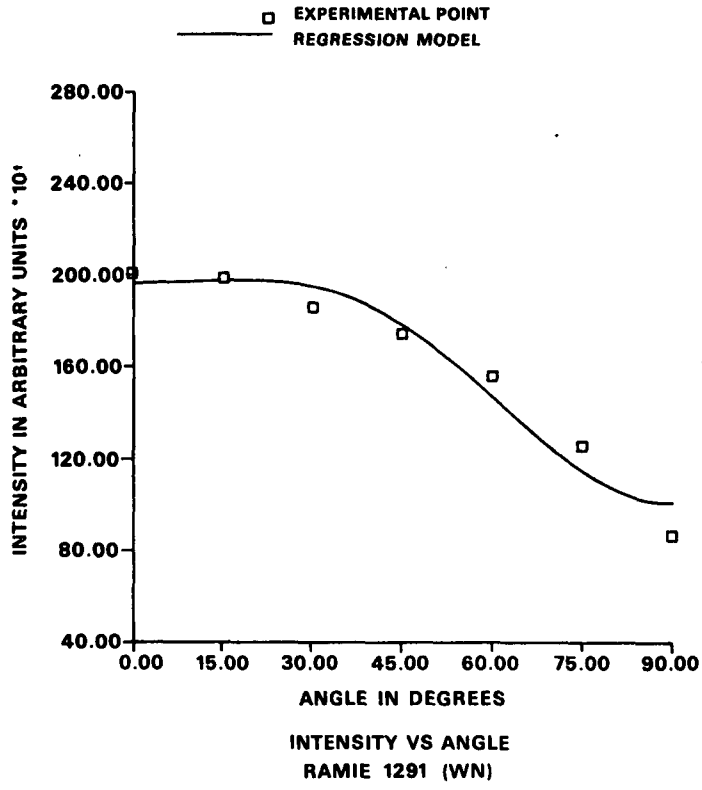

Figure 101. Intensity vs. angle - ramie 1291 (WN).

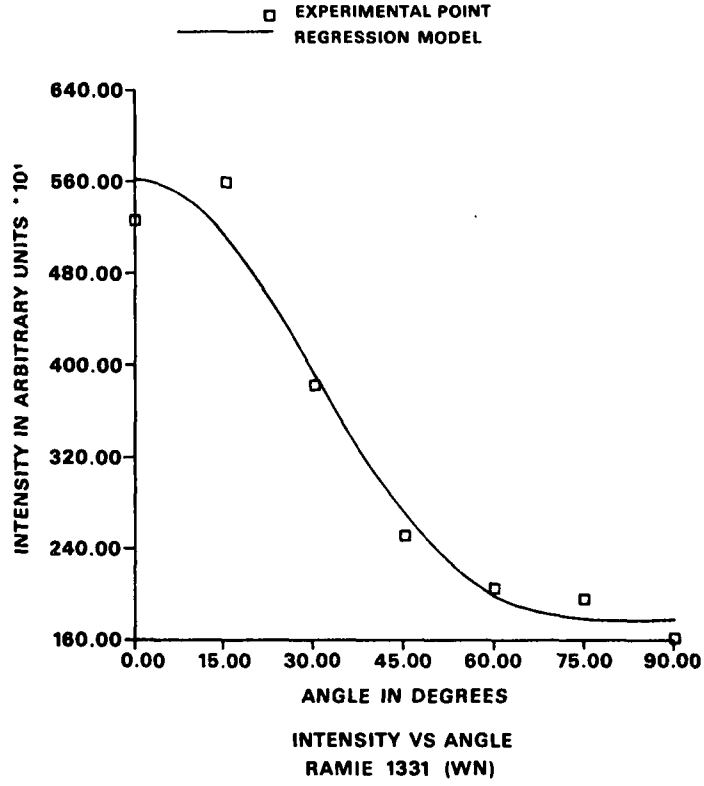

Figure 102. Intensity vs. angle - ramie 1331 (WN).

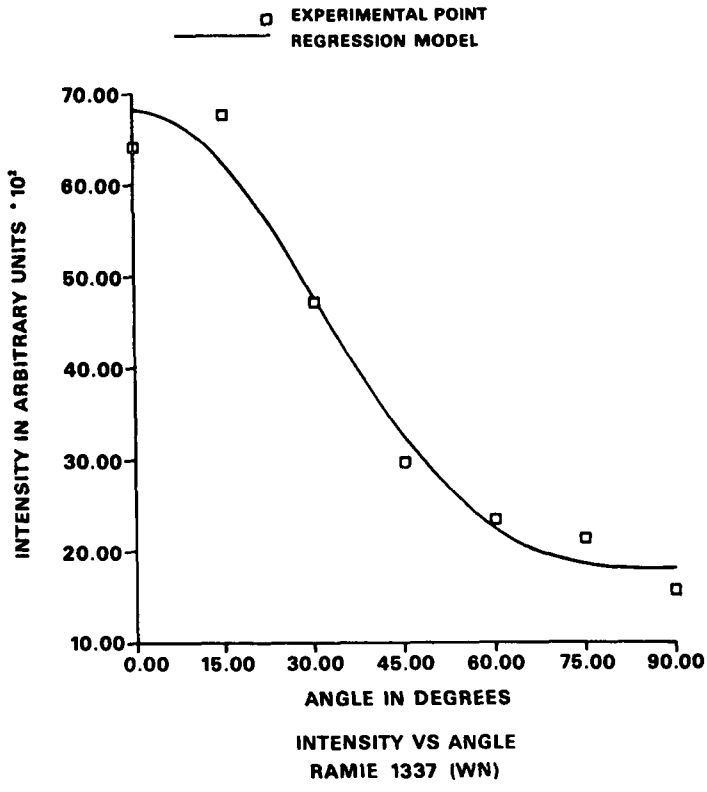

Figure 103. Intensity vs. angle - ramie 1337 (WN).

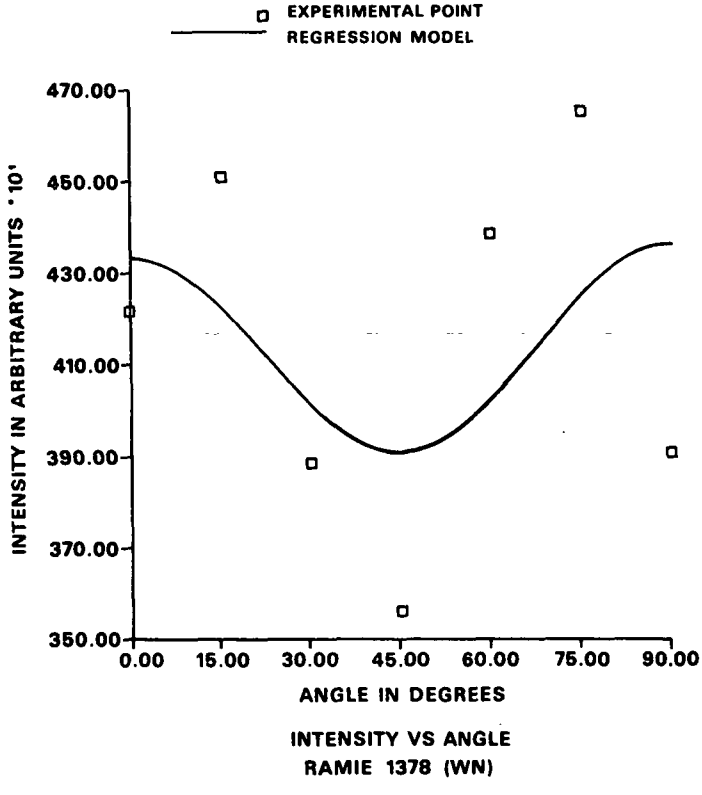

Figure 104. Intensity vs. angle - ramie 1378 (WN).

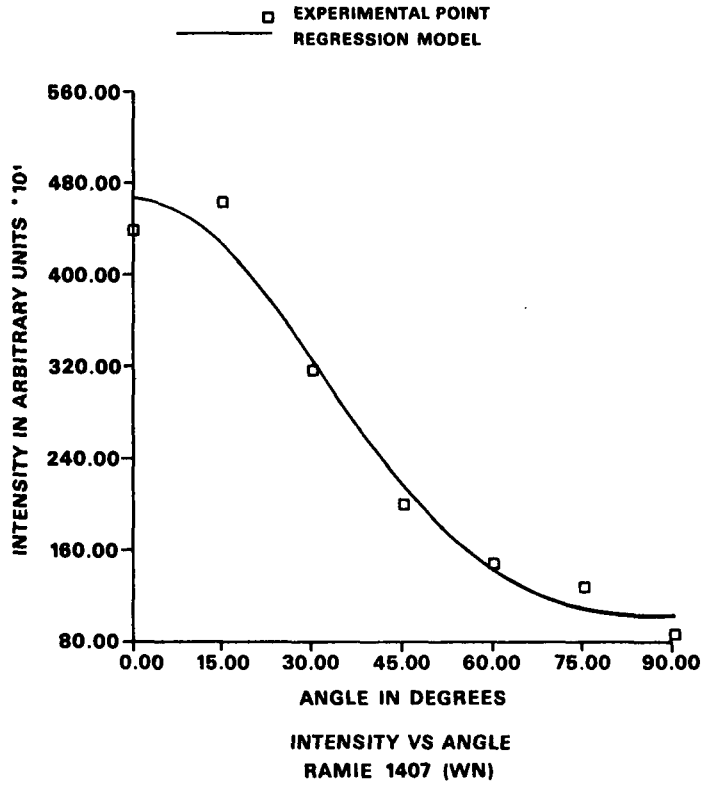

Figure 105. Intensity vs. angle - ramie 1407 (WN).

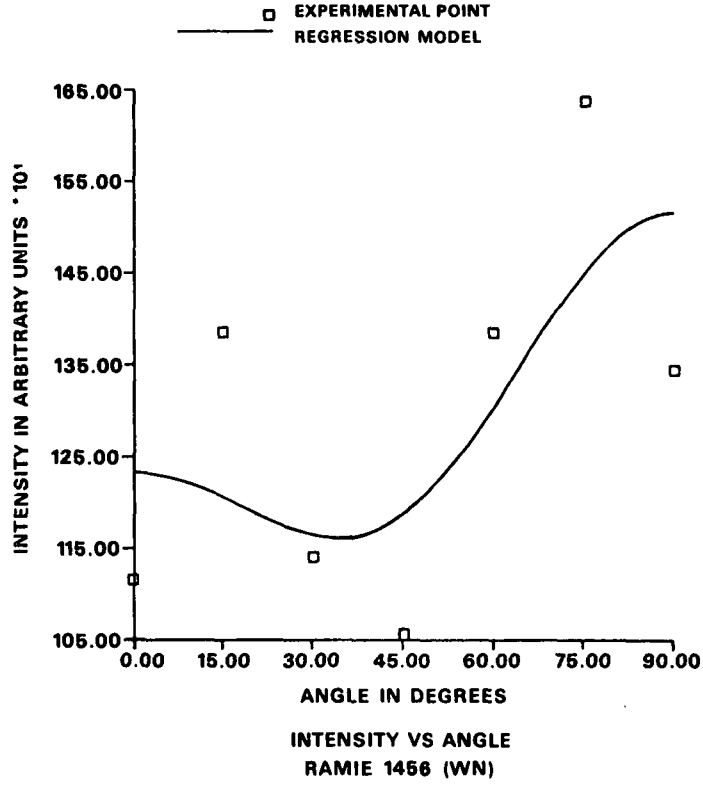

Figure 106. Intensity vs. angle - ramie 1456 (WN).

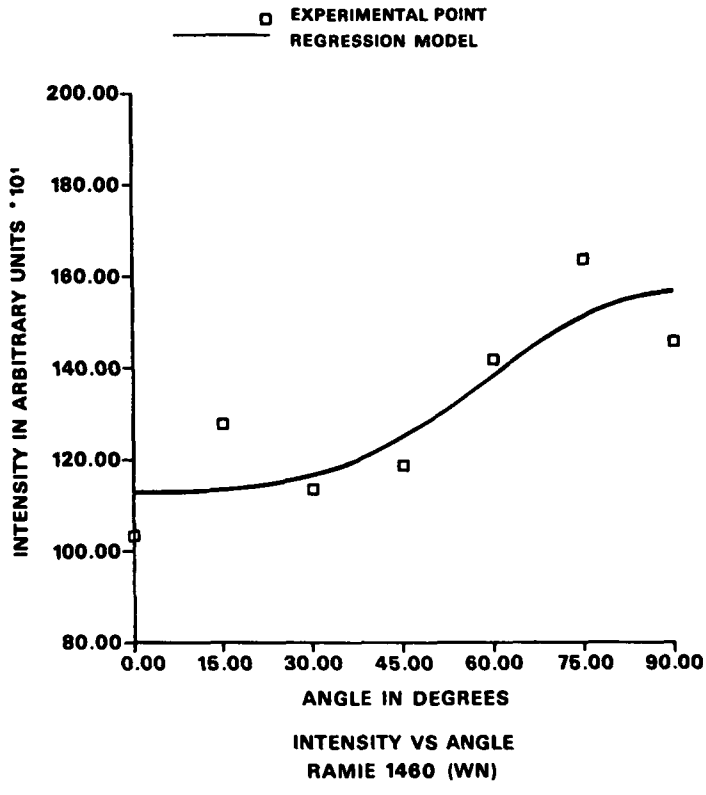

Figure 107. Intensity vs. angle - ramie 1460 (WN).

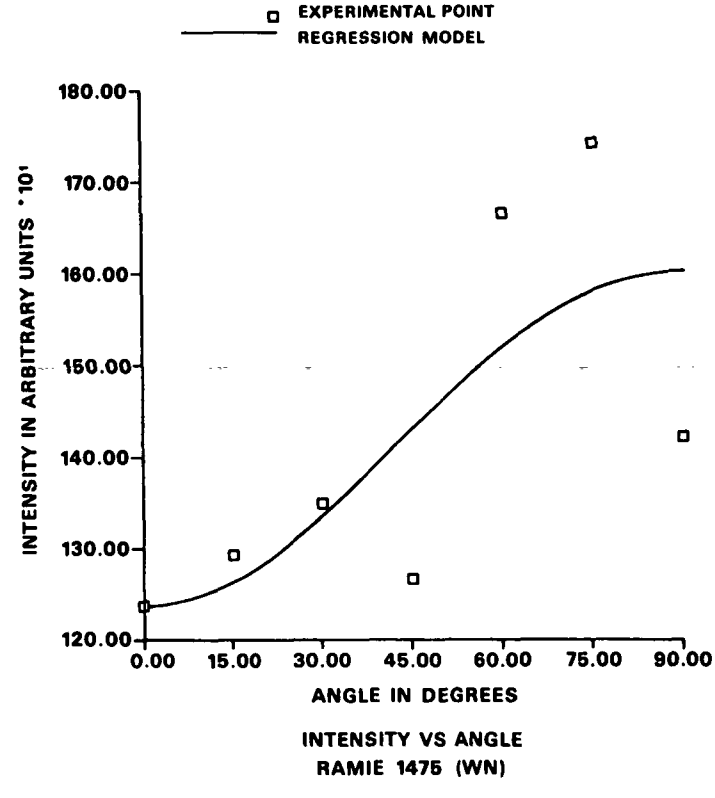

Figure 108. Intensity vs. angle - ramie 1475 (WN).

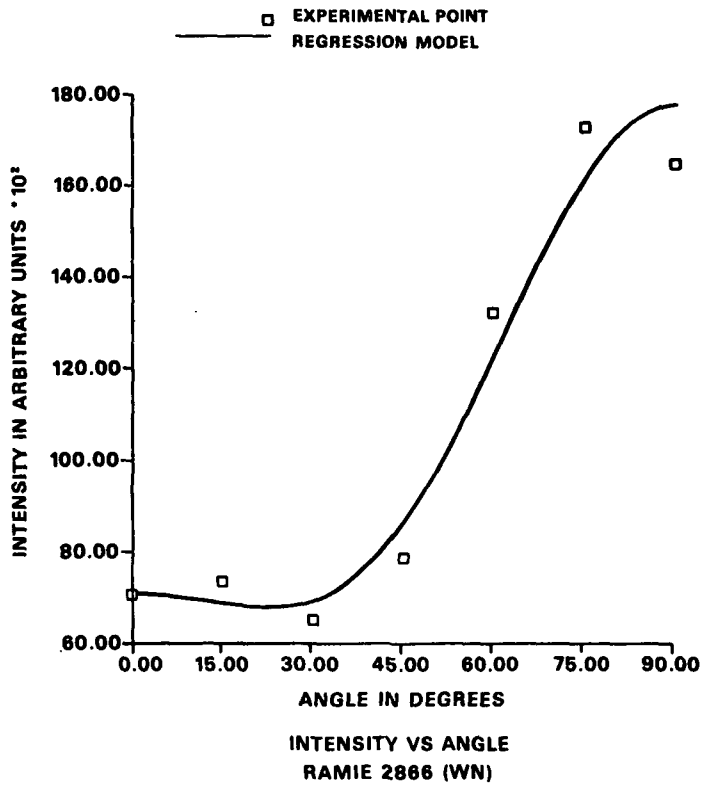

Figure 109. Intensity vs. angle - ramie 2866 (WN).

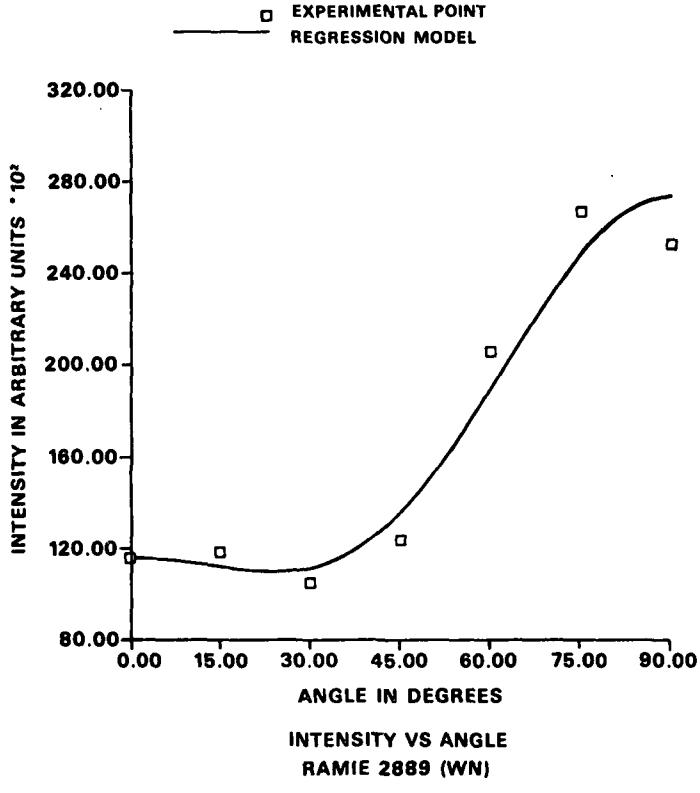

Figure 110. Intensity vs. angle - ramie 2889 (WN).

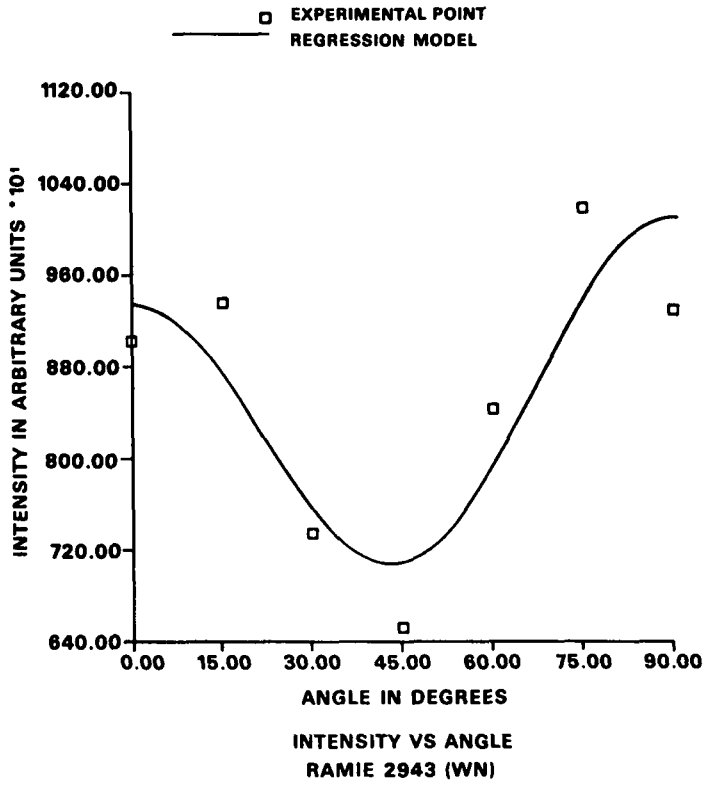

Figure 111. Intensity vs. angle - ramie 2943 (WN).

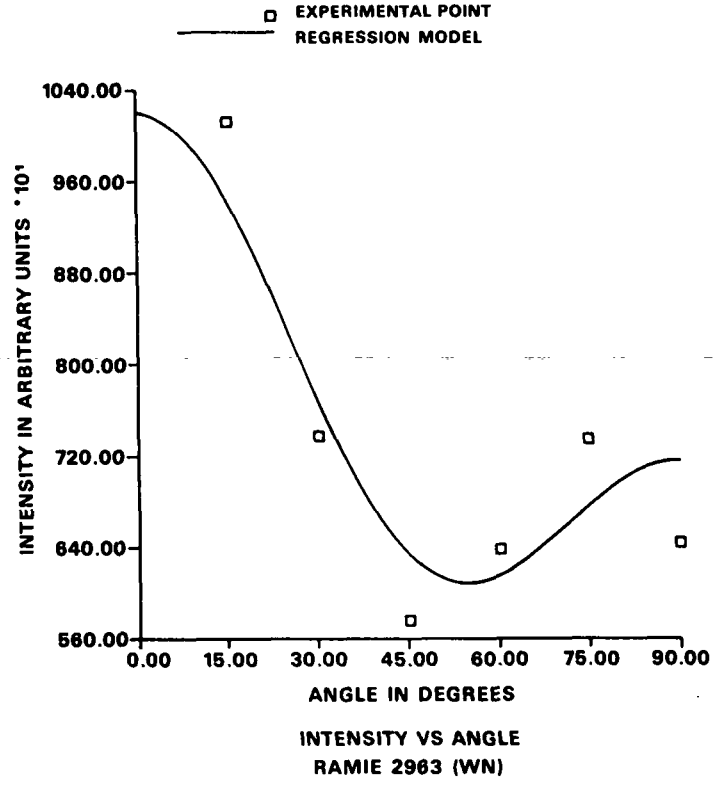

Figure 112. Intensity vs. angle - ramie 2963 (WN).

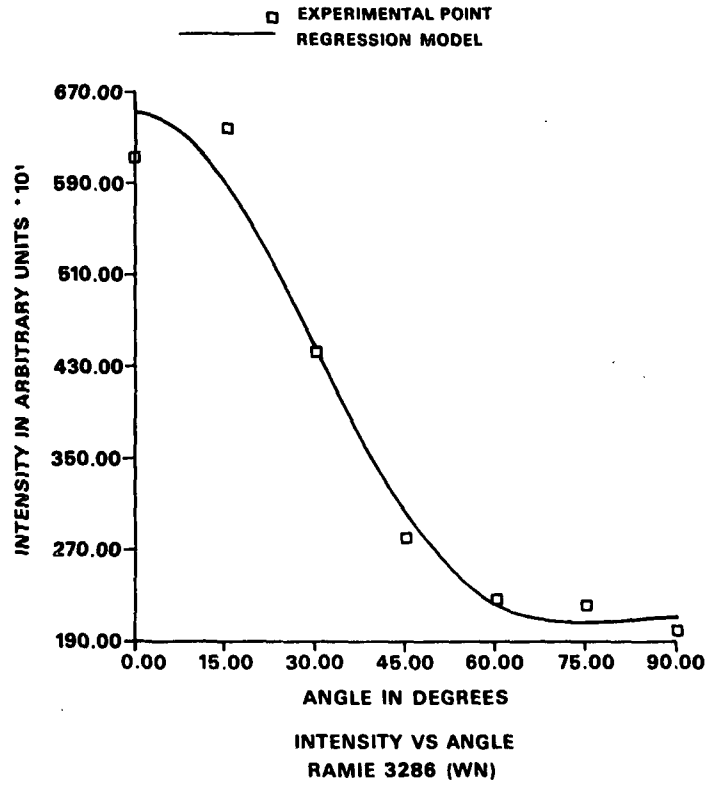

Figure 113. Intensity vs. angle - ramie 3286 (WN).

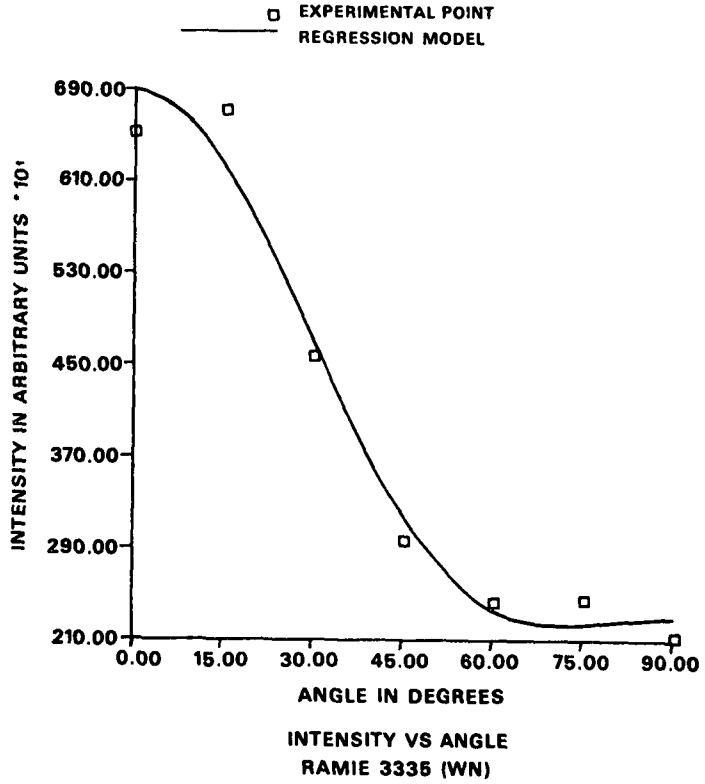

Figure 114. Intensity vs. angle - ramie 3335 (WN).

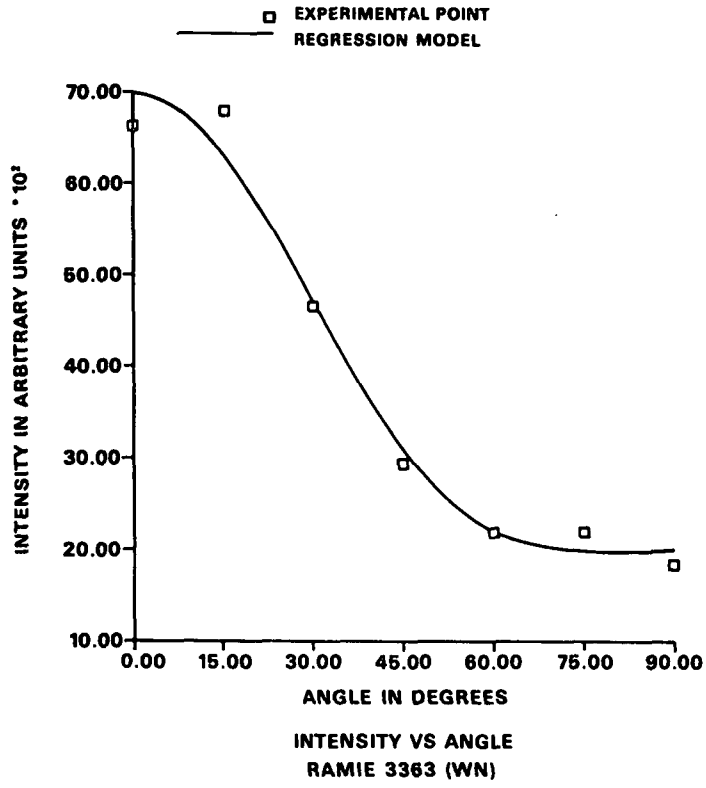

Figure 115. Intensity vs. angle - ramie 3363 (WN).

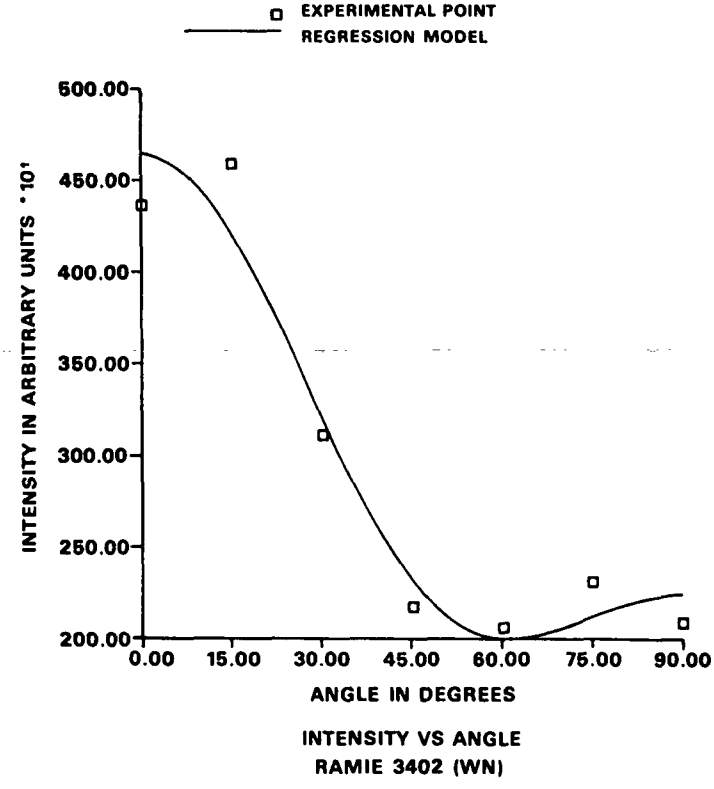

Figure 116. Intensity vs. angle - ramie 3402 (WN).

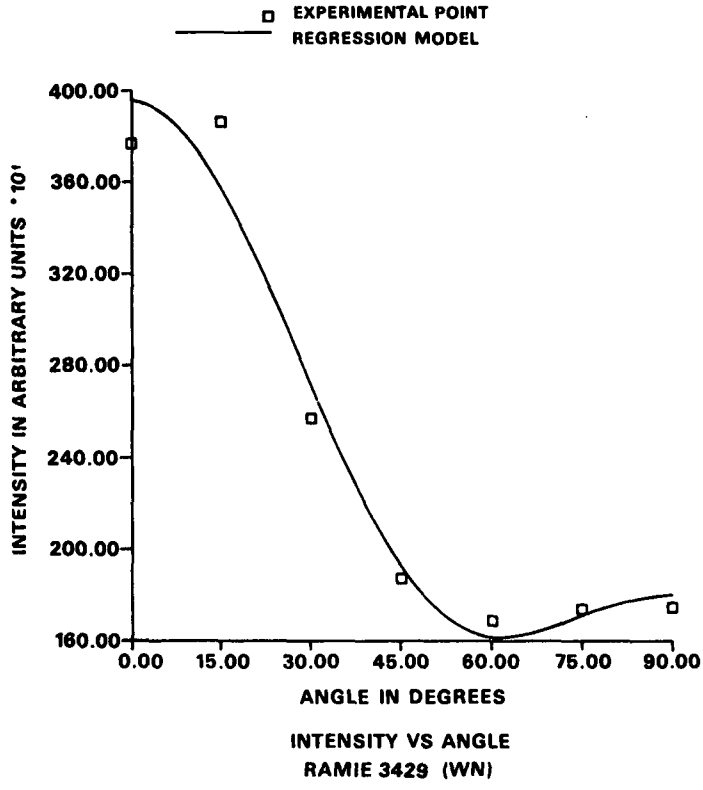

Figure 117. Intensity vs. angle - ramie 3429 (WN).